by ERNST JA STELLER

INVASION

IN COLORECTAL LIVER METASTASES

INVASION IN COLORECTAL LIVER METASTASES

Thesis, Faculty of Medicine, University Utrecht, the Netherlands, with summary in Dutch
Proefschrift, Medische faculteit, Universiteit Utrecht, Nederland, met een samenvatting in het Nederlands

The work described in this thesis was supported by a personal grant from the Dutch Cancer Society and the Wijnand M. Pon foundation.

Publication of this thesis was financially supported by: Afdeling Heelkunde UMC Utrecht, Chipsoft BV, Thermo Fisher Scientific, Panasonic biomedical, Bayer HealthCare, Pfizer Oncology, Takeda Nederland BV

ISBN/EAN: 978-94-90944-08-7
Cover design: Myra Nijman www.myranijman.nl
Lay out: Wendy Schoneveld, www.wenziD.nl
Printed by: PrintSupport4U, Meppel

INVASION
IN COLORECTAL LIVER METASTASES

(met een samenvatting in het Nederlands)

PROEFSCHRIFT

ter verkrijging van de graad van doctor

aan de Univerisiteit Utrecht

op gezag van de rector magnificus, prof. dr. G.J. van der Zwaan,

ingevolge het besluit van het college voor promoties

in het openbaar te verdedigen op

donderdag 6 juni 2013 des middags te 12.45 uur

door

Ernst Johan Abraham Steller

geboren op 7 augustus 1981 te Capelle aan den IJssel

Promotor: Prof. dr. I.H.M. Borel Rinkes
Co-promotor: Dr. O. Kranenburg

Aan Imke en mijn ouders

CONTENT

CHAPTER 1

1

General introduction and outline of the thesis

INTRODUCTION

Liver metastases account for the vast majority of colorectal cancer deaths. Still, the events necessary for metastasis formation are largely unknown. Understanding the biological processes leading to colorectal cancer (CRC) and to colorectal liver metastasis formation, is key to finding a cure. Many faulty signaling pathways have been identified in intestinal epithelial tumor cells. However, none has resulted in the identification of a therapy able to selectively kill colorectal tumor cells or stop cancer development. This may be due to the activation of "rescue" pathways or to tumor cell independence of those pathways. Identification of the molecular signaling cascades on which tumor cells depend for their survival and metastatic spread is therefore essential for treating cancer. The ultimate goal of cancer therapy is to specifically induce tumor cell death. This thesis studies the role of the well known apoptosis inducing receptor CD95 in CRC and liver metastasis formation and investigates the early stages of metastasis formation in the liver.

PART I

Apoptosis

Apoptosis is the process of programmed cell death which is essential in embryonic development but also plays an important role in cancer development. This highly orchestrated cell death is morphologically characterized by cell shrinkage and rounding, enhancement of the cytoplasm density, condensation of the chromatin and fragmentation into so-called apoptotic bodies. These bodies are taken up by neighboring cells or phagocytes, avoiding an immune response. Apoptosis can be initiated by the cell itself when it is not able to repair internal damage (intrinsic apoptosis) but it can also be triggered by extracellular signals, for instance from neighboring cells or immune cells (extrinsic apoptosis)[3,4] (Figure 1).

Death receptors

Several cell surface receptors can activate apoptosis, upon binding to their ligand. Eight distinct 'death receptors' have been characterized: CD95 (also known as FAS/APO-1/DR2), TNF-receptor 1 (TNF-R1/p55/p60/CD120a/DR1), TNF-related apoptosis-inducing ligand receptor 1 (TRAILR1/DR4/APO-2), DR3 (APO-3/LARD/TRAMP/WSL1, TNF-related apoptosis-inducing ligand receptor 2 (TRAIL-R2/KILLER/TRICK2/DR5), DR6 (TNFRSF21), ectodysplasin A receptor (EDAR) and nerve growth factor receptor (NGFR)5. These receptors are distinguished by a cytoplasmic region of $\pm$ 80 residues which is termed the death domain. Stimulation of the receptor by binding to one of the death receptor ligands, CD95Ligand (CD95L or FASL), tumor necrosis factor (TNF), TL1A, TNF-related apoptosis inducing ligand (TRAIL), ectodysplasin A (EDA1), APO-3 ligand (APO-3L) or nerve growth factor (NGF), activates intracellular signaling cascades leading to programmed cell death[5,6].

CD95

The discovery of CD95 as a death receptor was made accidentally in the lab of Dr. Yonehara in 1989. In order to obtain a monoclonal antibody against interferon alpha mice were immunized with the human fibroblast cell line FS-7 and, surprisingly, an antibody which killed multiple human cell lines was obtained[7]. The human antigen recognized by the antibody was termed

the FS-7-associated surface (or FAS) antigen, which was later renamed CD95[7]. Also in 1989 in the laboratory of Dr. Krammer a different antibody (termed anti-APO-1) was developed which induced apoptotic cell death in human lymphoblast cell lines and was later discovered to activate CD95[8]. By cloning the cDNA of both FAS and APO-1 it was revealed that both antibodies recognized the same human protein[9]. The identification of the cDNA for CD95 made it possible to create a monoclonal antibody against mouse CD95. This antibody was produced in a hybridoma cell line from hamsters which were immunized with CD95-overexpressing cells[10]. When the resulting antibody against CD95 was injected in the peritoneal cavity all mice rapidly died due to fulminant hepatitis. This was caused by CD95-mediated apoptosis of hepatocytes[10]. In 1993, the ligand for CD95 (CD95L) was first described[11]. When investigating T-cell mediated cytotoxicity a lymphocyte cell line (d10S) was identified which killed target cells via the CD95-CD95L pathway[12]. From these cells the CD95L cDNA was cloned and its resulting protein was shown to induce cell death upon binding to its receptor on CD95 overexpressing cell lines[11]. The CD95 gene was identified in mice on chromosome 19 near an allele which had been mapped for an autosomal recessive mutation called *lpr* (lymphoproliferation)[13]. DNA extraction from *lpr* mice showed a rearrangement in the CD95 gene and no mRNA expression of CD95[14]. Mice carrying a *gld* (generalized lymphoproliferative disease) mutation were known to have a clinical syndrome identical to that of *lpr* mice. The cause of the *gld* phenotype was a point mutation in the CD95ligand gene on chromosome 1[15]. The *lpr* and *gld* phenotypes are characterized by progressive enlargement of all lymph node groups, enlargement of the spleen, lymphoid infiltrates, and autoimmune disease[16]. A similar clinical presentation is observed in patients with autoimmune lymphoproliferative syndrome (ALPS)[17]. Subsequently, it was confirmed that these patients had a defect in the gene encoding CD95, resulting in non-detectable cell surface expression[18]. This linked defects in CD95 signaling to human disease.

CD95 apoptosis signaling

At present CD95L is the only known ligand for CD95. CD95L can activate its receptor as a membrane bound form (mCD95L) to stimulate apoptosis[2,11,19]. Upon binding to mCD95L the intracellular death domain of CD95 recruits the death inducing signaling complex (DISC) which results in activation of caspase 8. Caspase 8 activation plays a central role in transduction of the apoptotic signal finally resulting in cell death (Figure 1). mCD95L can be cleaved by matrix metalloproteinases (MMPs) into a soluble form (sCD95L)[20]. sCD95L activates several non-apoptotic signaling pathways but is not very efficient in inducing apoptosis[2,21,22] (Figure 1).

CD95 expression

CD95 is expressed in various tissues including the thymus, lung, liver, small and large intestine, heart and spleen and on cells of the immune system[23,24]. On the contrary, CD95L is expressed more selectively by activated T cells, natural killer cells, B lymphocytes, plasma cells and on Paneth cells in the small intestine[11]. Furthermore, constitutive CD95L expression is seen in the eye and testis, where it is implicated in creating an environment of immune privilege by killing infiltrating CD95-expressing cytotoxic T-cells[25].

CD95, CD95L, and cancer

Many human tumors express CD95 and CD95L, including those of colorectal, breast, renal, hepatocellular, and lung origin[26-28]. Expression levels of CD95L are frequently upregulated with tumor progression while CD95 expression levels remain similar to or are downregulated when compared to non-cancerous tissue[27,29,30].

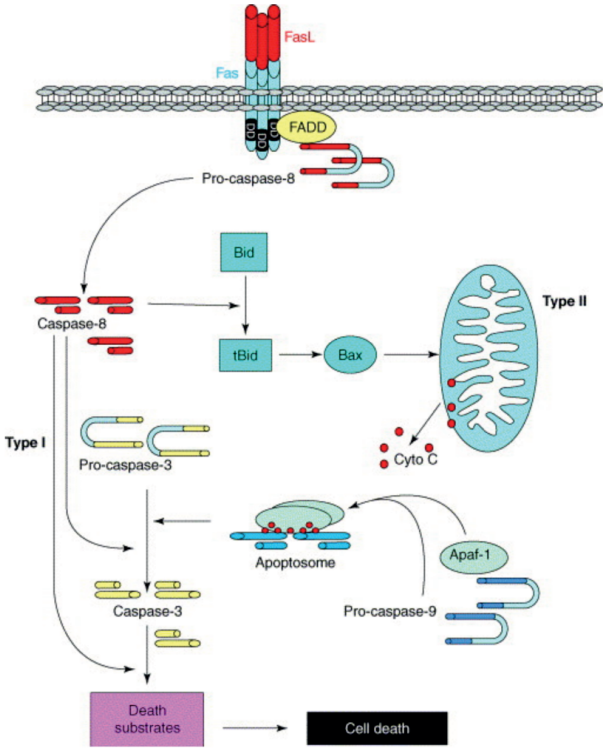

Figure 1. CD95 death receptor signaling (adapted from Houston et al 2004[1]).

Death ligands can trigger apoptosis in many different tumor cell lines *in vitro* and as such are potential anti-cancer therapeutic agents[31]. The stimulation of death receptors as anti-cancer therapy is based on the assumption that CD95 and other death receptors primarily induce apoptosis. A large proportion of human tumors acquire an inactivating mutation in p53, thereby becoming resistant to chemotherapy and radiation therapy, which both rely on p53-induced apoptosis (Ashkenazi 1999[31]). Death receptors induce apoptosis independently of the tumor suppressor p53[32]. Thus, a combination of chemo or radiation therapy with death receptor activation could enhance anti-cancer effects. However, CD95-stimulating antibodies, when injected intra-abdominally, are highly hepatotoxic[10]. Despite the dependency of this toxic effect on the FcγRIIB tail of agonistic CD95 antibodies, it argues against the use of agonistic antibodies in cancer patients[33]. More importantly, not all tumors undergo apoptosis upon CD95 stimulation. Treatment of these apoptosis-resistant tumors with CD95-activating compounds could result in activation of pro-tumorigenic signaling pathways and holds the potential danger of stimulating rather then inhibiting tumor growth[34,35] (this thesis). In short, application of agonistic death receptor antibodies or any of the death receptor ligands as death receptor anti-cancer therapy should be approached with great care.

Pro-tumorigenic affects of CD95/CD95L signaling

Evidence pointing to a role for CD95 / CD95L in the pathogenesis of cancer was provided by studies which showed a negative association between CD95L expression and prognosis in breast[36,37], ovarian[38], colorectal[39,40] and liver cancer[41]. In colorectal cancer, for example,

expression levels of CD95L are higher in the liver metastases when compared to their matched primary tumor and this is related to a poorer prognosis[39,40].
Several hypotheses about the involvement of the CD95 system in carcinogenesis were tested. First, the upregulation of expression of CD95L in tumors could create an environment of immune privilege, similar to what is observed in the testis or the eye. This would enable tumor outgrowth by elimination of activated and infiltrating CD95 expressing T lymphocytes[38,42,43]. This so-called "tumor counter attack" hypothesis was questioned when CD95L overexpressing xenografts implanted in mice resulted in attraction of neutrophils that infiltrated the tumor and displayed local tumoricidal activity leading to complete tumor eradication[44,45]. Moreover, it was shown in different tumor types that CD95L expression of the tumor led to the recruitment of pro-inflammatory cells which stimulated tumor growth by secreting tumor promoting cytokines[46-48] (this thesis).
Second, as early as 1993 it was observed that in addition to stimulating apoptosis CD95 also stimulates proliferation[49]. Since then multiple reports have published on the non-apoptotic functions of CD95 signaling. These include proliferation, survival, differentiation and invasion[34,46,50-55]. Several mechanisms could control the switch between apoptotic and non-apoptotic signaling by CD95. First, a certain threshold in the strength of the CD95 signal is required to induce apoptosis, lower levels of stimulation can lead to non-apoptotic signaling[53]. Second, CD95 signaling can be modified by extracellular signals and/or mutations in tumor cells[34,51]. Third, inactivation of the apoptotis-inducing activity of CD95 could be due to downregulation of CD95, its pro-apoptotic signaling molecules, or by upregulation of anti-apoptotic proteins such as Bcl-2 or cFLIP[50]. However, the exact mechanisms that control CD95 signaling output to apoptosis, proliferation, differentiation, invasion or survival, after CD95L binding to CD95, remain largely unclear.

CD95, CD95L, and invasion

Invasion is crucial for tumor cells to metastasize. Not only does CD95L act as a potent chemoattractant for neutrophils and other myeloid cells[56], stimulation of CD95 could also lead to a migratory and invasive phenotype of apoptosis-resistant tumor cells[34,50,52,57]. Several proteins have been suggested to be involved in CD95 mediated invasion. These proteins regulate the expression of extracellular matrix remodeling factors or the formation of cellular protrusions by rearrangement of the cytoskeleton, essential for migration. Among them are caspase-8, ERK1/2 and NF-kB activation[50], the MEK1/ERK/p35 pathway[52], PI3K activation[57] and KRAS/Raf1 signaling[34]. Most of these CD95 invasion signaling pathways seem to function independent of the death domain of the receptor. However, caspase-8 mediated CD95 induced invasion does seem to be mediated through the death domain[50]. As such it is not completely clear which signaling domains of the CD95 receptor are involved in CD95 stimulated invasion and if these signaling domains are dependent on each other in signaling invasion.

Migration, invasion, and metastasis of colorectal cancer

Colorectal cancer (CRC) is the third leading cause of cancer related death in the world, with over 600 000 deaths a year (http://globocan.iarc.fr/factsheet.asp#BOTH). The high mortality rate of CRC is primarily due to the formation of liver metastases, which arise in approximately 50-60% of all cases of CRC[58].
Metastases of primary colorectal tumors develop through a distinct sequence of biological processes that allow the tumor cell to move from the primary tumor to a distant secondary site. The primary epithelial tumor is a solid mass of cells in which the cell-cell interactions are

tight and essential for intercellular signaling[59]. In order to invade the surrounding environment the cell-cell interactions have to be disrupted. Subsequent dissemination of the migratory cells from the primary tumor can take place after degradation of the encapsulating basement membrane. When encountering blood or lymph vessels the metastasizing cell invades through the endothelial cell layer (intravasation) and enters the circulation[60]. Within the portal circulation, which drains the blood from the gut, the cell has to evade elimination by the immune system and survive shear stress when arrested in the sinusoids of the liver[60]. Next, the disseminated cells extravasate by invading the sinusoidal endothelial layer and degrading the basement membrane before being able to colonize the liver tissue[60]. Within the liver the tumor cell has to evade attacks from the local immune system and migrate to a niche favorable for colonization. Once grown into a micrometastasis the morphology of the liver metastasis often closely resembles the morphology of the primary tumor.

In order to be able to metastasize it is hypothesized that an epithelial cell, dependent on cell-cell interactions for survival, undergoes the transition to a more anchorage independent mesenchymal-like cell (epithelial to mesenchymal transition (EMT))[61]. The transformation to the mesenchymal phenotype allows migration, invasion of surrounding tissue and apoptosis resistance, all traits considered essential for metastases formation[61]. When a micrometastasis is formed in the liver the tumor cell is believed to undergo mesenchymal to epithelial transition (MET) and revert from a migratory invading phenotype back to a static, tightly packed, proliferating carcinoma cell[61].

Many mouse studies and cell culture experiments have demonstrated that carcinoma cells can acquire a mesenchymal phenotype and express mesenchymal markers[62]. These mesenchymal-like cells have been closely related to invasion and are considered to be the cells that disseminate from the primary tumor and ultimately form metastasis[59,62]. A direct causal link between EMT and metastasis has been suggested in several different tumor subtypes like breast and lung carcinomas[9,62-64]. Recently, an elegant experiment with a spontaneously metastasizing pancreatic cancer model in mice has proven that EMT is a driving and transient phenomenon of pancreatic metastasis by showing that the disseminating cell has a mesenchymal phenotype and that MET occurs when the distant organ has been colonized[65].

The reason that the role of EMT in cancer metastasis is still met with skepticism is the difficulty of demonstrating EMT in human cancer metastasis. Identification of invading mesenchymal-like cells among surrounding stroma cells in the primary tumor is problematic since most EMT markers are expressed in all epithelial or all mesenchymal cells, lacking specificity for tumor cells which obtained mesenchymal properties. However, some studies have shown EMT in human cancer metastasis. For example, partial loss of the epithelial marker E-cadherin is associated with carcinoma progression and poor prognosis in human breast cancer[66]. Also in human breast cancer, circulating tumor cells (CTCs) with a mesenchymal-like phenotype are associated with poor survival[67-69].

EMT has also been suggested to be the driving force in metastasis formation in CRC. This assumption is largely based on observational studies in which a mesenchymal morphology of cells at the invasive front is reported and pathways or proteins possibly involved in EMT have been observed in cell lines and mouse studies[70,71]. For human CRC, EMT is described as the budding of mesenchymal-like dedifferentiated cells at the invasive front of the primary tumor together with the translocation of B-catenin expression from the cell membrane to the nucleus[72]. Moreover, a correlation between an EMT-signature and prognosis in stage II and III CRC was shown by gene expression profiling[73]. Despite these reports it is still not clear if mesenchymal-like cells are more potent in forming colorectal liver metastasis, because no

actual observations are reported in human disease (*in vitro* or *in vivo*) showing that mesenchymal-like cells are more potent in forming metastases compared to epithelial-like cells.
In summary, the observational evidence of EMT in the biology of cancer is extensive but functional evidence proving EMT/MET in metastasis of human disease is still scarce.

PART II

Imaging
Most mechanistic insights into metastasis formation are derived from xenograft studies in rodents. Typically, a tumor cell line known to metastasize *in vivo* is injected at the orthotopic site and spontaneous metastases develop. Alternatively, tumor cells are injected into the bloodstream to experimentally form metastases in the first organ encountered within the microcirculation, usually the lung or liver. Techniques originally used to visualize cellular processes involved in tumor and metastasis formation (for example histochemistry, visual inspection or end-stage measurements (number of metastatic foci)) only allow for a static observation and are mainly limited to studying multi-cellular processes in micro- or macrometastases. However, the crucial seeding phases of metastasis formation depend on the dynamics of single cells.

Visualization of single cell dynamics has had a major impulse when it became possible to express fluorescent proteins in cells[74]. This allowed for studying the function of a protein of interest *in vitro* at subcellular level with high resolution laser microscopes. Moreover, rodents genetically engineered to express fluorescent proteins or cells permitted application of microscopic visualization *in vivo*, a technique which was termed intravital microscopy (IVM). IVM allows for dynamic *in vivo* imaging of tumors and metastasis at subcellular resolution and single disseminating cells can be observed for multiple days to weeks[75] (this thesis). Moreover, from a clinical perspective, the development of IVM permits real time *in vivo* studies on the cellular effect of anti-cancer drug treatment on tumor and 'healthy' cells. Furthermore, possible associated therapeutic resistance mechanisms in tumors could be visualized.
Fluorescent high-resolution IVM only permits imaging up to 1mm in depth[75]. This limits visualization to superficial tissue (i.e. skin) or to sites that have been surgically exposed (i.e. mammary fat pad). It has also been possible to image the lung, an organ subject to primary tumor growth as well as metastases formation[76,77]. However, these studies required invasive surgery to expose the organ of interest which limited the duration of IVM to a few hours and interfered with normal anatomy and physiology. The development of imaging windows which are placed on the organ or tumor of interest allowed for repetitive and long term imaging of the same animal without manipulating the organ, tumor or microenvironment. These IVM windows have made it possible to visualize the formation of new blood vessels in the tumor[78-80], tumor cell invasion and intravasation[81], and tumor cell colonization of a distant site[82]. The advances of IVM have mostly been applied to image the early steps of metastasis formation in the primary tumor. Several studies have attempted to image the dynamics of the disseminated tumor cell which arrives in the secondary organ and forms a metastasis. For example, metastasis to the lung[76], bone marrow[83], lymph nodes[84] and spleen[85] have been investigated by surgically exposing the respective organs. Sequential imaging over time, of the identical location or cells, only succeeded with the cranial imaging window, in which a coverslip is placed directly on top

of the murine brain. This made it possible to visualize colonization and dormancy of metastasizing tumor cells in the secondary organ over time[82]. The adaptation of imaging windows for use on other secondary organs (i.e. liver / lung / lymph nodes) allows visualization of the dynamics of the metastatic process in more common organs of metastasis and potentially will enable the development of additional strategies for the treatment of human cancer. Moreover, this will aid in understanding why metastases occur and survive.

OUTLINE OF THE THESIS

In part I of this thesis, the pro-tumorigenic capacities of CD95 and CD95L in colorectal cancer and liver metastasis formation are investigated.

In **chapter 2**, we present an overview of the role of CD95 in colorectal cancer. In this chapter the literature regarding both experimental (*in vitro* as well as *in vivo*) and clinical studies on CD95 in colorectal cancer is reviewed. Both the apoptotic and the non-apoptotic functions of CD95 are addressed and a model is presented in which the tumor-suppressing and tumor-promoting activities of CD95/CD95L together determine colorectal tumor behavior.

As metastasis formation is the leading cause of death in colorectal cancer patients we sought to investigate how CD95 signaling contributes to liver metastasis formation. CD95 signals invasion which is a critical property for tumor cells in order to be able to metastasize. For an epithelial cancer cell to become migratory and invasive it has to acquire a dynamic actin cytoskeleton. In **chapter 3** we describe how CD95 signals invasion through a pathway involving the platelet derived growth factor receptor (PDGFR), phospholipase C (PLC) and cofilin mediated actin remodeling.

Chapter 4 reviews the available literature concerning intracellular signaling pathways through which CD95 stimulates invasion in non-apoptotic cells. CD95-stimulated invasion is essential in inflammation, neurobiology and tumor biology. In this review we postulate that CD95 signals invasion by stimulating the production of extra-cellular matrix-degrading proteases and by stimulating the formation of actin-driven cell protrusions.

In **chapter 3** we identified the PDGFR as a critical component of CD95-stimulated invasion. In **chapter 6**, we set out to asses the role of PDGFRB in metastatic colorectal cancer. We show that epithelial-to-mesenchymal transition leads to PDGFR expression on the primary epithelial colorectal tumor cell and that platelets bind to tumor cells in the circulation. Activation of these platelets in the liver sinusoids leads to PDGF excretion and more efficient metastasis formation.

In part II of this thesis better understanding of the dynamic processes involved in colorectal liver metastasis formation is obtained by visualization of these processes. Potentially, this could lead to new targets for interfering in metastasis formation. Part II of this thesis investigates colorectal tumor cell colonization of the liver by intravital imaging through a newly developed abdominal imaging window.

From experimental imaging studies of the primary tumor it is known that invasion plays a crucial role in the initial steps of dissemination. However, it is unclear what exactly happens when the

disseminated tumor cell arrives in the secondary organ and forms a metastasis. In **chapter 7** we developed an imaging window that allowed for long term and sequential imaging of single colorectal tumor cells in the liver. Here we studied the rate-limiting steps in metastasis formation in the first few days after arrival of the disseminated tumor cell in the liver. Furthermore, it is investigated how drug-treatment can reduce colonization capacity.

In **chapter 8** a protocol for using the newly developed abdominal imaging window is presented which discusses the design of the window and the surgical procedures needed for implantation in detail.

REFERENCE LIST

1. Houston, A et al. The Fas signaling pathway and its role in the pathogenesis of cancer. Curr.Opin.Pharmacol. 4, 321-326. 2004.
2. O' Reilly, LA et al. Membrane-bound Fas ligand only is essential for Fas-induced apoptosis. Nature 461, 659-663. 2009.
3. Hotchkiss, RS et al. Cell death. N.Engl.J.Med. 361, 1570-1583. 2009.
4. Thornberry, NA et al. Caspases: enemies within. Science 281, 1312-1316. 1998.
5. Lavrik, I et al. Death receptor signaling. J.Cell Sci. 118, 265-267. 2005.
6. Peter, ME et al. Does CD95 have tumor promoting activities?. Biochim.Biophys.Acta 1755, 25-36. 2005.
7. Yonehara, S et al. A cell-killing monoclonal antibody (anti-Fas) to a cell surface antigen co-downregulated with the receptor of tumor necrosis factor. J.Exp.Med. 169, 1747-1756. 1989.
8. Trauth, BC et al. Monoclonal antibody-mediated tumor regression by induction of apoptosis. Science 245, 301-305. 1989.
9. Oft, M et al. TGFbeta signaling is necessary for carcinoma cell invasiveness and metastasis. Curr. Biol. 8, 1243-1252. 1998.
10. Ogasawara, J et al. Lethal effect of the anti-Fas antibody in mice. Nature 364, 806-809. 1993.
11. Suda, T et al. Molecular cloning and expression of the Fas ligand, a novel member of the tumor necrosis factor family. Cell 75, 1169-1178. 1993.
12. Rouvier, E et al. Fas involvement in Ca(2+)-independent T cell-mediated cytotoxicity. J.Exp.Med. 177, 195-200. 1993.
13. Watanabe, T et al. A molecular genetic linkage map of mouse chromosome 19, including the lpr, Ly-44, and Tdt genes. Biochem.Genet. 29, 325-335. 1991.
14. Watanabe-Fukunaga, R et al. Lymphoproliferation disorder in mice explained by defects in Fas antigen that mediates apoptosis. Nature 356, 314-317. 1992.
15. Takahashi, T et al. Generalized lymphoproliferative disease in mice, caused by a point mutation in the Fas ligand. Cell 76, 969-976. 1994.
16. Cohen, PL et al. *Lpr* and gld: single gene models of systemic autoimmunity and lymphoproliferative disease. Annu.Rev.Immunol. 9, 243-269. 1991.
17. Sneller, MC et al. A novel lymphoproliferative/autoimmune syndrome resembling murine lpr/gld disease. J.Clin.Invest 90, 334-341. 1992.
18. Rieux-Laucat, F et al. Mutations in Fas associated with human lymphoproliferative syndrome and autoimmunity. Science 268, 1347-1349. 1995.
19. Tanaka, M et al. Expression of the functional soluble form of human fas ligand in activated lymphocytes. EMBO J. 14, 1129-1135. 1995.
20. Kayagaki, N et al. Metalloproteinase-mediated release of human Fas ligand. J.Exp.Med. 182, 1777-1783. 1995.
21. Suda, T et al. Membrane Fas ligand kills human peripheral blood T lymphocytes, and soluble Fas ligand blocks the killing. J.Exp.Med. 186, 2045-2050. 1997.
22. Tauzin, S et al. The naturally processed CD95L elicits a c-yes/calcium/PI3K-driven cell migration pathway. PLoS.Biol. 9, e1001090. 2011.
23. French, LE et al. Fas and Fas ligand in embryos and adult mice: ligand expression in several immune-privileged tissues and coexpression in adult tissues characterized by apoptotic cell turnover. J.Cell Biol. 133, 335-343. 1996.
24. Leithauser, F et al. Constitutive and induced expression of APO-1, a new member of the nerve growth factor/tumor necrosis factor receptor superfamily, in normal and neoplastic cells. Lab Invest 69, 415-429. 1993.
25. Green, DR et al. The role of Fas ligand in immune privilege. Nat.Rev.Mol.Cell Biol. 2, 917-924. 2001.
26. Debatin, KM et al. Death receptors in chemotherapy and cancer. Oncogene 23, 2950-2966. 2004.
27. Moller, P et al. Expression of APO-1 (CD95), a member of the NGF/TNF receptor superfamily, in normal and neoplastic colon epithelium. Int.J.Cancer 57, 371-377. 1994.
28. Timmer, T et al. Fas receptor-mediated apoptosis: a clinical application?. J.Pathol. 196, 125-134. 2002.
29. Bennett, MW et al. Fas ligand upregulation is an early event in colonic carcinogenesis. J.Clin.Pathol. 54, 598-604. 2001.
30. Peduto, EL et al. Fas and Fas ligand expression in tumor cells and in vascular smooth-muscle cells of colonic and renal carcinomas. Int.J.Cancer 81, 772-778. 1999.
31. Ashkenazi, A et al. Apoptosis control by death and decoy receptors. Curr.Opin.Cell Biol. 11, 255-260. 1999.
32. Levine, AJ. p53, the cellular gatekeeper for growth and division. Cell 88, 323-331. 1997.
33. Xu, Y et al. Fc gamma Rs modulate cytotoxicity of anti-Fas antibodies: implications for agonistic antibody-based therapeutics. J.Immunol. 171, 562-568. 2003.
34. Hoogwater, FJ et al. Oncogenic K-Ras turns death receptors into metastasis-promoting receptors in human and mouse colorectal cancer cells. Gastroenterology 138, 2357-2367. 2010.
35. Peter, ME et al. The CD95 receptor: apoptosis revisited. Cell 129, 447-450. 2007.
36. Mottolese, M et al. Prognostic relevance of altered Fas (CD95)-system in human breast cancer. Int.J.Cancer 89, 127-132. 2000.
37. Reimer, T et al. FasL:Fas ratio--a prognostic factor in breast carcinomas. Cancer Res. 60, 822-828. 2000.
38. Munakata, S et al. Expressions of Fas ligand and other apoptosis-related genes and their prognostic significance in epithelial ovarian neoplasms. Br.J.Cancer 82, 1446-1452. 2000.
39. Mann, B et al. FasL is more frequently expressed in liver metastases of colorectal cancer than in matched primary carcinomas. Br.J.Cancer 79, 1262-1269. 1999.

40. Nozoe, T et al. Fas ligand expression is correlated with metastasis in colorectal carcinoma. Oncology 65, 83-88. 2003.
41. Ito, Y et al. The status of Fas and Fas ligand expression can predict recurrence of hepatocellular carcinoma. Br.J.Cancer 82, 1211-1217. 2000.
42. Bennett, MW et al. The Fas counterattack *in vivo*: apoptotic depletion of tumor-infiltrating lymphocytes associated with Fas ligand expression by human esophageal carcinoma. J.Immunol. 160, 5669-5675. 1998.
43. Houston, A et al. Fas ligand expressed in colon cancer is not associated with increased apoptosis of tumor cells *in vivo*. Int.J.Cancer 107, 209-214. 2003.
44. Arai, H et al. Gene transfer of Fas ligand induces tumor regression *in vivo*. Proc.Natl.Acad.Sci.U.S.A 94, 13862-13867. 1997.
45. Seino, K et al. Antitumor effect of locally produced CD95 ligand. Nat.Med. 3, 165-170. 1997.
46. Chen, JJ et al. Regulation of the proinflammatory effects of Fas ligand (CD95L). Science 282, 1714-1717. 1998.
47. Matsumoto, N et al. Caspase-8- and JNK-dependent AP-1 activation is required for Fas ligand-induced IL-8 production. FEBS J. 274, 2376-2384. 2007.
48. Park, DR et al. Fas (CD95) induces proinflammatory cytokine responses by human monocytes and monocyte-derived macrophages. J.Immunol. 170, 6209-6216. 2003.
49. Alderson, MR et al. Fas transduces activation signals in normal human T lymphocytes. J.Exp.Med. 178, 2231-2235. 1993.
50. Barnhart, BC et al. CD95 ligand induces motility and invasiveness of apoptosis-resistant tumor cells. EMBO J. 23, 3175-3185. 2004.
51. Desbarats, J et al. Fas engagement accelerates liver regeneration after partial hepatectomy. Nat.Med. 6, 920-923. 2000.
52. Desbarats, J et al. Fas engagement induces neurite growth through ERK activation and p35 upregulation. Nat.Cell Biol. 5, 118-125. 2003.
53. Legembre, P et al. Induction of apoptosis and activation of NF-kappaB by CD95 require different signaling thresholds. EMBO Rep. 5, 1084-1089. 2004.
54. Sun, M et al. The cytoplasmic domain of Fas ligand costimulates TCR signals. J.Immunol. 177, 1481-1491. 2006.
55. Zuliani, C et al. Control of neuronal branching by the death receptor CD95 (Fas/Apo-1). Cell Death. Differ. 13, 31-40. 2006.
56. Seino, K et al. Chemotactic activity of soluble Fas ligand against phagocytes. J.Immunol. 161, 4484-4488. 1998.
57. Kleber, S et al. Yes and PI3K bind CD95 to signal invasion of glioblastoma. Cancer Cell 13, 235-248. 2008.
58. Welch, JP et al. The clinical correlation of an autopsy study of recurrent colorectal cancer. Ann. Surg. 189, 496-502. 1979.
59. Kalluri, R. EMT: when epithelial cells decide to become mesenchymal-like cells. J.Clin.Invest 119, 1417-1419. 2009.
60. Steeg, PS. Tumor metastasis: mechanistic insights and clinical challenges. Nat.Med. 12, 895-904. 2006.
61. Hanahan, D et al. Hallmarks of cancer: the next generation. Cell 144, 646-674. 2011.
62. Yang, J et al. Epithelial-mesenchymal transition: at the crossroads of development and tumor metastasis. Dev.Cell 14, 818-829. 2008.
63. Siegel, PM et al. Cytostatic and apoptotic actions of TGF-beta in homeostasis and cancer. Nat.Rev. Cancer 3, 807-821. 2003.
64. Thomson, S et al. Kinase switching in mesenchymal-like non-small cell lung cancer lines contributes to EGFR inhibitor resistance through pathway redundancy. Clin.Exp.Metastasis 25, 843-854. 2008.
65. Rhim, AD et al. EMT and dissemination precede pancreatic tumor formation. Cell 148, 349-361. 2012.
66. Vincent-Salomon, A et al. Host microenvironment in breast cancer development: epithelial-mesenchymal transition in breast cancer development. Breast Cancer Res. 5, 101-106. 2003.
67. Cristofanilli, M et al. Circulating tumor cells: a novel prognostic factor for newly diagnosed metastatic breast cancer. J.Clin.Oncol. 23, 1420-1430. 2005.
68. Gradilone, A et al. Circulating tumour cells lacking cytokeratin in breast cancer: the importance of being mesenchymal. J.Cell Mol.Med. 15, 1066-1070. 2011.
69. Raimondi, C et al. Epithelial-mesenchymal transition and stemness features in circulating tumor cells from breast cancer patients. Breast Cancer Res.Treat. 130, 449-455. 2011.
70. Bates, RC et al. The epithelial-mesenchymal transition (EMT) and colorectal cancer progression. Cancer Biol.Ther. 4, 365-370. 2005.
71. Brabletz, T et al. Invasion and metastasis in colorectal cancer: epithelial-mesenchymal transition, mesenchymal-epithelial transition, stem cells and beta-catenin. Cells Tissues.Organs 179, 56-65. 2005.
72. Brabletz, T et al. Variable beta-catenin expression in colorectal cancers indicates tumor progression driven by the tumor environment. Proc.Natl.Acad. Sci.U.S.A 98, 10356-10361. 2001.
73. Loboda, A et al. EMT is the dominant program in human colon cancer. BMC.Med.Genomics 4, 9. 2011.
74. Beerling, E et al. Intravital microscopy: new insights into metastasis of tumors. J.Cell Sci. 124, 299-310. 2011.
75. Zomer, A et al. Real-time intravital imaging of cancer models. Clin.Transl.Oncol. 13, 848-854. 2011.
76. Kimura, H et al. Real-time imaging of single cancer-cell dynamics of lung metastasis. J.Cell Biochem. 109, 58-64. 2010.

77. Kreisel, D et al. *In vivo* two-photon imaging reveals monocyte-dependent neutrophil extravasation during pulmonary inflammation. Proc.Natl.Acad. Sci.U.S.A 107, 18073-18078. 2010.
78. Abdul-Karim, MA et al. Automated tracing and change analysis of angiogenic vasculature from *in vivo* multiphoton confocal image time series. Microvasc.Res. 66, 113-125. 2003.
79. Farhadi, MR et al. Combined inhibition of vascular endothelial growth factor and platelet-derived growth factor signaling: effects on the angiogenesis, microcirculation, and growth of orthotopic malignant gliomas. J.Neurosurg. 102, 363-370. 2005.
80. Fukumura, D et al. Tumor microvasculature and microenvironment: novel insights through intravital imaging in pre-clinical models. Microcirculation. 17, 206-225. 2010.
81. Kedrin, D et al. Intravital imaging of metastatic behavior through a mammary imaging window. Nat.Methods 5, 1019-1021. 2008.
82. Kienast, Y et al. Real-time imaging reveals the single steps of brain metastasis formation. Nat.Med. 16, 116-122. 2010.
83. Sipkins, DA et al. *In vivo* imaging of specialized bone marrow endothelial microdomains for tumour engraftment. Nature 435, 969-973. 2005.
84. Mempel, TR et al. T-cell priming by dendritic cells in lymph nodes occurs in three distinct phases. Nature 427, 154-159. 2004.
85. Grayson, MH et al. Confocal fluorescent intravital microscopy of the murine spleen. J.Immunol. Methods 256, 55-63. 2001.

PART I | CD95 AND COLORECTAL CANCER

CHAPTER 2

2

CD95 signaling in colorectal cancer

Biochimica Biophysica Acta. 2012 Aug;1826(1):189-98

Frederik J.H. Hoogwater*, Ernst J.A Steller*, B. Florien Westendorp,
Inne H.M. Borel Rinkes and Onno Kranenburg

* *Equal contribution*

Department of Surgery, University Medical Center Utrecht, The Netherlands

ABSTRACT

CD95 and its ligand (CD95L) are widely expressed in colorectal tumors, but their role in shaping tumor behaviour is unclear. CD95 activation on tumor cells can lead to apoptosis, while CD95L attracts neutrophils, suggesting a function in tumor suppression. However, CD95 can also promote tumorigenesis, at least in part by activating non-apoptotic signaling pathways that stimulate tumor cell proliferation, invasion and survival. In addition, CD95 signaling in stromal cells and tumor-infiltrating inflammatory cells has to be taken into account when addressing the function of CD95 and its ligand in colorectal tumor biology. We present a model in which the tumor-suppressing and tumor-promoting activities of CD95/CD95L together determine colorectal tumor behaviour. We also discuss how these multiple activities are changing our view of CD95 and CD95L as potential therapeutic targets in the treatment of colorectal cancer. We conclude that locking CD95 in apoptosis-mode may be a more promising anti-cancer strategy than simply inhibiting or stimulating CD95.

INTRODUCTION

The 'death receptor' CD95 and its ligand (CD95L) are frequently expressed in colorectal tumors. In many cell types, CD95 activation results in programmed cell death (apoptosis). The CD95 system may therefore suppress tumor development by promoting tumor cell apoptosis. However, many colorectal tumors express CD95 and CD95L without dying and recent data suggest that their function in colorectal cancer is not limited to stimulating tumor cell apoptosis. At least two levels of complexity need to be considered. First, CD95 can activate alternative – non-apoptotic – signaling pathways that promote tumor cell proliferation, migration, invasion, and even survival. Second, multiple cell types within a tumor may express CD95. Depending on their response to CD95 stimulation these cell types may either positively or negatively influence tumor development.

Here we review the literature describing a role for CD95 and CD95L in colorectal cancer. We discuss the relationship between expression levels, tumor behaviour, and clinical outcome. In addition, we provide an overview of the diversity of CD95 signaling modes in tumor and non-tumor cells and discuss how CD95 signaling output is controlled. We present a model in which the tumor-suppressing and tumor-promoting activities of CD95/CD95L together determine tumor behaviour. Finally, we discuss how these multiple activities are changing our view of CD95 and CD95L as potential therapeutic targets in the treatment of colorectal cancer.

EXPRESSION AND FUNCTION OF CD95 AND CD95 LIGAND (CD95L)

In the normal intestine

CD95 is expressed in a large variety of tissues, including the intestinal tract[1,2]. Along the intestinal tract, CD95 is uniformly expressed at the basolateral side of all epithelial cells[2,3]. By contrast, CD95L is mainly expressed on lymphoid cells including T, B, and NK cells [4-8] and on myeloid cells, such as activated neutrophils[9]. Epithelial cells of the intestinal tract do not express CD95L, except for the differentiated Paneth cells which reside at the bottom of the crypts in the small intestine[10]. In the colon, Paneth cells are scarce, and expression of CD95L is restricted to a few lamina propria cells [10] (Figure 1). The exclusive expression of CD95L in Paneth cells is intriguing, as these cells are flanked by intestinal stem cells and provide essential signals for stem cell maintenance[11]. However, it is not likely that CD95L itself would represent such a stem cell maintenance signal, as mice lacking CD95L do not display gross intestinal abnormalities. Intestinal stem cells generate a population of proliferating transit-amplifying cells, which migrate up along the crypt-villus axis and differentiate into specialized cell types. These are eventually eliminated by apoptosis at the luminal surface[12]. Regardless of their position along the crypt-villus axis, epithelial cells are equally sensitive to CD95L-induced apoptosis[13]. Furthermore, mice lacking functional CD95 or CD95L display normal intestinal morphology and apoptotic cell count[13]. The function of CD95 and CD95L in epithelial cells of the normal colon is therefore still obscure.

During inflammatory bowel disease (IBD) and IBD-associated carcinogenesis

Under conditions of chronic intestinal inflammation (inflammatory bowel disease; IBD) the number of apoptotic epithelial cells increases dramatically[14,15]. In IBD, the intestinal tissue is infiltrated by T cells expressing high levels of CD95L[16]. Furthermore, CD95L-neutralizing antibodies ameliorate disease parameters[17]. This suggests that CD95 signaling is implicated in

IBD, possibly by promoting T cell CD95L-mediated apoptosis in intestinal epithelial cells. IBD can be modelled in mice by exposing them to dextran sodium sulphate (DSS). To assess the contribution of CD95 and CD95L to IBD, several studies have made use of mice lacking either functional CD95L (*gld*/*gld*; generalized lymphoproliferative disease[18,19]) or CD95 (*lpr*/*lpr*; lymphoproliferation[18,19]). CD95L-deficiency reduced the infiltration of neutrophils into the colon following DSS exposure and attenuated IBD[20,21]. By contrast, selective loss of CD95 in the intestinal epithelial cell compartment resulted in increased destruction of epithelial cells and in severely reduced tissue regeneration[22]. Thus, during colitis, epithelial CD95 unexpectedly promotes epithelial cell survival and tissue repair, rather than apoptosis and tissue destruction[21]. In line with these mouse studies, human colonocytes from IBD patients are markedly resistant to CD95-induced apoptosis[23]. Taken together, CD95L may play a role in the homing and/or activation of tissue-damaging inflammatory cells during IBD, but apoptosis of epithelial cells is not mediated by CD95 (Figure 2).

It may have been expected that CD95-deficient mice, displaying aggravated IBD, would be more prone to colorectal tumor development. However, IBD-associated tumor development was not significantly different between CD95-proficient and -deficient mice. Possibly, this could be due to the loss of pro-tumorigenic CD95 signaling in epithelial cells neutralizing the pro-tumorigenic effect of excessive IBD (see below)[21].

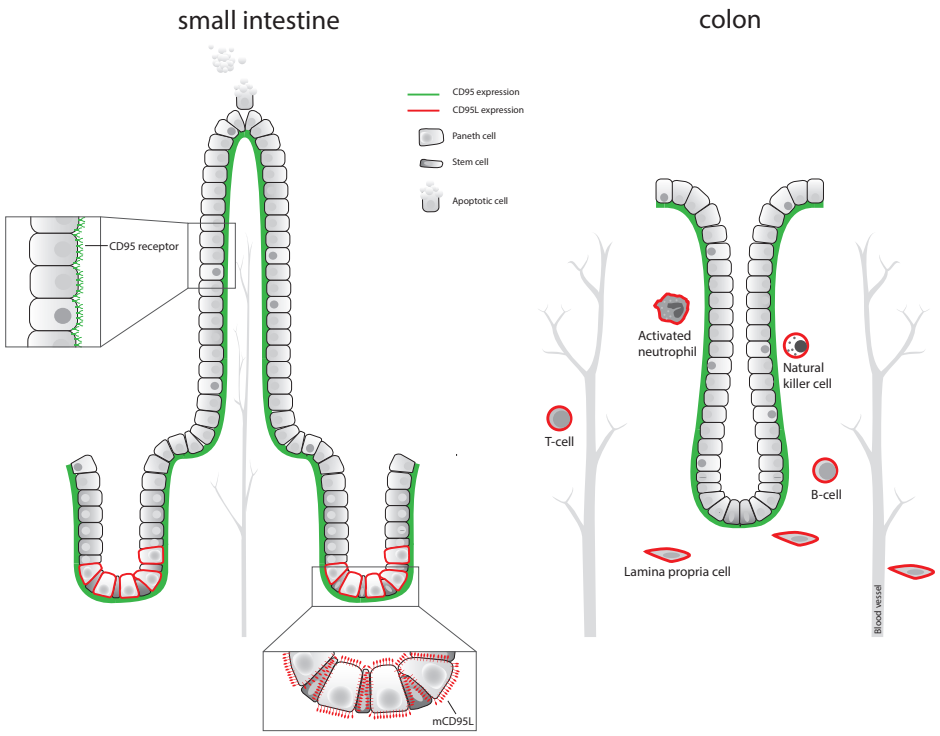

Figure 1. Expression of CD95 and CD95-ligand in the small intestine and the colon. Along the intestinal tract CD95 is ubiquitously expressed in all epithelial cells. CD95-ligand however, is expressed exclusively in the Paneth cells of the small intestine. In the colon, Paneth cells are scarce, and CD95-ligand is only expressed in occasional lamina propria cells, B cells, plasma cells, NK cells and/or neutrophils.

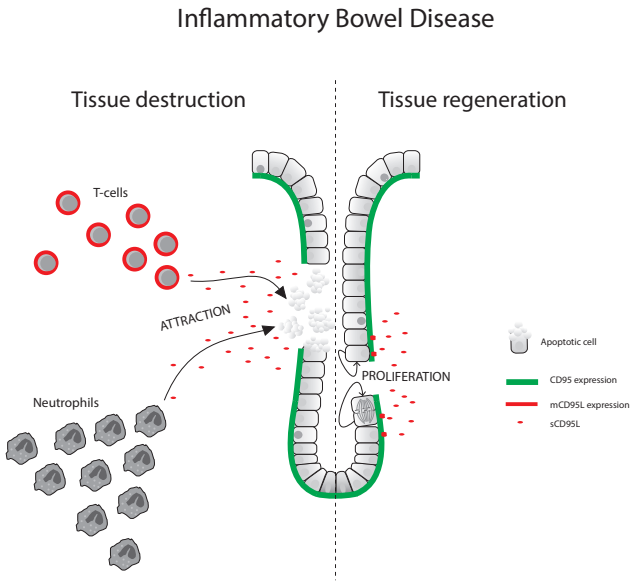

Figure 2. The two faces of CD95/CD95L in inflammatory bowel disease. CD95L causes attraction of neutrophils and T cells that mediate tissue destruction. Attraction of these cell types may either be due to direct secretion of soluble CD95L itself, or indirectly to CD95L-stimulated production of inflammatory cytokines. The destruction process itself is not primarily mediated by CD95, as IBD epithelium is relatively resistant to CD95L-induced apoptosis. Rather CD95 acts as a stimulator of tissue regeneration, presumably by stimulating proliferation of the regenerating epithelium.

During colorectal cancer development

Immunohistochemistry studies have shown that the expression of CD95 is diminished in a subpopulation of colorectal tumors[3,24], and that low expression of CD95 in the primary tumor predicts metastatic tumor recurrence[25]. Nevertheless, low levels of CD95 are maintained in most colorectal tumors[26,27] and this may be sufficient to activate pro-tumorigenic signaling pathways. Furthermore, inactivating mutations such as those found in Autoimmune Lymphoproliferative Syndrome (ALPS) have not been detected in colorectal tumors[28]. Presumably, this is due to the fact that CD95 is not primarily an apoptosis inducer in colonic epithelial cells *in vivo* (see above). For instance, survival signaling by CD95 requires far lower thresholds of receptor stimulation than those required to induce apoptosis[29,30]. Therefore, low level expression of CD95 in colorectal tumors does not imply that the receptor is inactive.

The expression of CD95L is gradually increased during progression from (early) adenoma to colorectal carcinoma and metastasis[31-33]. CD95 and CD95L are co-expressed in the majority of adenomas and carcinomas but this does not result in apoptosis[27,31]. In fact, high levels of CD95L are associated with poor prognosis[34,35]. These findings suggest that autocrine non-apoptotic CD95 signaling may be a general phenomenon in neoplastic colorectal lesions, starting early during tumor development.

CD95 AS A SUPPRESSOR OF COLORECTAL TUMOR GROWTH AND METASTASIS FORMATION

Stimulation of tumor cell apoptosis

Several studies suggest that the progression and metastatic spread of apoptosis-sensitive tumors may be negatively controlled by the CD95/CD95L system[25,36-41], although none of these studies focused on (models of) colorectal cancer. CD95L (and TRAIL) can trigger apoptosis in a variety of colorectal tumor cell lines[42-47]. However, the tumor cell response to CD95L or CD95-activating antibodies added *in vitro* may not adequately reflect how CD95 signals in the context of tumor tissue. CD95 is frequently downregulated in colorectal tumors which may contribute to apoptosis resistance. Whether CD95 is an efficient apoptosis inducer in tumors that retain CD95 is unclear, but most colorectal tumors express both CD95 and CD95 ligand without dying spontaneously (see above).

Interestingly, CD95 is a p53 target gene and may therefore contribute to apoptosis under conditions in which p53 is activated, for instance in response to chemotherapy[38,48]. Indeed, increased expression of CD95 by chemotherapeutics like 5FU contributes to apoptosis of colorectal cancer cell lines *in vitro*[49]. In line with this, treatment of colorectal cancer patients with 5FU increased tumor cell apoptosis and concomitant upregulation of CD95[50]. It is presently unknown whether the induction of CD95 by chemotherapy is related to *TP53* mutation status, and/or to response rates and clinical outcome in colorectal cancer patients. Alternatively, upregulation of CD95 may help cells recover from 5-FU-induced injury (see below).

Recruitment of tumoricidal neutrophils by CD95L

CD95L is a potent chemoattractant and activation signal for neutrophils *in vitro* and *in vivo*[9,51-54]. Overexpression of CD95L in colorectal tumor xenografts in mice results in attraction of neutrophils that infiltrate the tumor and display local tumoricidal activity which can even lead to complete tumor eradication[55-58]. In the APC^{min} model, ubiquitous loss of functional CD95L in the *gld* background promotes polyp formation and this is associated with a reduced influx of neutrophils (not lymphoid cells), rather than with tumor cell apoptosis[20]. Loss of functional CD95 in the *lpr* background also promotes Apc-loss-driven polyp formation, but this was associated with an increased influx of lymphoid cells (not neutrophils) and increased signaling through the Akt survival pathway[59]. The striking differences between these two models highlight the complexity of CD95/CD95L biology in shaping intestinal tumor development. A common theme in all studies using GEM models for intestinal tumor development is that the CD95/CD95L system appears to be a critical regulator of the inflammatory component of these lesions, but not a prominent inducer of tumor cell apoptosis. It is presently unknown how CD95L-dependent neutrophil infiltration in human colorectal tumors affects their development and/or metastatic potential.

Stimulation of anti-tumor immunity

Neutrophils attracted by CD95L may impair tumor growth not only through direct cytotoxic effects, but also by promoting the development of $CD8^+$ T cell-dependent antitumor immunity[56-58,60]. Activation of CD95 on dendritic cells induces their maturation and promotes the secretion of chemokines and cytokines that attract neutrophils and T cells[61-64]. In addition, CD95 expressed on $CD4^+$ helper T cells is critical for generating cytotoxic T lymphocyte (CTL) responses[65]. Conversely, immunosuppressive regulatory T cells (Treg) express CD95 acting as an apoptosis inducer[66,67]. These functions of CD95 could help boost T cell responses against

CD95L-expressing tumor cells. Although none of the above studies focussed on colorectal cancer, studies in human colon cancer biopsies have shown that infiltration of primary tumors by memory and cytotoxic T cells is associated with reduced metastatic spread and a better prognosis[68]. This suggests that tumor progression and metastasis formation is suppressed by the adaptive immune system, in which CD95 plays a central role.

CD95 AS A STIMULATOR OF COLORECTAL TUMOR GROWTH AND METASTASIS FORMATION

Apoptosis in tumor infiltrating lymphocytes (TIL) – "counterattack"

Activated T cells are highly sensitive to cell death induced by CD95L, which is important for T cell contraction following a normal T cell response. It has been proposed that CD95L-expressing tumors can kill tumor-infiltrating activated T cells in a CD95-dependent manner[33,69-72]. This has been referred to as the tumor "counterattack". However, the relevance of the CD95L-mediated counterattack *in vivo* is debated[73]. This is primarily based on results showing that over-expressed CD95L in tumor cells caused tumor rejection and development of anti-tumor immunity, rather than tolerance through induction of T cell apoptosis[53,58,74].

Apoptosis in hepatocytes

Injection of CD95-activating antibodies into mice causes severe hepatitis due to massive hepatocyte apoptosis[75,76]. CD95 also mediates hepatocyte apoptosis induced by concanavalin-A and acetaminophen[77,78]. Colorectal liver metastases express high levels of CD95L and may therefore induce apoptosis in nearby hepatocytes[32,79]. Indeed, apoptotic hepatocytes are frequently detected at the margin of colorectal liver metastases. CD95 expression in hepatocytes allows them to be killed by CD95L-expressing tumor infiltrating lymphocytes and/or tumor cells. A direct consequence of hepatocyte killing by invasive tumor cells could be that tumor invasion into the surrounding liver tissue is facilitated[79]. By simultaneously promoting hepatocyte apoptosis and tumor cell invasion (see below) CD95L may play an important role in facilitating metastasis outgrowth in the liver.

Attraction of pro-tumorigenic inflammatory cells

CD95 ligand is a potent inducer of inflammation by stimulating the expression and release of inflammatory factors such as interleukin 1β, interleukin 8, MCP1 (monocyte chemotactic protein-1), IP10 (interferon-gamma-induced protein 10), MIG (monokine induced interferon-gamma), keratinocyte-derived chemokine, MIP1α and 1β and MIP2 (macrophage inflammatory protein 2) from hepatocytes, monocytes and monocyte-derived macrophages[79-84]. These inflammatory cytokines and chemokines in turn promote influx and activation of neutrophils, which can subsequently promote tumor rejection[53,58,81-83]. However, influx of inflammatory cells into tumors can also generate a pro-tumorigenic microenvironment characterized by high levels of growth factors, pro-angiogenic factors and metalloproteases[85,86]. Indeed, chronically inflamed tissue is a pre-condition for tumor development in several organs, including the liver and the intestines[22,87]. Importantly, anti-CD95L antibodies or CD95-deficiency prevented inflammation-induced hepatocarcinogenesis, which demonstrates the pro-tumorigenic power of the CD95/CD95L system[88,89].

Non-apoptotic signaling; Lessons from other cell types

Many colorectal tumor cell lines display intrinsic resistance to apoptosis induced by CD95 and/or TRAIL-receptors[45,90]. Malignant transformation of intestinal epithelial cells may reduce their sensitivity to CD95L-induced apoptosis. Apoptosis is only one of a variety of potential outcomes of CD95 activation on tumor cells. Alternative outcomes include proliferation, invasion and cell survival[91-93].

Proliferation

In a recent landmark study it was shown that CD95 signaling is required for the maintenance of cell proliferation in tumor cell lines of diverse origin and for the initiation of liver tumors and endometroid tumors driven by oncogenic Kras88. The proliferation-stimulating capacity of CD95 was first demonstrated in a study showing that CD95 engagement accelerated liver regeneration after partial hepatectomy[94]. Cancer cells and hepatocytes in the regenerating liver require CD95 to activate Jun kinase (JNK) to drive cell proliferation[88,94]. In addition, CD95 ligand generates proliferation-stimulating and anti-apoptotic signals in quiescent hepatic stellate cells[95].

Invasion

The capacity of tumor cells to invade surrounding tissue and break through basement membranes is essential for dissemination and metastasis formation. CD95 can stimulate tumor cell migration and invasion (reviewed in[93]). CD95-stimulated invasion may be especially relevant under conditions of hypoxia[96]. Hypoxia has been associated with a more aggressive tumor phenotype. Recent data have shown that autocrine CD95 signaling contributes to hypoxia-induced colorectal tumor cell invasion and outgrowth of liver metastases[96].

In glioma cells, CD95 stimulates invasion by activating a tyrosine kinase pathway leading to activation of PI(3) kinase and, ultimately, expression of the matrix-degrading metalloproteases MMP2 and MMP9[85]. Furthermore, in a panel of apoptosis-resistant tumor cell lines derived from colon-, breast-, ovarian-, lung carcinoma and melanoma, CD95 signals migration via caspase-8 and ERK activation and expression of the serine protease uPA which is involved in remodelling fibrin-containing extracellular matrices[97].

Our own data show that CD95 activates the actin-severing protein cofilin to stimulate immediate actin remodelling and subsequent formation of cell protrusions in colorectal cancer cells[98,99]. Interestingly, also in these cells invasion signaling by CD95 was dependent on the activation of a tyrosine kinase, although in this case it was the PDGFR. Stimulation of CD95 causes PDGFR-mediated activation of phospholipase Cγ1 (PLCγ1) to induce plasma membrane PIP_2 hydrolysis[98]. This causes local cofilin activation which initiates actin remodelling[98]. Actin-driven formation of cell protrusions is considered to be essential for invasion and metastasis formation. Interestingly, during embryonic neural development and in adult neural progenitor cells, CD95 is constitutively expressed and promotes the branching and outgrowth of neurites rather than apoptosis[100-102]. The molecular mechanisms driving neurite outgrowth share many features with the mechanisms driving (tumor) cell migration. Both processes are orchestrated by the coordinated activation and inactivation of the Rho family GTPases RhoA, Rac and CDC42[103]. Both Rac and CDC42 can be activated by CD95[101,104]. Moreover, Rac activation plays an essential role during CD95-dependent stimulation of neurite outgrowth[101]. Whether Rac activation by CD95 also requires tyrosine kinase activity remains to be determined. Nevertheless, the capacity of CD95 to activate both Rac and the cofilin pathway strongly suggests that this 'death receptor' regulates core components of the machinery controlling cortical actin dynamics.

It thus appears that CD95 can have an impact on the invasive phenotype of tumor cells at

multiple levels. Which of these signals is/are the predominant force in CD95-stimulated invasion is likely to be cell type-specific.

Survival

One of the first non-apoptotic pathways that was found to be activated by CD95 is one that leads to the activation of the transcription factor NFκB[105-107]. NFκB activation in colorectal tumor cells is generally considered to be a survival signal which is required for colorectal tumor formation and tumor maintenance[87,108-110]. Hence, CD95 may primarily promote colorectal tumor cell survival by activating the NFκB pathway. A recent study identified CD95 and CD95-induced NFκB signaling as an essential survival pathway in lung cancer cells treated with EGFR inhibitors[111]. In addition, CD95 is required for survival and differentiation of adult neural stem cells[112].

DETERMINANTS OF CD95 SIGNALING OUTPUT

The fact that CD95 is more than just a death receptor and can have pleiotropic effects on (colorectal) tumor cell behaviour is now well established. Moreover, these non-apoptotic signal transduction pathways are beginning to be elucidated. Much less is known about the signals that determine how tumor cells will react to CD95 activation.

Modification and Localization of CD95

Palmitoylation (the covalent binding of fatty acids to cysteine residues of membrane proteins) of CD95 on the membrane-proximal residue Cys 199 directs it into membrane subdomains that are characterized by high glycolipid content[113,114]. Such subdomains are frequently referred to as 'rafts'. Interestingly, CD95 localization to lipid rafts is not only determined by its palmitoylation, but also by an extracellular domain that directly interacts with the glycosphingolipids that are enriched in the rafts[115]. Localization of CD95 to rafts is essential for efficient stimulation of apoptosis[113,116,117]. Palmitoylation of CD95 also promotes clustering of CD95 into high molecular weight complexes that recruit and activate caspase-8[114]. Indeed, caspase-8 activation occurs primarily in raft-like membrane subdomains[118]. In contrast, CD95 clustering and raft localization are not required for the activation of ERK and NFκB[97,115,119]. Furthermore, mutation of the glycosphingolipid interaction motif disables apoptosis signaling but promotes non-apoptotic signaling and this is associated with altered trafficking and internalization of activated CD95[115]. In addition, phosphatidylinositol 3'-kinase blocks CD95 aggregation and caspase-8 cleavage at the DISC by modulating lateral diffusion of the receptor[120]. Finally, apoptosis-inducing CD95 in colorectal cancer cells is internalized and degraded, but invasion-stimulating CD95 is localized to the invasive front and resistant to degradation[121]. Together, these studies suggest that the localization of CD95 to specific membrane subdomains may specify both its trafficking and its signaling output upon receptor stimulation.

cFLIP

Activation of caspase-8 and 10 in the DISC is limited by FLICE-inhibitory protein (cFLIP)[122,123]. cFLIP blocks caspase-8 activation in the DISC by occupying the caspase-8-binding site on the adaptor molecule FADD that is bound to the CD95/CD95L complex. In human colon cancer cells the long variant of FLIP ($FLIP_L$) plays a critical role in establishing apoptosis resistance[124].

In addition to inhibiting caspase-8 processing, cFLIPL also promotes CD95-stimulated activation of NFκB and ERK[125]. FLIP therefore acts as a determinant of CD95 signaling output rather than as a simple apoptosis-suppressor.

The KRAS oncogene

In the presence of mutant KRAS, CD95 and TRAIL-receptors preferentially stimulate migration and invasion of colorectal tumor cells, both *in vitro* and in liver metastases *in vivo*. Deletion of mutant KRAS is sufficient to switch these receptors back into apoptosis mode and abrogate metastatic capacity[121].

In new GEM models for intestinal tumorigenesis conditional loss of APC is combined with conditional activation of an activated Kras allele[126-129]. These mice develop invasive and sometimes metastatic[127] colorectal cancer. Whether CD95 controls apoptosis, inflammation and/or tumor progression in these models has so far not been evaluated. Indeed, the function of CD95 in APC-driven lesions (see above) could be quite distinct from its function in more advanced APC/Kras-induced tumors, given the ability of mutant Kras to lock CD95 in invasion-mode in late-stage colorectal tumor cells[121].

Raf1 suppression of ROK and LIMK1

Raf1 is best known as the Ras effector that mediates activation of the classical ERK pathway. However, the physiological function of Raf1 is to suppress apoptosis[130,131]. Strikingly, this does not require Raf1 kinase activity and is independent of its ability to activate the ERK pathway[130,131]. We identified Raf1 as the critical KRAS effector in mediating apoptosis resistance and maintaining metastatic capacity in colorectal cancer cells[130]. This suggests that the apoptosis-suppressing function of Raf1 during embryonic development is preserved during the pathophysiology of metastasis formation.

Multiple Raf1-binding proteins have been implicated in apoptosis suppression. First, Raf1 binding inactivates the pro-apoptotic kinase MST2[132,133]. Activation of CD95 causes disruption of the RAF1-MST2 complex, leading to activation of MST2 and increased apoptosis[133]. Second, Raf1 binds to and suppresses the activity of Rho-kinase (ROK)[134,135]. Oncogenic KRAS and Raf1 are potent suppressors of ROK activity in colorectal cancer cells[121]. ROK phosphorylates several downstream substrates, including the membrane-actin linker protein Ezrin. CD95 binds to ROK-phosphorylated Ezrin and is thereby targeted to the cortical actin cytoskeleton[136]. By inhibiting ROK and ROK-dependent Ezrin phosphorylation Raf1 reduces CD95 targeting to cortical actin and suppresses CD95-mediated apoptosis in fibroblasts[135].

In colorectal cancer cells Kras and Raf1 did not affect Ezrin phosphorylation, but strongly suppressed ROK-mediated phosphorylation of LIM-kinase 1 (LIMK1). LIMK1 inhibits the actin-severing protein cofilin and thereby stabilizes the cortical actin cytoskeleton. LIMK1 suppression by KRAS and Raf1 not only blocked apoptosis signaling but also allowed CD95 to stimulate tumor cell invasion and increase metastatic potential by allowing cofilin pathway activation [98,99,121]. Surprisingly little is known about the LIMK1-cofilin pathway in colorectal cancer. Functional studies implicating LIMK1 or other components of the cofilin pathway in colorectal carcinogenesis or metastasis formation are currently lacking.

CD95 IN COLORECTAL CANCER TREATMENT

The finding that many tumors express functional death receptors has raised enormous interest in exploiting them as targets for anti-cancer therapy, aiming to induce tumor cell apoptosis[137]. Several death receptor agonists are being tested for their safety and anti-tumor efficacy in clinical trials. These trials include patients with various types of cancer, including colorectal cancer. Unfortunately, tumor responses have so far been minimal[137,138].

CD95 as a target in cancer therapy

Pre-clinical studies showed that antibody-mediated systemic activation of CD95 in mice caused massive hepatocyte apoptosis resulting in fatal hepatitis[76,139]. This was dependent on FcγRIIB[140], suggesting that liver toxicity may be less pronounced when using non-antibody CD95-activating compounds, such as recombinant mega-CD95L (APO010) (www.clinicaltrials.gov). APO010 shows anticancer activity *in vitro* and in animal models carrying human xenografts of a variety of cancers, including multiple myeloma, non-small cell lung cancer (NSCLC) and ovarian cancer. APO010 appears to act synergistically with a variety of commonly used anticancer drugs[141]. Pre-clinical studies show that APO010 may cause moderate and reversible liver toxicity[141,142]. A phase I study in patients with solid tumors should reveal the safety and tolerability of APO010. Whatever the outcome of this study, hepatotoxicity will remain a major point of concern for the use of any CD95-activating compound in humans. Colorectal cancer primarily metastasizes to the liver. The evidence that CD95 has pro-tumorigenic signaling capacity is overwhelming. Therefore, there is a realistic danger that CD95-activating compounds will be toxic to the liver while stimulating growth and dissemination of the metastases it contains. Taken together, it is unlikely that such compounds will be effective against metastatic colorectal cancer.

Neutralization of CD95L in preclinical studies

Suppression of CD95 signaling offers the possibility of limiting inflammation and, possibly, inflammation-associated tumor growth. This has proven to be an effective strategy in the prevention of inflammation-associated hepatocarcinogenesis in mice[89]. In addition, suppression of CD95 signaling *in vivo* has also shown great therapeutic potential in limiting spinal cord injury, inflammatory lung disease, hepatitis, graft-versus-host disease and amyloid-β-associated neurodegeneration[143-147]. In these pre-clinical studies CD95L-neutralizing agents have proven to be non-toxic and well-tolerated. CD95L can be neutralized by CD95-Fc, a fusion protein consisting of the extracellular CD95L-binding part of CD95 and the Fc portion of human IgG1. Currently, a phase 1 clinical trial is testing the safety and tolerability of CD95-Fc in healthy volunteers and patients with spinal cord injury[148]. In addition, a phase II clinical trial is currently testing the effects of CD95-Fc treatment in glioblastoma patients (clinicaltrials.gov; NCT01071837).

CONCLUSIONS AND FUTURE PERSPECTIVE

It is presently unclear why low levels of CD95 and high levels of CD95L are both associated with tumor progression. This requires assessment of the function of tumor cell CD95 and CD95L during colorectal tumor initiation, progression and metastasis formation. In addition, CD95L-expressing immune cells and other stromal cells infiltrating into the lesions are likely to shape CD95-mediated control of tumor development (Table 1).

Effect of CD95L on:	Direct effect	Consequence
Tumor cells	Apoptosis Proliferation Invasion Survival	Tumor regression Tumor progression Tumor cell dissemination Tumor maintenance
Neutrophils	Infiltration into the tumor Secretion of cytokines/growth factors	Tumor regression Tumor progression
Macrophages	Secretion of cytokines/growth factors Secretion of metalloproteinases Secretion of pro-angiogenic factors	Influx inflammatory cells Matrix remodelling / tumor invasion Angiogenesis
Dendritic cells	Secretion of cytokines Establishing CTL response	Influx inflammatory cells Anti-tumor immunity
$CD4^+$ T_H cells	Establishing CTL response	Anti-tumor immunity
Regulatory T cells	Apoptosis	Reduced immune suppression
CTL	Apoptosis	Low levels intra-tumor CTL's ('counterattack')
Hepatocytes	Apoptosis Secretion of cytokines	Facilitates tumor cell invasion Influx inflammatory cells

Table 1 CD95L effector cells in and surrounding metastatic colorectal tumors.
T_H, T helper cell; CTL cytotoxic T lymphocyte.

The development of mouse models in which each of these factors is deleted in specific cellular compartments should provide insight into the multifaceted role of the CD95/CD95L system in controlling colorectal tumor development. The model presented in Figure 3 summarizes how CD95 signaling in tumor cells, immune cells and parenchymal cells together governs the behaviour of metastatic colorectal tumors.
Two major concerns limit the usefulness of CD95-activating drugs as therapeutics in colorectal cancer: (I) Hepatotoxicity, and (II) pro-tumorigenic effects on apoptosis-resistant tumor cells. Whether CD95-inhibiting drugs are safe and/or effective should be evaluated in preclinical and clinical studies. An even better approach would be to unravel the mechanism(s) that determine CD95 signaling output in colorectal cancer cells. On the basis of such information, compounds may be developed that lock CD95 in apoptosis mode. Such compounds, not necessarily targeting CD95 itself, may be more effective as anti-cancer agents than those that inhibit or stimulate CD95.

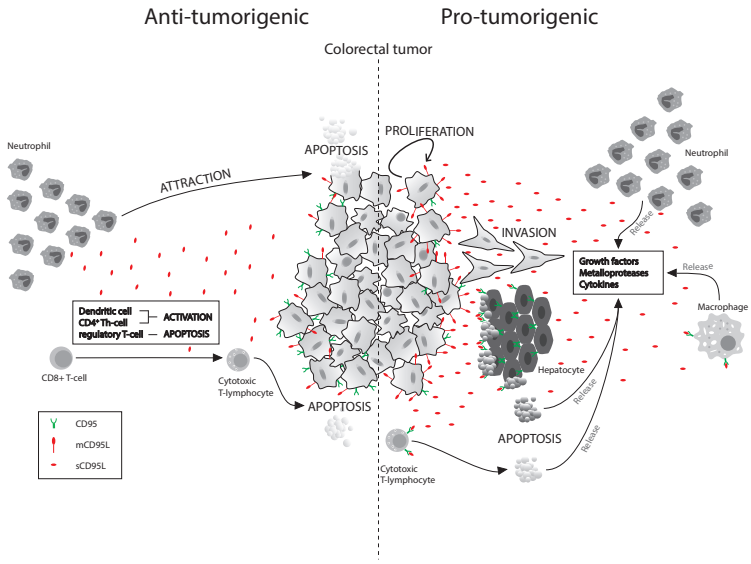

Figure 3. CD95 signaling in colorectal tumors. Soluble CD95L attracts T cells and neutrophils that can cause tumor cell apoptosis. Most likely, this is not mediated by activation of CD95 on tumor cells. CD95L may also play an important role in the development of antitumor immunity, as it stimulates dendritic cell (DC) maturation, and is essential for $CD4^+$ T cell. Thus, CD95 is expected to play a major role in the development of tumor-specific cytotoxic T lymphocytes (CTL). CD95L may also stimulate apoptosis of immune-suppressing regulatory T cells. Conversely, by activating CD95 on activated CTL's tumor-produced CD95L may limit anti-tumor immunity. This process has been referred to as the 'counter-attack'.
CD95 expressed on apoptosis-resistant tumor cells promotes proliferation and tissue invasion. In the case of liver metastases, invasion may be further facilitated by CD95L-induced apoptosis of tumor-surrounding hepatocytes. In addition, CD95 stimulation of hepatocytes, macrophages and neutrophils leads to secretion of a plethora of growth factors, cytokines and metalloproteases, which together form an inflammatory tumor-promoting micro-environment.

REFERENCE LIST

1 L. E. French, et al., "Fas and Fas ligand in embryos and adult mice: ligand expression in several immune-privileged tissues and coexpression in adult tissues characterized by apoptotic cell turnover," J. Cell Biol. 133(2), 335 (1996).

2 J. Strater and P. Moller, "Expression and function of death receptors and their natural ligands in the intestine" Ann. N. Y. Acad. Sci. 915, 162 (2000).

3 P. Moller, et al., "Expression of APO-1 (CD95), a member of the NGF/TNF receptor superfamily, in normal and neoplastic colon epithelium" Int. J. Cancer 57(3), 371 (1994).

4 T. Brunner, et al., "Cell-autonomous Fas (CD95)/Fas-ligand interaction mediates activation-induced apoptosis in T-cell hybridomas" Nature 373(6513), 441 (1995).

5 J. Dhein, et al., "Autocrine T-cell suicide mediated by APO-1/(Fas/CD95)" Nature 373(6513), 438 (1995).

6 M. Hahne, et al., "Activated B cells express functional Fas ligand" Eur. J. Immunol. 26(3), 721 (1996).

7 S. T. Ju, et al., "Fas(CD95)/FasL interactions required for programmed cell death after T-cell activation" Nature 373(6513), 444 (1995).

8 A. H. Montel, et al., "Fas involvement in cytotoxicity mediated by human NK cells" Cell Immunol. 166(2), 236 (1995).

9 E. Letellier, et al., "CD95-ligand on peripheral myeloid cells activates Syk kinase to trigger their recruitment to the inflammatory site" Immunity. 32(2), 240 (2010).

10 P. Moller, et al., "Paneth cells express high levels of CD95 ligand transcripts: a unique property among gastrointestinal epithelia " Am. J. Pathol. 149(1), 9 (1996).

11 T. Sato, et al., "Paneth cells constitute the niche for Lgr5 stem cells in intestinal crypts" Nature 469(7330), 415 (2011).

12 G. L. Eastwood, "Gastrointestinal epithelial renewal" Gastroenterology 72(5 Pt 1), 962 (1977).

13 J. Strater and P. Moller, "CD95 (Fas/APO-1)/CD95L in the gastrointestinal tract: fictions and facts" Virchows Arch. 442(3), 218 (2003).

14 L. Chen, et al., "Cell death in the colonic epithelium during inflammatory bowel diseases: CD95/Fas and beyond" Inflamm. Bowel. Dis. 16(6), 1071 (2010).

15 J. Strater, et al., "CD95 (APO-1/Fas)-mediated apoptosis in colon epithelial cells: a possible role in ulcerative colitis" Gastroenterology 113(1), 160 (1997).

16 H. Ueyama, et al., "High Fas ligand expression on lymphocytes in lesions of ulcerative colitis" Gut 43(1), 48 (1998).

17 N. Dan, et al., "Ameliorating effect of anti-Fas ligand MAb on wasting disease in murine model of chronic colitis" Am. J. Physiol Gastrointest. Liver Physiol 285(4), G754-G760 (2003).

18 P. L. Cohen and R. A. Eisenberg, "Lpr and gld: single gene models of systemic autoimmunity and lymphoproliferative disease" Annu. Rev. Immunol. 9, 243 (1991).

19 S. Nagata and T. Suda, "Fas and Fas ligand: *lpr* and *gld* mutations" Immunol. Today 16(1), 39 (1995).

20 B. Fingleton, K. J. Carter, and L. M. Matrisian, "Loss of functional Fas ligand enhances intestinal tumorigenesis in the Min mouse model" Cancer Res. 67(10), 4800 (2007).

21 S. M. Park, et al., "CD95 is cytoprotective for intestinal epithelial cells in colitis" Inflamm. Bowel. Dis. 16(6), 1063 (2010).

22 L. M. Coussens and Z. Werb, "Inflammation and cancer" Nature %19-26;420(6917), 860 (2002).

23 J. B. Seidelin and O. H. Nielsen, "Attenuated apoptosis response to Fas-ligand in active ulcerative colitis" Inflamm. Bowel. Dis. 14(12), 1623 (2008).

24 Eberl L. Peduto, et al., "Fas and Fas ligand expression in tumor cells and in vascular smooth-muscle cells of colonic and renal carcinomas" Int. J. Cancer 81(5), 772 (1999).

25 J. Strater, et al., "Impaired CD95 expression predisposes for recurrence in curatively resected colon carcinoma: clinical evidence for immunoselection and CD95L mediated control of minimal residual disease" Gut 54(5), 661 (2005).

26 M. W. Bennett, et al., "Fas ligand upregulation is an early event in colonic carcinogenesis" J. Clin. Pathol. 54(8), 598 (2001).

27 H. Li, et al., "Human and mouse colon cancer utilizes CD95 signaling for local growth and metastatic spread to liver" Gastroenterology 137(3), 934, 944 (2009).

28 T. Sjoblom, et al., "The consensus coding sequences of human breast and colorectal cancers" Science 314(5797), 268 (2006).

29 I. N. Lavrik, et al., "Analysis of CD95 threshold signaling: triggering of CD95 (FAS/APO-1) at low concentrations primarily results in survival signaling " J. Biol. Chem. 282(18), 13664 (2007).

30 P. Legembre, et al., "Induction of apoptosis and activation of NF-kappaB by CD95 require different signaling thresholds" EMBO Rep. 5(11), 1084 (2004).

31 M. W. Bennett, et al., "Fas ligand upregulation is an early event in colonic carcinogenesis" J. Clin. Pathol. 54(8), 598 (2001).

32 B. Mann, et al., "FasL is more frequently expressed in liver metastases of colorectal cancer than in matched primary carcinomas " Br. J. Cancer 79(7-8), 1262 (1999).

33 J. O'Connell, et al., "Fas ligand expression in primary colon adenocarcinomas: evidence that the Fas counterattack is a prevalent mechanism of immune evasion in human colon cancer" J. Pathol. 186(3), 240 (1998).

34 F. J. Hoogwater, et al., "Circulating CD95-ligand as a potential prognostic marker for recurrence in patients with synchronous colorectal liver metastases" Anticancer Res. 31(12), 4507 (2011).

35 T. Nozoe, et al., "Fas ligand expression is correlated with metastasis in colorectal carcinoma" Oncology 65(1), 83 (2003).

36 C. L. Hall, et al., "Essential role for hematopoietic Fas ligand (FasL) in the suppression of melanoma lung metastasis revealed in bone marrow chimeric mice" Clin. Exp. Metastasis 21(3), 251 (2004).

37 K. Liu and S. I. Abrams, "Alterations in Fas expression are characteristic of, but not solely responsible for, enhanced metastatic competence" J. Immunol. 170(12), 5973 (2003).

38 H. L. Maecker, et al., "Epigenetic changes in tumor Fas levels determine immune escape and response to therapy" Cancer Cell 2(2), 139 (2002).

39 J. P. Medema, et al., "Immune escape of tumors *in vivo* by expression of cellular FLICE-inhibitory protein" J. Exp. Med. 190(7), 1033 (1999).

40 L. B. Owen-Schaub, et al., "Fas and Fas ligand interactions suppress melanoma lung metastasis" J. Exp. Med. 188(9), 1717 (1998).

41 L. B. Owen-Schaub, "Fas function and tumor progression: use it and lose it" Cancer Cell 2(2), 95 (2002).

42 N. Finnberg, A. J. Klein-Szanto, and W. S. El-Deiry, "TRAIL-R deficiency in mice promotes susceptibility to chronic inflammation and tumorigenesis" J. Clin. Invest 118(1), 111 (2008).

43 E. Oikonomou, et al., "Newly established tumourigenic primary human colon cancer cell lines are sensitive to TRAIL-induced apoptosis *in vitro* and *in vivo*" Br. J. Cancer 97(1), 73 (2007).

44 R. M. Pitti, et al., "Induction of apoptosis by Apo-2 ligand, a new member of the tumor necrosis factor cytokine family" J. Biol. Chem. 271(22), 12687 (1996).

45 C. M. van Geelen, E. G. de Vries, and Jong S. de, "Lessons from TRAIL-resistance mechanisms in colorectal cancer cells: paving the road to patient-tailored therapy" Drug Resist. Updat. 7(6), 345 (2004).

46 S. R. Wiley, et al., "Identification and characterization of a new member of the TNF family that induces apoptosis" Immunity. 3(6), 673 (1995).

47 H. Yao, et al., "Expression of FAP-1 by human colon adenocarcinoma: implication for resistance against Fas-mediated apoptosis in cancer" Br. J. Cancer 91(9), 1718 (2004).

48 L. B. Owen-Schaub, et al., "Wild-type human p53 and a temperature-sensitive mutant induce Fas/APO-1 expression" Mol. Cell Biol. 15(6), 3032 (1995).

49 U. McDermott, et al., "Effect of p53 status and STAT1 on chemotherapy-induced, Fas-mediated apoptosis in colorectal cancer" Cancer Res. 65(19), 8951 (2005).

50 H. H. Backus, et al., "5-Fluorouracil induced Fas upregulation associated with apoptosis in liver metastases of colorectal cancer patients" Ann. Oncol. 12(2), 209 (2001).

51 S. Buonocore, et al., "Dendritic cells overexpressing CD95 (Fas) ligand elicit vigorous allospecific T-cell responses *in vivo*" Blood 101(4), 1469 (2003).

52 S. Buonocore, et al., "Neutrophil-dependent tumor rejection and priming of tumoricidal CD8+ T cell response induced by dendritic cells overexpressing CD95L" J. Leukoc. Biol. 84(3), 713 (2008).

53 J. J. Chen, Y. Sun, and G. J. Nabel, "Regulation of the proinflammatory effects of Fas ligand (CD95L)" Science 282(5394), 1714 (1998).

54 L. Ottonello, et al., "Soluble Fas ligand is chemotactic for human neutrophilic polymorphonuclear leukocytes" J. Immunol. 162(6), 3601 (1999).

55 H. Arai, et al., "Gene transfer of Fas ligand induces tumor regression *in vivo*" Proc. Natl. Acad. Sci. U. S. A 94(25), 13862 (1997).

56 C. M. Cairns, et al., "Lymphotactin expression by engineered myeloma cells drives tumor regression: mediation by $CD4^+$ and CD8+ T cells and neutrophils expressing XCR1 receptor" J. Immunol. 167(1), 57 (2001).

57 M. R. Graf, R. M. Prins, and R. E. Merchant, "IL-6 secretion by a rat T9 glioma clone induces a neutrophil-dependent antitumor response with resultant cellular, antiglioma immunity" J. Immunol. 166(1), 121 (2001).

58 K. Seino, et al., "Antitumor effect of locally produced CD95 ligand" Nat. Med. 3(2), 165 (1997).

59 H. Guillen-Ahlers, et al., "Fas/CD95 deficiency in ApcMin/+ mice increases intestinal tumor burden" PLoS. ONE. 5(2), e9070 (2010).

60 M. Shimizu, et al., "Induction of antitumor immunity with Fas/APO-1 ligand (CD95L)-transfected neuroblastoma neuro-2a cells" J. Immunol. 162(12), 7350 (1999).

61 Z. Guo, et al., "Fas ligation induces IL-1beta-dependent maturation and IL-1beta-independent survival of dendritic cells: different roles of ERK and NF-kappaB signaling pathways" Blood 102(13), 4441 (2003).

62 Z. Guo, et al., "Fas signal links innate and adaptive immunity by promoting dendritic-cell secretion of CC and CXC chemokines" Blood 106(6), 2033 (2005).

63 M. Rescigno, et al., "Fas engagement induces the maturation of dendritic cells (DCs), the release of interleukin (IL)-1beta, and the production of interferon gamma in the absence of IL-12 during DC-T cell cognate interaction: a new role for Fas ligand in inflammatory responses" J. Exp. Med. 192(11), 1661 (2000).

64 E. Ullrich, et al., "Dendritic cells and innate defense against tumor cells" Cytokine Growth Factor Rev. 19(1), 79 (2008).

65 I. Puliaeva, et al., "Fas expression on antigen-specific T cells has costimulatory, helper, and down-regulatory functions *in vivo* for cytotoxic T cell responses but not for T cell-dependent B cell responses" J. Immunol. 181(9), 5912 (2008).

66 C. Reardon, A. Wang, and D. M. McKay, "Transient local depletion of Foxp3+ regulatory T cells during recovery from colitis via Fas/Fas ligand-induced death" J. Immunol. 180(12), 8316 (2008).

67 L. Strauss, C. Bergmann, and T. L. Whiteside, "Human circulating $CD4^+CD25^{high}Foxp3^+$

regulatory T cells kill autologous CD8+ but not CD4+ responder cells by Fas-mediated apoptosis" J. Immunol. 182(3), 1469 (2009).
68 J. Galon, et al., "Type, density, and location of immune cells within human colorectal tumors predict clinical outcome" Science 313(5795), 1960 (2006).
69 A. Houston, et al., "Fas ligand mediates immune privilege and not inflammation in human colon cancer, irrespective of TGF-beta expression" Br. J. Cancer 89(7), 1345 (2003).
70 F. H. Igney and P. H. Krammer, "Tumor counterattack: fact or fiction?" Cancer Immunol. Immunother. 54(11), 1127 (2005).
71 J. O'Connell, et al., "The Fas counterattack: Fas-mediated T cell killing by colon cancer cells expressing Fas ligand" J. Exp. Med. 184(3), 1075 (1996).
72 A. E. Ryan, et al., "Fas ligand promotes tumor immune evasion of colon cancer *in vivo*" Cell Cycle 5(3), 246 (2006).
73 N. P. Restifo, "Countering the 'counterattack' hypothesis" Nat. Med. 7(3), 259 (2001).
74 F. H. Igney, C. K. Behrens, and P. H. Krammer, "CD95L mediates tumor counterattack *in vitro* but induces neutrophil-independent tumor rejection *in vivo*" Int. J. Cancer 113(1), 78 (2005).
75 P. R. Galle, et al., "Involvement of the CD95 (APO-1/Fas) receptor and ligand in liver damage" J. Exp. Med. 182(5), 1223 (1995).
76 J. Ogasawara, et al., "Lethal effect of the anti-Fas antibody in mice" Nature 364(6440), 806 (1993).
77 Z. X. Liu, S. Govindarajan, and N. Kaplowitz, "Innate immune system plays a critical role in determining the progression and severity of acetaminophen hepatotoxicity" Gastroenterology 127(6), 1760 (2004).
78 Y. Tagawa, S. Kakuta, and Y. Iwakura, "Involvement of Fas/Fas ligand system-mediated apoptosis in the development of concanavalin A-induced hepatitis" Eur. J. Immunol. 28(12), 4105 (1998).
79 K. F. Yoong, et al., "Fas/Fas ligand interaction in human colorectal hepatic metastases: A mechanism of hepatocyte destruction to facilitate local tumor invasion" Am. J. Pathol. 154(3), 693 (1999).
80 K. Arai, et al., "IP-10 and Mig facilitate accumulation of T cells in the virus-infected liver," Cell Immunol. 219(1), 48 (2002).
81 S. Faouzi, et al., "Anti-Fas induces hepatic chemokines and promotes inflammation by an NF-kappa B-independent, caspase-3-dependent pathway" J. Biol. Chem. 276(52), 49077 (2001).
82 A. M. Hohlbaum, et al., "Fas ligand engagement of resident peritoneal macrophages *in vivo* induces apoptosis and the production of neutrophil chemotactic factors" J. Immunol. 167(11), 6217 (2001).
83 K. Miwa, et al., "Caspase 1-independent IL-1beta release and inflammation induced by the apoptosis inducer Fas ligand" Nat. Med. 4(11), 1287 (1998).
84 D. R. Park, et al., "Fas (CD95) induces proinflammatory cytokine responses by human monocytes and monocyte-derived macrophages" J. Immunol. 170(12), 6209 (2003).
85 S. Kleber, et al., "Yes and PI3K bind CD95 to signal invasion of glioblastoma," Cancer Cell 13(3), 235 (2008).
86 T. L. Whiteside, "The role of death receptor ligands in shaping tumor microenvironment" Immunol. Invest 36(1), 25 (2007).
87 F. R. Greten, et al., "IKKbeta links inflammation and tumorigenesis in a mouse model of colitis-associated cancer" Cell 118(3), 285 (2004).
88 L. Chen, et al., "CD95 promotes tumour growth," Nature 465(7297), 492 (2010).
89 Y. Nakamoto, et al., "Prevention of hepatocellular carcinoma development associated with chronic hepatitis by anti-fas ligand antibody therapy" J. Exp. Med. 196(8), 1105 (2002).
90 J. O'Connell, et al., "Altered mechanisms of apoptosis in colon cancer: Fas resistance and counterattack in the tumor-immune conflict" Ann. N. Y. Acad. Sci. 910:178-92; discussion;%193-5., 178 (2000).
91 J. T. Bridgham, et al., "All in the family: evolutionary and functional relationships among death receptors" Cell Death. Differ. 10(1), 19 (2003).
92 M. E. Peter, P. Legembre, and B. C. Barnhart, "Does CD95 have tumor promoting activities?" Biochim. Biophys. Acta 1755(1), 25 (2005).
93 M. E. Peter, et al., "The CD95 receptor: apoptosis revisited" Cell 129(3), 447 (2007).
94 J. Desbarats and M. K. Newell, "Fas engagement accelerates liver regeneration after partial hepatectomy," Nat. Med. 6(8), 920 (2000).
95 R. Reinehr, A. Sommerfeld, and D. Haussinger, "CD95 ligand is a proliferative and antiapoptotic signal in quiescent hepatic stellate cells" Gastroenterology 134(5), 1494 (2008).
96 M. W. Nijkamp, et al., "CD95 is a key mediator of invasion and accelerated outgrowth of mouse colorectal liver metastases following radiofrequency ablation" J. Hepatol. 53(6), 1069 (2010).
97 B. C. Barnhart, et al., "CD95 ligand induces motility and invasiveness of apoptosis-resistant tumor cells," EMBO J. 23(15), 3175 (2004).
98 E. J. Steller, et al., "The death receptor CD95 activates the cofilin pathway to stimulate tumour cell invasion" EMBO Rep. 12(9), 931 (2011).
99 E. J. Steller, Rinkes Borel, I, and O. Kranenburg, "How CD95 stimulates invasion" Cell Cycle 10(22), 3857 (2011).
100 J. Desbarats, et al., "Fas engagement induces neurite growth through ERK activation and p35 upregulation," Nat. Cell Biol. 5(2), 118 (2003).
101 W. Ruan, C. T. Lee, and J. Desbarats, "A novel juxtamembrane domain in tumor necrosis factor receptor superfamily molecules activates Rac1 and controls neurite growth" Mol. Biol. Cell 19(8), 3192 (2008).
102 C. Zuliani, et al., "Control of neuronal branching by the death receptor CD95 (Fas/Apo-1)" Cell Death. Differ. 13(1), 31 (2006).
103 Philipsborn A. von and M. Bastmeyer, "Mechanisms

of gradient detection: a comparison of axon pathfinding with eukaryotic cell migration" Int. Rev. Cytol. 263, 1 (2007).
104 M. C. Subauste, et al., "Rho family proteins modulate rapid apoptosis induced by cytotoxic T lymphocytes and Fas" J. Biol. Chem. 275(13), 9725 (2000).
105 S. Kreuz, et al., "NFkappaB activation by Fas is mediated through FADD, caspase-8, and RIP and is inhibited by FLIP" J. Cell Biol. 166(3), 369 (2004).
106 P. Legembre, B. C. Barnhart, and M. E. Peter, "The relevance of NF-kappaB for CD95 signaling in tumor cells" Cell Cycle 3(10), 1235 (2004).
107 A. Ponton, M. V. Clement, and I. Stamenkovic, "The CD95 (APO-1/Fas) receptor activates NF-kappaB independently of its cytotoxic function" J. Biol. Chem. 271(15), 8991 (1996).
108 M. Karin and A. Lin, "NF-kappaB at the crossroads of life and death" Nat. Immunol. 3(3), 221 (2002).
109 M. Karin, "Nuclear factor-kappaB in cancer development and progression" Nature 441(7092), 431 (2006).
110 E. Pikarsky, et al., "NF-kappaB functions as a tumour promoter in inflammation-associated cancer" Nature 431(7007), 461 (2004).
111 T. G. Bivona, et al., "FAS and NF-kappaB signaling modulate dependence of lung cancers on mutant EGFR" Nature 471(7339), 523 (2011).
112 N. S. Corsini, et al., "The death receptor CD95 activates adult neural stem cells for working memory formation and brain repair" Cell Stem Cell 5(2), 178 (2009).
113 K. Chakrabandhu, et al., "Palmitoylation is required for efficient Fas cell death signaling" EMBO J. 26(1), 209 (2007).
114 C. Feig, et al., "Palmitoylation of CD95 facilitates formation of SDS-stable receptor aggregates that initiate apoptosis signaling" EMBO J. 26(1), 221 (2007).
115 K. Chakrabandhu, et al., "The extracellular glycosphingolipid-binding motif of Fas defines its internalization route, mode and outcome of signals upon activation by ligand" Cell Death. Differ. 15(12), 1824 (2008).
116 C. Gajate and F. Mollinedo, "Cytoskeleton-mediated death receptor and ligand concentration in lipid rafts forms apoptosis-promoting clusters in cancer chemotherapy" J. Biol. Chem. 280(12), 11641 (2005).
117 A. O. Hueber, et al., "An essential role for membrane rafts in the initiation of Fas/CD95-triggered cell death in mouse thymocytes" EMBO Rep. 3(2), 190 (2002).
118 A. Eramo, et al., "CD95 death-inducing signaling complex formation and internalization occur in lipid rafts of type I and type II cells" Eur. J. Immunol. 34(7), 1930 (2004).
119 K. H. Lee, et al., "The role of receptor internalization in CD95 signaling" EMBO J. 25(5), 1009 (2006).
120 A. S. Varadhachary, et al., "Phosphatidylinositol 3'-kinase blocks CD95 aggregation and caspase-8 cleavage at the death-inducing signaling complex by modulating lateral diffusion of CD95" J. Immunol. 166(11), 6564 (2001).
121 F. J. Hoogwater, et al., "Oncogenic K-Ras turns death receptors into metastasis-promoting receptors in human and mouse colorectal cancer cells," Gastroenterology 138(7), 2357 (2010).
122 M. E. Guicciardi and G. J. Gores, "Life and death by death receptors" FASEB J. 23(6), 1625 (2009).
123 A. Krueger, et al., "Cellular FLICE-inhibitory protein splice variants inhibit different steps of caspase-8 activation at the CD95 death-inducing signaling complex" J. Biol. Chem. 276(23), 20633 (2001).
124 F. Zang, et al., "Critical role for c-FLIP(L) on Fas resistance in colon carcinoma cell line HT-29" Cell Biol. Int. 32(3), 329 (2008).
125 T. Kataoka, et al., "The caspase-8 inhibitor FLIP promotes activation of NF-kappaB and Erk signaling pathways" Curr. Biol. 10(11), 640 (2000).
126 K. M. Haigis, et al., "Differential effects of oncogenic K-Ras and N-Ras on proliferation, differentiation and tumor progression in the colon" Nat. Genet. 40(5), 600 (2008).
127 K. E. Hung, et al., "Development of a mouse model for sporadic and metastatic colon tumors and its use in assessing drug treatment" Proc. Natl. Acad. Sci. U. S. A 107(4), 1565 (2010).
128 K. P. Janssen, et al., "APC and oncogenic KRAS are synergistic in enhancing Wnt signaling in intestinal tumor formation and progression" Gastroenterology 131(4), 1096 (2006).
129 O. J. Sansom, et al., "Loss of Apc allows phenotypic manifestation of the transforming properties of an endogenous K-ras oncogene *in vivo*" Proc. Natl. Acad. Sci. U. S. A 103(38), 14122 (2006).
130 M. Huser, et al., "MEK kinase activity is not necessary for Raf-1 function" EMBO J. 20(8), 1940 (2001).
131 M. Mikula, et al., "Embryonic lethality and fetal liver apoptosis in mice lacking the c-raf-1 gene" EMBO J. 20(8), 1952 (2001).
132 J. Chen, et al., "Raf-1 promotes cell survival by antagonizing apoptosis signal-regulating kinase 1 through a MEK-ERK independent mechanism" Proc. Natl. Acad. Sci. U. S. A 98(14), 7783 (2001).
133 E. O'Neill, et al., "Role of the kinase MST2 in suppression of apoptosis by the proto-oncogene product Raf-1" Science 306(5705), 2267 (2004).
134 K. Ehrenreiter, et al., "Raf-1 regulates Rho signaling and cell migration" J. Cell Biol. 168(6), 955 (2005).
135 D. Piazzolla, et al., "Raf-1 sets the threshold of Fas sensitivity by modulating Rok-alpha signaling" J. Cell Biol. 171(6), 1013 (2005).
136 S. Fais, Milito A. de, and F. Lozupone, "The role of FAS to ezrin association in FAS-mediated apoptosis" Apoptosis. 10(5), 941 (2005).
137 J. C. Reed, "Drug insight: cancer therapy strategies based on restoration of endogenous cell death mechanisms" Nat. Clin. Pract. Oncol. 3(7), 388 (2006).
138 A. Ashkenazi, P. Holland, and S. G. Eckhardt, "Ligand-based targeting of apoptosis in cancer: the potential of recombinant human apoptosis ligand 2/Tumor necrosis factor-related apoptosis-inducing ligand (rhApo2L/TRAIL)," J. Clin. Oncol.

26(21), 3621 (2008).
139 K. Papenfuss, S. M. Cordier, and H. Walczak, "Death receptors as targets for anti-cancer therapy" J. Cell Mol. Med. 12(6B), 2566 (2008).
140 Y. Xu, et al., "Fc gamma Rs modulate cytotoxicity of anti-Fas antibodies: implications for agonistic antibody-based therapeutics" J. Immunol. 171(2), 562 (2003).
141 M. Russo, et al., "Exploring death receptor pathways as selective targets in cancer therapy" Biochem. Pharmacol. 80(5), 674 (2010).
142 I. Verbrugge, et al., "Combining radiotherapy with APO010 in cancer treatment" Clin. Cancer Res. 15(6), 2031 (2009).
143 V. M. Borges, et al., "Fas ligand triggers pulmonary silicosis" J. Exp. Med. 194(2), 155 (2001).
144 D. Demjen, et al., "Neutralization of CD95 ligand promotes regeneration and functional recovery after spinal cord injury" Nat. Med. 10(4), 389 (2004).
145 D. W. Ethell, R. Kinloch, and D. R. Green, "Metalloproteinase shedding of Fas ligand regulates beta-amyloid neurotoxicity" Curr. Biol. 12(18), 1595 (2002).
146 T. Kondo, et al., "Essential roles of the Fas ligand in the development of hepatitis" Nat. Med. 3(4), 409 (1997).
147 K. Miwa, et al., "Therapeutic effect of an anti-Fas ligand mAb on lethal graft-versus-host disease" Int. Immunol. 11(6), 925 (1999).
148 U. Fischer and K. Schulze-Osthoff, "Apoptosis-based therapies and drug targets" Cell Death. Differ. 12 Suppl 1, 942 (2005).

PART I | CD95 AND COLORECTAL CANCER

CHAPTER 3

3

The death receptor CD95 activates the cofilin pathway to stimulate tumor cell invasion

EMBO Rep. 2011 Sep 1;12(9):931-7

Ernst J.A. Steller[1]*, Laila Ritsma[2]*, Danielle A.E. Raats[1], Frederik J.H. Hoogwater[1], Benjamin L. Emmink[1], Klaas M. Govaert[1], Jamila Laoukili[1], Inne H.M. Borel Rinkes[1], Jacco van Rheenen[2], Onno Kranenburg[1]

* *Equal contribution*

[1] Department of Surgery, University Medical Center Utrecht, the Netherlands
[2] Hubrecht Institute-KNAW and University Medical Center Utrecht, the Netherlands

ABSTRACT

The 'death receptor' CD95 promotes apoptosis via well-defined signaling pathways. In colorectal cancer cells CD95 primarily stimulates migration and invasion via pathways that are incompletely understood. Here we identify a novel CD95-activated tyrosine kinase pathway that is essential for CD95-stimulated tumor cell invasion. We show that CD95 promotes tyrosine 783 phosphorylation of phospholipase C-γ1 (PLC-γ1) via the platelet-derived growth factor receptor beta (PDGFR-β), resulting in ligand-stimulated PIP_2 hydrolysis. PIP_2 hydrolysis liberates the actin-severing protein cofilin from the plasma membrane to initiate cortical actin remodeling. Cofilin activation is required for CD95-stimulated formation of membrane protrusions and increased tumor cell invasion.

INTRODUCTION

Death receptors on tumor cells can suppress metastasis formation by stimulating apoptosis[1-4]. Although CD95 is best known for its ability to induce apoptosis, it can also act as a promoter of tumor and metastasis formation by stimulating tumor cell proliferation, survival, and/or invasion[5-10]. We have recently shown that endogenous oncogenic KRAS, one of the first genes to be mutated during colorectal cancer development, can transform death receptors into invasion-stimulating receptors[7]. The signal transduction pathways that cause apoptosis downstream of activated CD95 have been well documented[11]. By contrast, much less is known about the factors that promote tumor cell invasion following CD95 stimulation. In many tumor cell lines, invasion is dependent on the actin-driven formation of membrane protrusions[12,13]. In the current report we provide evidence that activated CD95 promotes the formation of cell protrusions via a novel signaling pathway.

METHODS

Real time imaging

Cells were seeded in a Lab-Tek® Chambered #1.0 Borosilicate Coverglass System (Nalgene Nunc International, Rochester, NY14625, USA) and were mounted on a Zeiss Axiovert 200M microscope for live cell imaging (5% CO_2; 37°C) for 2 hours to 14 hours. Phase contrast images were captured every 2 minutes using a Photometics Coolsnap CCD camera (Scientific, Tuscon, AZ). Images were processed using Metamorph software (Universal imaging, Downington, PA). The number of protrusions was scored by off-line analysis of the generated videos and plotted as means $\pm$SEM. For real time fluorescence imaging, cells were placed on a Leica SP5 inverted microscope equipped with a 63x 1.3NA glycerol objective. Cells were kept in Leibovitz-15 buffered medium (Invitrogen, Breda, The Netherlands) at 37°C in a climate chamber.

Invasion assay

For *in vitro* invasion assay's 24-well BioCoat Matrigel invasion chambers (#354480, BD Biosciences, Alphen aan den Rijn) were used according to the manufacture's protocol. Cells were kept under serum free conditions overnight. In the upper compartment, $5x10^4$ cells/well were plated in 0.5 ml serum-free medium. The lower compartment contained 0.75 ml medium with 5% FCS. CD95L (10 ng/ml) was added to the lower compartment. Cells were pretreated overnight in both compartments with 1 µM U73122 and U73343 or with 2 µM Sunitinib for 1 hour before plating. Invasion chambers were incubated for 8 hrs. Cells in the upper compartment were removed with a cotton swap. Transmigrated cells were fixed in formaldehyde 3.7%, stained with DAPI, and counted by analyzing microscopic images (5-6 fields per membrane). Data are expressed relative to control. All assays were performed in triplicate and were repeated twice.

Checkerboard analysis

Checkerboard analysis was performed by adding 0, 2 and 10 ng/ml to the wells (bottom) and/or to the inserts (top) of the matrigel invasion chambers. Invasion assays were carried out as described above.

PIP_2 hydrolysis assay

Cells grown on coverslips were transiently transfected with mRFP-PH. The coverslips were mounted on a SP5 Leica confocal microscope. Images of RFP-PH were collected every 20 seconds and stored on the computer. Using a custom-made visual basics program, the images were imported and analyzed. Following a threshold step, background regions were determined and the background was measured and subtracted from the images. Cells were traced with a fixed threshold resulting in a binary image. Regions of the plasma membrane were determined by eroding the binary image with 6 pixels. The cytosol region was determined by eroding the binary image by another 4 pixels. Mean fluorescence level of the plasma membrane and cytosol region was measured and plotted over time. To calibrate the plasma membrane to cytosol translocation, ionomycin (5 μM) + 2mM calcium was added to induce a full membrane to cytosol translocation. PIP_2 hydrolysis was expressed as the ratio of fluorescent intensity of the plasma membrane to the cytosol as induced by CD95 compared to ionomycin/calcium.

Statistical analysis

Statistical differences between groups were analyzed by an unpaired two sided t-test. Data are expressed as mean $\pm$ SEM. A p-value of <0.05 was considered statistically significant ($* < 0.05$).

RESULTS AND DISCUSSION

To study invasion signaling pathways downstream of CD95 we employed the Kras mutant murine colorectal cancer cell line C26. CD95 primarily signals motility and invasion in these cells[7,9] (Figure 1A). Checkerboard analysis further showed that CD95-ligand (CD95L) promotes directed (chemotaxis) rather than non-directed (chemokinesis) tumor cell migration (Figure 1B). Real-time imaging showed that non-stimulated C26 cells spontaneously formed cell protrusions in a random fashion with, on average, 1-2 protrusions per cell. Upon stimulation with CD95L the number of protrusions increased to 4-6 per cell and this caused a significant increase in total cell area of ~35% over a period of 30 minutes (Figure 1C). Knockdown of the endogenous mutant $Kras^{D12}$ allele largely prevented CD95-induced formation of cell protrusions and invasion and allowed CD95 to induce apoptosis (Figure 1A and supplementary Figure S1). Stimulation of another murine colorectal cancer cell line (MC38) with CD95L also resulted in increased migration, the formation of cell protrusions and tumor cell invasion (supplementary Figure S2). The polymerization of actin monomers into filamentous actin (F-actin) at the leading edge of migrating cells generates the forces that drive the formation of cell protrusions. Actin polymerization occurs mainly at one end of the filament, named the 'barbed end', and assembly of F-actin is controlled by tight regulation of the number of barbed ends. One of the key proteins in this process is the actin-binding protein cofilin, which can increase the number of barbed ends by severing existing F-actin[14] and by its intrinsic actin-nucleation activity[15]. Cofilin is inactivated by LIM kinase (LIMK1)-mediated phosphorylation on serine 3 which is located in the actin-binding domain. The phospho-group on serine 3 inhibits cofilin binding to F-actin and renders it inactive[16-20]. We next tested whether CD95-stimulated formation of cell protrusions was cofilin-dependent by overexpressing LIMK1. As expected, LIMK1 transfection into C26 cells resulted in the phosphorylation (inactivation) of cofilin on serine 3 (pS3-Cofilin) (Supplementary Figure S3). Cofilin inhibition by LIMK1 largely prevented the formation of cell protrusions and

the increase in cell area (Figure 1C) and strongly reduced the invasive capacity of control and CD95L-stimulated C26 cells (Figure 1D). Rather, prolonged stimulation of C26-LIMK1 cells caused apoptosis (Figure 1D). Together the data indicate that CD95 promotes the formation of cell protrusions in a LIMK1-suppressible fashion, strongly suggesting that it is a cofilin-dependent phenomenon.

The activity of cofilin is negatively regulated by LIMK1-mediated serine 3 phosphorylation[16,20] and by binding to plasmamembrane phosphatidylinositol (4,5)-bisphosphate (PIP_2)[21,22]. If CD95 activates cofilin by S3 dephosphorylation, one would expect cofilin phosphorylation to decrease in response to CD95L. However, phosphoS3-cofilin levels in C26 cells are low due to Kras/Raf1-mediated suppression of LIMK1[7] and were unaffected by stimulation with CD95L (Figure 2A) Therefore, it seems unlikely that CD95 activates cofilin by promoting its dephosphorylation.

In breast cancer cells, EGF stimulation causes local PLC-γ1-mediated PIP_2 hydrolysis that liberates cofilin from inhibition by PIP_2 [21,22]. PLC-γ1 is activated by growth factors through phosphorylation of tyrosine residue 783, which increases its PIP_2 hydrolysis activity[23].

Stimulation of C26 or MC38 cells with CD95L caused an increase in Tyr783-PLC-γ1 phosphorylation without altering cofilin Ser3 phosphorylation (Figure 2A and Figure 4C). PIP_2 hydrolysis can be detected by using the PLC-δ1 PH domain fused to red fluorescent protein (RFP) (mRFP-PH) as a PIP_2 probe[24-26]. In resting C26 cells, mRFP-PH is bound to PIP_2 in the plasma membrane (Figure 2B; left panel). Stimulation with CD95L induced a rapid 40-50% translocation of mRFP-PH from the membrane to the cytosol (Figure 2B). Interestingly, PIP_2 hydrolysis following CD95L stimulation occurred concomitantly with the formation of cell protrusions and the increase in cell area (Figure 2B; lower left panel).

The results so far suggest that CD95L promotes cofilin activation to induce cell protrusions, possibly via PLC-γ1-mediated PIP_2 hydrolysis. To test the requirement for PLC in CD95L-stimulated formation of cell protrusions and invasion, C26 cells were treated with the PLC inhibitor U73122. As expected, U73122 inhibited CD95L-stimulated PIP_2 hydrolysis (Figure 3A). Strikingly, in U73122-treated cells CD95L caused an increase in plasma membrane PIP_2 levels. This could point to activation of PIP-5 kinase following CD95L-stimulation. Importantly, U73122 not only prevented PIP_2 hydrolysis, but also blocked CD95L-stimulated formation of cell protrusions and the increase in total cell area (Figure 3B). In addition, RNAi-mediated suppression of PLC- γ1 significantly reduced the CD95L-stimulated increase in cell area (Figure 3B). Transwell assays further showed that U73122 treatment or PLC- γ1 knockdown strongly reduced CD95L-stimulated invasion of C26 and MC38 cells (Figures 3C and 3D).

PLC-γ1 is a growth factor-responsive PLC that is activated by receptor and/or non-receptor tyrosine kinases, including Src family kinases (SFK's) and the PDGFR-β[23,27]. Interestingly, SFK's are activated by CD95 and may play a role both in apoptosis and invasion signaling[8,28]. However, the small molecule SFK inhibitor SU6656[29] had no effect on CD95L-stimulated Y783-PLC-γ1 phosphorylation in C26 cells (data not shown). To search for candidate PLC-γ1-kinases, C26 cells were stimulated with EGF and PDGF. PDGF, but not EGF, effectively stimulated PLC-γ1 phosphorylation in C26 cells (Figure 4A). Interestingly, PLC-γ1 activation is required for PDGFR-induced cell migration[30]. CD95L caused a marked increase in phosphorylation of tyrosine 1021 of the PDGFR-β, which mediates binding to and activation of PLC-γ1 (Figure 4B)[27]. To assess whether PDGFR-β activity may play a role in CD95L-stimulated PLC-γ1 phosphorylation and tumor cell invasion, cells were treated with AG1296, a specific PDGFR inhibitor or Sunitinib, a PDGFR/VEGFR inhibitor. Both AG1296 and Sunitinib completely blocked CD95-stimulated phosphorylation of PLC-γ1 (Figure 4C).

A

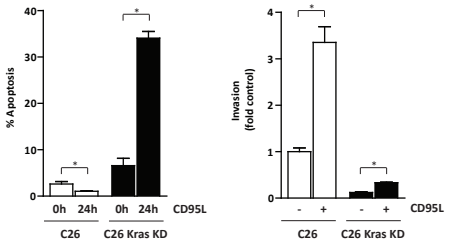

B

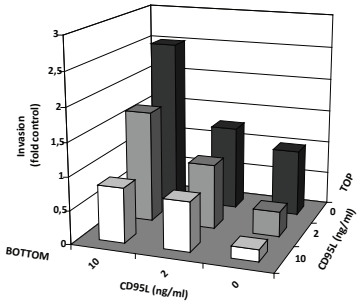

[CD95L] BOTTOM	[CD95L] TOP		
	0	2	10
0	1 ± 0,34	0,38 ± 0,08 (* 0,04)	0,18 ± 0,04 (* 0,01)
2	1,26 ± 0,81 (0,63)	0,97 ± 0,12 (0,90)	0,74 ± 0,42 (0,46)
10	2,50 ± 0,48 (* 0,01)	1,67 ± 0,45 (0,11)	0,82 ± 0,48 (0,64)

C

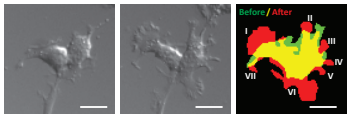

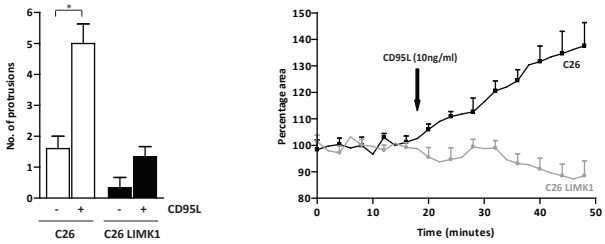

D

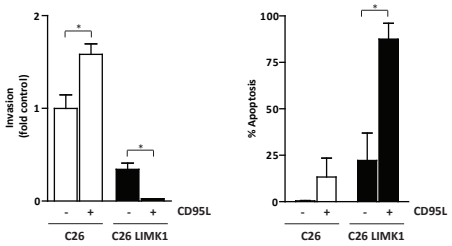

Figure 1. CD95 ligand stimulates rapid cofilin-dependent formation of cell protrusions and an increase in cell area. A. C26 and C26KrasKD cells were treated with CD95L (10ng/ml) for 24 hrs and were stained with propidium iodide (PI). The apoptotic sub-G1 fraction was determined by FACS analysis (Left panel). C26 and C26Kras KD cells were plated on Matrigel-coated membranes in transwell chambers and were allowed to invade for 8 hours in the presence or absence of CD95L (10ng/ml) (Right panel). The bar graph shows fold increase relative to non-stimulated controls (=1). Error bars represent SEM based on 2 independent experiments performed in triplicate. **B.** Checkerboard analysis in which CD95L (ng/ml; 8 hrs) was added to the insert (TOP) or to the well (BOTTOM) of the Matrigel invasion chamber. All conditions were tested in 3-5 independent experiments. Numbers represent fold change of the number of invaded cells relative to control (no CD95L in either compartment), +/- SEM (p-value). Significance was tested using the student's t test (unpaired; double-sided). **C.** C26 cells were transiently transfected with LIMK-GFP or GFP and were analyzed by real-time imaging before and after stimulation with CD95L (10 ng/ml). DIC images were used to determine the number of protrusions before and after stimulation. Inset shows C26 cells before (left panel) and after (middle panel) CD95L stimulation. The right image is a merge of binary threshold images at both time points. Yellow represents no change; Red represents increased protrusion formation; Green represents membrane retraction. Numbers indicate new protrusion formed. Scale bar represents 10μm. The generated images were also used to measure the total cell areas over time before and after stimulation (arrow) by using ImageJ software (n=4). These values were plotted as the percentage of average cell area before stimulation (Right panel). * indicates significance based on p values < 0.05. **D.** C26 and C26-LIMK1 cells were treated with CD95L (10ng/ml) for 24 hrs and apoptosis and invasion were assessed as in A (n=3). * indicates significance based on p values < 0.05.

In addition, RNAi-mediated suppression of PDGFR-β expression strongly reduced CD95L-stimulated PLC-γ1 phosphorylation and cell area enlargement (Figure 4D). Moreover, Sunitinib, AG1296 and PDGFR-β-targeted siRNA's all prevented basal and CD95L-stimulated tumor cell invasion (Figure 4E and 4F). These results strongly suggest that CD95L promotes PLC-γ1 Y783-phosphorylation via the PDGFR-β.

In conclusion, our results identify a novel CD95-initiated signaling pathway involving PDGFR-β-mediated PLC-γ1 activation and PIP_2 hydrolysis. Future work should address how CD95 stimulates PDGFR-β tyrosine phosphorylation and whether this requires PDGF binding to the receptor. Alternatively, a direct interaction between activated CD95 and the PDGFR-β could recruit the latter into the CD95 signaling complex, which contains tyrosine kinase activity[31]. In this scenario, CD95 stimulation could cause PDGFR-β activation in a PDGF-independent manner.

Earlier work has implicated caspase-8 and ERK in CD95-stimulated tumor cell invasion[5]. More recently, it was shown that CD95 activates tyrosine kinases (Yes, Syk) to promote the expression of matrix-degrading metalloproteinases, thereby facilitating tissue invasion of tumor cells and myeloid cells[8,32]. The present study shows that tyrosine kinase activation by CD95 also results in the rapid actin-driven formation of cell protrusions, a process that is essential for tumor cell invasion. Thus, CD95 can promote tumor cell invasion via distinct pathways. The specific tyrosine kinases involved and the dominance of each of these pathways in determining invasive behavior will most likely be cell-type dependent.

We propose a model in which CD95 stimulates PDGFR-β-mediated PLC activation and PIP_2 hydrolysis. The consequent release of cofilin from the plasma membrane and the continued suppression of LIMK1 by Kras/Raf1 together allow robust activation of the cofilin pathway. Cofilin-generated actin barbed ends serve as nucleation points for de novo actin polymerization. This process is driven by the small GTPases Rac and Cdc42 which are also activated following CD95 stimulation[33,34]. Cofilin and Rac/Cdc42 cooperate to stimulate actin polymerization which causes the formation of cell protrusions[22]. This process is essential for tumor cell invasion and, presumably, for metastasis formation.

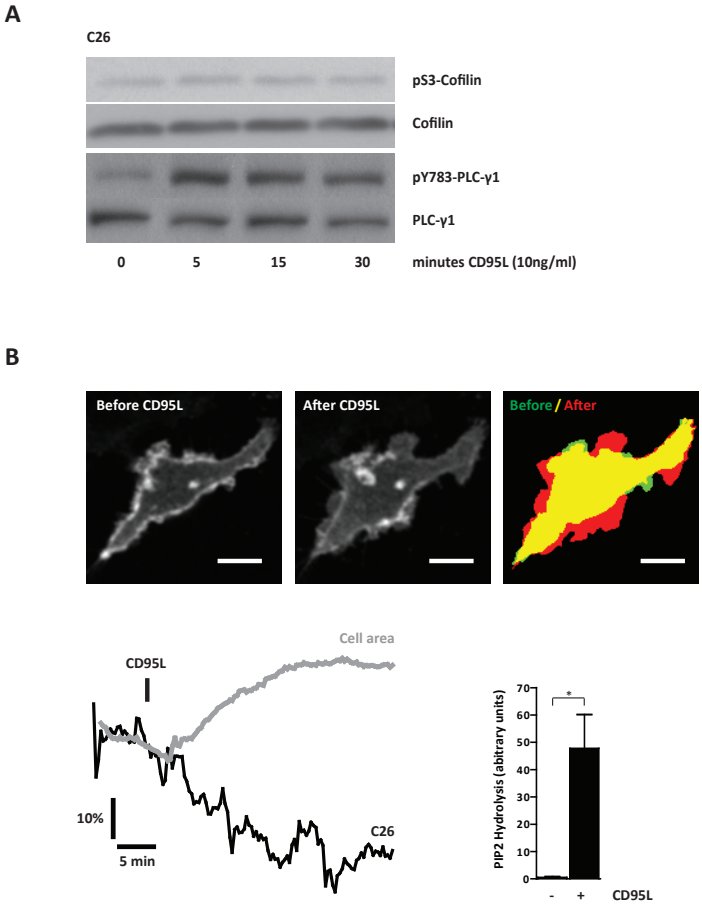

Figure 2. CD95 ligand stimulates phospholipase C-γ1 Tyr783 phosphorylation and PIP2 hydrolysis. A. C26 cells were treated with CD95L (10ng/ml) for the indicated periods of time. Cell lysates were prepared and analyzed for cofilin serine 3 phosphorylation (pS3-Cofilin), total cofilin, tyrosine 783 phosphorylation of PLC-γ1 (pY783-PLC-γ1) and total PLC-γ1 by Western blotting. **B.** Cells were transiently transfected with mRFP-PH and analyzed by real-time confocal microscopy. Images represent mRFP-PH in C26 cells before stimulation (left) and 15 minutes after stimulation with CD95L (10 ng/ml) (middle). Scale bar represents 5μm. Plotting of total cell area (measured by DIC images) and PIP_2 hydrolysis (measured using mRFP-PH) over time shows that addition of CD95L (10ng/ml) (black bar) caused a simultaneous increase in cell area and PIP_2 hydrolysis (Left lower panel). The average of 5 independent experiments is plotted (n=5). The right lower panel shows a quantification of maximal CD95L-induced PIP_2 hydrolysis, relative to ionomycin-induced maximum translocation of the mRFP-PH probe (100%). Significance was tested using the student's t test (unpaired; double-sided). * $p < 0.05$.

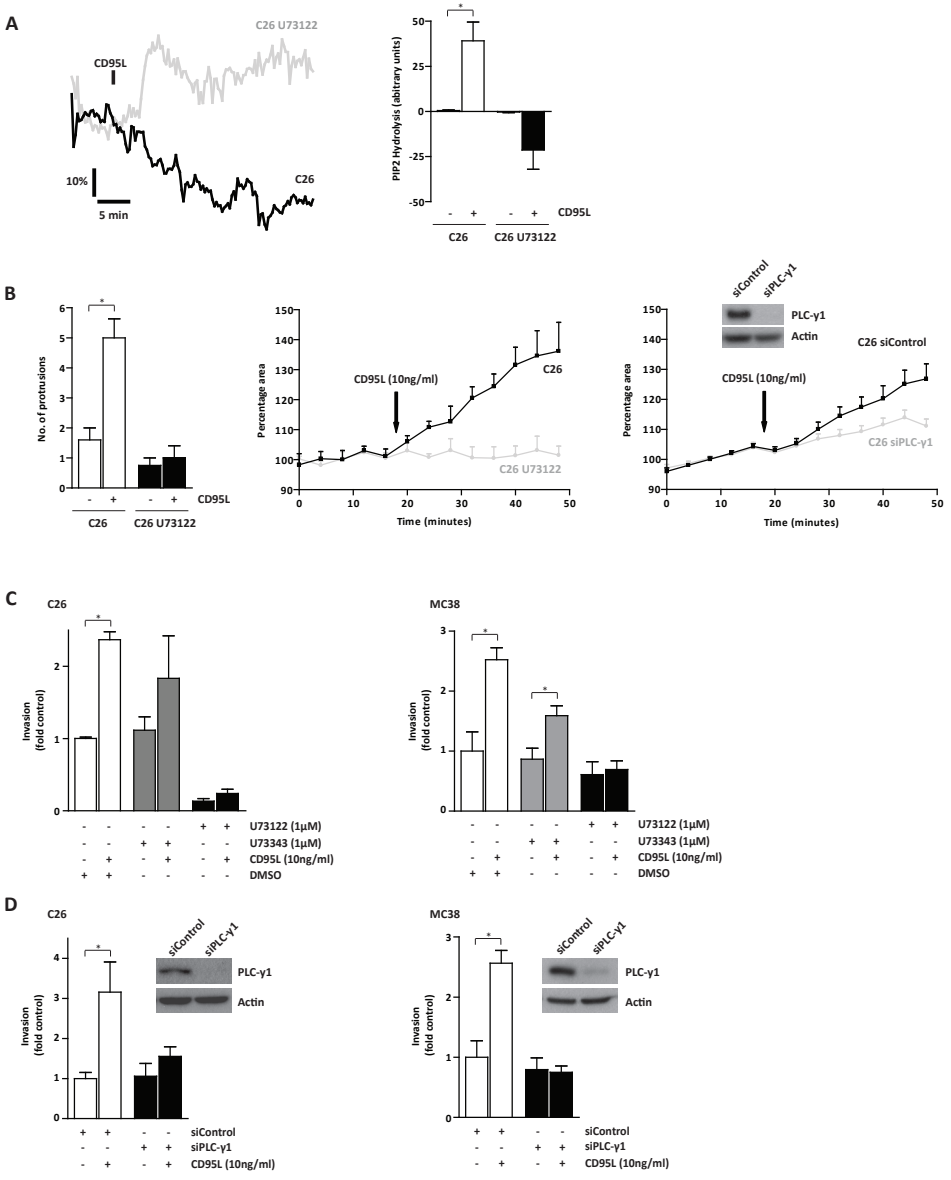

Figure 3. CD95 ligand-induced tumor cell invasion requires PLC-γ1 activation. A. C26 cells were transiently transfected with mRFP-PH. After 24 hours cells were either pre-treated with U73122 (5μM) or with vehicle (DMSO) for 1 hour prior to stimulation with CD95L (10 ng/ml). PIP_2 hydrolysis was measured over time as in Figure 2B. **B.** C26 cells were either pre-treated with U73122 (5μM) or with vehicle (DMSO) for 1 hour prior to stimulation with CD95L (10 ng/ml). Knockdown of PLC-γ1 was established by transfection of siRNA's 2 days prior to stimulation. Cells were analyzed by real-time imaging. The number of cell protrusions and the increase in cell area was measured as in Figure 1B. **C.** Transwell invasion assays of C26 and MC38 cells treated with U73343 or U73122 were performed as in Figure 1A. Data are from 2 independent experiments performed in triplicate. **D.** Transwell invasion assays of C26 and MC38 cells transfected by control or PLC-γ1 siRNA's (n=2). Significance was tested using the student's t test (unpaired; double-sided). * $p < 0.05$

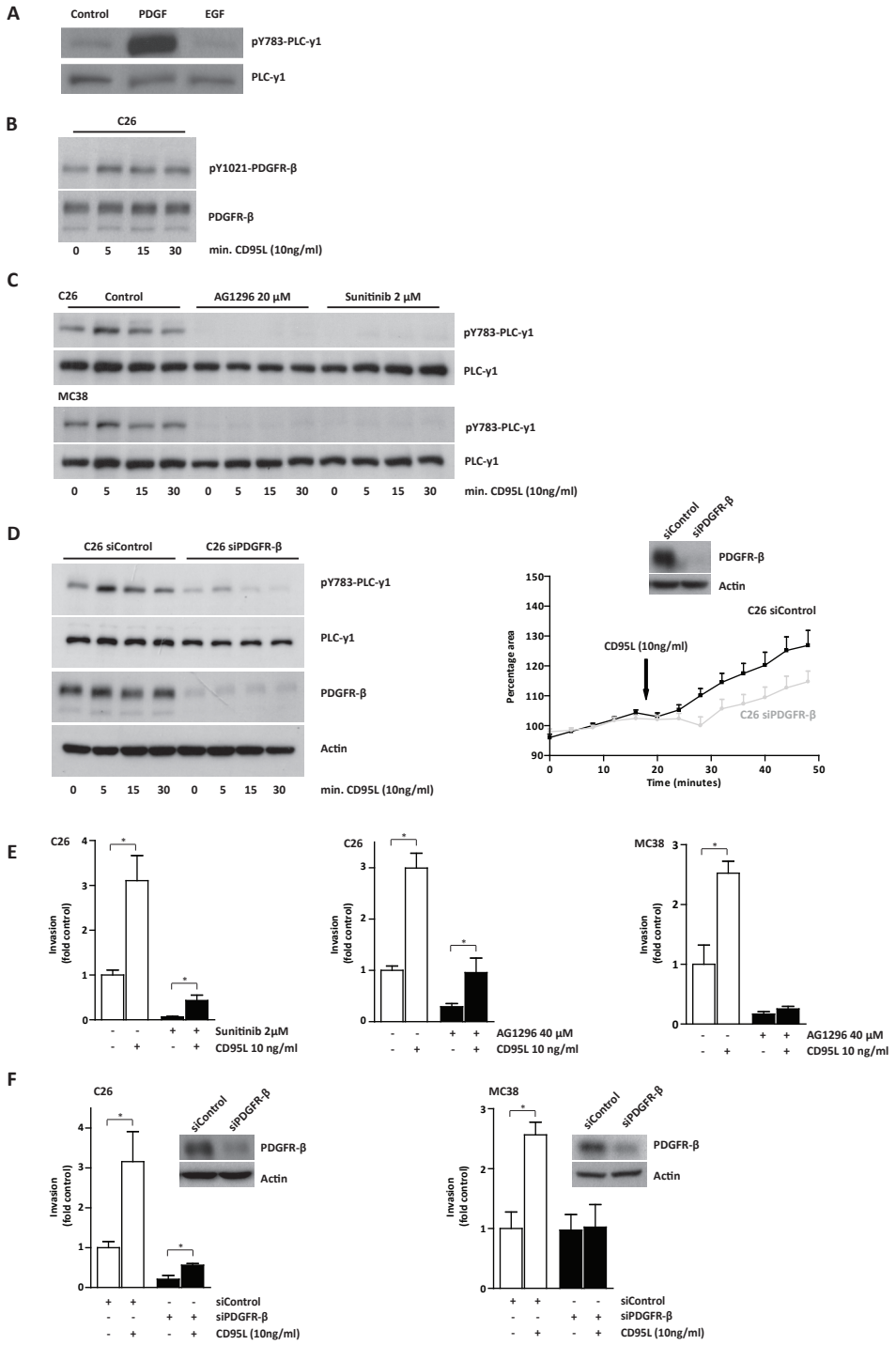

Figure 4. PDGFR-β mediates CD95-stimulated PLC-γ1 phosphorylation and tumor cell invasion. A. C26 cells were stimulated with PDGF or EGF and pY783-PLC-γ1 was assessed by western blotting. **B.** C26 cells were stimulated with CD95L and PDGFR-β phosphorylation on Y1021 was assessed by western blotting. **C.** C26 and MC38 cells were pre-treated with Sunitinib (2μM) or AG1296 (20 μM) for 16 hours and were subsequently stimulated with CD95L for 5, 15 or 30 minutes. Cell lysates were prepared and analyzed for pY783-PLC-γ1 by western blotting. **D.** C26 cells were transfected with siRNA's against PDGFR-β and stimulated for the indicated time points with CD95L. Y783-PLC-γ1 phosphorylation and PDGFR-β knockdown were assessed by western blotting. Cell area enlargement (right panel) was measured as in Figure 1A. **E.** Transwell invasion assays of C26 and MC38 cells treated with Sunitinib, AG1296 or vehicle. Data are from 2 independent experiments (n=2) performed in triplicate. **F.** Transwell invasion assay of C26 and MC38 cells transfected with control or PDGFR-β-targeting siRNA's (n=2). Significance was tested using the student's t test (unpaired; double-sided). * $p < 0.05$

REFERENCE LIST

1. Koshkina, NV et al. Fas-negative osteosarcoma tumor cells are selected during metastasis to the lungs: the role of the Fas pathway in the metastatic process of osteosarcoma. Mol.Cancer Res. 5, 991-999. 2007.
2. Smyth, MJ et al. Tumor necrosis factor-related apoptosis-inducing ligand (TRAIL) contributes to interferon gamma-dependent natural killer cell protection from tumor metastasis. J.Exp.Med. 193, 661-670. 2001.
3. Takeda, K et al. Involvement of tumor necrosis factor-related apoptosis-inducing ligand in surveillance of tumor metastasis by liver natural killer cells. Nat.Med. 7, 94-100. 2001.
4. Yang, D et al. Downregulation of IFN-gammaR in association with loss of Fas function is linked to tumor progression. Int.J.Cancer 122, 350-362. 2008.
5. Barnhart, BC et al. CD95 ligand induces motility and invasiveness of apoptosis-resistant tumor cells. EMBO J. 23, 3175-3185. 2004.
6. Chen, L et al. CD95 promotes tumour growth. Nature 465, 492-496. 2010.
7. Hoogwater, FJ et al. Oncogenic K-Ras turns death receptors into metastasis-promoting receptors in human and mouse colorectal cancer cells. Gastroenterology 138, 2357-2367. 2010.
8. Kleber, S et al. Yes and PI3K bind CD95 to signal invasion of glioblastoma. Cancer Cell 13, 235-248. 2008.
9. Nijkamp, MW et al. CD95 is a key mediator of invasion and accelerated outgrowth of mouse colorectal liver metastases following radiofrequency ablation. J.Hepatol. 53, 1069-1077. 2010.
10. Peter, ME et al. The CD95 receptor: apoptosis revisited. Cell 129, 447-450. 2007.
11. Strasser, A et al. The many roles of FAS receptor signaling in the immune system. Immunity. 30, 180-192. 2009.
12. Wang, W et al. The activity status of cofilin is directly related to invasion, intravasation, and metastasis of mammary tumors. J.Cell Biol. 173, 395-404. 2006.
13. Wang, W et al. The cofilin pathway in breast cancer invasion and metastasis. Nat.Rev.Cancer 7, 429-440. 2007.
14. Ichetovkin, I et al. Cofilin produces newly polymerized actin filaments that are preferred for dendritic nucleation by the Arp2/3 complex. Curr.Biol. 12, 79-84. 2002.
15. Andrianantoandro, E et al. Mechanism of actin filament turnover by severing and nucleation at different concentrations of ADF/cofilin. Mol.Cell 24, 13-23. 2006.
16. Arber, S et al. Regulation of actin dynamics through phosphorylation of cofilin by LIM-kinase. Nature 393, 805-809. 1998.
17. Bamburg, JR. Proteins of the ADF/cofilin family: essential regulators of actin dynamics. Annu.Rev. Cell Dev.Biol. 15, 185-230. 1999.
18. Bernard, O. Lim kinases, regulators of actin dynamics. Int.J.Biochem.Cell Biol. 39, 1071-1076. 2007.
19. Moriyama, K et al. Phosphorylation of Ser-3 of cofilin regulates its essential function on actin. Genes Cells 1, 73-86. 1996.
20. Yang, N et al. Cofilin phosphorylation by LIM-kinase 1 and its role in Rac-mediated actin reorganization. Nature 393, 809-812. 1998.
21. van Rheenen, J et al. EGF-induced PIP_2 hydrolysis releases and activates cofilin locally in carcinoma cells. J.Cell Biol. 179, 1247-1259. 2007.
22. van Rheenen, J et al. A common cofilin activity cycle in invasive tumor cells and inflammatory cells. J.Cell Sci. 122, 305-311. 2009.
23. Kim, MJ et al. The mechanism of phospholipase C-gamma1 regulation. Exp.Mol.Med. 32, 101-109. 2000.
24. Stauffer, TP et al. Receptor-induced transient reduction in plasma membrane PtdIns(4,5)P2 concentration monitored in living cells. Curr.Biol. 8, 343-346. 1998.
25. van Rheenen, J et al. PIP_2 signaling in lipid domains: a critical re-evaluation. EMBO J. 24, 1664-1673. 2005.
26. Varnai, P et al. Visualization of phosphoinositides that bind pleckstrin homology domains: calcium- and agonist-induced dynamic changes and relationship to myo-[3H]inositol-labeled phosphoinositide pools. J.Cell Biol. 143, 501-510. 1998.
27. Ronnstrand, L et al. Identification of two C-terminal autophosphorylation sites in the PDGF beta-receptor: involvement in the interaction with phospholipase C-gamma. EMBO J. 11, 3911-3919. 1992.
28. Schlottmann, KE et al. Activation of Src-family tyrosine kinases during Fas-induced apoptosis. J. Leukoc.Biol. 60, 546-554. 1996.
29. Blake, RA et al. SU6656, a selective src family kinase inhibitor, used to probe growth factor signaling. Mol.Cell Biol. 20, 9018-9027. 2000.
30. Kundra, V et al. Regulation of chemotaxis by the platelet-derived growth factor receptor-beta. Nature 367, 474-476. 1994.
31. Sancho-Martinez, I et al. Tyrosine phosphorylation and CD95: a FAScinating switch. Cell Cycle 8, 838-842. 2009.
32. Letellier, E et al. CD95-ligand on peripheral myeloid cells activates Syk kinase to trigger their recruitment to the inflammatory site. Immunity. 32, 240-252. 2010.
33. Ruan, W et al. A novel juxtamembrane domain in tumor necrosis factor receptor superfamily molecules activates Rac1 and controls neurite growth. Mol.Biol.Cell 19, 3192-3202. 2008.
34. Subauste, MC et al. Rho family proteins modulate rapid apoptosis induced by cytotoxic T lymphocytes and Fas. J.Biol.Chem. 275, 9725-9733. 2000.

SUPPLEMENTARY METHODS

Cell culture

MC38, C26 and C26KrasKD cells were described before[1,2]. Cells were cultured in Dulbecco's Modified Eagle's Medium (DMEM; Dulbecco, ICM Pharmaceuticals, Costa Mesa, CA) supplemented with 5% (v/v) fetal calf serum, 2mM ultraglutamine, 0.3 mg/ml streptomycin, and 100 U/ml penicillin. Cells were kept at 37°C in a humidified atmosphere containing 5% CO_2.

Antibodies and reagents

The following antibodies were obtained from Cell Signaling Technology Inc., Danvers, MA: rabbit pS3Cofilin (#3311S), rabbit Cofilin (#3312), rabbit pY783-PLC-γ1 (#2821), rabbit PLC-γ1 (#2822), rabbit pY1021-PDGFR-β (#2227), rabbit PDGFR-β (#4564). Secondary peroxidase-conjugated antibodies were from Dako (Glostrup, Denmark). The following reagents were used in this study: CD95 Ligand (CD95L), membrane bound (#01-210) from Upstate Cell Signaling Solutions, Lake Placid, NY. U73122 (sc-3574) Santa Cruz Biotechnology, Santa Cruz, CA. U-73343 (sc-201422) Santa Cruz Biotechnology, Santa Cruz, CA. Sunitinib malate salt (S-8803) was from LC Laboratories, Woburn, MA. AG1296 (#658551) was from EMD4Biosciences, San Diego, CA. siRNA OTP SMARTpools were transfected using reverse transfection with Hiperfect (Qiagen) according to the manufacturers' guidelines. Gene names and siRNA sequences of the siRNA library are listed in supplementary material Table S1.

DNA constructs and transfections

pWPT-GFP was a kind gift of Prof. Didier Trono. The expression construct for LIMK1 was a kind gift of Prof John Condeelis[3]. The mRFP-PH construct was described before[4]. Transfections were performed using Lipofectamine 2000^{tm} (Invitrogen 11668-019) according to the manufacturer's protocol.

Apoptosis assay

Cells were fixed in 70% ice-cold ethanol and incubated for 2h at 4°C. To assess the cell-cycle profile, fixed cells were treated with RNAse and DNA was stained with propidium iodide (PI). All samples were analysed by flow cytometry using Cell Quest and Modfit software (Becton Dickinson, Breda, the Netherlands).

Migration assay

Migration of MC38 cells was assessed by tracking cells, in x and y directions, over time in real time. Images were acquired every five minutes for 9 hours on a Leica AF7000 inverted microscope for live cell imaging (5%CO_2, 370C). Analysis was performed using ImageJ software. The x and y starting coordinates were subtracted from each measured coordinate, resulting in tracks that all start at 0,0 (x,y).

SUPPLEMENTARY FIGURES

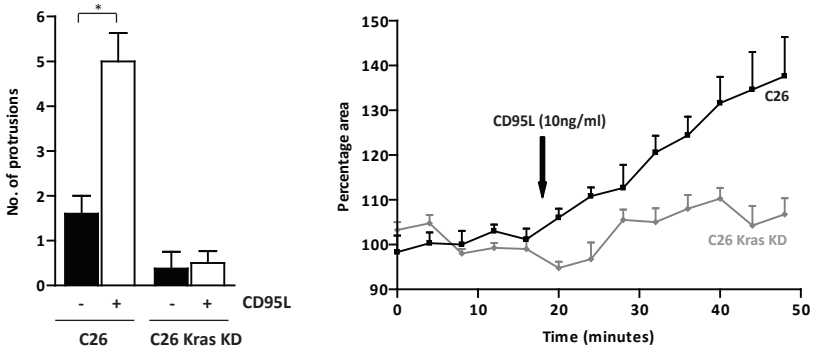

Figure S1. Knockdown of mutant Kras in C26 cells abrogates CD95L-induced formation of cell protrusions and cell area enlargement. C26 and C26KrasKD cells were stimulated with CD95L (10 ng/ml) and were analyzed for the number of cell protrusions and for total cell area by real-time imaging exactly as in Figure 1. n=4. *p<0.05.

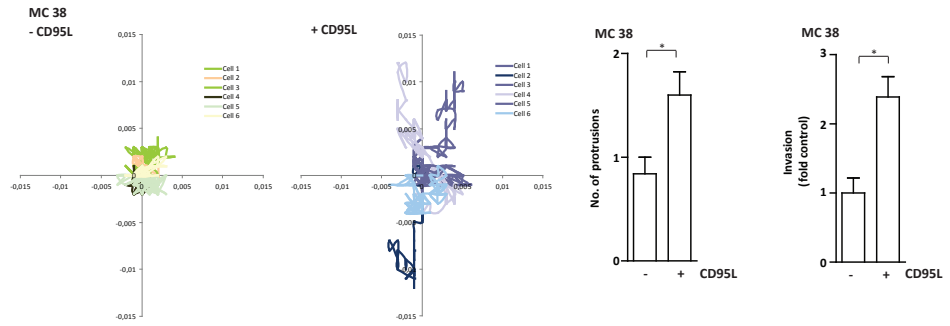

Figure S2. CD95L induces migration, protrusion formation and invasion in MC38 cells. Left panel: MC38 cells were observed by live cell imaging. ImageJ software was used to track individual cells over time before and after addition of CD95L (10 ng/ml; n=6). Right panel: MC38 cells were either left unstimulated or were stimulated for 30 minutes with CD95L (10 ng/ml) for protrusion analysis. The number of cell protrusions and tumor cell invasion were performed and assessed exactly as in Figure 1.

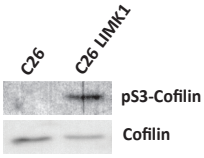

Figure S3. Overexpression of LIMK1 increases pS3-Cofilin levels. Cells were transiently transfected with expression constructs encoding LIMK1-GFP or GFP and were sorted by flow cytometry on the basis of GFP expression. The levels of pS3-Cofilin and total Cofilin were analyzed by Western Blotting.

	Sequence	Concentration	Knockdown time	Manufacturer
OTP Non-Targeting Pool	Control siRNA	20nM	48-72 hrs	Dharmacon
PDGFR-β OTP SMARTpool	CAGCGAGGUUUCACUGGUA GAACGACCAUGGCGAUGAG GGAAGCGUAUCUAUAUCUU UAGAUUACGUGCCCAUGUU	20nM	48-72 hrs	Dharmacon
PLC-γ1 OTP SMARTpool	CUGCUAAGGAGAACGGUGA UCAGAAAGGUGCUUGGCGA GCAAAAUGAAGCUACGCUA GAUCAAGCACUGCCGAGUA	20nM	48-72 hrs	Dharmacon

Table S1. Overview of siRNA smartpools used in this study.

REFERENCE LIST

1. Rosenberg, SA et al. A new approach to the adoptive immunotherapy of cancer with tumor-infiltrating lymphocytes. Science 233, 1318-1321. 1986.
2. Smakman, N et al. Dual effect of Kras(D12) knockdown on tumorigenesis: increased immune-mediated tumor clearance and abrogation of tumor malignancy. Oncogene 24, 8338-8342. 2005.
3. Wang, W et al. The activity status of cofilin is directly related to invasion, intravasation, and metastasis of mammary tumors. J.Cell Biol. 173, 395-404. 2006.
4. van Rheenen, J et al. PIP2 signaling in lipid domains: a critical re-evaluation. EMBO J. 24, 1664-1673. 2005.

PART I | CD95 AND COLORECTAL CANCER

CHAPTER 4

4

How CD95 stimulates invasion

Cell Cycle. 2011 Nov 15;10(22):3857-62

Ernst J. A. Steller, Inne H. M. Borel Rinkes and Onno Kranenburg

Department of Surgery, University Medical Center Utrecht, the Netherlands

ABSTRACT

CD95 is best known for its capacity to induce apoptosis, but also activates multiple non-apoptotic signaling pathways. In particular, CD95 promotes migration and tissue invasion of apoptosis-resistant cell types, and this plays a central role in inflammation, neurobiology, and tumor biology. CD95 induces invasion by stimulating the expression of extracellular matrix (ECM)-degrading proteases, and by stimulating the formation of actin-driven cell protrusions through Rac and the cofilin pathway. In this review we discuss how CD95-initiated signaling pathways may cooperate to facilitate cell migration and tissue invasion.

INTRODUCTION

In 1992 and 1994 it was discovered that mutations in CD95 (Fas/Apo1) and CD95 ligand (Fas ligand/Apo1 ligand) were the underlying cause of the autoimmune lymphoproliferative syndrome (ALPS) in *lpr* and *gld* mice respectively[1,2]. This was due to defective apoptosis signaling in lymphoid cells. Similar apoptosis defects due to mutations in CD95 were found in human ALPS patients[3,4]. Hence, subsequent studies on the CD95 system primarily focused on apoptosis regulation. However, over the years it has become clear that CD95 also activates a number of non-apoptotic signaling pathways (reviewed in[5]). Activation of non-apoptotic signaling cascades by CD95 can result in increased cell proliferation, survival, inflammation, differentiation, migration and invasion[5]. The first indication that CD95 ligand could promote cell migration and tissue invasion came from studies on CD95L-overexpressing tumors and transplanted pancreatic islets. In these studies ectopic expression of CD95L caused infiltration of neutrophils into tumor tissue and into the transplanted islets[6-8]. It was subsequently found that CD95L is a potent chemoattractant for neutrophils and other myeloid cells[9]. Later, it was shown that CD95L promotes migration and invasion of kidney epithelial cells[10] and a variety of apoptosis-resistant tumor cells[11-14].

The signal transduction events that link activated CD95 to increased migration and invasion are beginning to be elucidated. CD95-stimulated invasion requires at least two independent signaling pathways, one leading to increased expression of extracellular matrix-degrading proteases, and the other causing rapid actin-driven formation of cell protrusions. In addition, CD95 also affects factors that are implicated in cell adhesion. In the present report we discuss the sequence of signaling events that promote invasion following activation of CD95.

Increased expression of metalloproteases and uPA

CD95L can be shedded into the circulation following cleavage by metalloproteases[15,16]. Circulating –soluble – CD95L (sCD95L) is unable to induce apoptosis, but activates non-apoptotic pro-tumorigenic signaling pathways[17], including cell migration and invasion[18]. The signaling pathway that leads to apoptosis is initiated by the cytoplasmic 'death domain' (DD) in CD95. By contrast, CD95-induced migration and invasion does not appear to require an intact DD[9,12,19,20]. Nevertheless, in some tumor cell lines invasion signaling by CD95 depends on caspase-8[11] and, by inference, on the DD to which it is recruited.

A general requirement for CD95-induced invasion is the stimulation of tyrosine kinase activity[13,18,21,22]. CD95 is found in a complex with Src-family tyrosine kinases[23], it stimulates tyrosine kinase activity[23,24] and it is phosphorylated on tyrosine itself[25] (reviewed in[26]). In addition to activating tyrosine kinases of the Src family, CD95 also activates the EGFR in hepatocytes and hepatic stellate cells[27], the PDGF receptor in invasion-prone tumor cells[22], and Syk in myeloid cells[21]. How CD95 stimulation leads to tyrosine kinase activation is still largely unclear. Likewise, the exact sequence of tyrosine phosphorylation events downstream of CD95 remains to be established. Regardless of the nature of these initiating events, CD95 activation results in tyrosine phosphorylation of a number of distinct signaling proteins including caspase-8[28], the catalytic subunit of phosphatidylinositol-3-kinase (p110-PI3K)[29], and the scaffold protein TRIP6[19]. Caspase-8 is phosphorylated on tyrosine 380 by c-Src[30]. As such, it is proteolytically inactive, but becomes a docking site for Src homology domain 2 (SH2)-containing proteins, including c-Src itself and the p85 subunit of PI3K[31-33]. In glioma cells, the Src-family kinase Yes and p85-PI3K are recruited into the CD95 complex to mediate PI3K activation. However, the specific tyrosine-phosphorylated docking sites in the CD95 complex were not determined[13]. Yes (but

not caspase-8) was detected in the migration-inducing CD95 complex in lymphocytes and lymphoma cells[18]. This suggests that tyrosine-phosphorylated docking proteins other than caspase-8 may link CD95 to p85 recruitment and PI3K activation. Activation of the PI3K pathway downstream of tyrosine kinase activity appears to be commonly observed following CD95L stimulation and to be essential for CD95-induced (tumor) cell invasion[13,18,21]. Interestingly, activation of PI3K appears to be especially important during the metastatic process[34,35]. The identity of the CD95-activated tyrosine kinase(s) and the specific tyrosine-phosphorylated docking proteins mediating p85 recruitment are likely to be cell type specific.

Active PI3K recruited to the plasmamembrane by the CD95 signaling complex phosphorylates phosphatidylinositol-4,5,-bisphosphate (PIP_2) to generate PIP_3 in the plasmamembrane. PIP_3 recruits PDK1 and Akt in the classical signal transduction pathway that mediates Akt activation in response to growth factor stimulation. Akt phosphorylates several substrates involved in cell cycle progression and survival[36]. Importantly, Akt is a potent inducer of tumor cell invasion by stimulating expression of metalloproteases (MMP's) and urokinase plasminogen activator (uPA) via the transcription factor NFκB[37]. CD95 stimulates expression of MMP's and uPA and this is required for tumor cell migration[11,13,18]. CD95 is a potent stimulator of NFkB, although not exclusively via Akt[11,37-39]. CD95-induced NFκB activation also involves caspase-8, RIP1, and TRAF2, a scaffold for activation of the IκB kinase complex[40-43].

Another pathway linking CD95-stimulated Akt to increased MMP expression involves phosphorylation of glycogen synthase kinase 3 B (GSK3B), which results in GSK3B destruction[13,44]. GSK3B negatively controls Wnt pathway activity by targeting B-catenin for degradation, thereby preventing the activation of TCF/B-catenin (Wnt) target genes. In glioma cells this pathway allows CD95 to promote Wnt-pathway-dependent MMP expression[13]. Indeed, MMP-2, MMP-9, membrane-type MMP, and urokinase plasminogen activator (uPA) have all previously been identified as Wnt target genes[45,46].

CD95 may also affect MMP and/or uPA expression by activating the ERK and JNK mitogen-activated protein kinase pathways. JNK phosphorylates and thereby activates c-Jun, which is part of the AP-1 transcription factor. Interestingly, AP-1 activates expression of several MMP genes[47]. Furthermore, pharmacological inhibition of the ERK-activating kinase MEK reduced CD95-induced uPA gene induction[11].

Together, the data suggest that CD95-stimulated invasion depends on increased expression of uPA and MMP's and that this is due to activation of the Akt, NFκB, Wnt and/or MAPK signaling pathways (Figure 1). The relative contribution of each of these pathways, and the cross-talk between them, may vary from cell type to cell type. How MMP's and uPA contribute to (tumor) cell invasion has been extensively reviewed elsewhere (see for instance[48,49]).

Remodelling of the actin cytoskeleton and formation of cell protrusions

CD95 is constitutively expressed during embryonic neural development and in adult neural progenitor cells. In these cells it stimulates the branching and outgrowth of neurites rather than apoptosis[20,50,51]. The molecular mechanisms driving neurite outgrowth share many features with the mechanisms driving (tumor) cell migration. Both processes are orchestrated by the coordinated activation and inactivation of the Rho family GTPases RhoA, Rac and CDC42[52]. PIP_3 generated by CD95-activated PI3K not only causes activation of Akt (see above) but may also cause mobilization of the Rac-activating exchange factors Vav and Tiam[53]. Rac is a key mediator of cortical actin remodelling downstream of a large variety of migration- and invasion-inducing cytokine and growth factor receptors[54]. Rac promotes the formation of actin-based lamellar cell protrusions which are essential for cell migration[54], for instance during the

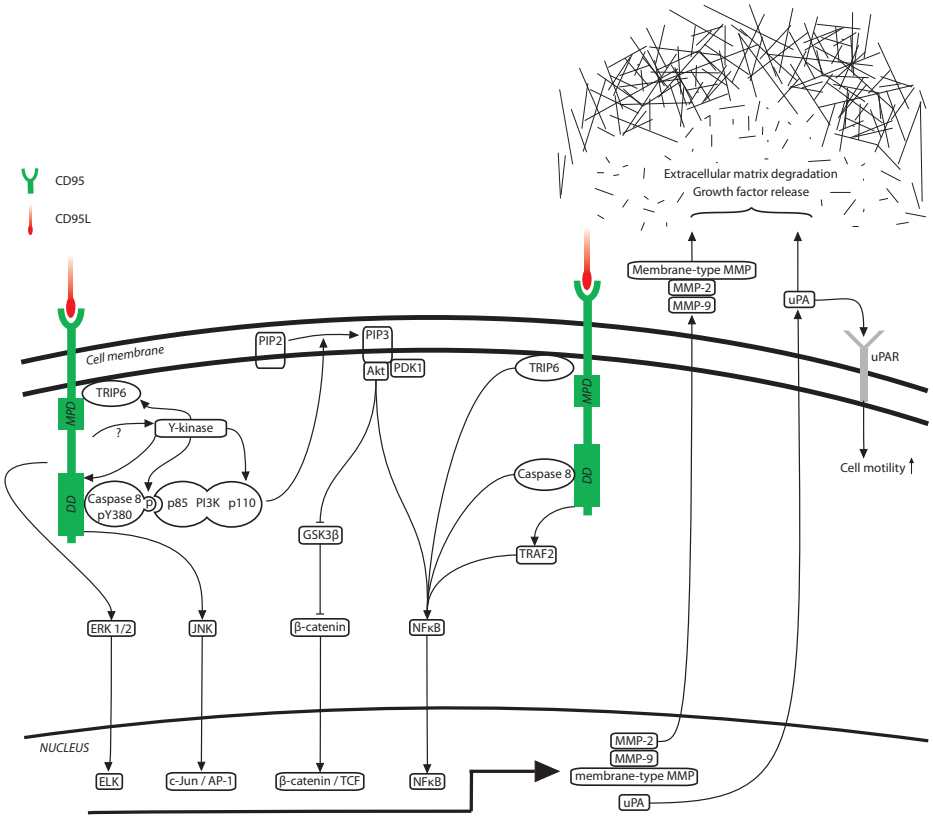

Figure 1. CD95 stimulates expression of extracellular matrix-degrading proteases. CD95 stimulates tyrosine kinase activity via an unknown mechanism. CD95-activated tyrosine kinases include Src-family kinases and tyrosine kinase receptors like PDGFR and EGFR. Active tyrosine kinases phosphorylate docking proteins (caspase-8, TRIP6, others) or serve as tyrsosine-phosphorylated docking sites themselves. PI3K is recruited into the CD95 complex, for instance by binding of the p85-PI3K SH2 domain to tyrosine-phosphorylated caspase-8. Subsequent activation of Akt then promotes activation of the transcription factors NFκB and B-catenin/TCF. TRIP6, caspase-8 and/or TRAF2 have also been implicated in CD95 activation of NFκB. In parallel, CD95 activates the ERK and JNK MAPK pathways, leading to activation of the Elk1 and AP1 transcription factors. Metalloproteases and urokine plasminogen activator (uPA) are among the most prominently upregulated genes in response to CD95 stimulation. These enzymes primarily cause proteolytic processing of extracellular matrix (ECM) components, like laminin, fibrin, and collagen, thus facilitating cell migration through ECM. ECM processing may also lead to the release of invasion-stimulating ECM-bound growth factors and/or ECM fragments.

outgrowth of neurites, the homing of neutrophils to injured tissue and tissue invasion by metastatic cancer cells. CD95L-stimulates Rac activity and this is essential for CD95-induced neurite outgrowth[20]. Interestingly, CD95-induced Rac activation occurs independently of the death domain (DD)[20]. Likewise, CD95-induced tumor cell invasion and neutrophil migration also occur independently of the DD[9,12]. This strongly suggests that the invasion- and apoptosis-promoting signaling pathways already diverge at the level of the receptor.

The signal transduction pathway linking CD95 to Rac activation is currently unknown. A contribution of PI3K-induced recruitment of Vav and/or Tiam seems likely, but has so far not been investigated. CD95 may also stimulate Rac activity via its interaction with Ezrin. A conserved membrane-proximal domain (MPD), but not the death domain, is required for binding of CD95

to Ezrin and for Rac activation[20]. The MPD is located between the transmembrane domain and the death domain. Ezrin can promote activation of Rho GTPases, including Rac, by binding and sequestering RhoGDI[55]. Whether this underlies Rac activation by CD95 is not known.

Rac activates the WAVE complex to stimulate Arp2/3-dependent formation of branched actin networks that drive protrusion of the cell membrane[56,57]. Free actin barbed ends are generated from existing actin filaments by the cofilin family of actin-severing proteins[58]. Actin barbed ends then serve as nucleation points for de novo Rac-stimulated actin polymerization[56,57]. Concomitant activation of the cofilin pathway and Rac results in increased actin 'treadmilling' which is the basis for actin-based cell locomotion[56,57]. Cofilin is normally kept inactive by binding to plasmamembrane PIP_2[59]. CD95 stimulates local plasma membrane PIP_2 hydrolysis which results in activation of the cofilin pathway[22]. This is mediated by CD95-induced activation of the PDGFR and tyrosine phosphorylation (activation) of the PIP_2-hydrolyzing enzyme phospholipase Cγ1 (PLC-γ1)[22]. Indeed, CD95-induced formation of cell protrusions, tumor cell invasion and metastasis formation are cofilin-dependent phenomena[12,22]. Taken together, we propose that activation of the cofilin pathway following CD95 stimulation generates actin barbed ends that serve as nucleation sites for Rac-stimulated cortical actin remodelling (Figure 2). This drives the formation of cell protrusions, which is essential during tumor cell migration, invasion and metastasis.

Integrins and focal adhesions

Interestingly, the CD95 MPD is not only essential for Rac activation, but also for binding to TRIP6, a scaffold protein that promotes focal adhesion turnover and tumor cell invasion[19,60,61]. By binding to the CD95-MPD, TRIP6 also interferes with FADD binding to the death domain[19].

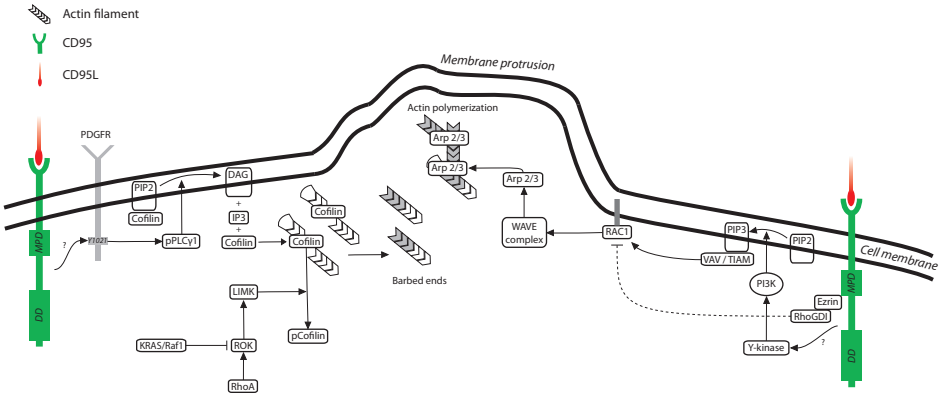

Figure 2. CD95 stimulates the formation of cell protrusions by activating the cofilin pathway and Rac. CD95 promotes tyrosine 1021 (Y1021) phosphorylation of the PDGFR which is the preferred docking site for phospholipase C-γ1 (PLC-γ1). How CD95 stimulates tyrosine kinase activity is not known. PLC-γ1 subsequently hydrolyses phosphatidylinositol-4,5-bisphosphate (PIP_2) in the plasmamembrane, which releases the actin-severing protein cofilin. Active cofilin generates free actin barbed ends which serve as nucleation sites for *de novo* actin polymerization. CD95 also activates the small GTPase Rac via its membrane-proximal domain (MPD). The exact mechanism is not known but may involve sequestration of the Rac exchange factors Vav and/or Tiam following tyrosine kinase-dependent activation of PI3K and generation of PIP_3. In addition, CD95 may sequester RhoGDI via MPD-bound ezrin. CD95-stimulated Rac activates the WAVE complex to promote Arp2/3-dependent actin polymerization and consequent formation of cell protrusions.

Following CD95 stimulation TRIP6 associates with CD95 and is a substrate for Src-mediated tyrosine phosphorylation[19]. This promotes TRIP6 association with focal adhesion molecules such as Crk and p130^{Cas}. By interfering with FADD binding and by stimulating invasion and focal adhesion turnover, TRIP6 could be an important determinant of CD95 signaling output. Furthermore, caspase-8 is part of the focal adhesion complex and promotes adhesion-induced Rac activation and the formation of cell protrusions[62,63]. An intriguing possibility is that CD95 may promote caspase-8 recruitment to focal adhesions, rather than to its own DD.

In addition to stimulating the expression of matrix-remodelling proteases and promoting actin-based cell motility, CD95 also stimulates integrin-dependent cell adhesion. CD95 promotes adhesion of macrophages to ICAM[21], presumably involving the B2 integrin LFA-1[64]. Furthermore, CD95 increases binding of epithelial renal tubular cells to vitronectin by stimulating expression of B8-integrin, and this is required for CD95-stimulated cell migration[10]. The signal transduction pathway(s) coupling activated CD95 to increased integrin expression and cell adhesion are currently unknown, but are likely to play an essential role in CD95-stimulated (tumor) cell invasion.

Concluding Remarks

In apoptosis-resistant cells CD95 promotes tissue invasion and migration by activating specific signaling pathways that promote cell adhesion, remodelling of the extracellular matrix, and the formation of action-based cell protrusions. The signal transduction pathways that link activated CD95 to these phenomena have partly been elucidated. An interesting theme in CD95 invasion signaling is that activation of at least some of these pathways does not require an intact death domain. Further research is required to assess which of the signaling pathway(s) discussed above is/are the predominant force in CD95-stimulated invasion in any given cell type. Furthermore, the transactivation of tyrosine kinases by CD95 is incompletely understood, as is the function of caspase-8. Given the prominent role for CD95 invasion signaling in both inflammation and tumor biology, it is expected that these and other questions will continue to be the topic of intense research over the coming years.

REFERENCE LIST

1. Takahashi, T et al. Generalized lymphoproliferative disease in mice, caused by a point mutation in the Fas ligand. Cell 76, 969-976. 1994.
2. Watanabe-Fukunaga, R et al. Lymphoproliferation disorder in mice explained by defects in Fas antigen that mediates apoptosis. Nature 356, 314-317. 1992.
3. Fisher, GH et al. Dominant interfering Fas gene mutations impair apoptosis in a human autoimmune lymphoproliferative syndrome. Cell 81, 935-946. 1995.
4. Rieux-Laucat, F et al. Mutations in Fas associated with human lymphoproliferative syndrome and autoimmunity. Science 268, 1347-1349. 1995.
5. Peter, ME et al. The CD95 receptor: apoptosis revisited. Cell 129, 447-450. 2007.
6. Allison, J et al. Transgenic expression of CD95 ligand on islet beta cells induces a granulocytic infiltration but does not confer immune privilege upon islet allografts. Proc.Natl.Acad.Sci.U.S.A 94, 3943-3947. 1997.
7. Kang, SM et al. Fas ligand expression in islets of Langerhans does not confer immune privilege and instead targets them for rapid destruction. Nat. Med. 3, 738-743. 1997.
8. Seino, K et al. Antitumor effect of locally produced CD95 ligand. Nat.Med. 3, 165-170. 1997.
9. Seino, K et al. Chemotactic activity of soluble Fas ligand against phagocytes. J.Immunol. 161, 4484-4488. 1998.
10. Jarad, G et al. Fas activation induces renal tubular epithelial cell beta 8 integrin expression and function in the absence of apoptosis. J.Biol.Chem. 277, 47826-47833. 2002.
11. Barnhart, BC et al. CD95 ligand induces motility and invasiveness of apoptosis-resistant tumor cells. EMBO J. 23, 3175-3185. 2004.
12. Hoogwater, FJ et al. Oncogenic K-Ras turns death receptors into metastasis-promoting receptors in human and mouse colorectal cancer cells. Gastroenterology 138, 2357-2367. 2010.
13. Kleber, S et al. Yes and PI3K bind CD95 to signal invasion of glioblastoma. Cancer Cell 13, 235-248. 2008.
14. Nijkamp, MW et al. CD95 is a key mediator of invasion and accelerated outgrowth of mouse colorectal liver metastases following radiofrequency ablation. J.Hepatol. 53, 1069-1077. 2010.
15. Kayagaki, N et al. Metalloproteinase-mediated release of human Fas ligand. J.Exp.Med. 182, 1777-1783. 1995.
16. Tanaka, M et al. Expression of the functional soluble form of human fas ligand in activated lymphocytes. EMBO J. 14, 1129-1135. 1995.
17. O' Reilly, LA et al. Membrane-bound Fas ligand only is essential for Fas-induced apoptosis. Nature 461, 659-663. 2009.
18. Tauzin, S et al. The naturally processed CD95L elicits a c-yes/calcium/PI3K-driven cell migration pathway. PLoS.Biol. 9, e1001090. 2011.
19. Lai, YJ et al. The adaptor protein TRIP6 antagonizes Fas-induced apoptosis but promotes its effect on cell migration. Mol.Cell Biol. 30, 5582-5596. 2010.
20. Ruan, W et al. A novel juxtamembrane domain in tumor necrosis factor receptor superfamily molecules activates Rac1 and controls neurite growth. Mol.Biol.Cell 19, 3192-3202. 2008.
21. Letellier, E et al. CD95-ligand on peripheral myeloid cells activates Syk kinase to trigger their recruitment to the inflammatory site. Immunity. 32, 240-252. 2010.
22. Steller, EJ et al. The death receptor CD95 activates the cofilin pathway to stimulate tumour cell invasion. EMBO Rep. 12, 931-937. 2011.
23. Atkinson, EA et al. A physical interaction between the cell death protein Fas and the tyrosine kinase p59fynT. J.Biol.Chem. 271, 5968-5971. 1996.
24. Schlottmann, KE et al. Activation of Src-family tyrosine kinases during Fas-induced apoptosis. J. Leukoc.Biol. 60, 546-554. 1996.
25. Daigle, I et al. Death receptors bind SHP-1 and block cytokine-induced anti-apoptotic signaling in neutrophils. Nat.Med. 8, 61-67. 2002.
26. Sancho-Martinez, I et al. Tyrosine phosphorylation and CD95: a FAScinating switch. Cell Cycle 8, 838-842. 2009.
27. Reinehr, R et al. CD95 ligand is a proliferative and antiapoptotic signal in quiescent hepatic stellate cells. Gastroenterology 134, 1494-1506. 2008.
28. Cursi, S et al. Src kinase phosphorylates Caspase-8 on Tyr380: a novel mechanism of apoptosis suppression. EMBO J. 25, 1895-1905. 2006.
29. Gulbins, E et al. Cellular stimulation via CD95 involves activation of phospho-inositide-3-kinase. Pflugers Arch. 435, 546-554. 1998.
30. Stupack, DG. Caspase-8 as a therapeutic target in cancer. Cancer Lett. 2010.
31. Barbero, S et al. Identification of a critical tyrosine residue in caspase 8 that promotes cell migration. J.Biol.Chem. 283, 13031-13034. 2008.
32. Finlay, D et al. Critical role for caspase-8 in epidermal growth factor signaling. Cancer Res. 69, 5023-5029. 2009.
33. Senft, J et al. Caspase-8 interacts with the p85 subunit of phosphatidylinositol 3-kinase to regulate cell adhesion and motility. Cancer Res. 67, 11505-11509. 2007.
34. Schmidt-Kittler, O et al. PI3Kalpha inhibitors that inhibit metastasis. Oncotarget. 1, 339-348. 2010.
35. Zawel, L. P3Kalpha: a driver of tumor metastasis?. Oncotarget. 1, 315-316. 2010.
36. Fresno Vara, JA et al. PI3K/Akt signaling pathway and cancer. Cancer Treat.Rev. 30, 193-204. 2004.
37. Kim, D et al. Akt/PKB promotes cancer cell invasion via increased motility and metalloproteinase production. FASEB J. 15, 1953-1962. 2001.
38. Legembre, P et al. The relevance of NF-kappaB for CD95 signaling in tumor cells. Cell Cycle 3, 1235-1239. 2004.
39. Naugler, WE et al. NF-kappaB and cancer-identifying targets and mechanisms. Curr.Opin. Genet.Dev. 18, 19-26. 2008.
40. Geserick, P et al. RIP-in CD95-induced cell death:

The control of alternative death receptors pathways by cIAPs. Cell Cycle 9, 2689-2691. 2010.
41. Kreuz, S et al. NFkappaB activation by Fas is mediated through FADD, caspase-8, and RIP and is inhibited by FLIP. J.Cell Biol. 166, 369-380. 2004.
42. Maelfait, J et al. Non-apoptotic functions of caspase-8. Biochem.Pharmacol. 76, 1365-1373. 2008.
43. Trauzold, A et al. CD95 and TRAF2 promote invasiveness of pancreatic cancer cells. FASEB J. 19, 620-622. 2005.
44. Cross, DA et al. Inhibition of glycogen synthase kinase-3 by insulin mediated by protein kinase B. Nature 378, 785-789. 1995.
45. Neth, P et al. Wnt signaling regulates the invasion capacity of human mesenchymal stem cells. Stem Cells 24, 1892-1903. 2006.
46. Wu, B et al. Wnt signaling induces matrix metalloproteinase expression and regulates T cell transmigration. Immunity. 26, 227-239. 2007.
47. Reuben, PM et al. Regulation of matrix metalloproteinase (MMP) gene expression by protein kinases. Front Biosci. 11, 1199-1215. 2006.
48. Kessenbrock, K et al. Matrix metalloproteinases: regulators of the tumor microenvironment. Cell 141, 52-67. 2010.
49. McMahon, B et al. The plasminogen activator system and cancer. Pathophysiol.Haemost. Thromb. 36, 184-194. 2008.
50. Desbarats, J et al. Fas engagement induces neurite growth through ERK activation and p35 upregulation. Nat.Cell Biol. 5, 118-125. 2003.
51. Zuliani, C et al. Control of neuronal branching by the death receptor CD95 (Fas/Apo-1). Cell Death. Differ. 13, 31-40. 2006.
52. von Philipsborn, A et al. Mechanisms of gradient detection: a comparison of axon pathfinding with eukaryotic cell migration. Int.Rev.Cytol. 263, 1-62. 2007.
53. Rivard, N. Phosphatidylinositol 3-kinase: a key regulator in adherens junction formation and function. Front Biosci. 14, 510-522. 2009.
54. Hall, A. Rho GTPases and the control of cell behaviour. Biochem.Soc.Trans. 33, 891-895. 2005.
55. Takahashi, K et al. Direct interaction of the Rho GDP dissociation inhibitor with ezrin/radixin/moesin initiates the activation of the Rho small G protein. J.Biol.Chem. 272, 23371-23375. 1997.
56. Derivery, E et al. Generation of branched actin networks: assembly and regulation of the N-WASP and WAVE molecular machines. Bioessays 32, 119-131. 2010.
57. Le, CC et al. Regulation of actin assembly associated with protrusion and adhesion in cell migration. Physiol Rev. 88, 489-513. 2008.
58. van Rheenen, J et al. A common cofilin activity cycle in invasive tumor cells and inflammatory cells. J.Cell Sci. 122, 305-311. 2009.
59. van Rheenen, J et al. EGF-induced PIP2 hydrolysis releases and activates cofilin locally in carcinoma cells. J.Cell Biol. 179, 1247-1259. 2007.
60. Lai, YJ et al. c-Src-mediated phosphorylation of TRIP6 regulates its function in lysophosphatidic acid-induced cell migration. Mol.Cell Biol. 25, 5859-5868. 2005.
61. Takizawa, N et al. Supervillin modulation of focal adhesions involving TRIP6/ZRP-1. J.Cell Biol. 174, 447-458. 2006.
62. Barbero, S et al. Caspase-8 association with the focal adhesion complex promotes tumor cell migration and metastasis. Cancer Res. 69, 3755-3763. 2009.
63. Helfer, B et al. Caspase-8 promotes cell motility and calpain activity under nonapoptotic conditions. Cancer Res. 66, 4273-4278. 2006.
64. Long, EO. ICAM-1: getting a grip on leukocyte adhesion. J.Immunol. 186, 5021-5023. 2011.

PART I | CD95 AND COLORECTAL CANCER

CHAPTER 5

5

PDGFRB promotes liver metastasis formation of mesenchymal-like colorectal tumor cells

Neoplasia. 2013 Feb;15(2):204-17

Ernst J.A. Steller [1], Danielle A. Raats [1], Jan Koster [4], Bert Rutten [2], Klaas M. Govaert [1], Benjamin L. Emmink [1], Nikol Snoeren [1], Sander R van Hooff [3], Frank CP Holstege [3], Coen Maas [2], Inne H.M. Borel Rinkes [1], Onno Kranenburg[1]

[1] Department of Surgery, University Medical Center Utrecht, the Netherland
[2] Department of Haematology, University Medical Center Utrecht, the Netherlands
[3] Department of Molecular Cancer Research, University Medical Center Utrecht, the Netherlands
[4] Department of Oncogenomics, Academic Medical Center Amsterdam, the Netherlands

ABSTRACT

In epithelial tumors the PDGF Receptor B (PDGFRB) is mainly expressed by stromal cells of mesenchymal origin. Tumor cells may also acquire PDGFRB expression following epithelial-to-mesenchymal transition (EMT), which occurs during metastasis formation. Little is known about PDGFRB signaling in colorectal tumor cells. We studied the relationship between PDGFRB expression, EMT and metastasis in human colorectal cancer (CRC) cohorts by analysis of gene expression profiles. PDGFRB expression in primary CRC was correlated with short disease-free and overall survival. PDGFRB was co-expressed with genes involved in platelet activation, TGFB signaling and EMT in three CRC cohorts. PDGFRB was expressed in mesenchymal-like tumor cell lines *in vitro* and stimulated invasion and liver metastasis formation in mice. Platelets, a major source of PDGF, preferentially bound to tumor cells in a non-activated state. Platelet activation caused robust PDGFRB tyrosine phosphorylation on tumor cells *in vitro* and in liver sinusoids *in vivo*. Platelets also release TGFB, which is a potent inducer of EMT. Inhibition of TGFB signaling in tumor cells caused partial reversion of the mesenchymal phenotype and strongly reduced PDGFRB expression and PDGF-stimulated tumor cell invasion. These results suggest that PDGFRB may contribute to the aggressive phenotype of colorectal tumors with mesenchymal properties, most likely downstream of platelet activation and TGFB signaling.

INTRODUCTION

Multiple receptor tyrosine kinases (RTKs) and their growth factor ligands have been implicated in cancer progression and metastasis. Among these are the platelet-derived growth factor receptors (PDGFRs)[1]. Stimulation of the PDGFR leads to activation of intracellular signaling pathways which can promote cell migration, invasion, survival, and proliferation[2,3].
Expression of PDGFRs is mainly restricted to mesenchymal cell types[2]. Activating mutations in PDGFRs are found in gastrointestinal stromal tumors[1]. In colorectal carcinomas PDGFR expression appears to be mainly expressed by stromal cells and pericytes[4,5]. However, PDGFRB can also be expressed by colorectal tumor cell lines[3,6], similar to the mesenchymal marker vimentin[7]. We have recently shown that PDGFRB primarily signals invasion in colorectal tumor cells[3]. In line with this, PDGFR signaling contributes to the aggressive behavior of other epithelial tumor types such as breast, liver and pancreas carcinomas[8-10]. High PDGFR expression correlates with advanced stage disease and poor prognosis in all these tumor types[6,8-11].
While most epithelial tumor cells do not express PDGFRs, they may acquire PDGFR expression following epithelial-to-mesenchymal transition (EMT)[12-19]. EMT is thought to contribute to metastasis formation in multiple tumor types by generating tumor cells with decreased cell-cell adhesion and enhanced invasive and clonogenic properties[20]. In breast cancer, circulating tumor cells with a mesenchymal-like phenotype are associated with poor survival[21-23]. Breast and lung cancer cells acquire PDGFR expression following EMT which is essential for their metastatic potential[18,24]. A prominent inducer of EMT is transforming growth factor beta (TGFB)[20]. Recently, it was shown that TGFB stimulation of colorectal cancer cells promotes invasive mesenchymal-like growth of murine colorectal tumor cells and increased metastatic capacity[25]. A potential role for the PDGFR was not investigated in that study. Taken together, the above studies suggest that PDGFR expression, like EMT, could be a transient phenomenon that may facilitate the metastatic process. This could play a role at the primary tumor site, but also in the circulation and/or at the secondary organ site.
Disseminated tumor cells are surrounded by platelets, which are a major source of PDGF[2]. Tumor cell-associated platelet aggregation and micro-thrombus formation occurs when tumor cells get trapped in the microvasculature of the distant organ[26-30]. This can be mediated by cancer-specific mucins which contain multiple binding sites for platelets, leukocytes and endothelial cells[31]. Once activated, platelets promote metastasis formation by releasing specific growth factors, including LPA and TGFB[25,32-34]. In line with their prominent pro-metastatic activity, high platelet counts are associated with poor prognosis in many cancer types, including colorectal cancer[32,35,36].
In the present report we show that PDGFRB expression in human colorectal cancer is strongly correlated with platelet activation, TGFB signaling and EMT. We also show that PDGFRB signaling in mesenchymal-like tumor cells contributes to invasion and liver metastasis formation.

MATERIALS AND METHODS

Bioinformatic analyses
Most analyses were performed using the R2 microarray analysis and visualization platform. (http://r2.amc.nl). Expression of PDGFR and EGFR across datasets was done by choosing the 'Megasampler' option in R2 and selecting all 9 colorectal tumor datasets.

Disease-free survival (DFS) data are available for three of the datasets (Jorissen[37], Smith[38], Snoeren[39]). In addition, two datasets contain overall survival (OS) data (Smith, Snoeren). The association of PDGFRB expression with DFS and OS was determined by using the Kaplan Meijer option in R2. Median PDGFR expression levels were used as cutoff values. P values were determined by logrank test as described in Bewick *et al*[40].
KEGG pathway analysis was performed by choosing the 'KEGG Pathway Finder' option and setting the single gene association (Pearson correlation) p values to <e-10 (p value determined by t=r/sqrt((1-r^2)/(n-2)), distributed approximately as t with n-2 degrees of freedom) for each of the three datasets. The KEGG pathways that were significantly ($p<0.01$ chi square goodness of fit test) enriched in at least 2 out of 3 lists of PDGFR-associated genes were then identified and ordered according to significance, based on the combined p values (Stouffers z-trend) which were calculated with the web-based MetaP application (http://people.genome.duke.edu/~dg48/metap.php). A similar approach was used to identify Gene Ontology terms significantly enriched in the sets of PDGFR-associated genes. Here the p values for single gene associations was set to <e-7 for each dataset.
Genes that were significantly associated with PDGFRB within each of the identified KEGG pathways ($p<0.01$; chi square goodness of fit test) were identified by making use of the KEGG pathway gene filter option in R2. GeneVenn was then used to identify subsets of genes showing significant association with PDGFR expression in at least 2/3 datasets. The functional interconnectivity between the genes in these lists was visualized using the STRING tool for known and predicted protein-protein interactions (www.string-db.org). The lists were re-imported into R2 to generate heatmaps in which the tumors were ordered according to PDGFR expression levels from low to high using the largest dataset available (Jorissen; 290 tumors).
All human experiments were carried out with informed consent of the volunteers and under approval and accordance with the guidelines of the Medical Ethical Committee of the University Medical Center Utrecht, The Netherlands.

Cell culture

C26 and MC38 murine colorectal tumor cells cultured in Dulbecco's Modified Eagle's Medium (DMEM; Dulbecco, ICM Pharmaceuticals, Costa Mesa, CA) supplemented with 5% (v/v) fetal calf serum, 2mM ultraglutamine, 0.3 mg/ml streptomycin, and 100 U/ml penicillin. Cells were kept at 37°C in a humidified atmosphere containing 5% CO_2.
C26 luciferase were described before[41]. C26GFP and MC38GFP cell lines were generated by lentiviral transduction using pWPT-GFP (a kind gift from D. Trono).

Antibodies and reagents

The following antibodies were obtained from Cell Signaling Technology Inc.: rabbit pY1021-PDGFRB (#2227), rabbit PDGFRB (#4564). From BD pharmingen: PE-Cy5 mouse CD42b (551141), PE mouse P-selectin (Cd62P) (#555524), rat CD41 (#553847), mouse N-cadherin (#610920), mouse Fibronectin (#610077), rabbit active caspase 3 (#559565). From Santa Cruz Biotechnology Inc.: rabbit pY1021-PDGFRB (sc-12909-R) and from Thermo Fisher Scientific: rabbit KI67 (rm-9106-s). From Sigma–Aldrich: PDGFRB (HPA028499). From Emfret Analytics: rat anti-mouse P-selectin (#M130-2). Secondary peroxidase-conjugated antibodies were from Dako. The following reagents were used in this study: PDGF-BB Invitrogen (PGM0044), TGF-B1 Sigma Aldrich (H8541), Thrombin-receptor activating peptide (TRAP, SFLLRN) Bachem AG, PGI2 analog iloprost (ilomedine (R)) Bayer Schering Pharma AG, collagen-related peptide (CRP) was generated as described earlier[42], SB431524 Sigma Aldrich (#S4317). siRNA OTP SMARTpools

from Dharmacon were transfected using reverse transfection with Hiperfect (Qiagen) according to the manufacturers' guidelines. Gene names and siRNA sequences of the siRNA library are listed in supplementary material Figure S4C.

Platelet isolation
Human platelets were isolated as previously described[43]. In short, fresh whole blood was drawn from healthy volunteers into 3,2% tri-sodium citrate tubes (Greiner Bio-One B.V.). Platelet-rich-plasma (PRP) was prepared within 1 hour after collection by centrifugation at 160xg for 15 minutes at 20°C. Subsequently, 0.1 volume of acid-citrate dextrose (ACD) (containing 2.5% trisodium citrate, 1.5% citric acid and 2% D-glucose) was added to lower the pH to 6.5. PRP was spun down by centrifugation at 340xg for 15 minutes at 20°C. The platelet pellet was resuspended in Hepes-Tyrode buffer (containing 145 mmol/L NaCl, 5 mmol/L KCl, 0.5 mmol/L Na2HPO4, 1 mmol/L MgSO4, 10 mmol/L Hepes, 5 mmol/L Dglucose, pH 6.5). Prostacyclin (PGI2) (Cayman Chemical) was added to a final concentration of 10ng/ml and platelets were spun down at 340xg for 15 minutes at 20°C. The pellet was resuspended in Hepes-Tyrode buffer pH 7.2 at a platelet count of 2.0 x 10^{11} platelets/L. Platelets were allowed to return to a resting state for at least 30 minutes prior to usage.

Tumor cell platelet binding
GFP expressing tumor cells were harvested by brief trypsinization, washed and suspended in Hepes-Tyrode buffer to a final concentration of 1x10^5 cells/ml. In order to exclude clumps of cells the mixture was passed through a 40µm cell strainer. Tumor cells and platelets were mixed in a 1:10 ratio and incubated for 30 min at room temperature. Hereafter blocking was performed with FCS after which cells were washed with Hepes-Tyrode buffer by centrifugation at 400G for 10 minutes. Antibody binding (1:50) was allowed in Hepes-Tyrode buffer. After 30 min at room temperature the cell platelet suspension was washed and resuspended in Hepes-Tyrode buffer containing 2% formaldehyde. Cells were analyzed using flow cytometry.

Flow cytometry
The expression of a panel of cell surface markers was analyzed using a FACScalibur (BD Biosciences). All antibody incubation steps were carried out at room temperature. GFP expressing tumor cells were used and selected on fluorescent intensity. Doublets and clumps of tumor cells were excluded by size using doublet discrimination gating. For analysis of inactive platelets PE-Cy5 anti-CD42b was used. For analysis of active platelets PE anti-P-selectin was used as a marker. All samples were analysed by bivariate flow cytometry using Cell Quest software (Becton Dickinson).

Western blotting Western blotting was performed exactly as described before[41,44].

Invasion assay
For *in vitro* invasion assay's 24-well BioCoat Matrigel invasion chambers (#354480, BD Biosciences), with an 8-µm pore PET membrane coated with Matrigel basement membrane matrix, were used according to the manufacture's protocol. Cells were kept under serum free conditions overnight. In the upper compartment, 5 x 10^4 cells/well were plated in 0.5 ml serum-free medium. The lower compartment contained 0.75 ml medium with 0% FCS. PDGF (10 ng/ml) was added to the upper and/or lower compartment. For inhibitor experiments cells were pretreated with 10 µg/ml SB431524 overnight before plating and during the experiment in both

the upper and lower compartment. Invasion chambers were incubated for 8 hrs at 37°C in a humidified incubator with 5% CO_2. Remaining cells in the upper compartment were removed with a cotton swap. The transmigrated cells were fixed in formaldehyde 3.7% and stained with DAPI and were counted by analyzing microscopic images (5-6 fields per transwell membrane, magnification 10x). Data are expressed relative to control. All assays were performed in duplicate and were repeated twice.

In vitro proliferation assay

Cells (5000 cells/96-well) were plated and incubated at 37°C in a humidified atmosphere containing 5% CO_2. Proliferation was analyzed every 24hrs for 4 days by 3-(4,5 dimethylthiazolyl-2)-2,5-diphenyltetrazoleumbromide (MTT) assays (Roche Diagnostics) according to the manufacturer's instructions.

Immunohistochemistry

After harvesting, organs were either snap frozen in Tissue-Tek OCT using liquid nitrogen or fixed in 4% PFA and paraffin embedded. Frozen tissue was sectioned using a Leica cryotome CM 3050 (Mannheim, Germany), fixed with acetone, and an immunostaining was performed. Paraffin embedded tissues were sectioned by a Leica microtome RM 2235 (Mannheim, Germany) and stained according to standard histology protocols. For immunofluorescence, image acquisition and analysis was performed using a Zeiss Axiovert 200M and Zeiss LSM 510 Software.

Animals and surgery

Male Balb/c mice (10-12 weeks) were purchased from Charles River. Mice were housed under standard laboratory conditions and received food and water ad libitum. All surgical procedures were performed under isoflurane inhalation anesthesia. Prior to surgery, buprenorfine was administered intramuscularly to provide sufficient peri-operative analgesia. All animal experiments were carried out in accordance with the guidelines of the Animal Welfare Committee of the University Medical Center Utrecht, The Netherlands.

Liver metastasis mouse model

C26 cells expressing GFP- or luciferase were harvested by brief trypsinization. Colorectal liver metastases were induced as previously described[45,46]. In brief, single cell suspensions were prepared in phosphate-buffered saline to a final concentration of 7.5 x 10^4 cells/100 µl. Cells were injected into the parenchyma of the spleen. Ten minutes after injection, the spleen was removed. Induction and bioluminescence imaging of colorectal liver metastases was performed as described[41].

Hepatic Replacement Area

Tumor load in the liver was assessed in all liver lobes. Tumor load was scored as hepatic replacement area (HRA), that is, the percentage of liver tissue that had been replaced by tumor tissue, exactly as described before[47].

In brief, on hematoxylin and eosin (H&E) stained sections, at least 100 fields were selected using an interactive video overlay system, including an automated microscope (Q-Prodit; Leica Microsystems) at a 40x magnification. Using a four-point grid overlay, the ratio of tumor cells versus normal hepatocytes was determined for each field. Tumor load (HRA) was expressed as the average area ratio of all fields.

Statistical analysis Statistical differences between groups were analyzed by an unpaired two sided t-test. Data are expressed as mean ± SEM. A p-value of <0.05 was considered statistically significant (* < 0.05).

RESULTS

PDGFRB expression in primary CRC is associated with poor prognosis

Our previous results have implicated PDGFR signaling in the invasion of colorectal tumor cells *in vitro*[3]. Very little is known about the impact of PDGFR signaling on human colorectal tumor behavior. We first analyzed gene expression profiles of 9 different tumor cohorts to assess whether PDGFRB expression would be associated with clinical outcome. Figure 1A shows that PDGFRB and EGFR are expressed at considerable levels in colorectal tumors, although a direct comparison of the expression levels of both RTKs is not possible based on microarray data. One cohort of colorectal adenomas (T Colon 32 (Marra)) shows considerable less expression of PDGFRB. Immunohistochemistry staining for PDGFRB in colorectal cancer specimens demonstrated the expected stromal staining (Figure 1B). In addition, PDGFRB expression was also clearly observed in the tumor cells of 8/10 human CRC tumors (Figure 1B, Figure S1). We next assessed whether PDGFRB expression was correlated with survival in two cohorts of 232 and 290 primary CRC tumors[37,38] and a cohort of 119 liver metastases[39]. Using mean PDGFR levels as the cut-off value, we found that high PDGFRB expression in primary CRC tumors was correlated with shorter disease-free and overall survival (Figure 2A, B). This was not observed in liver metastases (Figure 2C).

PDGFRB expression is associated with ECM-receptor signaling, platelet activation, TGFB signaling and EMT

We next used bioinformatics tools of the R2 web application (http://r2.amc.nl) to search for processes, pathways and single genes associated with expression of PDGFRB in CRC. Searching the Kyoto Encyclopedia of Genes and Genomes (KEGG) pathway database revealed 7 pathways that were significantly associated with PDGFRB expression in the three separate tumor cohorts (Table 1). These include 'Extracellular Matrix-Receptor Interaction', 'Coagulation' and 'TGFB signaling'. Within the 'ECM-Receptor' pathway 46 genes were significantly correlated with PDGFRB in at least two out of three tumor cohorts (Figure S2A; p=6.7E-76). This gene set contains 15 collagens, 6 laminins, 8 integrins and 4 thrombospondins (Table S1; Figure S2A). All of the genes in this category were positively (rather than negatively) correlated with PDGFRB expression (Figure 3).

We noted that many of the genes within the ECM-Receptor class promote platelet activation, including collagens, laminins, thrombospondins, von Willebrand Factor and fibronectin (Table S1). Gene Ontology analysis of the genes co-expressed with PDGFRB in the separate tumor cohorts revealed that 'Platelet Activation', 'Platelet alpha-granule' and 'Platelet Degranulation' were indeed significantly overrepresented in all three cohorts (Table 1; p=1.9E-23). We identified a set of 41 'Platelet activation' genes which were significantly correlated with PDGFR expression in at least two out of three tumor cohorts. All of these correlations were positive (Table S1; Figure S2B). In addition, all except one (ALDOA) 'Platelet alpha-granule' genes were positively correlated with PDGFRB expression (Figure 3).

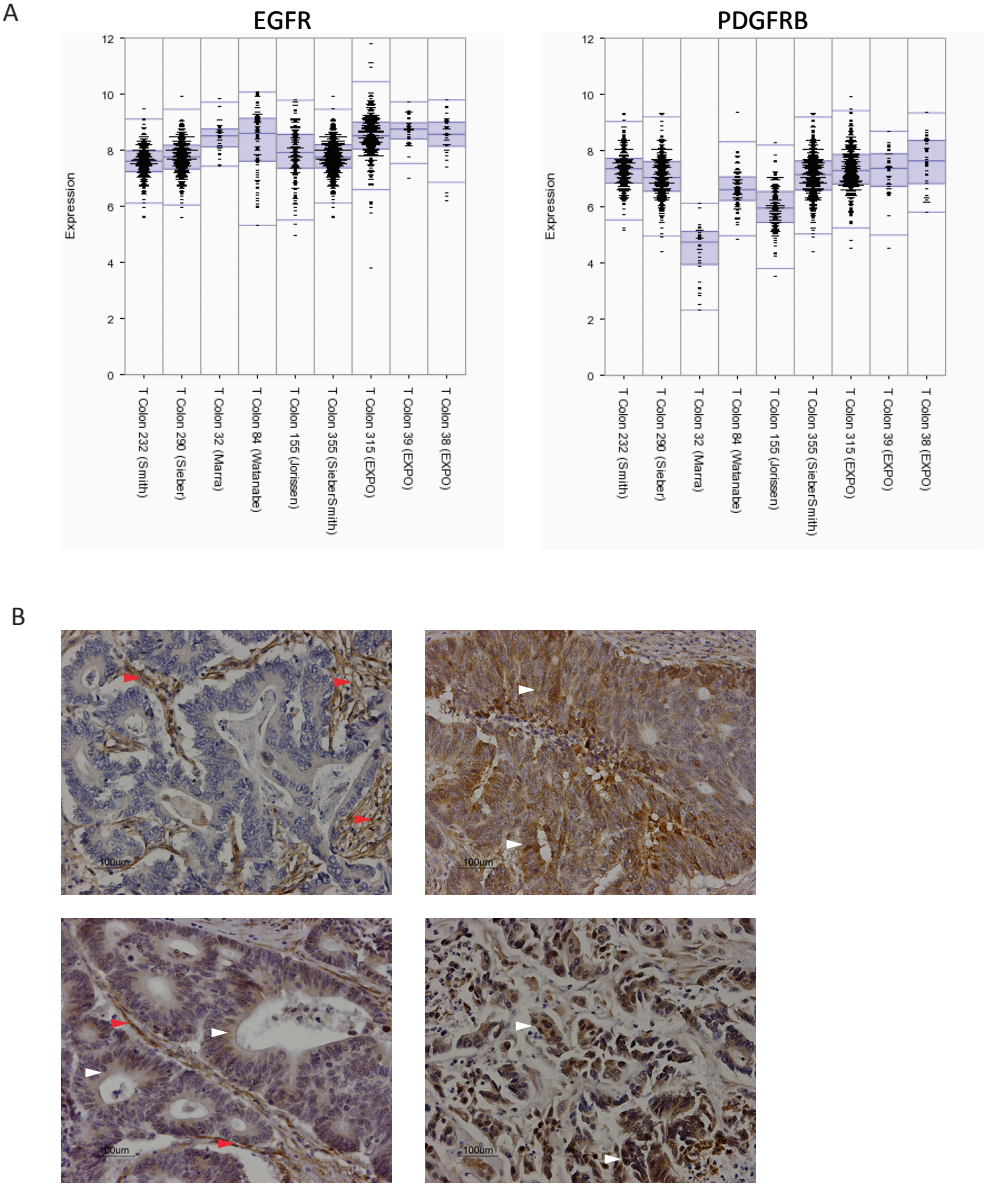

Figure 1. Expression of PDGFRB in human CRC.
A. mRNA levels of PDGFRB and EGFR of all tumors from 9 different cohorts were plotted. With the exception of one adenoma cohort, PDGFRB is expressed at considerable levels in multiple CRC cohorts. **B.** Immunohistochemistry analysis of the expression of PDGFRB in human colorectal tumors. Examples of tumors are shown in which PDGFRB is predominantly expressed in stromal cells (left upper panel) in both tumor cell and stromal compartments (left lower panel) and in tumor cells only (right upper and lower panels). Red arrowheads indicate expression in stromal tissue. White arrowheads indicate expression in tumor tissue.

Platelet activation promotes the metastatic capacity of tumor cells[32]. TGFB signaling has recently been identified as a major platelet-released pro-metastatic growth factor in a model of colorectal metastasis formation[25]. TGFB signaling was also one of the 7 KEGG pathways that were significantly associated with PDGFRB expression in all three tumor cohorts (Table 1; Table S1; Figure S2C; p=1.2E-8). A set of 28 overlapping 'TGFB pathway genes' was identified of which 22 were positively correlated with PDGFRB, including TGFB1, TGFB2, TGFB3 and TGFB-receptor 1 (TGFBR1). Mapping the PDGFRB-co-expressed genes on a TGFB pathway image shows enrichment of ligands, receptors, and signaling intermediates (Figure S3).

TGFB stimulation of epithelial tumor cells may lead to the acquisition of a more mesenchymal phenotype, which is associated with increased invasion and metastatic potential. Moreover, activated platelets promote EMT in tumor cells by secreting TGFB[25] which stimulates expression of the core transcription factors that mediate EMT (SNAI1, SNAI2, ZEB1, ZEB2, TWIST1 and TWIST2;[48]). Therefore, we next analyzed whether PDGFRB expression would be associated with these EMT-driving transcription factors. Indeed, PDGFRB was strongly associated with all 6 EMT-inducing transcription factors and with mesenchymal genes, such as vimentin and N-cadherin (CDH2) (Table S1; Figure 3). Conversely, PDGFRB was negatively correlated with epithelial genes, including E-cadherin (CDH1), Plakophilin-2 and Occludin (Table S1).

KEGG pathway	p value Snoeren	p value Smith	p value Jorissen	p value combined
ECM-receptor interaction	4,20E-12	3,90E-32	8,10E-15	3,33E-50
Focal adhesion	2,20E-10	5,70E-24	5,40E-11	1,42E-37
Malaria	7,90E-05	3,30E-15	5,40E-08	3,07E-23
Complement and coagulation cascades	1,30E-04	1,50E-08	7,10E-06	3,56E-15
Glycosaminoglycan biosynthesis	2,00E-02	2,80E-09	6,40E-06	2,97E-14
Amoebiasis	7,50E-05	1,10E-10	1,30E-03	1,08E-13
Phagosome	1,00E-02	1,00E-08	1,20E-04	1,76E-12
Leukocyte transendothelial migration	2,00E-02	1,50E-06	1,90E-05	1,47E-11
Cell adhesion molecules	4,00E-02	1,10E-04	1,50E-03	1,25E-07
Regulation of actin cytoskeleton	3,00E-02	1,10E-04	7,30E-03	7,23E-07
Vascular smooth muscle contraction	2,00E-03	5,40E-03	2,00E-02	1,54E-05
TGF-beta signaling pathway	4,40E-05	4,60E-03	7,00E-02	1,95E-05
GO pathway				
ECM	8.9E-44	1.4E-98	6.8E-27	5.2E-135
PDGF binding	2.7E-22	2.3E-18	4.5E-8	2.7E-34
Platelet activation	7.2E-9	5.1E-10	1.2E-9	1.9E-23
Platelet a-granule	2.2E-6	3.7E-13	1.2E-6	7.2E-21
Platelet degranulation	2.9E-3	3.8E-10	2.4E-9	1.2E-19
TGF-beta signaling pathway	4.4E-6	4.1E-4		1.7E-7

Table 1. Pathway analysis of genes co-expressed with PDGFRB in CRC.
PDGFRB-associated genes in each separate tumor cohort were analyzed for overrepresentation of KEGG pathways and GO terms by using R2. All KEGG pathways significantly associated with PDGFRB expression in at least 2 out of 3 datasets are shown. A limited set of GO terms that are related to those KEGG pathways is shown in addition. Combined p-values were calculated with the web-based MetaP software.

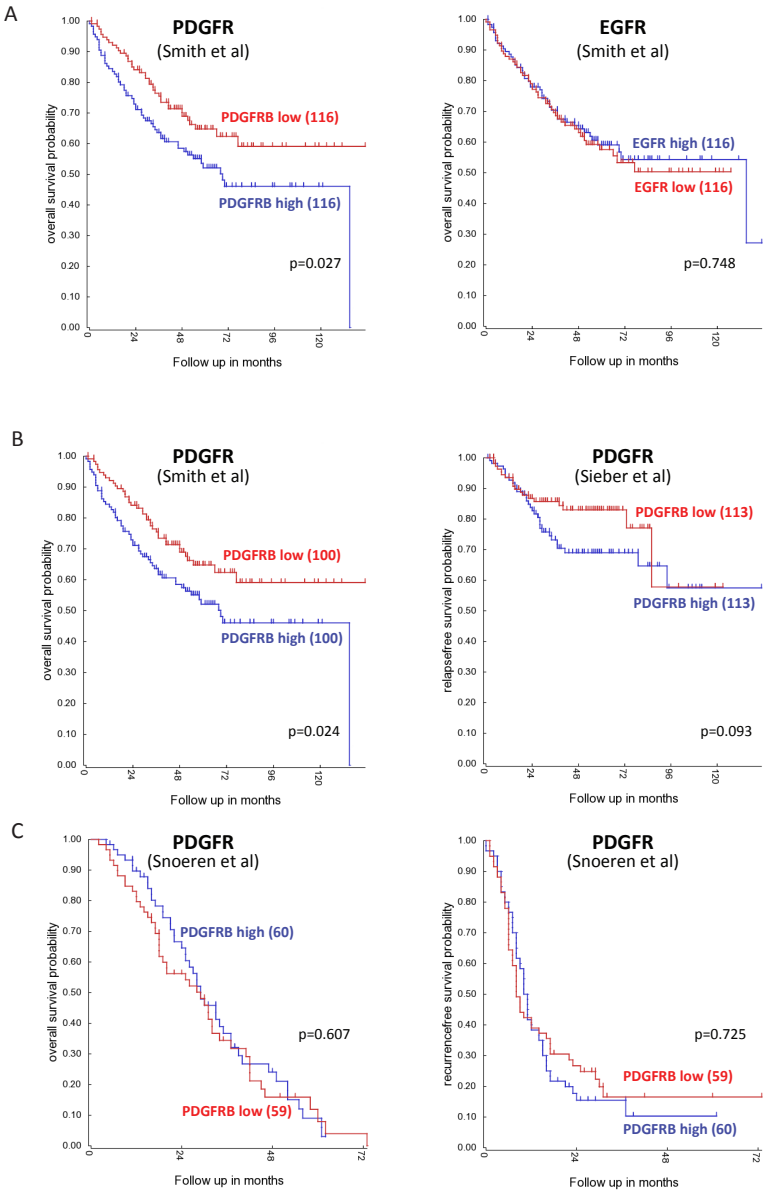

Figure 2. PDGFRB expression in primary CRC is associated with shorter disease-free and overall survival.
A. Expression levels of PDGFRB and EGFR were correlated with overall survival in a cohort of 232 primary CRC[38]. Median expression was used as a cutoff. Kaplan Meier curves show that expression of PDGFRB, but not EGFR, is associated with a significantly shorter overall survival. **B.** Expression levels of PDGFRB were correlated with disease-free survival in a cohort of 232 primary CRC[38] and a cohort of 290 primary CRC[37]. Median expression was used as a cutoff. Kaplan Meier curves show that expression of PDGFRB is associated with shorter disease-free survival in both cohorts. **C.** A possible correlation between PDGFRB levels with overall and disease-free survival was analyzed in a cohort of 119 colorectal liver metastasis [39]. Median expression was used as a cutoff. The Kaplan Meier curve shows that expression of PDGFRB is not significantly associated with shorter survival.

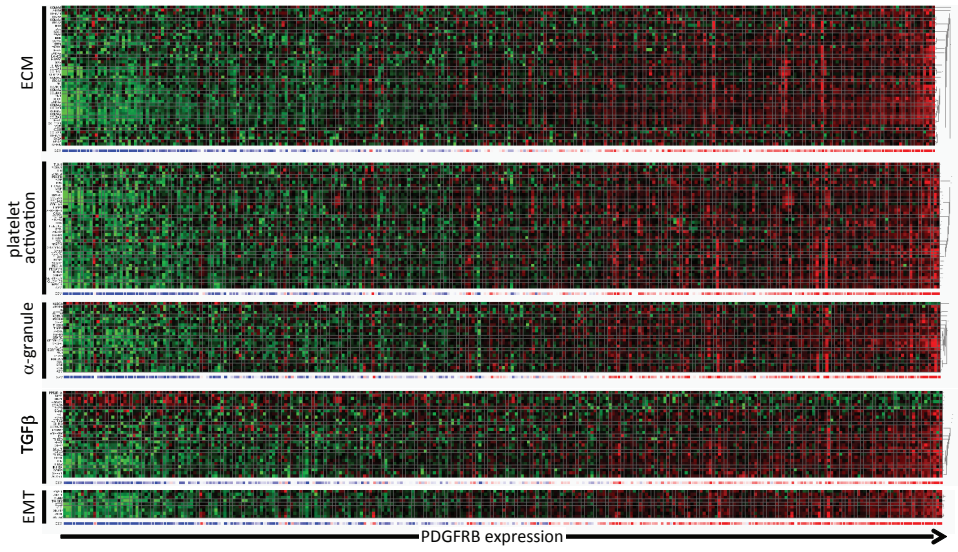

Figure 3. Co-expression of PDGFRB with genes governing ECM-Receptor Interaction, platelet activation, TGFB-pathway, and EMT in colorectal tumors.
Heatmap of the expression of genes co-expressed with the PDGFR in at least 2 out of 3 tumor cohorts in the categories "ECM-Receptor Interaction", 'Platelet Activation', 'Platelet alpha-Granule', 'TGFB pathway' and 'EMT'. The overlapping genes were identified by GeneVenn (Figure S1). An overview of the individual genes in these categories and their correlation with PDGFRB is presented in Table S1

PDGFRB in colorectal tumor cells signals invasion and metastases formation

The above results link PDGFRB expression to platelet activation, TGFB signaling, EMT and poor survival in human CRC. To test the function of PDGFRB in CRC cells, we performed Matrigel Transwell assays using PDGF-responsive C26 and MC38 colorectal cancer cells. Checkerboard analysis revealed that PDGF strongly promotes directed tumor cell migration (chemotaxis), whereas non-directed migration (chemokinesis) was not affected (Figure 4A). PDGF stimulation did not affect the growth rate of MC38 or C26 cells (Figure S4A).

Next, we assessed the contribution of PDGFRB to liver metastasis formation. To this end, PDGFRB expression was suppressed by transfecting short interfering RNA's (siRNA) into C26 cells expressing firefly luciferase. This resulted in efficient suppression of PDGFRB expression over a period of at least 4 days (Figure S5A). Expression levels returned to normal 6 days after transfection (Figure S5B). C26-siPDGFRB and control cells expressing scrambled siRNAs were injected into the spleens of syngenic Balb/c mice two days after transfection. Bioluminescence imaging over time showed that PDGFRB knockdown significantly reduced the outgrowth of liver metastases (Figure 4B). After 13 days the livers were removed and the Hepatic Replacement Area (HRA; % liver tissue occupied by tumor) was analyzed. PDGFRB knockdown had caused a significant drop in metastatic load (Figure 4B). Immunohistochemistry for active caspase 3 and KI67 on tumor tissue sections showed that suppression of PDGFRB expression had no effect on apoptosis or proliferation in liver metastases (Figure 4C). Likewise, PDGFRB knockdown had no effect on the *in vitro* growth rate of C26 or MC38 cells (Figure S4B).

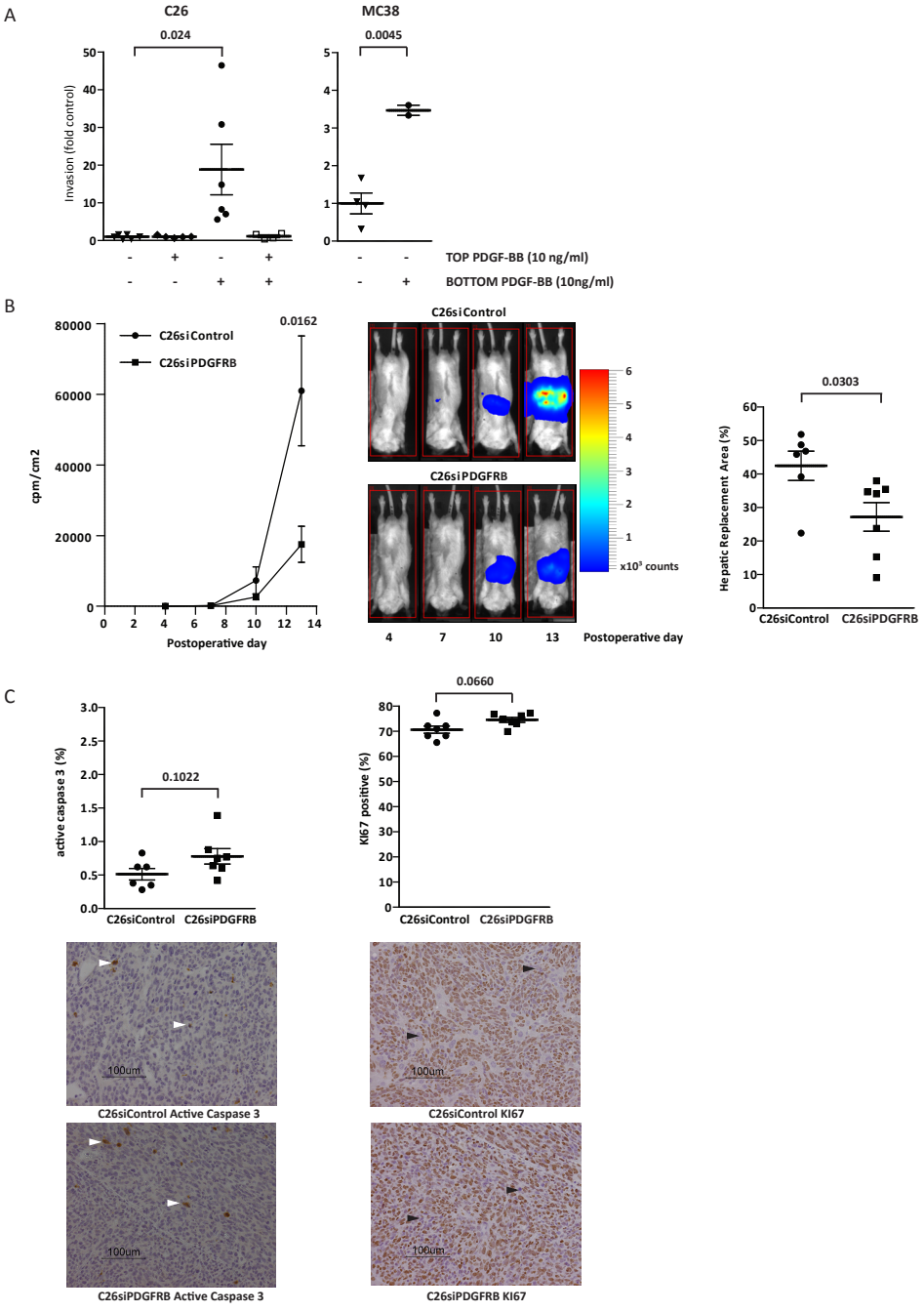

Figure 4. PDGFRB stimulates invasion and liver metastasis formation in colorectal cancer cell lines.
A. C26 cells and MC38 cells were cultured in Transwell chambers and invasion through Matrigel was assessed following addition of PDGF-BB (10ng/ml; 8 h) to the insert (top) or to the well (bottom) of the invasion chamber. All conditions were tested in duplicate in two independent experiments. Numbers represent fold change of the number of invaded cells relative to control (no PDGF-BB in either compartment). **B.** C26 cells expressing luciferase and either siRNAs targeting PDGFRB or control siRNAs were injected into the splenic parenchyma followed by splenectomy. The formation of liver metastases was then followed over time using bioluminescence imaging. Representative bioluminescence images of liver metastasis formation over time are depicted (scale bar represents bioluminescence counts). Two weeks after tumor cell injection the livers were harvested and the hepatic replacement area (HRA; liver area occupied/replaced by tumor tissue) was determined morphometrically. (n=7 mice per group) **C.** Sections of the livers harvested in B were analyzed for the presence of apoptotic caspase-3-positive cells (left panel; white arrowhead indicates active caspase-3 positive cell) and proliferating Ki67-positive cells (right panel; black arrowhead indicates Ki-67 negative cell) by immunohistochemistry. The bar graphs show the percentage positive cells measured in 5 high-power fields per mouse in 6 mice per condition. All error bars represent standard errors of the mean. Significance was tested using Student's t-test (unpaired; double sided).

ALK5 inhibition reduces PDGFRB expression and PDGF-stimulated invasion

The above results show that PDGFRB promotes invasion and liver metastasis formation. The C26 and MC38 cells that were used in this study display mesenchymal features including low expression of E-cadherin and high expression of N-cadherin and fibronectin (Figure 5A). Inhibition of constitutive TGFB signaling in C26 cells has previously been shown to lead to loss of the mesenchymal phenotype and to a concomitant loss of metastatic potential[49]. Indeed, treatment with the ALK5 inhibitor SB431524 blocked TGFB signaling in these cells (Figure S6) and strongly reduced basal fibronectin and N-cadherin expression, although this was not accompanied by re-expression of E-cadherin (Figure 5A). Importantly, ALK5 inhibition reduced PDGFRB expression and PDGF-stimulated tumor cell invasion (Figure 5A, B), indicating that PDGFRB expression and signaling in these cells requires TGFB signaling.

PDGF from platelets activates the PDGFRB on tumor cells

Circulating platelets are a major source of PDGF and have strong pro-metastatic activity[2,32]. Therefore, we assessed whether PDGF from platelets could stimulate the PDGFRB expressed on tumor cells. To this end, C26 and MC38 cells were exposed to PDGF or to platelets. Platelets were isolated from blood and were either left unstimulated, or were pre-stimulated with Thrombin Receptor Activating Peptide (TRAP). As expected, PDGF caused rapid tyrosine phosphorylation of the PDGFRB on C26 cells (Figure 6A). Non-stimulated platelets also induced some PDGFRB phosphorylation on C26 and MC38 cells, but this was drastically increased when platelets were pre-activated (Figure 6B, C). The time course of PDGFRB activation with (activated) platelets was similar to that induced by purified PDGF.

Tumor cells preferentially bind inactive platelets

Next, we used flow cytometry to study a potential interaction between tumor cells and platelets. Inactive platelets were isolated from donor blood and mixed with GFP-expressing tumor cells in a 10:1 ratio. Of all GFP-positive C26 and MC38 cells, 30-40% were also positive for the platelet marker CD42b (Figure 7A, S7B). Additionally, 5-10% of tumor cells were also positive for P-selectin, a marker for activated platelets (Figure 7A, S7B). Activation of platelets with TRAP prior to mixing with tumor cells did not change the total percentage of platelet-tumor cell events. Although 95% of the platelets were activated (Figure S7A), the vast majority of tumor cell-bound platelets were inactive (Figure 7A, S7B). Prevention of platelet activation by treatment

with Iloprost did not change the total percentage of platelet-bound tumor cells, but reduced the number of activated platelet-tumor cell events to undetectable levels (Figure 7A, S7B). Together, these results suggest that tumor cells preferentially bind inactive platelets.

PDGFRB phosphorylation on platelet-covered tumor cells in the liver sinusoids

To study the platelet-tumor cell interaction *in vivo* C26-GFP cells were injected into the spleen and the livers were harvested two hours after injection. Immunofluorescence microscopy

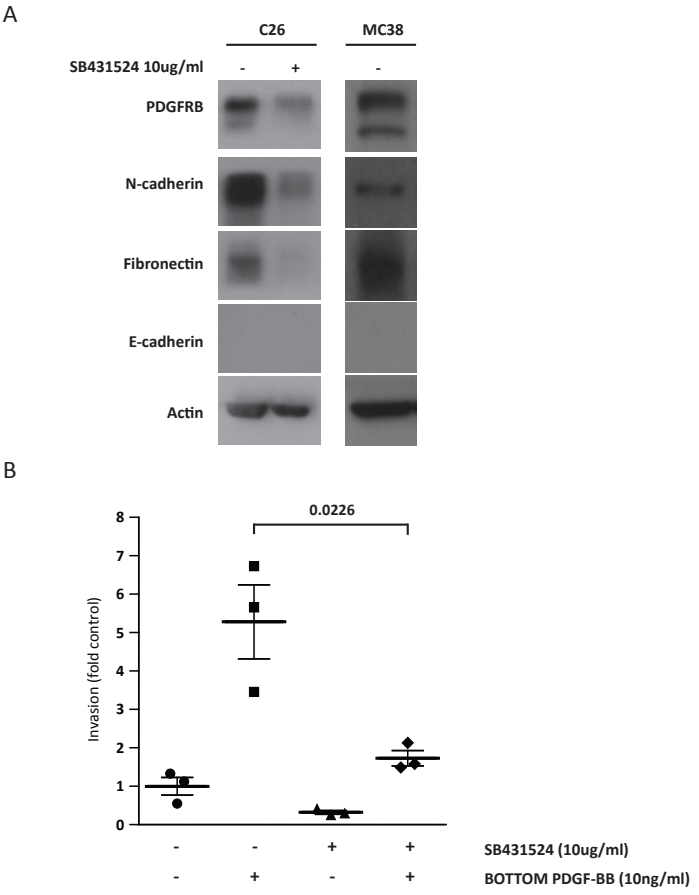

Figure 5. The ALK5 inhibitor SB431524 suppresses PDGFRB expression and PDGF-stimulated invasion.
A. C26 cells were incubated with SB431524 (10ng/ml) or vehicle for 1 week. Cells were lysed and expression of PDGFRB, N-cadherin, fibronectin, E-cadherin and actin was assessed by western blotting. **B.** C26 cells were cultured in Transwell chambers and invasion through Matrigel was assessed following addition of PDGF-BB (10ng/ml; 8 h) to the bottom well of the invasion chamber, in the presence or absence of SB431524 (10ng/ml). All conditions were tested in triplicate in two independent experiments. Numbers represent fold change of the number of invaded cells relative to control (no PDGF-BB added). All error bars represent standard errors of the mean. Significance was tested using Student's t-test (unpaired; double sided).

confirmed intra-sinusoidal localization of GFP-positive tumor cells (Figure 7B). Co-staining with CD41 showed that approximately 52% of all green tumor cells were surrounded by platelets. These cells also showed tyrosine phosphorylation of the PDGFRB (Figure 7B). By contrast, tumor cells that were not surrounded by CD41-positive platelets were negative for PDGFRB phosphorylation.

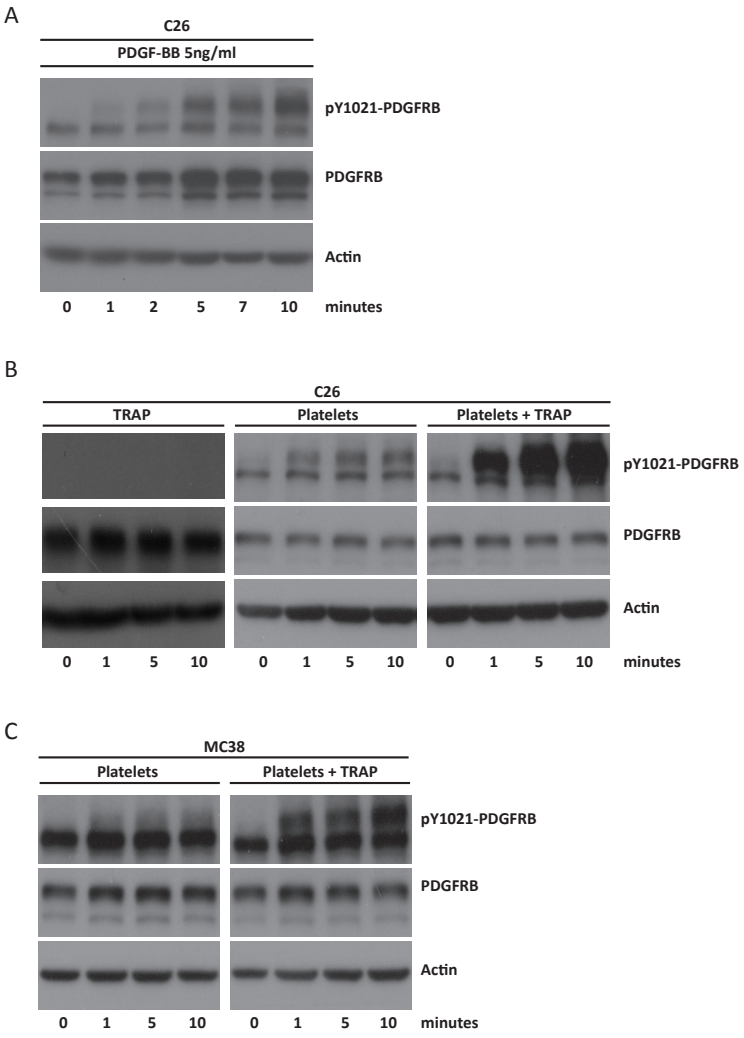

Figure 6. Activation of PDGFRB on colorectal cancer cell lines by activated platelets.
C26 cells were cultured in serum-free medium overnight and were subsequently stimulated with purified PDGF-BB 5ng/ml for different lengths of time (A), with Thrombin Receptor Activating Peptide (TRAP) 625μM alone, or with platelets ($25x10^6$/ml) that had been pre-activated or not (B). Platelet activation was performed by exposing them to TRAP 625μM. The same experiment was performed using MC38 cells (C). Stimulus-induced changes in expression and tyrosine 1021 phosphorylation of PDGFRB (pY1021-PDGFRB) was analyzed over time (0-10 minutes) by Western blotting.

A

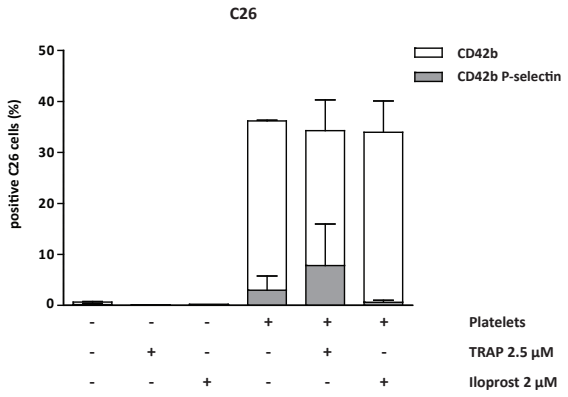

B

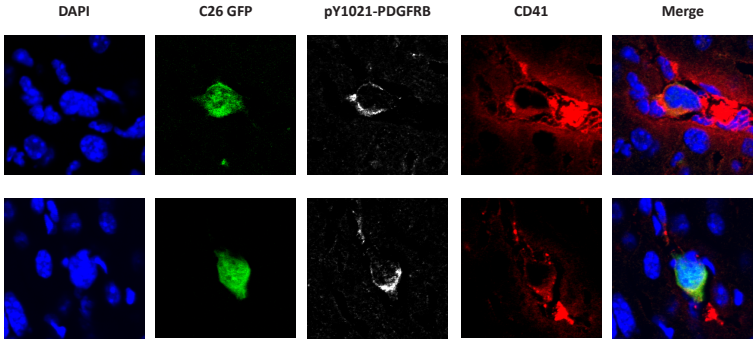

C

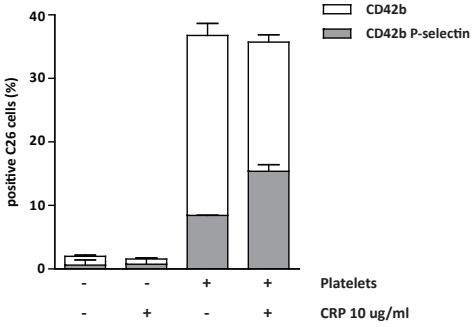

D

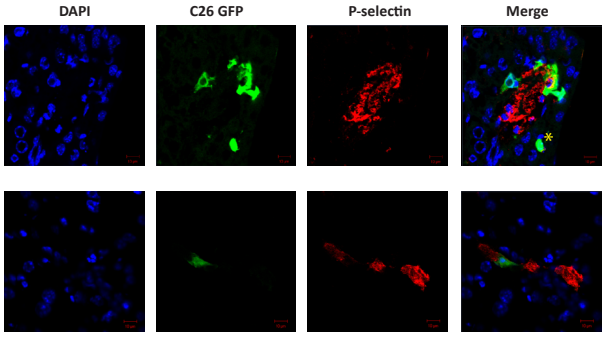

Figure 7. Platelets bind tumor cells and cause PDGFRB activation on tumor cells lodged in the liver sinusoids. **A.** GFP-expressing tumor cells and platelets were mixed in a 1:10 ratio. Before mixing platelets were non-treated, inactivated by iloprost (2μM) or activated by TRAP (2.5 μM) treatment as indicated. Two independent experiments were performed in duplicate. The fraction of tumor cells that were bound to non-activated and activated platelets was then analyzed by flow cytometry for GFP, CD42b and P-selectin. The white bars represent all tumor cell (GFP)-platelet ($CD42b^{+ve}$) events, while the grey bars represent tumor cell (GFP)-activated platelet ($CD42b^{+ve}$; P-$selectin^{+ve}$) events. **B.** GFP-expressing C26 tumor cells were injected into the spleen. After two hours the liver was perfused with PLP, harvested and processed for cryo-sectioning and immunofluorescence using anti-pY1021-PDGFRB (white) and CD41 (red) antibodies and DAPI (blue). CD41-positive platelet clusters were observed around ~52% of all sinusoid-arrested single tumor cells. These tumor cells were also positive for pPDGFRB. Representative images are shown. **C.** Tumor cells were mixed with platelets exactly as in A. Hereafter the mixture was treated with CRP (10μm/ml) as indicated. Two independent experiments were performed in duplicate. The mixture was subsequently analyzed by flow cytometry exactly as described in A. **D.** As in B cryo-sections were processed for immunofluorescence using anti-P-selectin (red) and DAPI (blue). P-selectin-positive tumor cells were identified surrounding ~50% of all GFP positive tumor cells. Representative images are shown, a tumor cell negative for P-selectin is indicated by *.

Activation of platelets in complex with tumor cells

To investigate if tumor cell-associated platelets are still responsive to activation by ECM components tumor cells were mixed with isolated platelets. To mimic ECM exposure collagen-related peptide (CRP) was added to the mixture and flow cytometry was used to study activation of platelets on platelet-tumor cell complexes. Approximately 40% of all tumor cells were covered by platelets, of which 8% was also positive for p-Sel. Thus, ~20% of tumor cell-bound platelets was activated (Figure 7C). After exposure to CRP the percentage of platelet-tumor cell complexes positive for P-selectin increased to +/- 45% (Figure 7C). This indicates that platelets associated to tumor cells are still responsive to activation by ECM components such as collagen. Next we analyzed C26-GFP tumor cells arrested in mouse liver sinusoids 2 hours after intrasplenic injection for P-selectin positivity by immunofluorescence (Figure 7D). Of 208 arrested tumor cells 105 (~50%) were also positive for P-selectin (Figure 7D), similar to the total percentage of platelet-covered tumor cells (52%, Figure 7B). Together, these results indicate that platelets in complex with tumor cells are activated following tumor cell lodging in the sinusoids and that this may be mediated by exposure to ECM components.

DISCUSSION

In the present report we provide evidence that mesenchymal-like colorectal tumor cells express PDGFRB which stimulates invasion and contributes to the metastatic capacity of such cells. Mounting evidence suggests that epithelial cells have to undergo EMT to efficiently seed metastases[18,20,50,51]. In a mouse model for spontaneous metastatic pancreas carcinoma the metastasizing tumor cells undergo EMT transiently and revert back to an epithelial phenotype in the distant organ[50]. Furthermore, recent studies in breast cancer patients have shown that a subpopulation of circulating tumor cells (CTCs) indeed has mesenchymal features and that high numbers of such cells predict poor prognosis[50,52-55]. The transient nature of EMT may explain why this phenomenon is hard to detect by immunohistochemistry on human tumor tissue sections. In addition, epithelial tumor cells with mesenchymal properties are distinct from true mesenchymal cells and may be hard to discriminate morphologically from their epithelial neighbors on tissue sections. Indeed, a considerable proportion of human colorectal tumors express moderate to high levels of the mesenchymal marker vimentin in the tumor cells without

appearing mesenchymal. This was associated with the presence of nuclear B-catenin, which helps drive the EMT-like process, but not with clear changes in epithelial morphology[7]. Likewise, PDGFRB expression in colorectal tumor cells has previously been documented[6]. In the current study we show that vimentin expression is strongly associated with PDGFRB expression and that this identifies an aggressive subset of CRC tumors (Table S1). We found that high PDGFRB expression in primary tumors correlates with tumor recurrence (metastasis formation), but also that this association was not found in already established metastases. Therefore, PDGFRB may primarily play a role in establishing distant metastases rather than in promoting the growth of established lesions.

Although the contribution of stromal cells to gene expression profiles of colorectal tumors is relatively small[56], we cannot exclude that stromal cells have contributed to PDGFRB expression in our analyses of the human tumor cohorts. Whatever that contribution may be, there is no doubt that EMT of tumor cells from diverse epithelial origins generates PDGFRB-expressing tumor cells with mesenchymal properties[12-14,16,19,24] (this study). Importantly, such cells become dependent on PDGFR signaling for efficient metastasis formation[18,24]. Expression of the PDGFRB in epithelial tumor cells is stimulated by TGFB[18,24] and by the EMT-driving transcription factor SNAIL[57]. Indeed, PDGFRB expression in CRC was strongly correlated with both TGFB signaling and with key EMT-driving transcription factors. Furthermore, inhibition of TGFB signaling reduced PDGFRB signaling in mesenchymal-like CRC cells (this study) and suppressed metastasis formation[49]. *Vice versa*, restoration of TGFB receptor signaling in human epithelial colorectal tumor cells with a mutation in TGFBR2 greatly enhanced tumor cell invasion[49].

EMT induced by TGFB or SNAIL results in enhanced expression of PDGFRB and ECM genes including collagens and fibronectin[57-59]. ECM deposition promotes platelet activation, which stimulates the metastatic process[32-34]. However, it is less clear during which steps in the metastatic cascade platelets may play a role. Most of the available evidence supports a role for platelets during initial metastasis establishment at distant sites. Micro-thrombi containing activated platelets are formed around tumor cells that are trapped in the microvasculature of the liver or the lungs[26-30](this study). This may help tumor cell extravasation and/or early

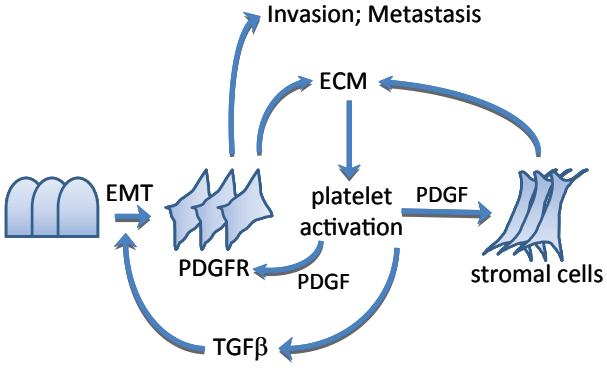

Figure 8. Working model for PDGFR signaling in metastatic CRC.
Tumors with high extracellular matrix content, including collagens, fibronectin and tenascin-C, are prone to platelet activation. Activated platelets produce TGFB which stimulates EMT and PDGFR expression in tumor cells. Platelets also produce PDGF which can then stimulate tumor cells and stromal cells in a paracrine fashion. Mesenchymal-like tumor cells are invasion-prone and have a relatively high capacity to seed distant metastases.

establishment of novel metastatic lesions. Interestingly, at least two key components of the metastatic niche, fibronectin and tenascin-C, are also potent inducers of platelet activation[60-63]. Furthermore, both ECM components are co-expressed with PDGFRB in CRC (Table S1). Platelet activation and subsequent EMT may also help tumor cells do detach from the primary tumor to disseminate.

We propose that aggressive colorectal tumors with high expression of PDGFRB and EMT genes may sustain their phenotype by high level matrix deposition resulting in an increased propensity for platelet activation. Activated platelets release TGFB which subsequently promotes EMT and PDGFR signaling in tumor and stromal cells (Figure 8). This self-sustaining series of events may operate both within the primary tumor and at distant sites.

REFERENCES

1. Ostman, A et al. PDGF receptors as targets in tumor treatment. Adv.Cancer Res. 97, 247-274. 2007.
2. Heldin, CH et al. Mechanism of action and in vivo role of platelet-derived growth factor. Physiol Rev. 79, 1283-1316. 1999.
3. Steller, EJ et al. The death receptor CD95 activates the cofilin pathway to stimulate tumour cell invasion. EMBO Rep. 12, 931-937. 2011.
4. Lindmark, G et al. Stromal expression of platelet-derived growth factor beta-receptor and platelet-derived growth factor B-chain in colorectal cancer. Lab Invest 69, 682-689. 1993.
5. Sundberg, C et al. Microvascular pericytes express platelet-derived growth factor-beta receptors in human healing wounds and colorectal adenocarcinoma. Am.J.Pathol. 143, 1377-1388. 1993.
6. Wehler, TC et al. PDGFRalpha/beta expression correlates with the metastatic behavior of human colorectal cancer: a possible rationale for a molecular targeting strategy. Oncol.Rep. 19, 697-704. 2008.
7. Veenendaal, LM et al. Differential Notch and TGF-beta signaling in primary colorectal tumors and their corresponding metastases. Cell Oncol. 30, 1-11. 2008.
8. Hwang, RF et al. Inhibition of platelet-derived growth factor receptor phosphorylation by STI571 (Gleevec) reduces growth and metastasis of human pancreatic carcinoma in an orthotopic nude mouse model. Clin.Cancer Res. 9, 6534-6544. 2003.
9. Maass, T et al. Liver specific overexpression of platelet-derived growth factor-B accelerates liver cancer development in chemically induced liver carcinogenesis. Int.J.Cancer 128, 1259-1268. 2011.
10. Seymour, L et al. Positive immunostaining for platelet derived growth factor (PDGF) is an adverse prognostic factor in patients with advanced breast cancer. Breast Cancer Res.Treat. 32, 229-233. 1994.
11. Kitadai, Y et al. Expression of activated platelet-derived growth factor receptor in stromal cells of human colon carcinomas is associated with metastatic potential. Int.J.Cancer 119, 2567-2574. 2006.
12. Campbell, CI et al. Mammary tumors that become independent of the type I insulin-like growth factor receptor express elevated levels of platelet-derived growth factor receptors. BMC.Cancer 11, 480. 2011.
13. Eckert, MA et al. Twist1-induced invadopodia formation promotes tumor metastasis. Cancer Cell 19, 372-386. 2011.
14. Fischer, AN et al. PDGF essentially links TGF-beta signaling to nuclear beta-catenin accumulation in hepatocellular carcinoma progression. Oncogene 26, 3395-3405. 2007.
15. Jechlinger, M et al. Expression profiling of epithelial plasticity in tumor progression. Oncogene 22, 7155-7169. 2003.
16. Lahsnig, C et al. ILEI requires oncogenic Ras for the epithelial to mesenchymal transition of hepatocytes and liver carcinoma progression. Oncogene 28, 638-650. 2009.
17. Smith, CL et al. Epicardial-derived cell epithelial-to-mesenchymal transition and fate specification require PDGF receptor signaling. Circ.Res. 108, e15-e26. 2011.
18. Thomson, S et al. Kinase switching in mesenchymal-like non-small cell lung cancer lines contributes to EGFR inhibitor resistance through pathway redundancy. Clin.Exp.Metastasis 25, 843-854. 2008.
19. Thomson, S et al. A systems view of epithelial-mesenchymal transition signaling states. Clin.Exp. Metastasis 28, 137-155. 2011.
20. Kalluri, R et al. The basics of epithelial-mesenchymal transition. J.Clin.Invest 119, 1420-1428. 2009.
21. Cristofanilli, M et al. Circulating tumor cells: a novel prognostic factor for newly diagnosed metastatic breast cancer. J.Clin.Oncol. 23, 1420-1430. 2005.
22. Gradilone, A et al. Circulating tumour cells lacking cytokeratin in breast cancer: the importance of being mesenchymal. J.Cell Mol.Med. 15, 1066-1070. 2011.
23. Raimondi, C et al. Epithelial-mesenchymal transition and stemness features in circulating tumor cells from breast cancer patients. Breast Cancer Res.Treat. 130, 449-455. 2011.
24. Jechlinger, M et al. Autocrine PDGFR signaling promotes mammary cancer metastasis. J.Clin. Invest 116, 1561-1570. 2006.
25. Labelle, M et al. Direct signaling between platelets and cancer cells induces an epithelial-mesenchymal-like transition and promotes metastasis. Cancer Cell 20, 576-590. 2011.
26. Erpenbeck, L et al. Inhibition of platelet GPIb alpha and promotion of melanoma metastasis. J.Invest Dermatol. 130, 576-586. 2010.
27. Im, JH et al. Coagulation facilitates tumor cell spreading in the pulmonary vasculature during early metastatic colony formation. Cancer Res. 64, 8613-8619. 2004.
28. Kawaguchi, T et al. Analysis of the lodgement and extravasation of tumor cells in experimental models of hematogenous metastasis. Cancer Metastasis Rev. 5, 77-94. 1986.
29. Kim, YJ et al. P-selectin deficiency attenuates tumor growth and metastasis. Proc.Natl.Acad. Sci.U.S.A 95, 9325-9330. 1998.
30. Tanaka, K et al. Intravital dual-colored visualization of colorectal liver metastasis in living mice using two photon laser scanning microscopy. Microsc. Res.Tech. 75, 307-315. 2012.
31. Kim, YJ et al. Distinct selectin ligands on colon carcinoma mucins can mediate pathological interactions among platelets, leukocytes, and endothelium. Am.J.Pathol. 155, 461-472. 1999.
32. Gay, LJ et al. Contribution of platelets to tumour metastasis. Nat.Rev.Cancer 11, 123-134. 2011.
33. Karpatkin, S et al. Role of adhesive proteins in platelet tumor interaction in vitro and metastasis

formation in vivo. J.Clin.Invest 81, 1012-1019. 1988.
34. Pearlstein, E et al. Effect of antiplatelet antibody on the development of pulmonary metastases following injection of CT26 colon adenocarcinoma, Lewis lung carcinoma, and B16 amelanotic melanoma tumor cells into mice. Cancer Res. 44, 3884-3887. 1984.
35. Lin, MS et al. Elevation of platelet count in patients with colorectal cancer predicts tendency to metastases and poor prognosis. Hepatogastroenterology 59, 1687-1690. 2012.
36. Sasaki, K et al. Impact of preoperative thrombocytosis on the survival of patients with primary colorectal cancer. World J.Surg. 36, 192-200. 2012.
37. Jorissen, RN et al. Metastasis-Associated Gene Expression Changes Predict Poor Outcomes in Patients with Dukes Stage B and C Colorectal Cancer. Clin.Cancer Res. 15, 7642-7651. 2009.
38. Smith, JJ et al. Experimentally derived metastasis gene expression profile predicts recurrence and death in patients with colon cancer. Gastroenterology 138, 958-968. 2010.
39. Snoeren, N et al. Exploring gene expression signatures for predicting disease free survival after resection of colorectal cancer liver metastases. PLoS.ONE. 7, e49442. 2012.
40. Bewick, V et al. Statistics review 12: survival analysis. Crit Care 8, 389-394. 2004.
41. Smakman, N et al. Validation of bioluminescence imaging of colorectal liver metastases in the mouse. J.Surg.Res. 122, 225-230. 2004.
42. Knight, CG et al. Collagen-platelet interaction: Gly-Pro-Hyp is uniquely specific for platelet Gp VI and mediates platelet activation by collagen. Cardiovasc.Res. 41, 450-457. 1999.
43. Korporaal, SJ et al. Platelet activation by oxidized low density lipoprotein is mediated by CD36 and scavenger receptor-A. Arterioscler.Thromb.Vasc. Biol. 27, 2476-2483. 2007.
44. Kranenburg, O et al. Regulating c-Ras function. cholesterol depletion affects caveolin association, GTP loading, and signaling. Curr.Biol. 11, 1880-1884. 2001.
45. Drixler, TA et al. Continuous administration of angiostatin inhibits accelerated growth of colorectal liver metastases after partial hepatectomy. Cancer Res. 60, 1761-1765. 2000.
46. Te Velde, EA et al. Enhanced antitumour efficacy by combining conventional chemotherapy with angiostatin or endostatin in a liver metastasis model. Br.J.Surg. 89, 1302-1309. 2002.
47. van der Bilt, JD et al. Ischemia/reperfusion accelerates the outgrowth of hepatic micrometastases in a highly standardized murine model. Hepatology 42, 165-175. 2005.
48. Peinado, H et al. Snail, Zeb and bHLH factors in tumour progression: an alliance against the epithelial phenotype?. Nat.Rev.Cancer 7, 415-428. 2007.
49. Oft, M et al. TGFbeta signaling is necessary for carcinoma cell invasiveness and metastasis. Curr. Biol. 8, 1243-1252. 1998.
50. Rhim, AD et al. EMT and dissemination precede pancreatic tumor formation. Cell 148, 349-361. 2012.
51. Siegel, PM et al. Cytostatic and apoptotic actions of TGF-beta in homeostasis and cancer. Nat.Rev. Cancer 3, 807-821. 2003.
52. Aktas, B et al. Stem cell and epithelial-mesenchymal transition markers are frequently overexpressed in circulating tumor cells of metastatic breast cancer patients. Breast Cancer Res. 11, R46. 2009.
53. Bonnomet, A et al. A dynamic in vivo model of epithelial-to-mesenchymal transitions in circulating tumor cells and metastases of breast cancer. Oncogene 31, 3741-3753. 2012.
54. Hou, JM et al. Clinical significance and molecular characteristics of circulating tumor cells and circulating tumor microemboli in patients with small-cell lung cancer. J.Clin.Oncol. 30, 525-532. 2012.
55. Kallergi, G et al. Epithelial to mesenchymal transition markers expressed in circulating tumour cells of early and metastatic breast cancer patients. Breast Cancer Res. 13, R59. 2011.
56. de Bruin, EC et al. Macrodissection versus microdissection of rectal carcinoma: minor influence of stroma cells to tumor cell gene expression profiles. BMC.Genomics 6, 142. 2005.
57. Argast, GM et al. Inducible expression of TGFbeta, snail and Zeb1 recapitulates EMT in vitro and in vivo in a NSCLC model. Clin.Exp.Metastasis 28, 593-614. 2011.
58. Thiery, JP et al. Epithelial-mesenchymal transitions in development and disease. Cell 139, 871-890. 2009.
59. Zeisberg, M et al. Fibroblasts derive from hepatocytes in liver fibrosis via epithelial to mesenchymal transition. J.Biol.Chem. 282, 23337-23347. 2007.
60. Kaplan, RN et al. VEGFR1-positive haematopoietic bone marrow progenitors initiate the pre-metastatic niche. Nature 438, 820-827. 2005.
61. Oskarsson, T et al. Breast cancer cells produce tenascin C as a metastatic niche component to colonize the lungs. Nat.Med. 17, 867-874. 2011.
62. Schaff, M et al. Novel function of tenascin-C, a matrix protein relevant to atherosclerosis, in platelet recruitment and activation under flow. Arterioscler.Thromb.Vasc.Biol. 31, 117-124. 2011.
63. Sleeman, JP. The metastatic niche and stromal progression. Cancer Metastasis Rev. 2012.

SUPPLEMENTAL

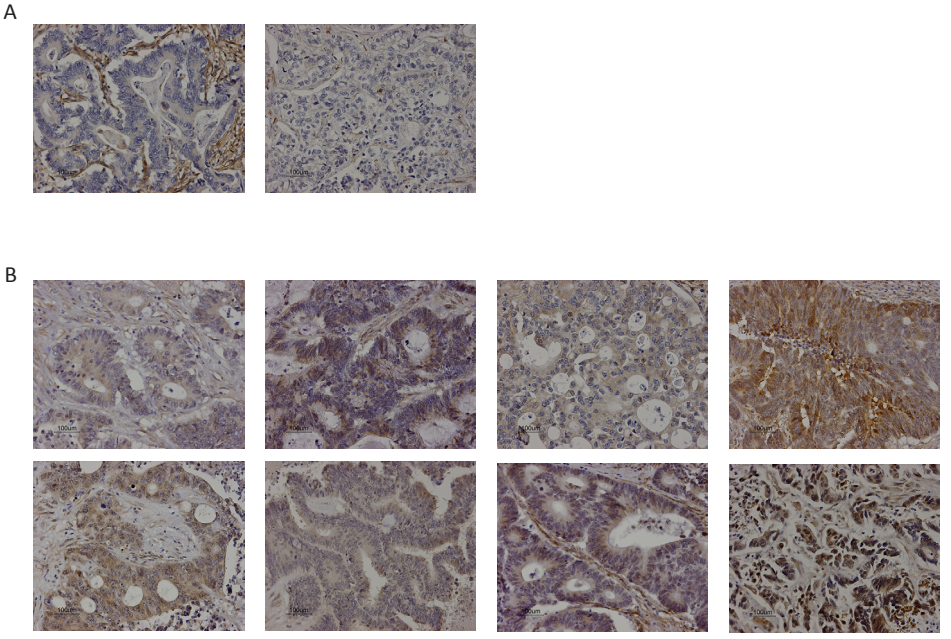

Figure S1. Immunohistochemistry analysis of the expression of PDGFRB in 10 human colorectal tumors.
A. In only two tumors PDGFRB is expressed in stromal cells only. **B.** In 8/10 tumors the tumor cell compartment was predominantly positive, sometimes accompanied by stromal staining.

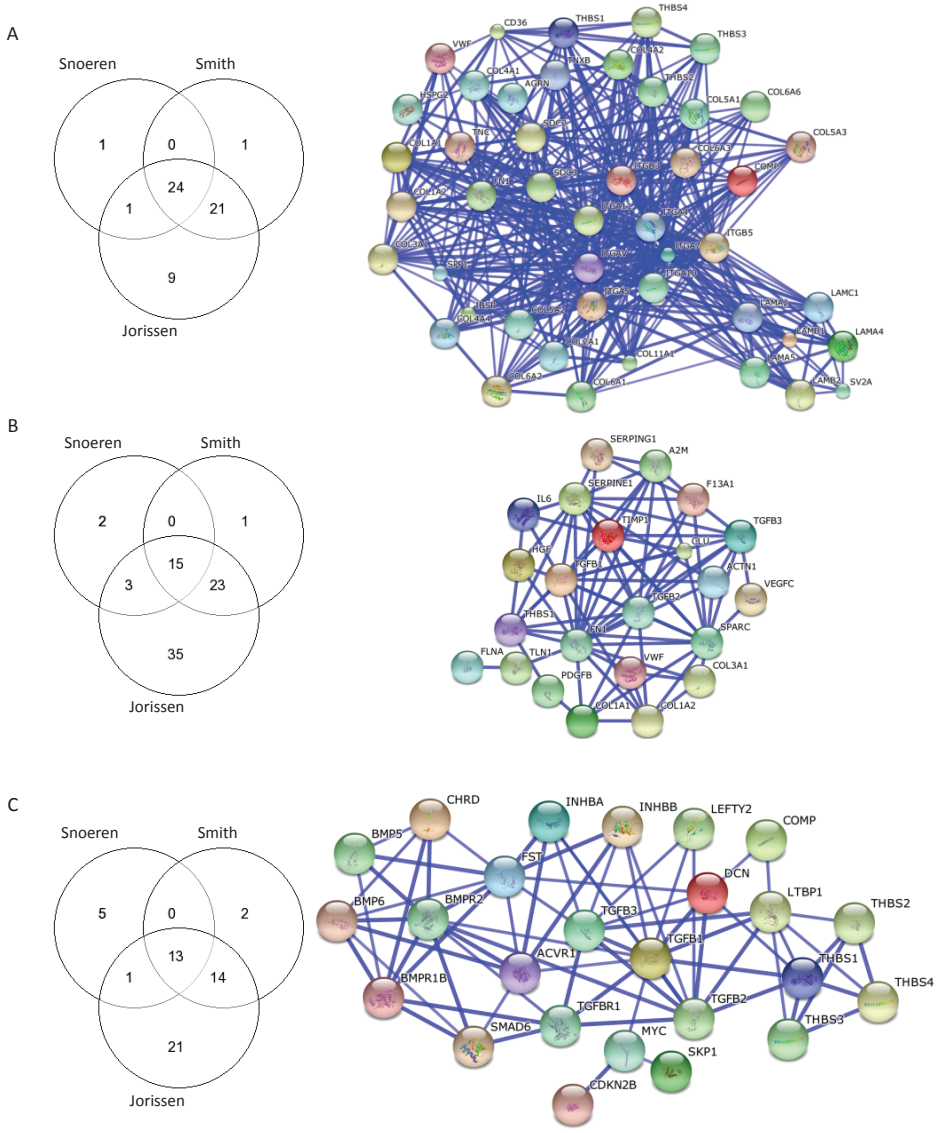

Figure S2.
A. Overlap between PDGFRB-associated genes from the three tumor cohorts in the ECM-Receptor Interaction pathway, **B.** the Platelet Activation pathway, and **C.** the TGFB pathway were identified by GeneVenn[1].
STRING analysis[2] was then used to visualize the high functional interconnectivity between the genes in these categories.

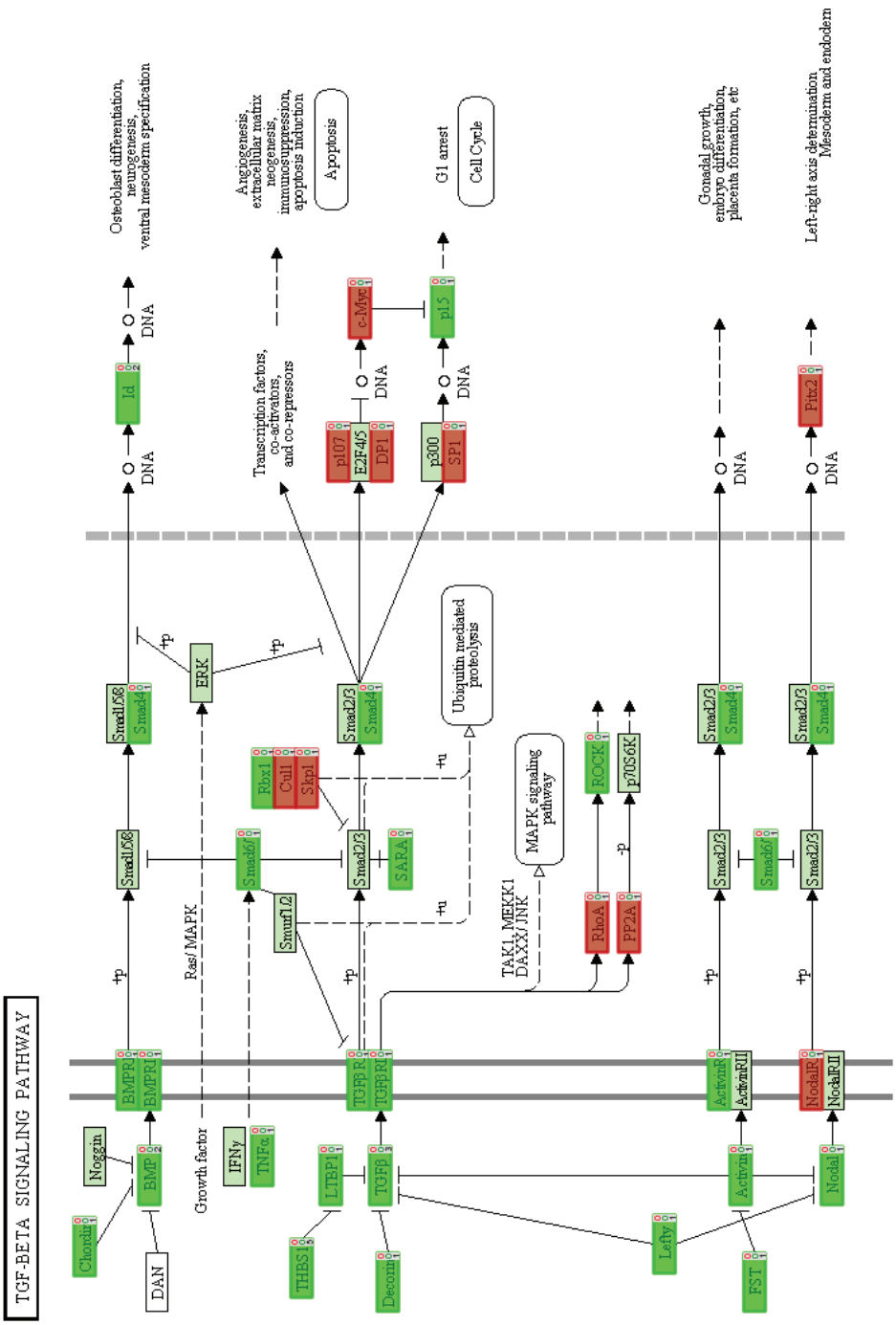

Figure S3. TGFB-pathway genes co-expressed with PDGFRB in CRC.
Genes within the TGFB KEGG pathway that are significantly associated with PDGFRB expression in a single cohort[3]. Positive correlations with PDGFRB are shown in green, negative correlations are shown in red.

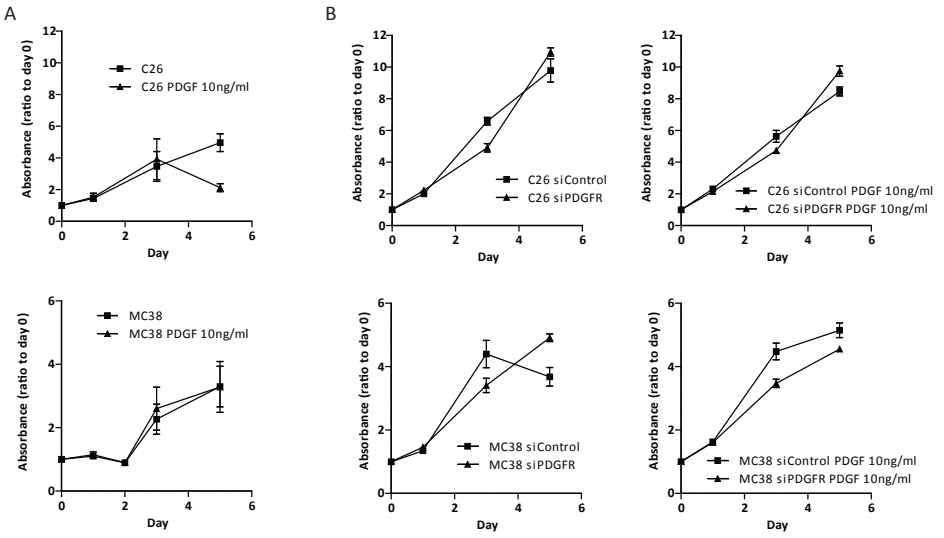

Figure S4. PDGF stimulation and PDGFRB knockdown do not affect proliferation of colorectal cancer cell lines. **A.** C26 and MC38 cells were stimulated with PDGF-BB (10ng/ml) for 0-5 days and growth curves were generated by MTT mitochondrial activity assays. The graphs represent 2 independent experiments performed in triplicate. Data are expressed as fold-change of absorbance values relative to day 0 (=1). Error bars reflect standard errors of the mean. **B.** PDGFRB expression in C26 and MC38 cells was suppressed by siRNA-mediated knockdown (See Fig S4 for confirmation of knockdown). Control cells received scrambled siRNAs. The resulting cell populations were then either left unstimulated or were stimulated with PDGF-BB. Growth curves over 0-5 days were then generated as in A.

A

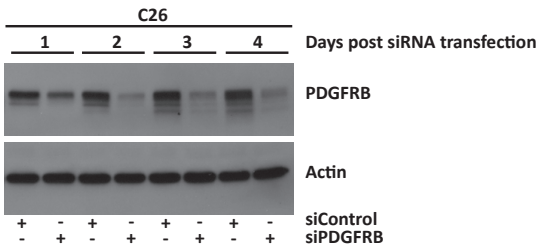

B

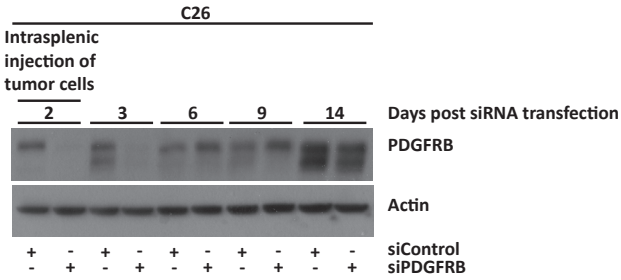

C

	Sequence	Concentration	Manufacturer
OTP Non-Targeting Pool	Control siRNA	20nM	Dharmacon
PDGFR-β OTP SMARTPool	CAGCGAGGUUUCACUGGUA GAACGACCAUGGCGAUGAG GGAAGCGUAUCUAUAUCUU UAGAUUACGUGCCCAUGUU	20nM	Dharmacon

Figure S5. Suppression of PDGFRB by short interfering RNA (siRNA) transfection in colorectal tumor cells
A. Western blot showing PDGFRB expression in C26 cells transfected with siRNA against PDGFRB or a control siRNA over time. **B.** Western blot showing PDGFRB expression in C26siPDGFRB expressing firefly luciferase transfected with siRNA against PDGFRB or a control siRNA over time. Cells were injected into the spleens of Balb/c mice 2 days post-transfection. **C.** Sequences of the siRNA smartpool targeting PDGFRB and the non-targeting siRNA pool that was used as a control.

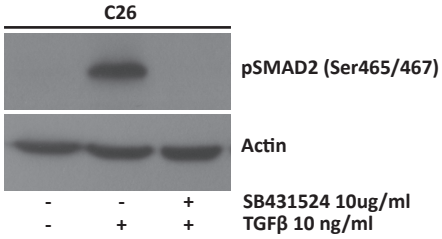

Figure S6. Validation of ALK5 inhibition by SB431524
Western blot showing SMAD2 phosphorylation following pre-treatment with the ALK5 inhibitor SB431524 (10µg/ml; 1week) and subsequent stimulation with TGFB (10 ng/ml; 45min).

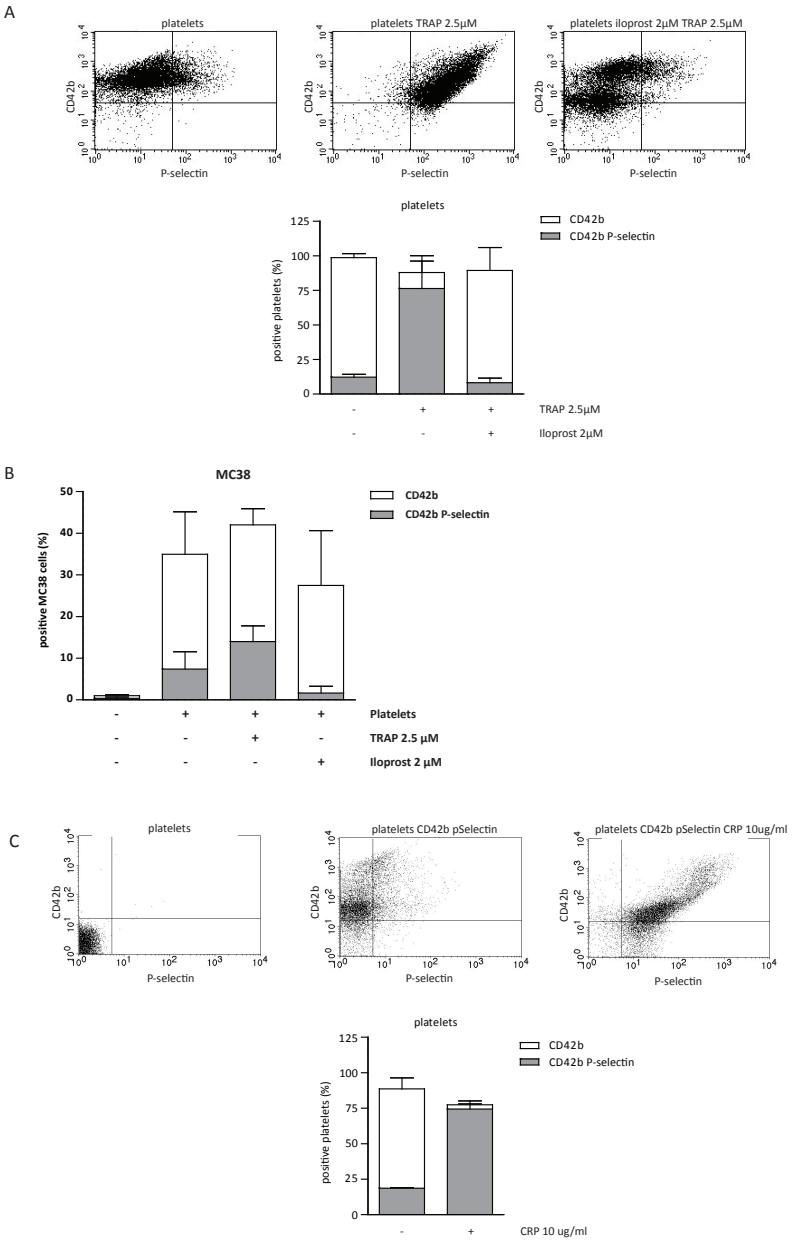

Figure S7. Validation of platelet activation by TRAP or CRP, prevention of activation by iloprost and repetition of platelet-tumor cell complex formation in MC38.

A. Flow cytometry analysis of CD42b and P-selectin expression on platelets isolated from donor blood. Platelets were either left untreated (left panel), were treated with TRAP (middle panel; 30min 2.5µM), or were pre-treated with Iloprost (30min; 2µM) and subsequently treated with TRAP (right panel). Bar graph represents data from 2 independent experiments. Error bars represent standard errors of the mean. **B.** MC38 tumor cell-platelet interactions were assessed exactly as in figure 7A. **C.** Flow cytometry analysis of CD42b and P-selectin expression on platelets isolated from donor blood. Platelets were untreated (middle panel) or treated with CRP (right panel; 15 min; 10 µg/ml). The bar graph represents the percentages of CD42b-positive platelets (white bar) and CD42b/P-selectin-positive platelets (grey bar).

Table S1. Genes co-expressed with PDGFRB in CRC.

GENES	R value	p value	R value	p value	R value	p value	R value
				ECM-Receptor interaction			
COL5A1	0,636	4,95E-14	0,783	4,43E-48	0,882	1,16E-94	0,767
THBS2	0,775	2,18E-23	0,694	6,04E-34	0,817	4,52E-70	0,762
LAMA4			0,660	6,84E-30	0,84	1,86E-77	0,750
COL5A2	0,674	4,98E-16	0,697	2,54E-34	0,873	1,66E-90	0,748
COL6A3	0,661	2,66E-15	0,726	1,95E-38	0,831	2,75E-74	0,739
COL4A2	0,66	2,29E-15	0,755	4,72E-43	0,725	6,54E-48	0,713
COL6A2	0,371	6,66E-05	0,848	1,02E-63	0,848	2,93E-80	0,689
COL5A3			0,682	1,90E-32	0,675	2,00E-39	0,679
COL6A1	0,404	1,20E-05	0,805	9,01E-53	0,825	1,26E-72	0,678
COL4A1	0,678	3,50E-16	0,611	1,16E-24	0,742	2,96E-51	0,677
ITGA5			0,729	7,89E-39	0,612	1,00E-30	0,671
COL1A2	0,553	2,92E-10	0,717	4,03E-37	0,699	3,36E-43	0,656
COL3A1	0,684	2,43E-16	0,631	1,33E-26	0,644	7,70E-35	0,653
SDC2	0,479	1,09E-07	0,602	6,79E-24	0,84	1,76E-77	0,640
HSPG2			0,698	1,82E-34	0,56	4,75E-25	0,629
COL11A1	0,441	1,45E-06	0,620	1,44E-25	0,725	7,59E-48	0,595
LAMB2	0,482	9,09E-08	0,670	4,87E-31	0,579	4,61E-27	0,577
LAMC1	0,493	4,59E-08	0,538	1,92E-18	0,654	2,91E-36	0,562
FN1	0,415	6,56E-06	0,605	3,98E-24	0,642	1,34E-34	0,554
LAMA2			0,487	6,31E-15	0,61	1,45E-30	0,549
ITGB5	0,631	8,30E-14	0,525	1,79E-17	0,486	1,96E-18	0,547
TNC			0,496	1,60E-15	0,591	2,33E-28	0,544
COMP	0,417	5,86E-06	0,496	1,67E-15	0,673	3,65E-39	0,529
THBS4			0,466	1,14E-13	0,569	5,41E-26	0,518
ITGAV			0,452	6,79E-13	0,549	5,71E-24	0,501
ITGA11	0,606	1,47E-12	0,518	4,91E-17	0,374	5,51E-11	0,499
COL1A1	0,602	1,94E-12	0,450	9,17E-13	0,387	1,08E-11	0,480
THBS3	0,315	8,89E-04	0,554	1,09E-19	0,519	3,30E-21	0,463
THBS1	0,379	4,64E-05	0,422	3,13E-11	0,578	6,51E-27	0,460
IBSP			0,376	4,97E-09	0,54	4,34E-23	0,458
SPP1			0,365	1,39E-08	0,533	1,89E-22	0,449
ITGA4			0,342	1,13E-07	0,485	2,54E-18	0,414
SDC3	0,485	7,83E-08	0,351	5,53E-08	0,381	2,38E-11	0,406
CD36			0,287	1,04E-05	0,481	5,47E-18	0,384
VWF	0,252	9,88E-03	0,461	2,20E-13	0,437	8,03E-15	0,383
ITGB3			0,325	5,09E-07	0,425	5,08E-14	0,375
ITGA7	0,421	4,91E-06	0,348	7,14E-08	0,349	1,19E-09	0,373
SV2A	0,349	1,96E-04			0,386	1,27E-11	0,368
COL2A1			0,301	3,50E-06	0,391	6,30E-12	0,346
AGRN			0,309	1,98E-06	0,372	7,32E-11	0,341
LAMB1	0,326	5,59E-04	0,349	6,29E-08	0,265	5,05E-06	0,313
LAMA5			0,262	5,86E-05	0,335	5,72E-09	0,299
COL4A4			0,257	7,93E-05	0,308	9,90E-08	0,283
COL6A6			0,190	3,82E-03	0,289	5,66E-07	0,240
ITGA10			0,190	3,91E-03	0,288	6,51E-07	0,239
TNXB			0,274	2,58E-05	0,198	6,80E-04	0,236
				Platelet activation			
COL5A1	0,636	4,95E-14	0,783	4,43E-48	0,882	1,16E-94	0,767
THBS2	0,775	2,18E-23	0,694	6,04E-34	0,817	4,52E-70	0,762
LAMA4			0,660	6,84E-30	0,84	1,86E-77	0,750
COL5A2	0,674	4,98E-16	0,697	2,54E-34	0,873	1,66E-90	0,748
COL6A3	0,661	2,66E-15	0,726	1,95E-38	0,831	2,75E-74	0,739

Table S1. continued

GENES	R value	p value	R value	p value	R value	p value	R value
				Platelet activation			
COL4A2	0,66	2,29E-15	0,755	4,72E-43	0,725	6,54E-48	0,713
COL6A2	0,371	6,66E-05	0,848	1,02E-63	0,848	2,93E-80	0,689
COL5A3			0,682	1,90E-32	0,675	2,00E-39	0,679
COL6A1	0,404	1,20E-05	0,805	9,01E-53	0,825	1,26E-72	0,678
COL4A1	0,678	3,50E-16	0,611	1,16E-24	0,742	2,96E-51	0,677
ITGA5			0,729	7,89E-39	0,612	1,00E-30	0,671
COL1A2	0,553	2,92E-10	0,717	4,03E-37	0,699	3,36E-43	0,656
COL3A1	0,684	2,43E-16	0,631	1,33E-26	0,644	7,70E-35	0,653
SDC2	0,479	1,09E-07	0,602	6,79E-24	0,84	1,76E-77	0,640
HSPG2			0,698	1,82E-34	0,56	4,75E-25	0,629
COL11A1	0,441	1,45E-06	0,620	1,44E-25	0,725	7,59E-48	0,595
LAMB2	0,482	9,09E-08	0,670	4,87E-31	0,579	4,61E-27	0,577
LAMC1	0,493	4,59E-08	0,538	1,92E-18	0,654	2,91E-36	0,562
FN1	0,415	6,56E-06	0,605	3,98E-24	0,642	1,34E-34	0,554
LAMA2			0,487	6,31E-15	0,61	1,45E-30	0,549
ITGB5	0,631	8,30E-14	0,525	1,79E-17	0,486	1,96E-18	0,547
TNC			0,496	1,60E-15	0,591	2,33E-28	0,544
COMP	0,417	5,86E-06	0,496	1,67E-15	0,673	3,65E-39	0,529
THBS4			0,466	1,14E-13	0,569	5,41E-26	0,518
ITGAV			0,452	6,79E-13	0,549	5,71E-24	0,501
ITGA11	0,606	1,47E-12	0,518	4,91E-17	0,374	5,51E-11	0,499
COL1A1	0,602	1,94E-12	0,450	9,17E-13	0,387	1,08E-11	0,480
THBS3	0,315	8,89E-04	0,554	1,09E-19	0,519	3,30E-21	0,463
THBS1	0,379	4,64E-05	0,422	3,13E-11	0,578	6,51E-27	0,460
IBSP			0,376	4,97E-09	0,540	4,34E-23	0,458
SPP1			0,365	1,39E-08	0,533	1,89E-22	0,449
ITGA4			0,342	1,13E-07	0,485	2,54E-18	0,414
SDC3	0,485	7,83E-08	0,351	5,53E-08	0,381	2,38E-11	0,406
CD36			0,287	1,04E-05	0,481	5,47E-18	0,384
VWF	0,252	9,88E-03	0,461	2,20E-13	0,437	8,03E-15	0,383
ITGB3			0,325	5,09E-07	0,425	5,08E-14	0,375
ITGA7	0,421	4,91E-06	0,348	7,14E-08	0,349	1,19E-09	0,373
SV2A	0,349	1,96E-04			0,386	1,27E-11	0,368
COL2A1			0,301	3,50E-06	0,391	6,30E-12	0,346
AGRN			0,309	1,98E-06	0,372	7,32E-11	0,341
LAMB1	0,326	5,59E-04	0,349	6,29E-08	0,265	5,05E-06	0,313
LAMA5			0,262	5,86E-05	0,335	5,72E-09	0,299
COL4A4			0,257	7,93E-05	0,308	9,90E-08	0,283
COL6A6			0,190	3,82E-03	0,289	5,66E-07	0,240
ITGA10			0,190	3,91E-03	0,288	6,51E-07	0,239
TNXB			0,274	2,58E-05	0,198	6,80E-04	0,236
				TGFβ pathway			
THBS2	0,775	1,89E-23	0,694	5,05E-33	0,817	6,20E-69	0,762
DCN	0,810	4,87E-27	0,607	1,55E-23	0,747	1,16E-51	0,721
INHBA	0,639	6,83E-14	0,672	2,16E-30	0,774	1,51E-57	0,695
TGFB3	0,694	5,41E-17	0,626	2,20E-25	0,667	1,36E-37	0,662
TGFB1	0,549	1,02E-09	0,721	1,32E-36	0,704	2,53E-43	0,658
LTBP1	0,676	6,58E-16	0,461	9,92E-13	0,635	4,42E-33	0,591
COMP	0,417	1,66E-05	0,496	9,60E-15	0,673	1,76E-38	0,529
THBS3	0,315	2,57E-03	0,554	5,76E-19	0,519	1,22E-20	0,463
THBS1	0,379	1,41E-04	0,422	1,43E-10	0,578	3,08E-26	0,460
ID4	0,661	4,49E-15	0,260	2,29E-04	0,394	1,70E-11	0,438

Table S1. continued

GENES	R value	p value	R value	p value	R value	p value	R value
				TGFβ pathway			
ACVR1	0,314	2,48E-03	0,383	1,00E-08	0,564	8,02E-25	0,420
THBS4	0,172	6,00E-02	0,466	5,51E-13	0,569	2,37E-25	0,402
TGFBR1	0,272	2,80E-03	0,308	6,83E-06	0,545	5,12E-23	0,375
CDKN2B	0,361	3,28E-04	0,345	3,43E-07	0,385	4,63E-11	0,364
CHRD	0,164	7,00E-02	0,373	2,55E-08	0,386	4,30E-11	0,308
TGFB2	0,001	9,90E-01	0,374	2,39E-08	0,538	2,33E-22	0,304
FST	-0,002	9,80E-01	0,478	1,15E-13	0,337	1,37E-08	0,271
INHBB	0,301	4,01E-03	0,247	5,13E-04	0,252	3,23E-05	0,267
BMPR1B	-0,015	8,70E-01	0,363	6,13E-08	0,422	3,20E-13	0,257
BMP6	0,173	6,00E-02	0,236	8,89E-04	0,266	1,03E-05	0,225
BMPR2	0,007	9,40E-01	0,334	8,27E-07	0,323	5,83E-08	0,221
LEFTY2	0,027	7,70E-01	0,243	6,44E-04	0,374	1,77E-10	0,215
SMAD6	0,156	9,00E-02	-0,231	1,15E-03	-0,224	2,51E-04	-0,100
BMP5	0,126	1,70E-01	-0,328	1,32E-06	-0,203	9,49E-04	-0,135
SKP1	0,199	3,00E-02	-0,243	6,39E-04	-0,380	8,38E-11	-0,141
PPP2R1A	-0,344	6,97E-04	0,041	5,40E-01	-0,286	2,21E-06	-0,196
PPP2CA	-0,072	4,30E-01	-0,191	9,08E-03	-0,376	1,35E-10	-0,213
MYC	-0,271	2,80E-03	-0,207	4,17E-03	-0,342	7,70E-09	-0,273
				EMT			
SNAI2	0,606	2,80E-13	0,815	4,30E-70	0,639	5,20E-28	0,687
ZEB2	0,687	6,50E-18	0,780	1,10E-60	0,539	6,50E-19	0,669
ZEB1			0,743	3,60E-52	0,543	3,60E-19	0,643
TWIST2			0,688	4,60E-42	0,551	8,70E-20	0,620
SNAI1	0,514	2,20E-09	0,344	1,70E-09	0,416	4,20E-11	0,425
TWIST1	-0,137	1,40E-01	0,715	1,30E-46	0,670	1,50E-31	0,416
				Mesenchymal			
VIM	0,656	5,50E-16	0,782	4,00E-61	0,695	8,80E-35	0,711
ACTA2	0,679	2,00E-17	0,656	4,90E-37	0,631	3,40E-27	0,655
FN1	0,415	2,80E-06	0,642	4,90E-35	0,605	1,50E-24	0,554
CDH2	0,373	2,90E-05	0,649	5,20E-36	0,544	2,70E-19	0,522
				Epithelial			
plakophilin 2	-0,333	2,10E-04	-0,396	2,50E-12	-0,334	1,80E-07	-0,354
Occludin	-0,168	7,00E-02	-0,402	1,10E-12	-0,369	6,80E-09	-0,313
CDH1	-0,324	3,20E-04	-0,394	3,50E-12	-0,200	2,20E-03	-0,306
Villin	-0,295	1,10E-03	-0,293	3,70E-07	-0,229	4,30E-04	-0,272

Association of individual genes from KEGG and GO pathways that are significantly associated with PDGFRB expression in all three tumor cohorts. Individual genes were included if they were significantly associated with PDGFRB in at least 2/3 datasets. The genes are ordered according to the strength of the correlation across datasets (Mean R value; last column).

REFERENCES

1. Pirooznia,M., Nagarajan,V., and Deng,Y. 2007. GeneVenn - A web application for comparing gene lists using Venn diagrams. Bioinformation. 1:420-422.
2. Jensen,L.J., Kuhn,M., Stark,M., Chaffron,S., Creevey,C., Muller,J., Doerks,T., Julien,P., Roth,A., Simonovic,M. et al 2009. STRING 8--a global view on proteins and their functional interactions in 630 organisms. Nucleic Acids Res. 37:D412-D416.
3. Jorissen,R.N., Gibbs,P., Christie,M., Prakash,S., Lipton,L., Desai,J., Kerr,D., Aaltonen,L.A., Arango,D., Kruhoffer,M. et al 2009. Metastasis-Associated Gene Expression Changes Predict Poor Outcomes in Patients with Dukes Stage B and C Colorectal Cancer. Clin. Cancer Res. 15:7642-7651.

PART II | IMAGING OF METASTASIS

CHAPTER 6

6

Intravital Microscopy through an Abdominal Imaging Window Reveals a Pre-Micrometastasis Stage during Liver Metastasis

Science Translational Medicine. 2012 Oct 31;4(158) p. 158ra145

Laila Ritsma[2]*, Ernst J. A. Steller[1]*, Evelyne Beerling[2], Cindy J. M. Loomans[2], Anoek Zomer[2], Carmen Gerlach[3], Nienke Vrisekoop[2], Daniëlle Seinstra[2], Leon van Gurp[2], Ronny Schäfer[2], Daniëlle A. Raats[1], Anko de Graaff[2], Ton N. Schumacher[3], Eelco J. P. de Koning[2,4], Inne H. Borel Rinkes[1], Onno Kranenburg[1]* and Jacco van Rheenen[2]*

** Equal contribution*

1 Department of Surgery, University Medical Center Utrecht, the Netherlands
2 Hubrecht Institute-KNAW and University Medical Center Utrecht, the Netherlands
3 Department of Immunology, the Netherlands Cancer Institute, Amsterdam, the Netherlands
4 Department of Nephrology and Department of Endocrinology, Leiden University Medical Center, the Netherlands

ABSTRACT

Cell dynamics in subcutaneous and breast tumors can be studied through conventional imaging windows with intravital microscopy. By contrast, visualization of the formation of metastasis has been hampered by the lack of long-term imaging windows for metastasis-prone organs, such as the liver. Here, we developed an abdominal imaging window (AIW) to visualize distinct biological processes in the spleen, kidney, small intestine, pancreas, and the liver. The AIW can be used to visualize processes for up to 1 month, as we demonstrate with islets cell transplantation. Furthermore, we have used the AIW to image the single steps of metastasis formation in the liver over the course of 14 days. We observed that single extravasated tumor cells proliferated to form "pre-micrometastases" in which cells lacked contact with neighboring tumor cells and were active and motile within the confined region of the growing clone. The clones then condensed into micrometastases where cell migration was strongly diminished, but proliferation continued. Moreover, the metastatic load was reduced by suppressing tumor cell migration in the pre-micrometastases. We suggest that tumor cell migration within pre-micrometastases is a contributing step that can be targeted therapeutically during liver metastasis formation.

INTRODUCTION

Cancer-related mortality is predominantly caused by metastatic tumor growth in secondary organs such as the liver. Metastasis is a multistep process, which requires cells to escape from the primary tumor, survive in the circulation, enter a distant organ, and grow out in this new environment[1]. Furthermore, angiogenesis is required for the outgrowth of small metastases (micrometastases) into macroscopically detectable metastases (macrometastases with a diameter > 500 um)[2]. For the development of effective therapeutic agents targeting metastasis and angiogenesis, techniques are required to identify processes underlying metastatic growth and therapy resistance. Intravital microscopy (IVM) allows the visualization and analysis of tumor cell dynamics in live animals in real time, and may therefore lead to the discovery of novel steps during metastasis formation, which may be used in the design of therapeutics[3].

The dynamic behavior of tumor cells that escape from the primary tumor has been extensively studied using high resolution IVM in mice[4-8]. A small number of studies have also imaged the colonization of organs that are prone to metastasis, such as the lungs[9], bone marrow[10], lymph nodes[11], spleen[12], and liver[13,14]. Nonetheless, these organs are anatomically inaccessible by microscopes and should be surgically exposed, which precludes long-term imaging. Therefore, the long-term dynamic aspects of colonization are largely unknown. Cranial imaging windows can be used for multiple-day imaging, and have allowed investigators to image the formation of brain metastases[15]. However, brain tissue, isolated from the circulation by the blood-brain barrier, has a unique environment and therefore the steps to colonization may not be representative for other organs, such as the lungs and the liver. Other commonly used imaging windows cannot be utilized to image metastasis-prone organs, because of their inability to fix organs by 'clamping' (dorsal skin fold chamber[16]), or by their poor abdominal fixation and window-induced organ damage [e.g. mammary window[17-19]]. New lung imaging windows have been designed that allow imaging for up to 3 hours[20,21], but these cannot be used to image metastatic outgrowth over multiple days.

Short-term (<24 h) videomicroscopy studies of liver colonization identified many early events in liver metastasis, such as survival and growth[13,14]. In order to link cellular behavior to successful colonization, the formation of a clone should be followed longitudinally. For this, new long-term imaging windows are required that enable studying long-term dynamic events. Here, we have developed an imaging window for abdominal organs, which has allowed us to study cancer cell migration during the different phases of hepatic colonization in detail. We identified migration as a facilitating "pre-micrometastasis" step during the early colonization of liver metastases that can potentially be targeted therapeutically.

MATERIALS AND METHODS

Cell culture and generation of stable cell lines

C26 colorectal tumor cells were cultured in Dulbecco's Modified Eagle's Medium + GlutaMAX (DMEM; GIBCO, Invitrogen Life technologies) supplemented with 5% (v/v) fetal bovine serum (Sigma), 100 µg/ml streptomycin, and 100 U/ml penicillin (Invitrogen Life Technologies). Cells were kept at 37°C in a humidified atmosphere containing 5% CO2. C26 H2B-Dendra2, C26 Dendra2, C26 mCherry, and C26 lifeact-GFP were generated using standard lentiviral transfection (Supplementary Methods). Afterwards, cells were either sorted by flow cytometry,

grown as a polyclonal population, or single cell clones were selected and combined to form a polyclonal population.

Animal models

All experiments were carried out in accordance with the guidelines of the Animal Welfare Committee of the Royal Netherlands Academy of Arts and Sciences, The Netherlands. Female BALB/c (10-12 weeks), C57BL/6 mice (10-12 weeks) and MIP-GFP mice were purchased from Jackson laboratory. 129P2/OlaHsd and FVB/n (The Jackson Laboratory) mice were crossed to obtain female 129P2/OlaHsd;FVB/n mice and were used to measure AIW post-surgical behavior and blood count. Female E-cadherin-mCFP, Lrg5-EGFP-Ires-CreERT2 and R26R-confetti mice were a kind gift from H. Clevers (Hubrecht Institute). Mice were housed under standard laboratory conditions and received food and water ad libitum. U73122 (Santa Cruz Biotechnology; dissolved in 100% DMSO) and DMSO were both dissolved in PBS (final concentration 5% v/v DMSO) and animals were treated by intraperitoneal injection every other day with 200 ul of 120 ug/ml U73122 or 5% DMSO.

Liver metastasis assay

C26 cells were harvested by brief trypsinization. Colorectal liver metastases were induced as described previously[23]. In brief, single-cell suspensions were prepared to a final concentration of 7.5 x 10^4 cells/100 ul PBS. Through the incision made for implanting the AIW, cells were injected into the parenchyma of the spleen. To circumvent outgrowth of tumor cells in the spleen and to prevent the tumor cells from leaving the spleen at later time points, we removed the spleen 10 minutes after injection of the tumor cells. We did not observe arrival of new cells in the liver after splenectomy. For the mice used for intravital imaging, a liver AIW was implanted immediately after the splenectomy.

Intravital microscopy

Mice were sedated using isoflurane inhalation anesthesia (1.5 to 2% v/v isoflurane in O_2), and placed within a custom-designed imaging box. The isoflurane was introduced through a facemask, and ventilated by an outlet on the other side of the box. The imaging window was placed through a hole in the bottom of the box. The imaging box and microscope were kept at 32°C by a climate chamber. Mouse vitals were monitored during imaging using the MouseOx system (Starr Lifescience Corp.). Imaging was performed on an inverted Leica TCS SP5 AOBS two-photon microscope with a chameleon Ti:Sapphire pumped Optical Parametric Oscillator (Coherent Inc.). For more details on microscopy, see Supplementary Methods.

Tracking of C26 tumor cells

C26 cells (7.5×10^4) were injected into the spleens of BALB/c mice. Each day, a large overview image of stitched high resolution images (tile scan) was taken through the liver AIW (minimum of 3 mm x 3 mm). Maximum projections of the 3D volumes (150-300 um deep) were generated from the IVM images. Next, the SHG signal was manually overlayed for the various positions containing cells using ImageJ software (NIH).

To determine track distance and displacement of cells in the liver parenchyma, intrahepatic tumor cells and their metastases were imaged using the AIW at day 2 (pre-micrometastases) and day 5 (micrometastases). Where indicated, mice were treated with DMSO or U73122 according to the treatment schedule. Three-dimensional volumes (z-stacks) were collected every hour for 10 hours (Figure 3, C and D) or every 10 minutes for 3 hours (Figure 4, A and B)

and cells were tracked manually with an ImageJ plugin (NIH). The XYZ position was determined over time and the displacement and track distance was calculated by Microsoft Excel.
To monitor the *in vivo* growth rate of pre-micrometastases, the intrasplenically injected C26 cells and their pre-micrometastases were tracked over multiple days. Cells per pre-micrometastasis were counted 1 and 2 days after injection, and the growth rate was calculated using the following formula: LOG(cell count day1/cell count day2)/LOG(2).

Statistical analysis
A Student's t test was used to determine if there was a significant difference between two means. $P < 0.05$ was considered significant. If there was no normal distribution present (tested using a Shapiro Wilk test), or if n was less than 20, a non-parametric Mann-Whitney U test was performed. For the clonal analysis, a G-test (based on the log-likelihood ratio) was performed to determine if our findings were different from the theoretical findings based on the synergistic growth hypothesis. A one-way or two-way ANOVA was used to compare 3 or more samples.

RESULTS

Characterizing response to the abdominal imaging window
The presently available imaging windows (Figure S1A) were ultimately not suitable for abdominal organs, such as the liver. Therefore, we designed the abdominal imaging window (AIW), which consists of a reusable titanium ring with a 1-mm groove on the side and a coverslip on top, tightly secured in the skin and abdominal wall by a purse-string suture (Figure 1A; Figure S1B; movie S1). The purse-string suture is located within the groove of the ring and there is no direct opening to the abdomen with subsequent danger of infections.
Existing imaging windows remain in place for periods ranging from days to weeks[15,16,18]. To record the time until dislodgement of the AIW occurred, we implanted the window onto several abdominal mouse organs. The window did not dislodge from the abdominal wall or skin for an average of 5 weeks $\pm$ 3.9 days (SEM, n = 12), with a maximum of 63 days (Figure S2A). To detect potential discomfort caused by the AIW, we assessed the post-operative behavior of mice according to a clinical appearance scoring system[22]. We measured the reactivity, appearance, and behavior of mice carrying an AIW, and found a majority of normal scores (Figure S2, B to D). One day after surgery, the weight of all animals was slightly reduced (approximately 5% of total body weight), but returned to normal from day 5 onwards (Figure S2E). For the remaining weeks, a steady increase in weight was observed as expected for aging mice. Mice were not impaired in their mobility with the AIW, as demonstrated by their ability to stretch their bodies to get food. Furthermore, we did not observe any visual signs of inflammation or necrosis of the skin surrounding the AIW. The white blood cell count one day before, and 1, 4, 6, and 8 days after surgery was normal, indicating the absence of leukocytosis or leukopenia (Figure S2F). The red blood cell count was elevated one day after surgery, likely owing to loss of fluids during abdominal surgery, but returned to basal levels by day 4 (Figure S2G).
Liver regions that were behind the AIW and liver regions of mice without an AIW (control) were compared. We did not find any difference in the number of lymphocytes between the two groups (Figure S2H). For both the control and the AIW tissue, we observed neutrophils in the sinusoids (fenestrated capillaries), but not in between hepatocytes (Figure S2I). These data suggest the absence of a local inflammatory response upon AIW insertion. In order to test

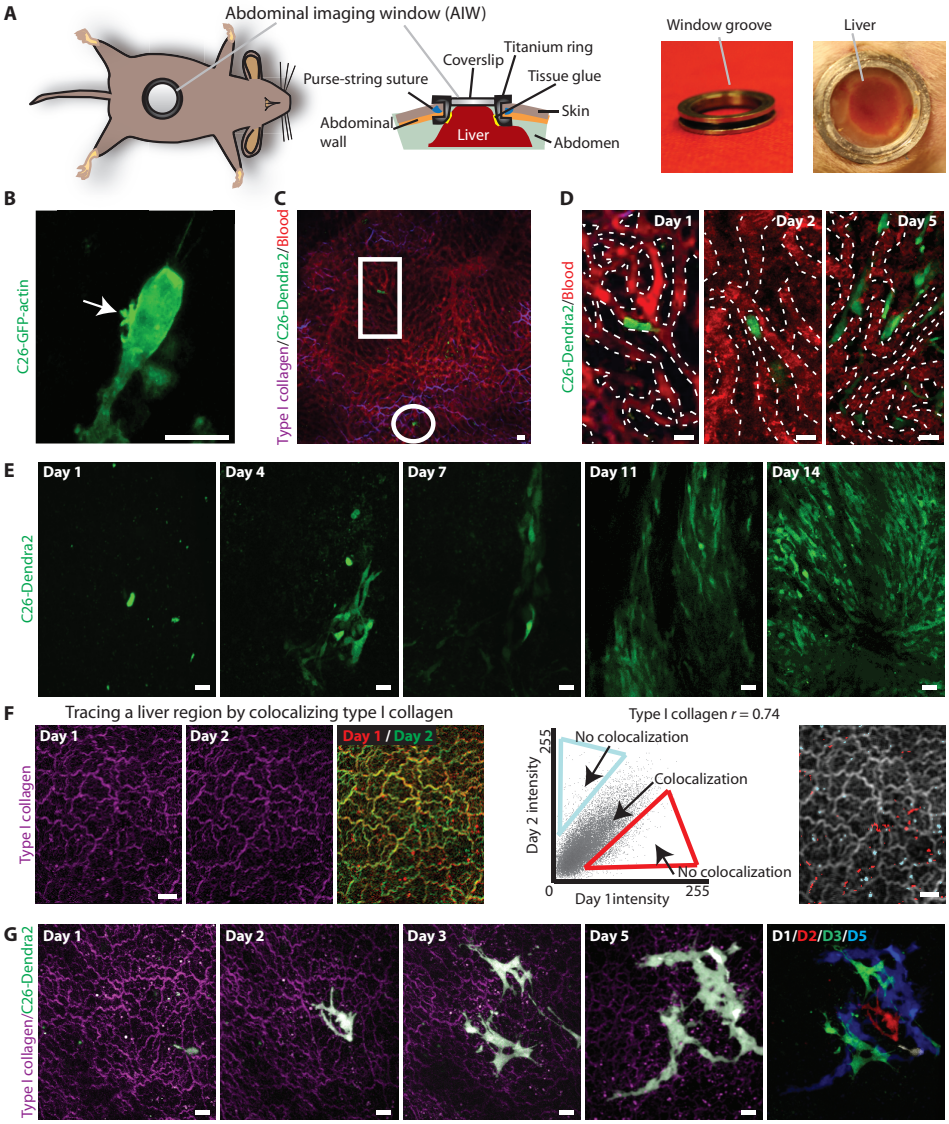

Figure 1. The abdominal imaging window as a tool to study liver metastasis over multiple imaging sessions. Intravital microscopic (IVM) images of tumor cells, the vasculature, and type I collagen [second harmonic generation (SHG)] were taken through the AIW surgically implanted above the liver. **A.** Cartoons and pictures of the AIW. **B.** High resolution image of a C26 GFP-actin cell within the liver. Actin-rich protrusions are marked by the arrow. **C.** Overview of the liver vasculature, and stalled C26 tumor cells. The circled and boxed area highlights two stalled cells. Type I collagen is shown via SHG in purple. **D.** Images of the vasculature and C26 tumor cells at days 1, 2, and 5 after injection. The dotted lines outline the sinusoids. **E.** Long-term (14-day) tracing of liver colonization. **F.** Images of type I collagen taken at the indicated time points. A merged image highlights the colocalization (yellow). To the right, a Pearson's correlation coefficient (r) and a scatter plot of the type I collagen images. The selected non-colocalizing pixels from the scatterplot, as indicated by the blue and red boxes, were replotted in the IVM image of day 1. **G.** Long-term (5-day) tracing of the outgrowth of an individual cell into a micrometastasis. All scale bars, 20 μm.

whether the AIW can lead to alterations in the structure of the abdominal tissue, hematoxylin and eosin (H&E)–stained sections were analyzed to identify possible necrotic zones and to look for abnormalities within the liver tissue architecture. We could not detect necrotic zones or any architectural differences between sections of non-perturbed and window-fixed livers (Figure S2J). Furthermore, there was no difference between the number of apoptotic cells in tissue that was behind an AIW and in the tissue of control animals (Figure S2K).
We also encountered a few challenges when using the AIW. An unavoidable problem is the breakage of the coverslip, which happens in 3% of all cases. Moreover, one week after implantation, encapsulation of the abdominal organ by connective tissue led to a drift of the organ in 20% of the cases where the abdominal organ was not touching the coverslip of the AIW. This drift caused the imaging site to be located beyond the maximum imaging depth of our microscope (~800 um), obscuring imaging resolution and sharpness of our images. Tissue motion caused by respiration can also result in imaging distortions. To reduce this, we used an inverted microscope and the surgical procedure was optimized for each abdominal organ (Supplementary Methods). Lastly, an imaging box (Figure S3A) that fits the stage of our multiphoton microscope (Figure S3B) was designed in order to stably fix the AIW above the objective.

Repetitive tumor-cell imaging with the AIW

We aimed to visualize the formation of liver metastases from individual colorectal tumor cells. For *in vivo* imaging of liver metastasis formation, we used a standardized liver metastasis assay[23] in which mouse colorectal tumor cells (C26 cells) expressing fluorescent proteins were injected into the splenic parenchyma of syngeneic BALB/c mice. To test whether the AIW could potentially be used to study the formation of liver metastases, we first visualized individual C26 cells in the liver parenchyma through the AIW with subcellular resolution (Figure 1B), as exemplified by the cell protrusions enriched in GFP-labeled actin. Ten minutes after intrasplenic injection of C26 cells transfected with fluorescent Dendra2 (day 1), individual colorectal cells were trapped in the sinusoids of the liver (Figure 1, C and D). These sinusoids are highly permeable and can be easily traversed by tumor cells[24]. In line with this, at days 2 and 5, cells could be seen outside the sinusoids (Figure 1D).
To visualize the colonization of the liver parenchyma by fluorescent C26 cells that are trapped in the sinusoids, we retraced areas of interest over multiple imaging sessions (14 days) using an AIW that contained a gridded coverslip (Figure 1E; Figure S1B). For retracing with subcellular accuracy, we used type I collagen structures as reference points [visualized by second harmonic generation (SHG)][25] (Figure 1, F and G; Figure S4). To illustrate the ability to retrace areas using type I collagen fibers, we quantified the colocalization of the fibers of an area at day 1 and day 2 by plotting the intensities of similar pixels of both images in a scatterplot and calculated the Pearson's correlation coefficient, r (Figure 1F). The pixels in the scatterplots of well-aligned images will appear along the diagonal, whereas pixels of unaligned images will be located off the diagonal (no colocalization). Importantly, when we retraced imaging regions the next day, the two images aligned well and r ranged from 0.2 to 1, depending on the signal-to-noise ratio in the images (Figure 1F). As a non-retraced negative control, we analyzed the same images but flipped the second image (Figure S4A). As expected, the r of the non-retraced negative control dropped towards zero (we will refer to the correlation coefficient for this negative control as rflip). This method allowed us to trace the liver colonization over the course of 5 days (Figure 1G) as illustrated by the high r and low rflip (Figure S4B). After 5 days, type I collagen in the initial imaging area got lost due to tumor growth, preventing the retracing at subcellular accuracy.

Metastasis growing from a single founder cell

The increase in the number of cells in the growing micrometastasis can either be explained by multiple trapped cells that cluster (synergistic growth) or by the clonal growth of an individual cell (Figure S5). Earlier work suggests that most metastases are clonal[26], thus it was expected that our C26 tumor model also grew clonally. However, we cannot exclude synergistic growth of our model. In order to determine whether multiple tumor cells need to cluster to initiate proliferation and growth of a metastasis or whether metastases grow from a single founder cell we co-injected the same number of two distinctly colored C26 tumor cell populations into the spleen. The different colors enabled us to trace progeny, even when cells were located within the same imaging field (Figure 2A). We found that 94% of the micrometastases in the liver were single-colored at day 5 (Figure 2B). Likewise, 97% of the macrometastases (>500 µm) consisted of a single color at day 14 (Figure 2, B and C). The color distribution in micro- and macrometastases was significantly different from the synergistic growth hypothesis ($P < 0.0001$, G-test). These data illustrate that most metastases are grown from a single founder cell. Importantly, differently colored tumor cell populations did not differ in their ability to form macrometastases (Figure 2D).

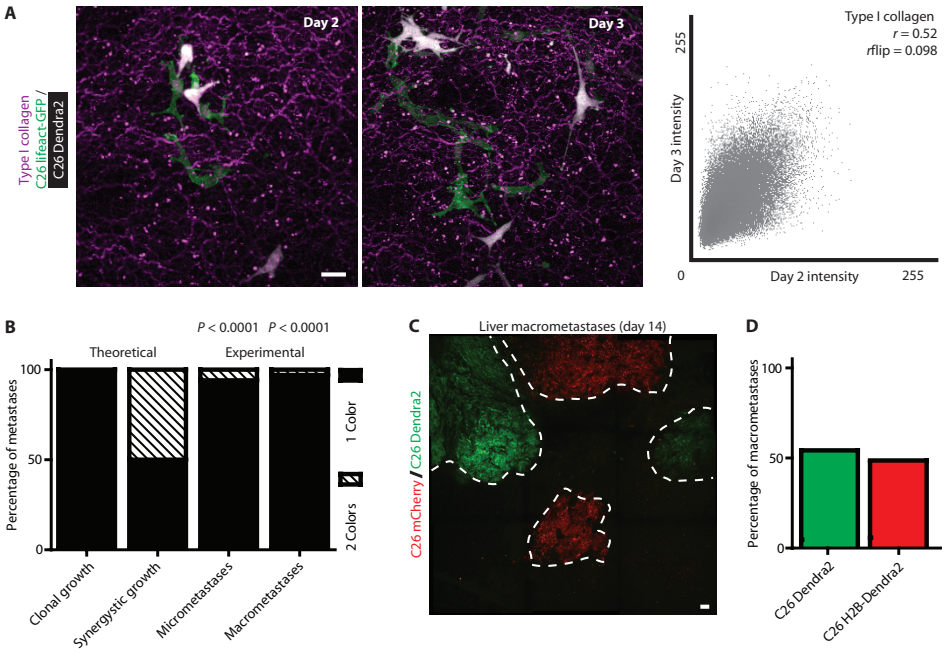

Figure 2. Clonal metastatic growth of C26 liver metastases. A. A mix of differently colored populations of C26 tumor cells were injected intrasplenically (more details in Figure S5) and imaged using the AIW at days 2 and 3. A corresponding scatter plot is shown. Scale bar, 20 um. **B.** Theoretical expected percentages of cell distribution (assuming two differently colored population of C26 cells) in metastases for clonal growth and for synergistic growth, and the experimental percentage from this study (n = 18 micrometastases in 4 mice, n = 39 macrometastases in 4 mice, P-values obtained using a G-Test). **C.** An *ex vivo* image of 14-day old liver metastases, each containing only one color. The dotted lines outline metastases. **D.** A graph is provided to show the percentage of macrometastases of each color in the liver (n = 39 metastases in 4 mice). Scale bar, 50 um.

A pre-micrometastatic stage with high tumor cell motility and proliferation

Next, we analyzed the outgrowth of single founder cells into metastatic colonies to explore potential unidentified contributing steps in the formation of metastases. A mix of differently colored C26 cells was monitored for 5 days following injection in the spleen. Within the first 24 hours, trapped tumor cells had left the vasculature and proliferated. The center of the progeny was on average located 71.5 ± 9.3 um (SEM) (~3 cell diameters) away from the arrival site. This deviation is larger than the theoretically calculated shift of two–cell-diameters in the unlikely case cells would divide asymmetrically towards one direction for this time frame, and therefore the observed shift suggests that the cells have migrated away from the arrival site. Interestingly, when examining the clones at different time points, a phenotypic difference was observed (Figure 1G). The cells of 3-day–old clones were surrounded mainly by liver parenchyma. Over the next two days, the cell density in the clones increased so that most cells were mainly surrounded by other tumor cells. To define these different stages, we refer to a clone as a "pre-micrometastasis" when the majority of cells have at least one-half of their cell surface surrounded by liver parenchyma (Figure 1G, day 3; Figure 3A). When less than 50% of the cells within a clone are mainly surrounded by liver parenchyma and when the clone is smaller than 500 um in diameter, we refer to this clone as a "micrometastasis" (Figure 1G, day 5; Figure 3A).

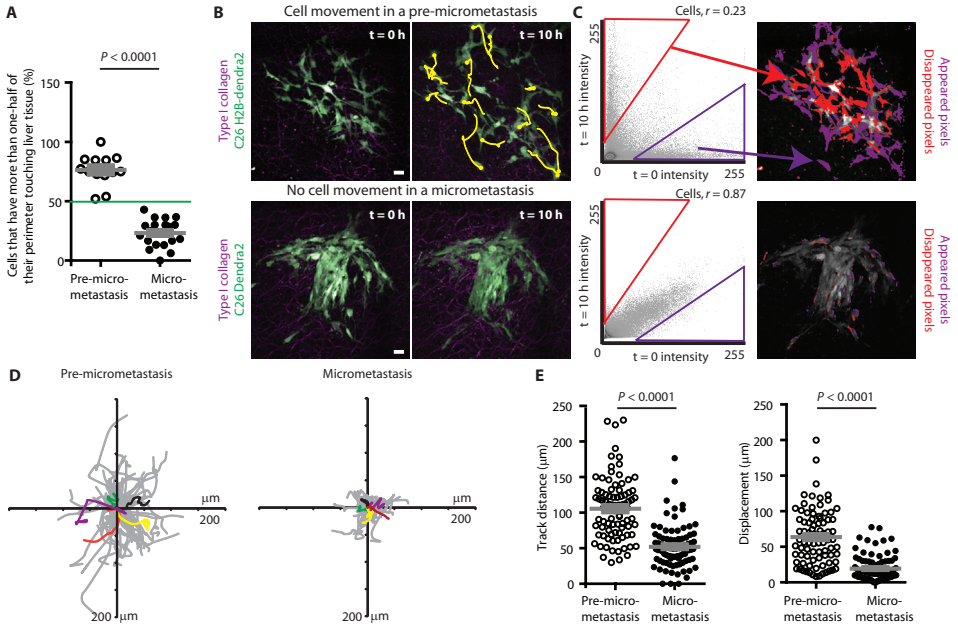

Figure 3. Migration within pre-micrometastases, but not within micrometastases in the liver. IVM images of type I collagen (SHG) and tumor cells were taken through the AIW. **A.** The percentage of cells in the clone that have at least one-half of their cell perimeter touching liver tissue. If the majority of the cells reach this criteria, we refer to this clone as a pre-micrometastasis (n ≥ 11 for each condition in ≥ 3 mice per condition). **B.** Representative images of cell movement over 10 hours. The yellow lines highlight the tracks of the tumor cells. Scale bars, 20 µm. **C.** A scatter plot and r of the cells shown in (B). The selected non-colocalizing pixels from the scatter plot (indicating cell movement, purple and red boxes), were replotted in the t = 0 IVM image shown in (B). **D.** The migration path of individually traced tumor cells (n ≥ 58 cells in 3 mice per condition). A few example migration tracks are shown in color. **E.** Quantification of the track distance and displacement of individual tumor cells after 10 hours. Data are from the cells tracked in (D). P-values obtained using a Mann Whitney U test. Data in (A) and (E) are means ± SEM.

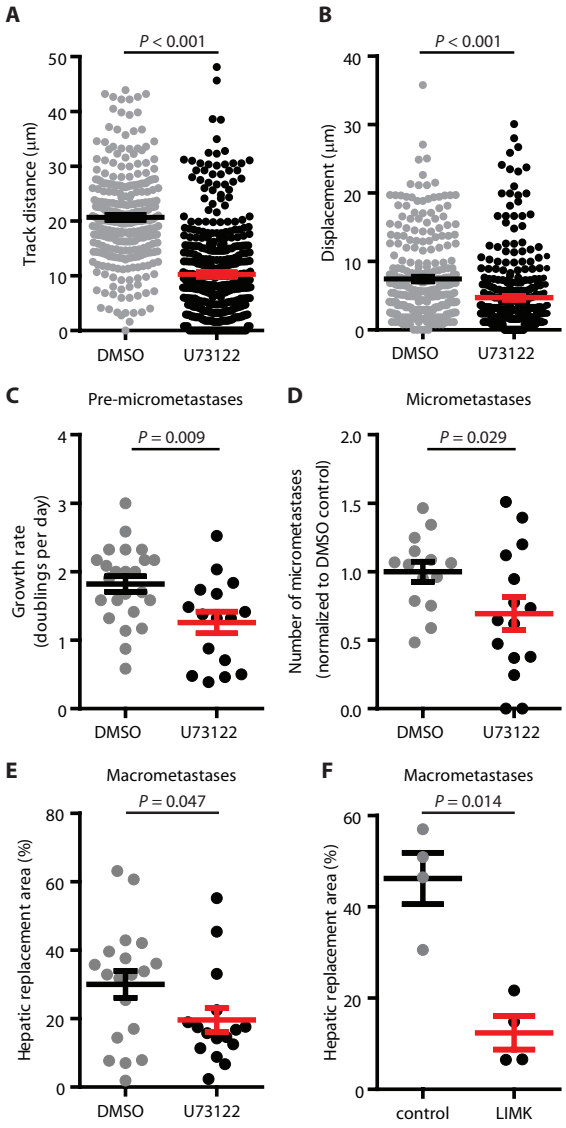

Figure 4. Migration and growth of pre-micrometastases treated with U73122. C26 tumor cells were injected intrasplenically and their intra-hepatic course was followed over time using a liver AIW. Animals were either treated after cells had left the vasculature according to the scheme depicted in figure S8. (**A** and **B**) The track distance (A) and displacement (B) of single pre-micrometastatic cells within 1 hour in treated animals (n > 282 cells in 5 mice per condition). **C.** The growth rate of pre-micrometastases in treated animals between day 2 and day 3 (n ≥ 16 clusters in ≥3 mice per condition). **D.** The number of micrometastases in H&E-stained liver sections from treated animals (n = 5 mice per condition). **E.** At day 14, livers were isolated and the hepatic replacement area (HRA) was determined (n = 15 sections in 5 mice per condition). **F.** C26 cells transfected with Lim kinase or control plasmid were injected intrasplenically. At day 14, livers were isolated and the HRA was determined (n = 5 mice per condition). Data are means ± SEM. P-values determined using a Mann Whitney U test.

In order to test whether cells in these phenotypically different stages display distinct behavior, we acquired 10-hour time-lapse movies of pre-micrometastases and micrometastases (Figure 3B). The cell signals detected at 0 and 10 hours were then compared in a scatter plot (Figure 3C). By subsequently highlighting the non-colocalizing (off-diagonal) pixels in the original microscopy image, we could see which cells had changed location between the 0- and 10-hour time points. Pre-micrometastases consisted of active cells that formed protrusions and were migratory (Figure 3, B to D). Although the cells in pre-micrometastases were migratory, disintegration did not occur because the cells changed direction often. In contrast to pre-micrometastases, cells within micrometastases were largely immotile and did not form protrusions (Figure 3, B to D; movie S2). In line with this, individual photomarked cells within micrometastases did not move (Figure S6). Both the mean total track distance (54.7 μm) and mean displacement (22.2 μm) of tumor cells within micrometastases were significantly less compared to pre-micrometastases (105.4 μm vs. and 63.6 μm, respectively) (Figure 3E).

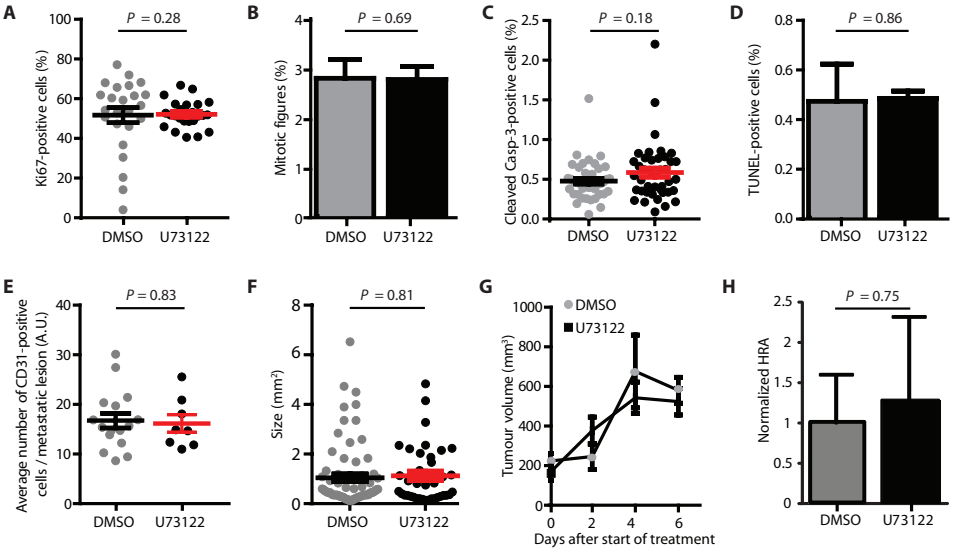

Figure 5. Proliferation, survival and vascularization of C26 macrometastases in the presence of U73122. Mice were injected intrasplenically with C26 cells and treated with DMSO or U73122 until macrometastases were formed. **A.** Liver sections of treated animals were stained for proliferation using a Ki67 antibody. The number of proliferating cells was determined in macrometastases (n > 40 fields in 3 mice per condition). **B.** The mitotic index was determined in liver sections of mice injected intrasplenically with C26 H2B-Dendra2 tumor cells (n > 40 fields in 3 mice per condition). **C.** Liver sections of treated animals were stained for apoptotic cells using a cleaved casp-3 antibody and cells were quantified in the macrometastases as a percentage of the total amount of cells (n > 40 fields in 3 mice per condition). **D.** Liver sections of treated animals were stained for TUNEL. The number of apoptotic cells was determined in macrometastases (n > 40 fields in 3 mice per condition). **E.** Liver sections of treated animals were stained for CD31⁺ blood vessels. The number of blood vessels within macrometastases was quantified (n > 8 metastases in 3 mice per condition). **F.** In treated animals, the size of macrometastases were determined in liver H&E sections (n > 38 metastases in 3 mice per condition). **G.** Mice were subcutaneously injected with C26 tumor cells and treated with U73122 or DMSO daily. The tumor growth rate was measured over time (n = 3 mice per condition). **H.** The bardiagram shows the normalized Hepatic Replacement Area of 14 day old macrometastases of animals treated from day 6 onwards according to the scheme depicted in figure S8C (n = 5 mice per condition). Data are means ± SEM. P-values determined using a Mann Whitney U test.

Pharmacological inhibition of migration and growth of cells in pre-micrometastases

The observation that tumor cells display active migration during the pre-micrometastatic stage raises the intriguing possibility that this could contribute to the efficiency of liver metastasis formation. We have recently established that the cofilin pathway is critical for migration of C26 cells, and that cofilin is activated following phospholipase C (PLC) activation[27]. Although the migration of leukocytes[28], neutrophils[29], and macrophages[30] is independent of PLC, migration and invasion of many tumor cell lines, including C26 cells, can be inhibited by the PLC inhibitor U73122 (Figure S7, A and B)[27,31]. To test whether the migration of C26 cells can be inhibited during the pre-micrometastatic stage, we treated mice with U73122 or DMSO (vehicle) after cells had left the vasculature (Figure S8A). Subsequently, we imaged *in vivo* migration of the tumor cells in pre-micrometastases through the liver AIW. U73122 significantly decreased the mean track distance 2-fold (Figure 4A) and the mean displacement 1.6-fold) (Figure 4B) of tumor cells in pre-micrometastases.

To test whether blocking cell migration in the pre-micrometastatic stage by U73122 treatment has an effect on liver metastasis formation, we analyzed the growth of pre-micrometastases. U73122 treatment significantly suppressed the growth rate of C26 pre-micrometastases *in vivo* by 1.7-fold (Figure 4C), which was in contrast to the *in vitro* growth response (Figure S7, C and D). This suggests that U73122 may affect growth in the pre-micrometastasis indirectly, by inhibiting migration. Furthermore, the diminished growth rate *in vivo* led to a 1.4-fold reduction in the number of pre-micrometastases that grew into micrometastases (Figure 4D). When blocking cell migration in the pre-micrometastatic and subsequent stages (Figure S8B), the metastatic area in relation to liver-tissue area [hepatic replacement area (HRA)] was also 1.5-fold diminished (Figure 4E). An alternative genetic approach to inhibit migration of C26 cells is the overexpression of the Lim kinase that phosphorylates and inhibits cofilin[27,32]. Similar to U73122 treatment, expression of Lim kinase reduced the HRA by 3.4 fold (Figure 4F).

Growth rate of micro- and macrometastases unaffected by U73122

If U73122 affects growth in the pre-micrometastasis by inhibiting migration, we hypothesized that U73122 would not inhibit growth in the micro- and macrometastases, because migration of cells is diminished at these stages. Growth is a balance of proliferation and cell death; thus, we determined the number of proliferating and apoptotic cells in liver sections of 14 day old macrometastases of mice that followed a prolonged treatment protocol (Figure S8B). We did not find significant differences in the number of proliferating (Ki67-positive) cells in metastases of these two animal groups (Figure 5A) or in the mitotic indices (Figure 5B). There were no significant differences in cleaved caspase-3 or TUNEL-positive cells in the two treatment groups (Figure 5, C and D). In order to test for potential effects of U73122 on microvasculature density, we stained the sections for CD31. There was no significant difference between the two treatment groups in microvasculature (Figure 5E). Moreover, U73122 did not inhibit growth of micrometastases into macrometastases, as the size of the 14 day old macrometastases was not reduced (Figure 5F).

These *in vivo* data agree with the *in vitro* results showing that U73122 treatment does not directly target proliferation and apoptosis of C26 cells. In line with this, the growth of subcutaneous C26 tumors was not affected by U73122 treatment (Figure 5G). This implies that the inhibition of growth of pre-micrometastases [with the subsequent effect on the HRA (Figure 4E)] by U73122 is indirectly achieved by inhibition of migration. Indeed, treatment only during the micrometastatic and macrometastatic stages (Figure S8C), where cells are

not migratory (from day 6 onward), did not affect the HRA (Figure 5H). Collectively, our results suggest that cell migration within pre-micrometastases is a contributing step of metastatic liver colonization.

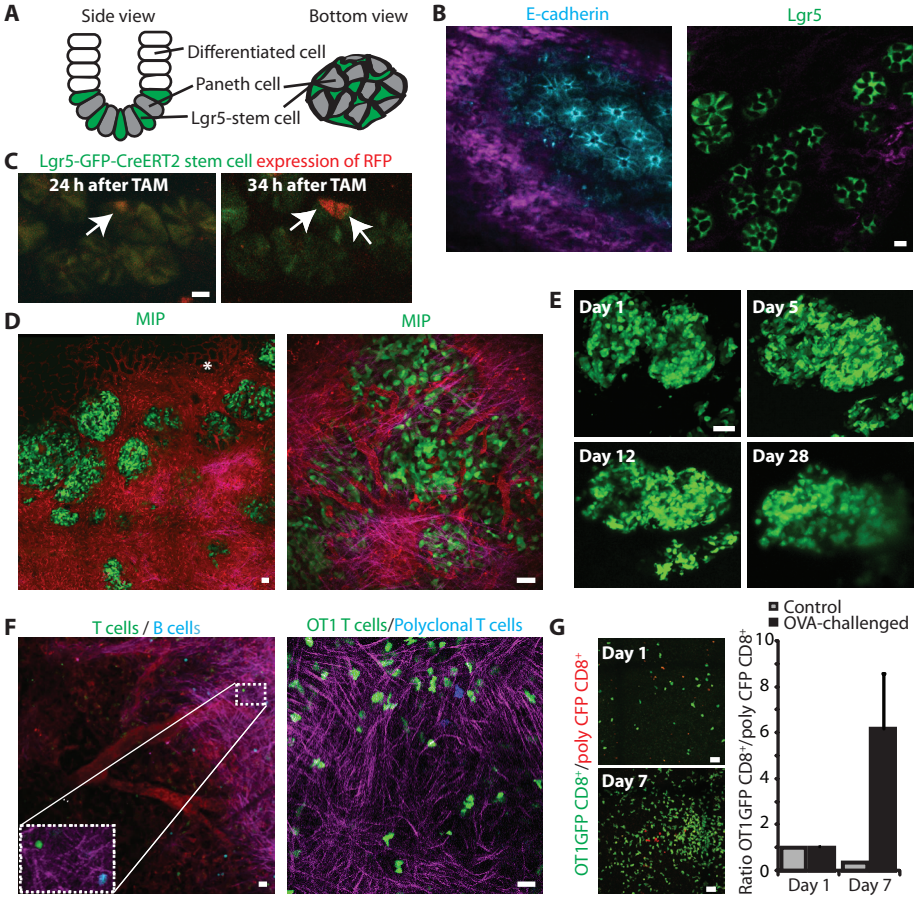

Figure 6. Subcellular visualization of abdominal organs. In all images type I collagen is shown in purple, the vasculature in red, and other cell types or structures as indicated. **A.** A cartoon showing intestinal stem cells and paneth cells within a crypt. **B.** IVM images of the small intestine in which the cell-cell adhesions (left) or LGR5$^+$ stem cells (right) are visible. **C.** Tracing was obtained by stochastically inducing the expression of one of the confetti colors (RFP) in the Lgr5-expressing stem cells using tamoxifen. The red-labeled stem cell proliferates and produces two red-labeled stem cells the next day (indicated by the white arrows). Scale bars, 10 µm. **D.** Images of insulin-producing B-cells that were transplanted under the kidney capsule. Left panel shows an overview of multiple islets, and the right panel shows a higher magnification of a single islet. The asterisk highlights the normal kidney vasculature. **E.** Images of a 28-day tracing experiment of islets of Langerhans that were transplanted the kidney capsule. Shown are images of the same islet at 1, 5, 12 and 28 days. Scale bar, 100 µm. **F.** IVM Images of T and B cells (left image), and of OT1-GFP CD8$^+$ T cells and poly-actin CFP CD8$^+$ T cells in the spleen (right image). Inset shows magnification of selected area. Scale bars represent 20 µm. G. IVM images of OTI GFP CD8$^+$ cells (green) and poly CFP CD8$^+$ cells (shown in red) were made of the same mouse on day 1 (left) and day 7 (right) after it was challenged with an OVA peptide in the presence of CpG. To the right, a bar diagram shows the ratios of the GFP/CFP cells normalized to day 1. The OVA challenged group consisted of 3 mice, the control group of 1 mouse. Data are means ± SEM.

Imaging abdominal organs long-term at subcellular resolution

To extend the utility of the AIW, we examined whether we could visualize abdominal organs other than the liver at subcellular resolution in living mice using multiphoton microscopy. We were able to visualize single cells in the small intestine, spleen, pancreas, and kidney (Figure 6). As an example of how the AIW could contribute to stem cell research, we have visualized stem cells positive for the leucine-rich-repeat-containing G-protein-coupled receptor 5 (Lgr5) in the crypts of the small intestine, which reside between the paneth cells in the epithelial layer (Figure 6, A and B). We visualized an individual $Lgr5^+$ stem cell division over the course of 3.5 hours using the AIW (Figure S9). To confirm division, we performed lineage-tracing experiments in GFP-labeled stem cells where, at day 1, expression of a red fluorescent label in one of the Lgr5+ cells was activated using tamoxifen (Supplementary Methods). On day 2, this new label was present in two daughter cells, but not in the surrounding cells (Figure 6C). In order to track these stem cells over multiple days, we used the vasculature as visual (fiducial) landmarks.

In another demonstration of long-term imaging through the AIW, we visualized the engrafment of GFP-labeled islets of Langerhans in the kidney (Figure 6D) and then traced the cells for 28 days through the AIW (Figure 6E). The vascularization of the islets containing b-cells was clearly visible at day 8 post-transplantation (Figure 6D).

We were also able to visualize insulin-producing b-cells through a pancreas AIW using a mouse insulin promoter-GFP (MIP-GFP) transgenic mouse model (Figure S10A), with pancreatic acinar cells visible at subcellular resolution (Figure S10B). In our last demonstration with the AIW, we intravenously transferred fluorescent B and $CD8^+$ T lymphocytes into the spleen and then followed the acute $CD8^+$ T cell response to antigen (ovalbumin peptide) challenge *in vivo* over multiple days (Figure 6, F and G; Figure S11) (Supplementary Methods). Tracking specific immune responses is an active area of imaging research, and using the spleen AIW we were able to quantify a T cell response 7 days after antigen challenge (Figure 6G; Figure S11A). Interestingly, additional information can be extracted from the IVM data, as we found individual $CD8^+$ T cells to be predominantly migratory and clustered $CD8^+$ T cells to be non-migratory (Figure S11B; movie S4), which likely reflects antigen recognition[33].

DISCUSSION

Long-term imaging of metastatic outgrowth and cancer treatment holds promise for discovering novel processes that may be exploited therapeutically[3]. In this study we describe the development of an AIW and have used it to image metastatic outgrowth in the liver at subcellular resolution. This high-resolution IVM technique can potentially be used to evaluate tumor recurrence after chemotherapy, which is a poorly understood phenomenon. We have used the AIW to identify a distinct intervention step during metastatic colonization to prevent formation of liver metastases. In this step, individual C26 tumor cells can proliferate into pre-micrometastases. In these pre-micrometastases, the cell density is low and cells display migratory behavior. Subsequently, the growing clones condense into micrometastases in which cell migration is strongly diminished. Our imaging study indicates that growth of pre-micrometastases is linked to migration, and that interfering with migration at this stage prevents liver metastasis formation, which could potentially retard tumor progression and improve patient survival rates.

In our study, we found that tumor cell migration supports the growth of pre-micrometastases, but not of micrometastases. Processes such as growth depend on the dynamic interplay between cell intrinsic properties and their microenvironment[34]. The different microenvironments experienced by tumor cells in pre-micrometastatic and micrometastatic stages may provide an explanation for the observed differential dependency on migration. Migration is possibly required for optimal positioning of the growing clone. Several migration-inducing genes have recently been linked to hepatic colonization of human colorectal cancer[35,36]. These genes potentially affect extravasation and niche-finding, and additionally they may affect the growth of pre-micrometastases.

Here, we were able to reduce migration in the pre-micrometastases by therapeutic intervention with the PLC inhibitor U73122, which led to reduced metastatic growth. Although U73122 reduced the metastatic burden by ~40%, this drug will not be the first choice of inhibitor for clinical purposes. We used U73122 because it effectively blocks migration without directly affecting proliferation and cell survival. However, the inhibition of metastatic load was not complete. A drug that affects other metastatic steps, such as proliferation or survival, in addition to downregulating migration, will be much more effective in reducing metastatic outgrowth. Nevertheless, migration is a well studied process, and many inhibitors of this process have already been developed which may serve as chemotherapeutic agents.

To study liver colonization, we used a standardized liver metastasis assay in which the colorectal carcinoma cell line C26 was intrasplenically injected. The C26 cell line generates carcinomas with an undifferentiated phenotype. As such, it may be a good model for metastasis development by undifferentiated colorectal carcinoma. Whether the processes described in this report also play a role during metastasis formation by well-differentiated colorectal carcinomas and/or by other tumor types has yet to be understood. With the recently developed protocols for isolating and expanding tumor-initiating cells directly from tumor resection specimens[37,38], this now seems feasible. Such studies should reveal the contribution of tumor cell migration during liver colonization across a large panel of human colorectal tumors. The demonstration of such a contribution would form an incentive to start evaluating the added value of migration-targeting drugs in the treatment of metastatic (colorectal) cancer.

Because inhibiting migration will only selectively target metastatic growth at the pre-micrometastatic stage, one can argue against the effectiveness of inhibiting migration as a treatment strategy when patients present themselves with a metastasized tumor. However, similar to tumor cells in the primary tumor, tumor cells within metastases invade and enter blood vessels leading to circulating tumor cells that seed secondary metastases[39,40]. In the clinical setting, it has also been observed that, even after successful resection of the primary tumor, tumor cells are detected in the blood that may seed new metastases[41]. This suggests that new metastases are constantly initiated. Interference of migration during the pre-micrometastasis phase could potentially inhibit the outgrowth of these new clones thereby blocking the expansion of metastasis, ultimately leading to prolonged survival of patients. The success of this potential therapeutic approach could be evaluated preclinically using the AIW.

REFERENCE LIST

1. Nguyen, DX et al. Metastasis: from dissemination to organ-specific colonization. Nat.Rev.Cancer 9, 274-284. 2009.
2. Hanahan, D et al. Hallmarks of cancer: the next generation. Cell 144, 646-674. 2011.
3. Amornphimoltham, P et al. Intravital microscopy as a tool to study drug delivery in preclinical studies Adv Drug Deliv Rev. 63, 119-128. 2011.
4. Beerling, E et al. Intravital microscopy: new insights into metastasis of tumors. J.Cell Sci. 124, 299-310. 2011.
5. Condeelis, J et al. Intravital imaging of cell movement in tumours. Nat Rev Cancer. 3, 921-930. 2003.
6. Lohela, M et al. Intravital imaging of stromal cell dynamics in tumors. Curr Opin Genet Dev 20, 72-78. 2010.
7. Ritsma, L et al. Intravital imaging of cell signaling in mice. 1, 3-11. 2012.
8. Sahai, E. Illuminating the metastatic process. 7, 737-749. 2007.
9. Kimura, H et al. Real-time imaging of single cancer-cell dynamics of lung metastasis. 109, 58-64. 2010.
10. Sipkins, DA et al. *In vivo* imaging of specialized bone marrow endothelial microdomains for tumour engraftment. 435, 969-973. 2005.
11. Mempel, TR et al. T-cell priming by dendriticcells in lymph nodes occurs in three distinct phases. 427, 154-159. 2004.
12. Grayson, MH et al. Confocal fluorescent intravital microscopy of the murine spleen. 256, 55-63. 2001.
13. Ito, S et al. Real-time observation of micrometastasis formation in the living mouse liver using a green fluorescent protein geneâ€˜tagged rat tongue carcinoma cell line. 93, 212-217. 2001.
14. Naumov, GN et al. Cellular expression of green fluorescent protein, coupled with high-resolution *in vivo* videomicroscopy, to monitor steps in tumor metastasis. 112, 1835-1842. 1999.
15. Kienast, Y et al. Real-time imaging reveals the single steps of brain metastasis formation. 16, 116-122. 2010.
16. Alexander, S et al. Dynamic imaging of cancer growth and invasion: a modified skin-fold chamber model 130, 1147-1154. 2008.
17. Gligorijevic, B et al. Dendra2 photoswitching through the Mammary Imaging Window. J.Vis.Exp. 2009.
18. Kedrin, D et al. Intravital imaging of metastatic behavior through a mammary imaging window. 5, 1019-1021. 2008.
19. Shan, S et al. A novel rodent mammary window of orthotopic breast cancer for intravital microscopy. 65, 109-117. 2003.
20. Kreisel, D et al. *In vivo* two-photon imaging reveals monocyte-dependent neutrophil extravasation during pulmonary inflammation. Proc.Natl.Acad. Sci.U.S.A 107, 18073-18078. 2010.
21. Looney, MR et al. Stabilized imaging of immune surveillance in the mouse lung. 8, 91-96. 2011.
22. Te Velde, EA et al. Impaired healing of cutaneous wounds and colonic anastomoses in mice lacking thrombin-activatable fibrinolysis inhibitor. 1, 2087-2096. 2003.
23. Drixler, TA et al. Continuous Administration of Angiostatin Inhibits Accelerated Growth of Colorectal Liver Metastases after Partial Hepatectomy. 60, 1761-1765. 2000.
24. Paku, SÃ et al. Organ-specificity of the extravasation process: An ultrastructural study. 18, 481-492. 2000.
25. Perentes, JY et al. *In vivo* imaging of extracellular matrix remodeling by tumor-associated fibroblasts. 6, 143-145. 2009.
26. Talmadge, JE et al. Evidence for the Clonal Origin of Spontaneous Metastases. 217, 361-363. 1982.
27. Steller, EJA et al. The death receptor CD95 activates the cofilin pathway to stimulate tumour cell invasion. 12, 931-937. 2011.
28. Jiang, H et al. Roles of phospholipase C beta2 in chemoattractant-elicited responses. 94, 7971-7975. 1997.
29. Li, Z et al. Roles of PLC-beta2 and -beta3 and PI3Kgamma in Chemoattractant-Mediated Signal Transduction. 287, 1046-1049. 2000.
30. Wang, Z et al. Phospholipase C beta3 deficiency leads to macrophage hypersensitivity to apoptotic induction and reduction of atherosclerosis in mice. 118, 195-204. 2008.
31. Mouneimne, G et al. Phospholipase C and cofilin are required for carcinoma cell directionality in response to EGF stimulation. 166, 697-708. 2004.
32. Hoogwater, FJH et al. Oncogenic K-Ras Turns Death Receptors Into Metastasis-Promoting Receptors in Human and Mouse Colorectal Cancer Cells. 138, 2357-2367. 2010.
33. Moreau, HD et al. Dynamic In Situ Cytometry Uncovers T Cell Receptor Signaling during Immunological Synapses and Kinapses *In Vivo*. Immunity 2012/06/12, 351-363. 2012.
34. Friedl, P et al. Cancer Invasion and the Microenvironment: Plasticity and Reciprocity. 147, 992-1009. 2011.
35. Ding, Q et al. APOBEC3G promotes liver metastasis in an orthotopic mouse model of colorectal cancer and predicts human hepatic metastasis. 121, 4526-4536. 2011.
36. Sun, L et al. P-Cadherin Promotes Liver Metastasis and Is Associated with Poor Prognosis in Colon Cancer. 179, 380-390. 2011.
37. Ricci-Vitiani, L et al. Identification and expansion of human colon-cancer-initiating cells. 445, 111-115. 2007.
38. Sato, T et al. Long-term Expansion of Epithelial Organoids From Human Colon, Adenoma, Adenocarcinoma, and Barrett's Epithelium. 141, 1762-1772. 2011.
39. Armstrong, AJ et al. Circulating Tumor Cells from Patients with Advanced Prostate and Breast Cancer Display Both Epithelial and Mesenchymal Markers 9, 997-1007. 2011.

40. Hou, JM et al. Circulating Tumor Cells as a Window on Metastasis Biology in Lung Cancer. 178, 989-996. 2011.
41. Ghossein, RA et al. Detection of circulating tumor cells in patients with localized and metastatic prostatic carcinoma: clinical implications. 13, 1195-1200. 1995.

SUPPLEMENTARY MATERIALS AND METHODS

DNA constructs and transfections

Dendra2 was cloned from the pDendra2 (Evrogen) into a pLV.CMV construct (a kind gift from P. Derksen, University Medical Center Utrecht). The pLV.CMV.H2B-Dendra2 construct was cloned by inserting H2B (from a H2B-YFP vector; a kind gift from G. Kops, University Medical Center Utrecht) into the pLV.CMV.Dendra2 construct. pLenti-lifeactGFP was a kind gift from O. Pertz (University of Basel). CMV-mCherry transfer vector was a kind gift from C. Löwik (Leiden University Medical Center). Transfections were performed using lipofectamine 2000tm (Invitrogen Life Technologies) according to manufacturer's protocol.

Antibodies and reagents

The MA rabbit Ki67 antibody was obtained from Thermo Fischer Scientific. The antibodies B220-PerCp-Cy5.5, CD19-APC, CD3-PE, CD4-APC, CD8-FITC, VA-2PE, CD8-PerCP-Cy5.5 and CD8-APC were obtained from BD Biosciences and were used for isolation and transfer of B and T lymphocytes. The antibody against cleaved caspase-3 was obtained from Cell Signaling Technology, the antibody against CD31 was obtained from BD Biosciences, and the secondary antibody Alexa Fluor 647 was obtained from Invitrogen. The TUNEL stain was performed using the Click-iT TUNEL Alexa Fluor 647 Imaging Assay kit from Invitrogen. OVA tetramer-APC was generated as described previously (48). The 70 kDa Dextran–Texas Red was obtained from Invitrogen Life Technologies.

Immunohistochemistry

After harvesting, organs were either snap frozen in Tissue Freezing Medium (Leica Microsystems Nussloch GmbH) using liquid nitrogen, or fixed in 4% PFA and paraffin-embedded. Frozen tissue was sectioned using a Leica cryotome CM 3050 and fixed with acetone for immunostaining with TUNEL or CD31. Paraffin-embedded tissues were sectioned by a Leica microtome RM 2235 and stained for Ki67, cleaved Casp-3, hematoxylin and eosin (H&E), Sudan Black B according to standard histological protocols.

AIW specifics

The AIW was prepared one day prior to surgery. It consists of a reusable titanium ring (14 mm outer diameter) with a 1-mm groove on the side which is made of the highest grade stainless steel ASTMF136-02A that meets ISO5832 part 3 and EN10204-3.1.B (FMI instrumet). On top, a 0.17-mm thick coverslip (Thermo Scientific, Menzel-Gläzer, 12 mm outer diameter) or a 0.17-mm thick photo-etched coverslip (Electron Microscopy Sciences, 12 mm ø) was glued using ethyl-cyanoacrylate glue (Super glue, Pattex power Gel, Henkel). The coverslips were coated with poly-L-lysine-g-poly(ethylene glycol)(SuSoS, Dübendorf). The size of the visible field of view was 10 mm in diameter, and the weight of the AIW was 0.45 g.

AIW surgery

All surgical procedures were performed under 2% isoflurane inhalation anesthesia. Prior to surgery, buprenorphine (3 ug per mouse) was administered intramuscularly to provide sufficient perioperative analgesia. During surgery, body temperature was maintained at 32°C by an electric heat pad. Surgical procedures were performed under aseptic conditions. Before surgery, the abdominal area of the mouse was shaved, and the skin was disinfected using 70% ethanol. A midline or left lateral flank (in case of a spleen or kidney window) incision was made through

skin and underlying abdominal wall. Next, the organ of interest was mobilized using sterile cotton tips. The wound edge (both the abdominal wall and the skin) was then sutured using a non-absorbable non-woven purse-string suture (4-0 prolene suture). Next, n-butyl cyanoacrylate or ethyl-cyanoacrylate glue was applied to the internal or abdominal side of the imaging ring, but not to the coverslip. Then the AIW was placed (glass side up) on top of the organ of interest. The glue firmly secured the organ of interest to the window ring. The glue was not in close proximity to the imaging site (coverslip) (Fig. 1A). After approximately 2 minutes, the skin and abdominal wall were placed within the window groove, and the sutures were tightened, firmly securing the window. After surgery, the mice were kept at 32°C until fully recovered from anesthesia. Mice were closely monitored for a few hours after surgery, and food was provided ad libitum within the cage.

To place the AIW over the liver, the following extra steps were taken. After the midline incision through skin and ventral abdominal wall the caudal part of the sternum (xyphoid process) was clamped and removed. Next, the falciform ligament was transected to create space between the liver and diaphragm. To ensure minimal movement from respiration and a secure anatomical position of the liver, a small piece of sterile cotton was placed in the gap created by dissecting the falciform ligament. To place the AIW over a kidney, the following extra steps were taken. First, GFP-positive islets were hand-picked from a collagenase-digested MIP-GFP pancreas just before transplantation under the renal capsule. After an incision through the skin and lateral abdominal wall was made on the left lateral flank, the kidney was located and positioned outside the abdominal wall. To ensure a permanent position behind the window, the abdominal wall was sutured with a purse-string suture and closed around the kidney vessels, securing the kidney in place but keeping the renal vasculature intact. Next, the skin was sutured with a purse-string suture and placed in the window groove as described above. Last, for the intestinal window, extra steps were taken to ensure that the intestine remained localized behind the window. Two pieces of silicone were glued against the coverslip on the inside of the window. The intestine was located between the silicone pieces, after which the pieces were stitched together above the intestine. This procedure ensured a stable position of the intestine against the coverslip.

Postoperative behavior

129P2/OlaHsd;FVB/n mice were assessed three times per week according to a predetermined clinical assessment score[22]. In short, the reactivity to animal handling, appearance, and behavior of the mice carrying an AIW were characterized every other day for several weeks using a scale with scores ranging from 0 to 3 as indicated in the figures. To calculate the percentage of postoperative weight loss, body weights were compared with those on day 1 (pre-operatively). For blood measurement, approximately 100 ul of blood was collected from the superficial temporal vein by sub-mandibular puncture one day prior to surgery, and 1, 4, 6, and 8 days after surgery. Red and white blood cell counts were assessed using a Cell-Dyn 1800 (Abbott Diagnostics).

C26 tumor formation

Cells were harvested by brief trypsinization [TrypLE, Invitrogen Life Technologies (0784)]. After centrifugation, single cell suspensions were prepared in phosphate-buffered saline to a final concentration of 5×10^5 cells/100 ul. Tumors were induced by subcutaneous injection of 5×10^5 cells into the flank of the mouse. Tumor growth rate was measured every other day. Horizontal (h) and vertical (v) diameters were determined, and tumor volume was calculated: $V = 4/3\pi(1/2[\sqrt{(h \times v)}]^3$. Mice were sacrificed when tumor volume reached approximately 700 mm^3.

Tumor load in the liver was assessed in all liver lobes and scored as hepatic replacement area (HRA), the percentage of liver tissue that had been replaced by tumor tissue.

***In vitro* migration, invasion, and proliferation assays**

Cells were plated on MatTek glass bottom dishes one day before imaging. Cells were treated with 1 uM U73122 or DMSO 30 minutes before imaging. Migration of C26 cells was assessed by tracking the cells in x and y directions over time. Images were acquired every 30 minutes for 11 hours on a Leica AF7000 inverted microscope for live cell imaging (5% CO_2, 37°C). Analysis was performed using ImageJ software. The x and y starting coordinates were subtracted from each measured coordinate, resulting in tracks that start at 0,0 (x,y).

For *in vitro* invasion assays, 24-well BioCoat Matrigel invasion chambers (BD Biosciences) were used according to the manufacturer's protocol. Cells were kept under serum-free conditions overnight. In the upper compartment, 1×10^4 cells/well were plated in 0.5 ml serum-free medium with DMSO or U73122 (1 μM). The lower compartment contained 0.75 ml medium with 5% fetal calf serum (FCS) with DMSO or U73122 (1 μM). Invasion chambers were incubated for 24 hours. Cells in the upper compartment were removed with a cotton swab. Transmigrated cells were fixed in 3.7% formaldehyde, stained with DAPI, and counted by analyzing microscopic images (10× objective, 5-6 fields per membrane). All assays were performed in duplicate and were repeated twice.

For proliferation assays, cells (50 cells/well plate) were plated and incubated at 37°C in a humidified atmosphere containing 5% CO_2. Proliferation was analyzed every 24 hours for 4 days by 3-(4,5-dimethylthiazolyl-2)-2,5-diphenyltetrazoleumbromide (MTT) assays (Roche Diagnostics) according to the manufacturer's instructions.

Apoptosis assay

Cells were fixed in 70% ice-cold ethanol and incubated for 2 hours at 4°C. To assess the cell-cycle profile, fixed cells were treated with RNAse (Roche diagnostics) and DNA was stained with propidium iodide (Sigma Aldrich). All samples were analyzed by flow cytometry using Cell Quest and Modfit software (Becton Dickinson).

***In vivo* lineage tracing of intestinal stem cells**

Lrg5-EGFP-Ires-CreERT2 were crossed with R26R-confetti mice. Double heterozygous mice were injected intraperitoneally with 5 mg tamoxifen (Sigma Aldrich, 30 mg/ml dissolved in regular sunflower oil 1 day prior to implantation of the AIW. Window implantation was performed as described. Intravital imaging was performed 24 and 34 hours after tamoxifen administration.

Transfer and imaging of B and T lymphocytes

B lymphocytes were purified from the spleens of two ACTB-CFP mice (The Jackson Laboratory) by immunomagnetic enrichment of CD19+ cells (CD19 microbeads; Miltenyi Biotec). T lymphocytes were purified by negative selection (Mouse T Lymphocyte Enrichment Set; BD Biosciences) from the spleens of histone 2B-GFP mice, ACTB-CFP, or OT1-GFP mice (The Jackson Laboratory). The purity of the B and T cell populations was between 68 and 95%, as determined by flow cytometry. A mixture of approximately 12×10^6 B cells and 12×10^6 T cells in PBS was injected intravenously (IV) into the tail vein of a sex-matched C57BL/6 recipient mouse that had received a spleen AIW 2 days before. The mice were imaged 3 hours after cell transfer and 5 minutes after IV injection of 70 kDa Dextran–Texas Red into the tail vein.

Imaging CD8 immune response in the spleen

A mixture of OT-I $CD8^+$ GFP (3×10^6) that specifically recognize the SIINFEKL peptide ($OVA^{257-264}$) and polyclonal CFP $CD8^+$ T cells (in a 1:1 or 1:5 ratio) was injected into the tail vein of a sex-matched C57BL/6 recipient mouse that had received a spleen AIW 3 days before. Six hours later the mice were injected with CpG/IFA/SIINFEKL (100 ul incomplete Freund's adjuvant (IFA), 50 ug CpG, 100 ug SIINFEKL peptide ($OVA^{257-264}$) in 100 ul water) at the tail base. Mice were imaged, and blood was collected on day 1, day 4, and day 7. Spleens were collected on day 7, and a single cell suspension was made using a cell strainer (70 um, BD Biosciences). Blood and splenocytes were analyzed by FACS using the following stains: OVA tetramer-APC, Valpha2-PE, and CD8-PerCP-Cy5.5. A maximum projection of the IVM images was made in ImageJ, and the CFP- and GFP-positive cells were counted manually.

Equipment and settings

All images were recorded on a Leica TCS SP5 AOBS two-photon microscope with a chameleon Ti:Sapphire pumped Optical Parametric Oscillator (Coherent Inc.). Different wavelengths between 700 nm and 1150 nm were used for excitation. Second harmonic generation signal (SHG) was obtained with a wavelength of 960 nm and detected with NDD2 (455-490 nm). Dendra2 was excited with a wavelength of 960 nm, CFP with a wavelength of 810 nm, GFP with a wavelength of 960 nm, mCherry with a wavelength of 1100 nm and Dextran 70kD Texas Red with a wavelength of 960 nm. The microscope is equipped with four non-descanned detectors (NDDs): NDD1 (<455 nm), NDD2 (455-490 nm), NDD3 (500-550 nm), NDD4 (560-650 nm). All images were acquired with a 25x (HCX IRAPO N.A.0.95 WD 2.5 mm) water objective (unless specified otherwise), using a zoom of 1x (unless stated otherwise), and a bit depth of 12 bit. All pictures were processed using ImageJ software; pictures were; smoothed (if necessary), cropped (if necessary), rotated (if necessary), contrasted (if necessary, only in a linear manner), and converted from 12 bit to 8 bit RGBs. Videos were corrected for XY and Z drift using custom-written software (codes on request available from J.v.R.).

SUPPLEMENTARY FIGURES

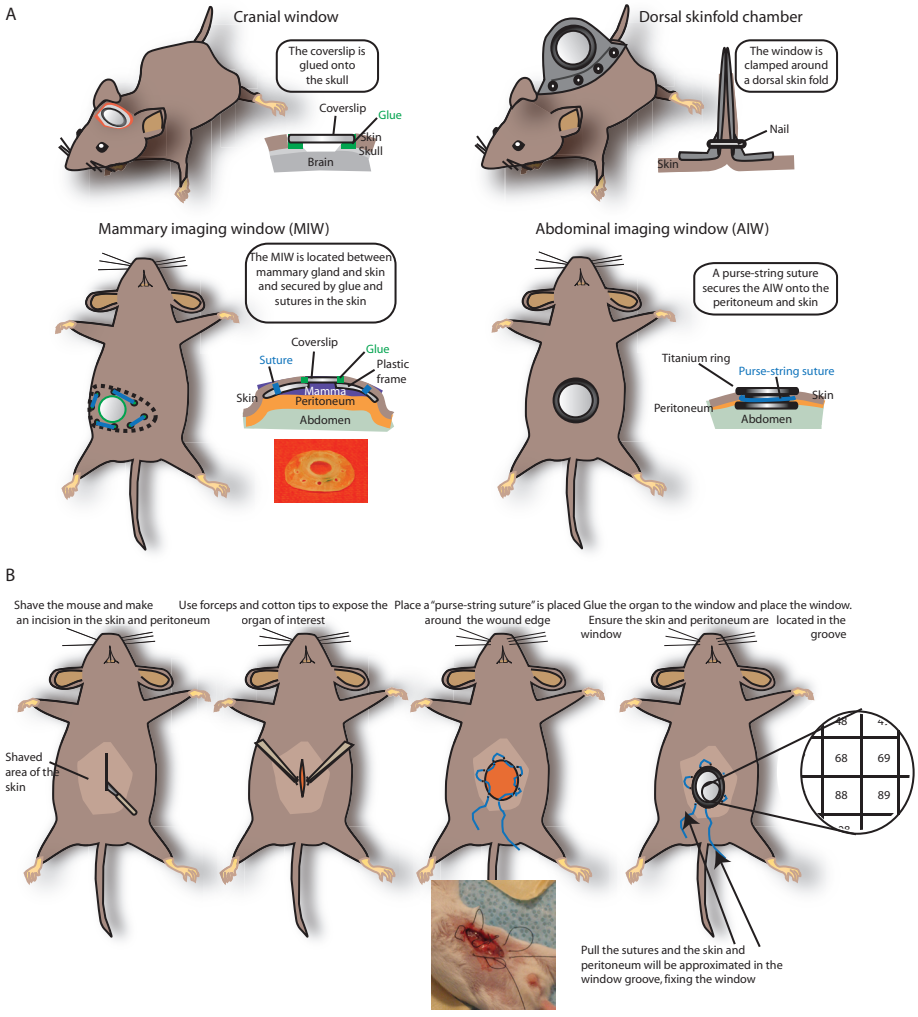

Figure S1. Comparison of imaging windows. A. Cartoons of the various imaging windows and their fixation method within the mouse. The cranial window is glued onto and secured by the skull of the mouse. The dorsal skinfold chamber is clamped on a fold of the skin, thereby strongly securing it onto the back of the mouse. The MIW is designed to be implanted on top of the mammary gland and sandwiched between the mammary gland and the skin. Sutures perpendicular to the MIW and the skin are used to secure the MIW. The crainial window, dorsal skinfold chamber and MIW technology cannot be simply applied to abdominal organs, since they do not contain bony tissue to secure a window (cranial window), cannot be clamped by a frame (dorsal skinfold chamber), and cannot be clamped in between tissues (MIW). The MIW inserted in the abdominal wall would simply "fall" into the abdominal cavity. Moreover, sutures perpendicular to the MIW would lead to a direct channel towards the abdomen of the mouse with subsequent danger of infections. Lastly, the design of the MIW required a large plastic frame which can collide with abdominal organs and cause potential tissue damage during mouse movement. For the MIW, this was not an issue since the mammary gland and peritoneum were protecting the underlying tissue. The AIW overcomes all the above mentioned problems. First, the AIW is designed to be kept in place by a horizontal suture (purse-string suture) and does not need clamping in between tissue. Second, the frame is much smaller which prevents collision with abdominal organs. Third, this design is made from titanium which enables the window to stay in the animal much longer. **B.** A cartoon of the surgical procedure of the AIW and a gritted coverslip. A picture of a mouse with a purse-string suture is shown.

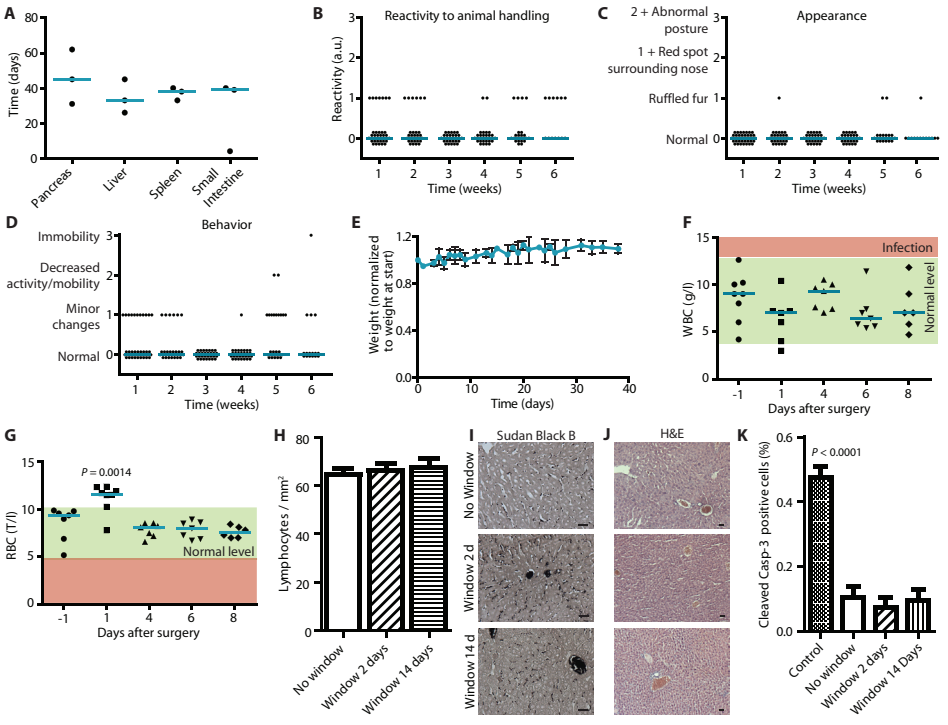

Figure S2. The AIW does not have deleterious effects in mice. A. AIWs were surgically inserted and the time they remained in place was determined (n = 3 mice per condition). (**B** to **D**) Every other day the reactivity to animal handling (B), appearance (the scale 1 to 3 represent normal to slow reactivity respectively) (C), and behavior (D) were assessed in 8 mice carrying an AIW using a clinical appearance scoring system. The combined measurements are depicted in the plots. **E.** The weight of the 8 mice carrying an AIW was measured over 40 days and plotted over time. Values are normalized to the weight of the mice just after surgery (which includes the AIW). (**F** and **G**) In the same mice, the blood was analyzed one day before and 1, 4, 6, and 8 days after surgery. The white blood cell count (WBC) (F) and the red blood cell (RBC) count (G) were measured and plotted over time. The green zone indicates physiological levels and the red zone elevated or diminished levels. On both data sets a one-way ANOVA was performed. **H.** In H&E-stained sections the number of lymphocytes was quantified at indicated time points (n = 12 fields of view, 3 mice per condition). A Kruskal-Wallis one-way ANOVA showed no differences between the means. **I.** Representative Sudan Black B stain marking neutrophils of liver tissue sections that were behind an AIW or were from a control liver (n = 3 mice per condition). Scale bar, 10 um. **J.** Representative H&E images of liver tissue sections that were behind a window or a section of a control liver (n = 3 mice per condition). Scale bar, 10 um. **K.** An immunostain for cleaved caspase-3 was performed in liver sections at indicated time points. As a positive control, liver metastases were used (n = 12 fields of view in 3 mice per condition). P-value obtained using a one-way ANOVA. All data are means ± SEM.

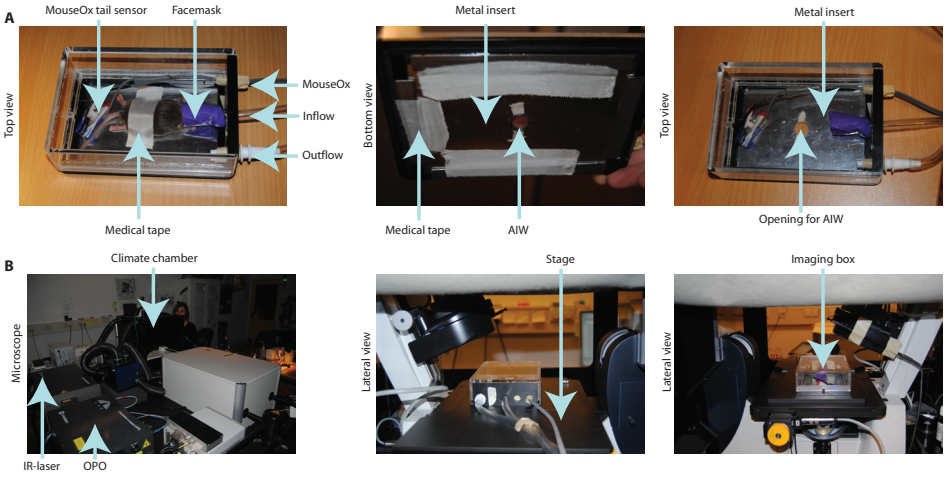

Figure S3. An imaging box fixes the AIW and exposes it to the objective. Mice carrying an AIW were sedated using isoflurane inhalation anesthesia (1.5 to 2% isoflurane v/v in O_2). **A.** Images showing the custom designed imaging box from different angles as indicated. **B.** Images showing the custom-designed imaging box placed on the stage above the objective of our microscope. Our setup contains a dark climate chamber which surrounds the whole microscope including the stage and objective.

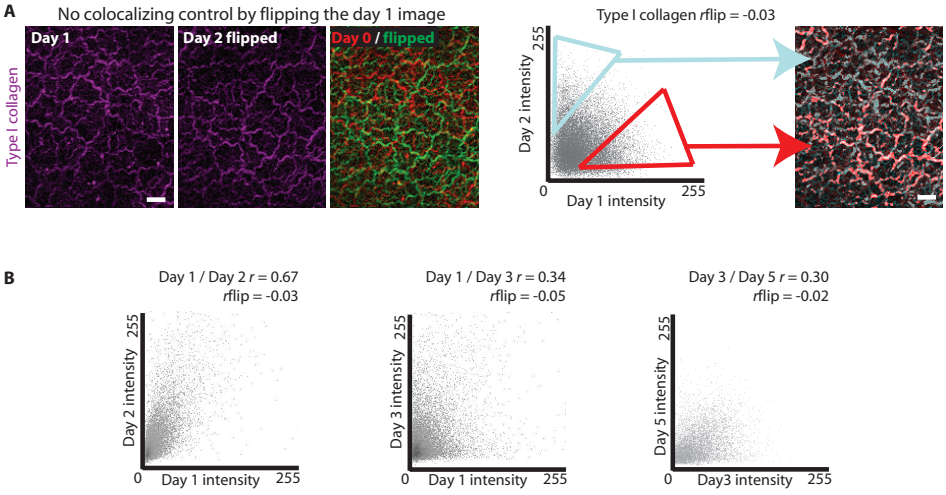

Figure. S4. Scatter plots of retraced areas during IVM. A. Non-overlapping images were generated by flipping the day 2 image in Figure 1F 180 degrees. The Pearson's correlation coefficient (rflip) and a scatter plot of the type I collagen images are shown, with selected non-colocalizing pixels from the scatterplot, as indicated by the blue and red boxes, replotted in the IVM image of day 1. Scale bars, 20 µm. (**B**) Shown are the scatterplots, the r and rflip of the images in Figure 1G.

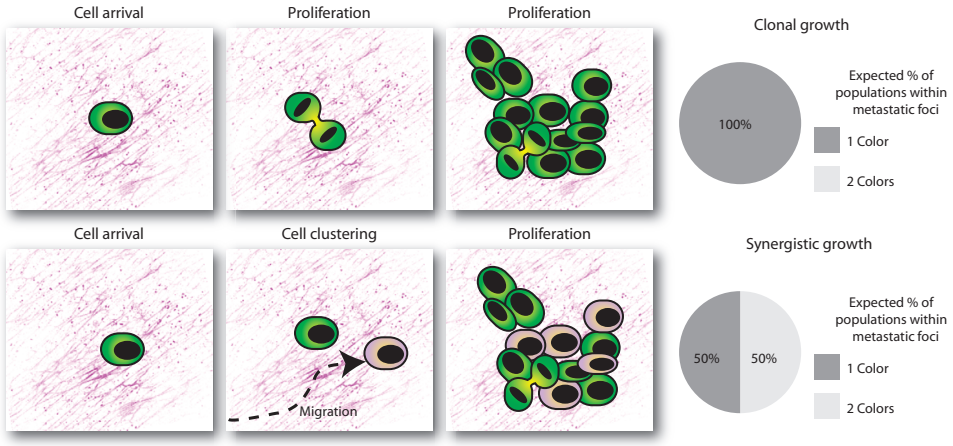

Figure S5. Clonal or synergistic metastatic growth within the liver. Cartoons explaining the clonal growth hypothesis (upper panels) and the synergistic growth hypothesis (lower panels). In the clonal growth hypothesis a metastasis grows from a single founder cell; according to the synergistic growth hypothesis a metastasis is formed from multiple founder cells. The pie charts (right panels) represent the expected percentage of metastatic foci that contain one or two populations of cells for each hypothesis.

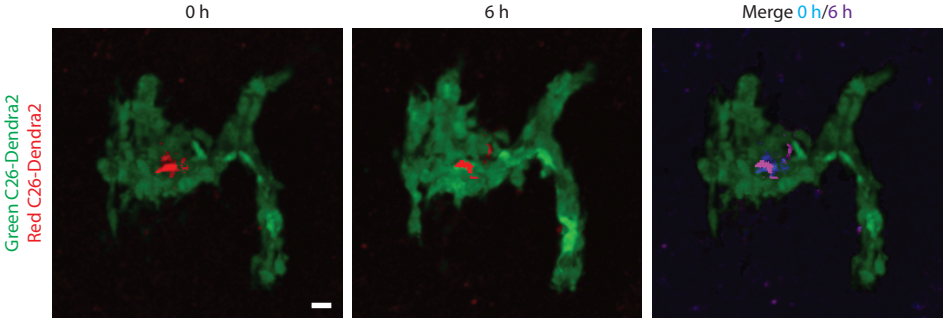

Figure S6. Photomarking and tracking of an individual cell within a micrometastasis. A representative experiment (n = 4) where an individual cell within a micrometastasis was photomarked by converting the green Dendra2 to red Dendra2. Green and red two-photon images were acquired at 0 and 6 hours. Shown are merged images from the green and red channels using an "or" function. The right panel shows a merged image in which the red channel at 0 hours is shown in blue, and the red channel at 6 hours in magenta. Scale bar, 20 µm.

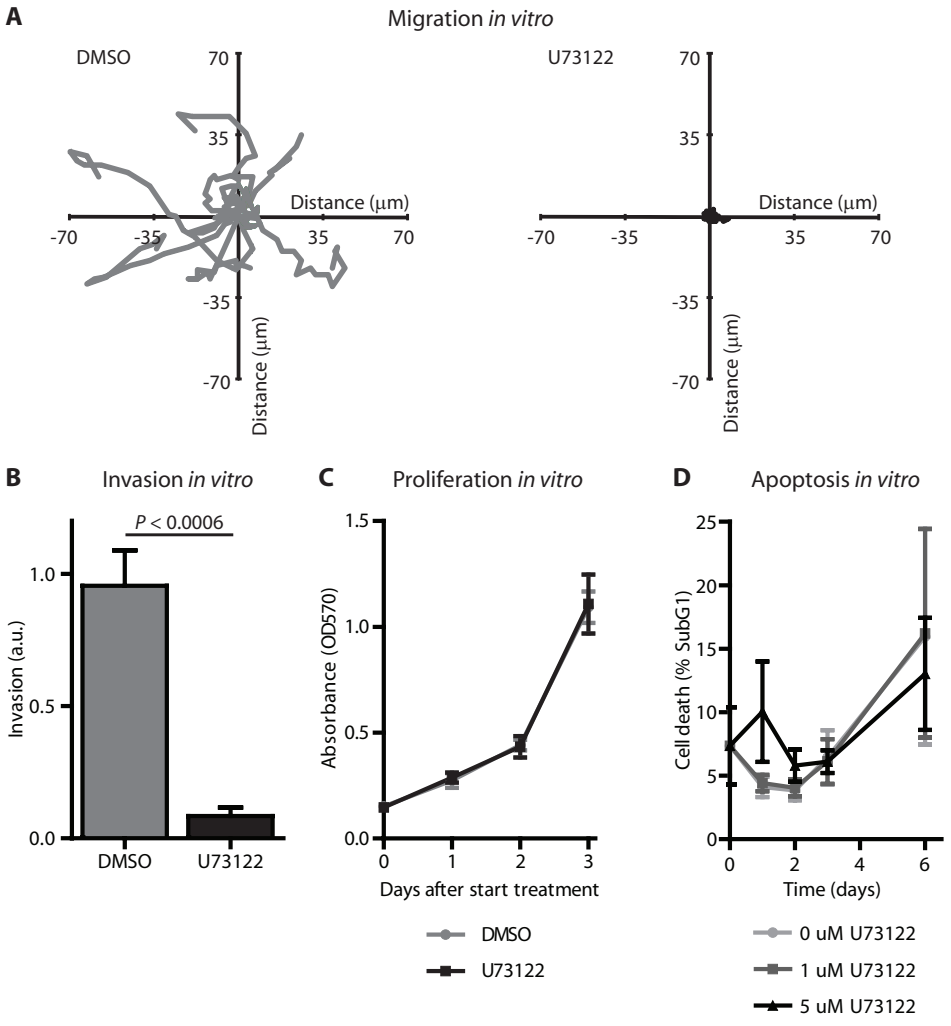

Figure S7. Inhibition of in vitro migration with U73122. A. Cells treated with DMSO or 1 uM U73122, and cell migration was traced over time. The tracks of 6 cells for each condition are plotted. **B.** C26 cells in transwell chambers were allowed to invade for 24 hours in the presence or absence of U73122 or DMSO (vehicle control). The bar graph shows fold increase relative to nonstimulated controls. Data are means ± SEM (n = 3 independent experiments performed in duplicate). P-value obtained using a non-parametric Mann Whitney U test. **C.** The increase of the number of C26 cells in response to U73122 was measured using the MMT assay. The graph shows the amount of light absorbance at OD570. Data are means ± SEM (n = 3). A two-way ANOVA revealed no significant differences. **D.** C26 cells were treated with varying concentrations of U73122 and the apoptotic sub-G1 fraction was determined by FACS analysis (n = 4 independent experiments performed in duplicate). A two-way ANOVA revealed no significant differences. Data are means ± SEM.

A TIMELINE Figure 4A-D

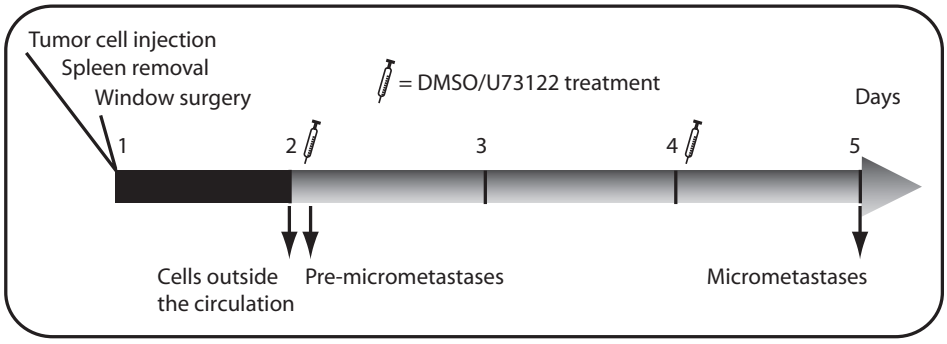

B TIMELINE Figure 4E and F ; Figure 5 ; figure S9

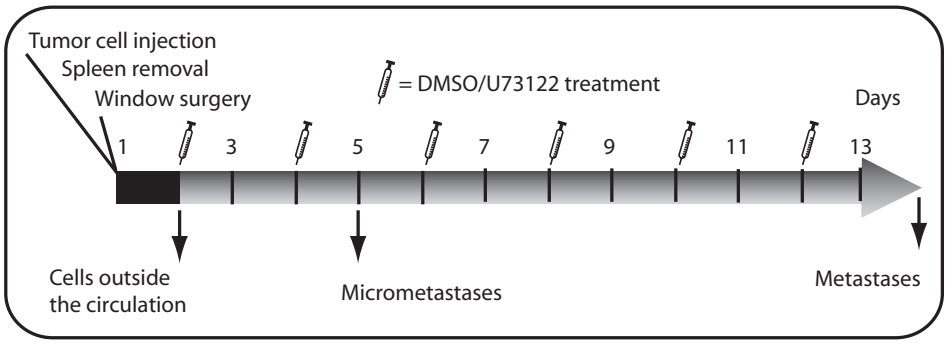

C TIMELINE Figure 5H

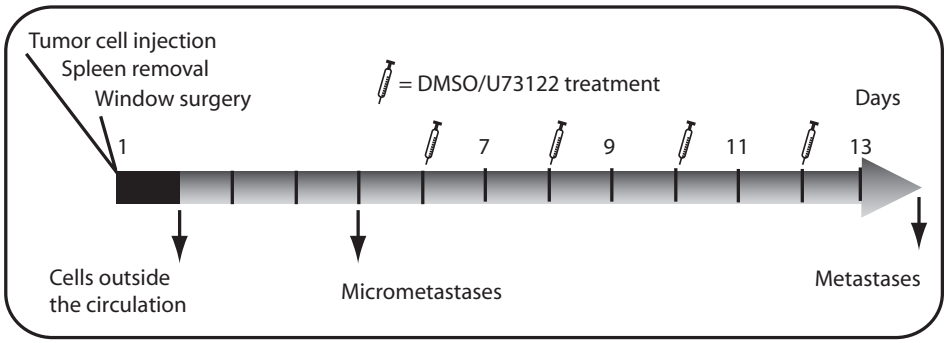

Figure S8. Timeline of mouse experiments treated with U73122. A. Schematic representation of the timeline of all experiments performed in Figure 4, A to D. Note that treatment starts after the cells have extravasated **B.** Schematic representation of the timeline of all experiments performed in Figure 4, E and F, and Figure 5. Note that treatment starts after the cells have left the circulation. **C.** Schematic representation of the timeline of experiments performed in Figure 5H. Note that treatment starts after the micrometastases are formed.

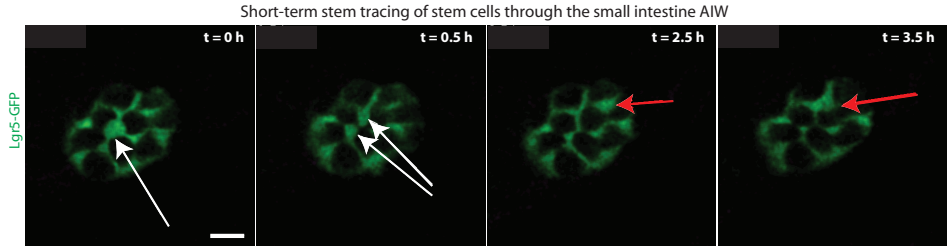

Figure S9. Intravital imaging of intestinal stem cells through the AIW. The AIW was surgically implanted on top of small intestine and images were taken through the AIW. A time series of images was acquired from the small intestine of a mouse that expresses CreERT2 and GFP driven by the Lgr5 promoter to label the stem cells. The white arrow points to a cell division, and the red arrow to a moving cell. Scale bar, 10 µm.

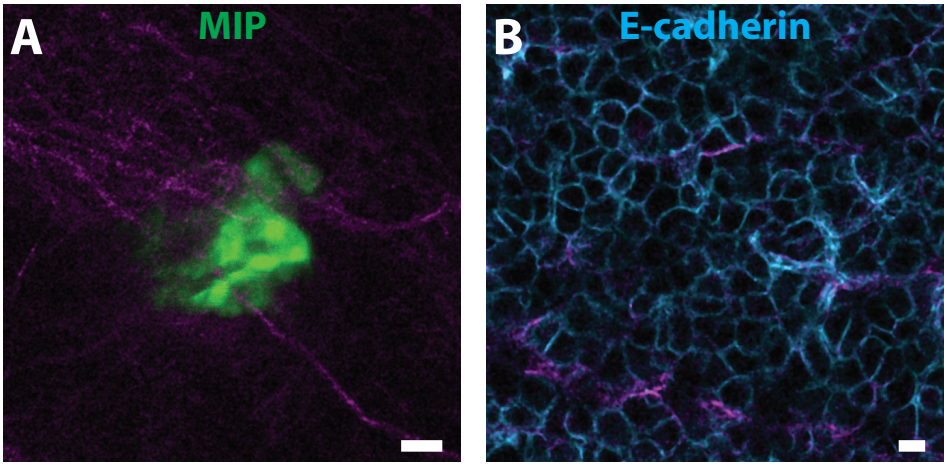

Figure S10. Intravital imaging of pancreatic tissue through the AIW. The AIW was surgically implanted on top of the pancreas. **A.** Image of the pancreas showing insulin-producing B-cells marked by MIP-GFP. **B.** The outline of the pancreatic cells marked by E-cadherin. Purple marks type I collagen. Scale bars, 30 µm.

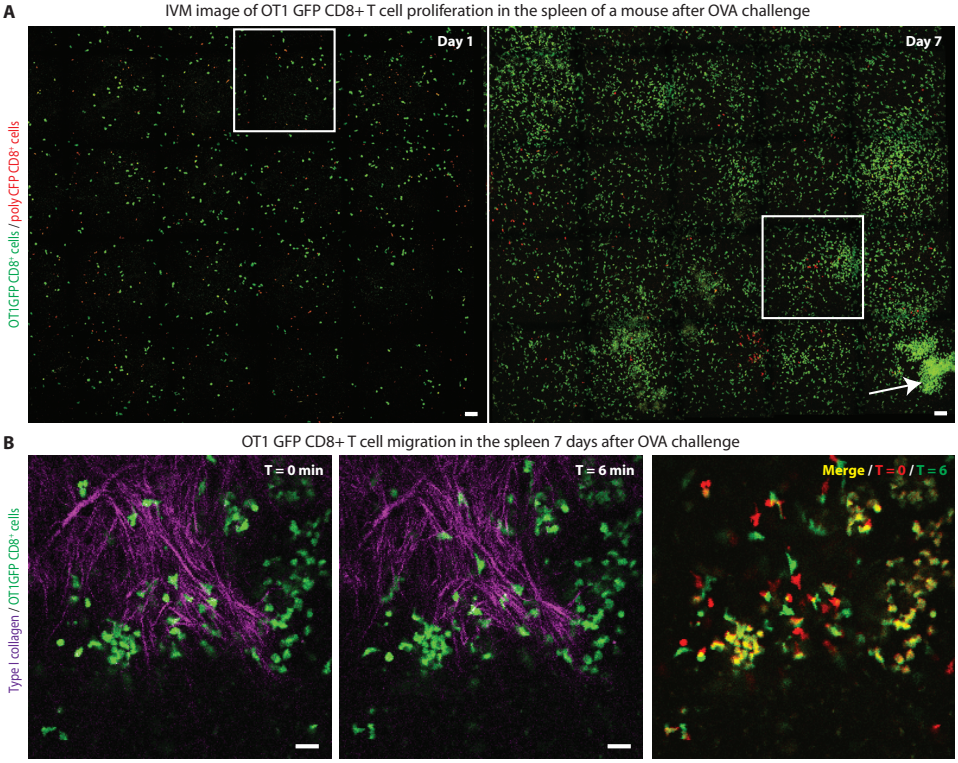

Figure S11. Intravital imaging of OVA-reacting T cells in the spleen through the AIW. A. IVM tile scans of OTI GFP CD8⁺ cells (green) and poly CFP CD8⁺ cells (shown in red) were made of the same mouse on day 1 and day 7 after it was challenged with an OVA peptide in the presence of CpG. An area with clustered T cells is indicated by the arrow. **B.** Still images from a time series taken every 30 seconds. An overlay of the green channels from 0 min (red) and 6 min (green) highlights migratory cells (red/green) and nonmigratory cells (yellow). Scale bars, 20 µm.

PART II | IMAGING OF METASTASIS

CHAPTER 7

7

Surgical implantation of an Abdominal Imaging Window for intravital microscopy

Nature Protocols 2013 Feb 21;8(3):583-94

Laila Ritsma[2]*, Ernst J.A. Steller[1]*, Saskia I.J. Ellenbroek[2], Onno Kranenburg[1], Inne H.M. Borel Rinkes[1]*, Jacco van Rheenen[2]*

* *Equal contribution*

[1] Department of Surgery, University Medical Center Utrecht, the Netherlands
[2] Hubrecht Institute-KNAW and University Medical Center Utrecht, the Netherlands

ABSTRACT

High-resolution intravital microscopy through imaging windows has become an indispensable technique for the long-term visualization of dynamic processes in living animals. Easily accessible sites such as the skin, the breast and the skull, can be imaged using various different imaging windows, however long-term imaging studies on cellular processes in abdominal organs are more challenging. These processes include colonization of the liver by metastatic tumor cells and development of an immune response in the spleen. We have recently developed an abdominal imaging window (AIW) which allows long-term imaging of the liver, the pancreas, the intestine, the kidney, and the spleen. Here, we describe the detailed protocol for the optimal surgical implantation of the AIW, which takes approximately 1 hour, and subsequent multiphoton imaging for up to one month.

INTRODUCTION

Subcellular imaging of tissue in living animals is often referred to as intravital imaging (IVM) and has become increasingly important for studying the dynamic aspects of physiological and pathological processes. Examples are the activation and contraction of immune and inflammatory reactions and the formation, spread, and vascularization of tumors. Histological techniques can also visualize tissue with high resolution, but generate snapshots of tissue status. By contrast, high resolution IVM can visualize the behavior of individual cells within tissue over time, often leading to new and unexpected insights[1,2].

Most high resolution IVM techniques are based on fluorescent light microscopy. Due to light scattering, the maximum imaging depth of fluorescent IVM techniques is one millimeter[3]. As a consequence, visualization of organs is restricted to either superficial tissue such as the skin, or to sites that have been surgically exposed. Exposure of organs for imaging requires invasive surgery and manipulation of organs from their anatomical position. These invasive procedures limit the duration of IVM experiments to a maximum period of 36 hours[4]. However, most physiological and pathological processes take place over longer time periods. The development of several imaging windows has provided new opportunities for studying these processes in real time. These windows allow multiple sequential imaging sessions over several days within the same living animal. Recently, we developed the Abdominal Imaging Window (AIW), a new window for intravital imaging of various abdominal organs previously inaccessible for long term sequential imaging[5].

Comparison with other windows

Currently, there are several windows available for intravital imaging, each providing access to different organs. The cranial imaging window is limited to imaging the brain and bone marrow[6-8]. The dorsal skinfold chamber is restricted to the skin and is frequently used for the visualization of subcutaneous tumor formation and angiogenesis[9-11]. The mammary imaging window (MIW) allows imaging of the mammary gland which has provided novel insights into the development of healthy and tumorigenic mammary tissue and early tumor growth[12-14]. Recently, a spinal chamber has been developed for *in vivo* imaging of spinal cord pathology[15].

Unfortunately, none of these windows permits visualization of abdominal organs. For instance, the cranial window is secured on the skull using glue[16], but the abdomen lacks bone structures onto which the window can be fixed. Dorsal skin fold chambers are also unsuitable for imaging abdominal organs, as these organs, unlike the skin, cannot be fixed between the frames of the window. The MIW is sandwiched between the mammary gland and the skin. For imaging abdominal organs the MIW is not suitable as the abdominal cavity lacks physical support for the window. In addition, the presence of a large plastic ring within the abdomen is likely to damage organs during animal movement. Therefore, we have developed a protocol for surgical implantation of an AIW that allows analysis of dynamic processes within abdominal organs.

The AIW, as described in Ritsma *et al*[5], consists of a titanium ring (titanium ASTMF136-02A that meets ISO5832 part 3 and EN10204-3.1.B) with a 1 mm groove on the side and a coverslip fixed on the top (170um thick) (Figure 1). The glass coverslip is secured using glue and can be easily replaced. After preparation of the window, the AIW is surgically implanted into the skin and abdominal wall, and held in position by a purse-string suture which is concealed within the groove of the AIW ring. Concealing the suture within the groove of the ring prevents mice from biting or pulling the sutures, which is frequently observed in other imaging windows. To further reduce the risk of dislodgement of the AIW, we make use of a non-woven non-resorbable

suture (prolene), which can be tightened once the window is inserted and which keeps the window secured for an average period of 5 weeks[5]. Moreover, the ring of the AIW is manufactured using a titanium alloy which allows it to be reused. This is in contrast to most other single-use plastic imaging windows. Among metals titanium has the best biocompatibility, is corrosion resistant, strong, 33% lighter than other stainless alloys and does not lead to inflammation following implantation[17]. Indeed, immunohistochemistry staining for inflammatory cells in tissue fixed to the ring and behind the coverslip did not show any signs of local inflammation. Furthermore, white blood cell counts of animals before and after window implantation did not indicate a systemic inflammatory response to the window[5]. However, as exudate accumulation behind the window was observed when the tissue of interest was not completely circularly fixed to the window frame, local inflammatory reactions elsewhere in the abdominal cavity cannot be excluded.

Using the AIW, we were able to image the arrival of single colorectal tumor cells in the hepatic microvasculature, and their expansion into (pre-)micrometastases and macrometastases[5]. Surprisingly, we observed that single extravasated tumor cells first grow into highly motile "pre-micrometastases" before forming non-motile micrometastasis. By genetically and chemically suppressing cell migration in pre-micrometastases total metastatic load was reduced, suggesting that tumor cell migration during the pre-micrometastasis stage contributes to efficient liver metastasis formation[5]. In addition, we visualized the activation of immune cells in the spleen, the division of stem cells in the small intestine, and b-cells in the pancreas. Moreover, we imaged transplanted pancreatic islets underneath the kidney capsule sequentially over a period of 28 days.

Optimized surgical procedures allow us to use the AIW for steady high resolution imaging of abdominal organs over long periods of time (max. 28 days) without considerable changes in the anatomical position of the window and without disturbing physiological processes[5]. Furthermore, the AIW is also an excellent tool for mammary gland imaging (LR, JvR unpublished data).

EXPERIMENTAL DESIGN

Window optimization

To improve the biocompatibility of the glass coverslip we coated it with polyethylene glycol (PEG). This prevents the development of an inflammatory/immune response against the foreign body.

For long term experiments, in which exudate can accumulate between the coverslip and the organ of interest, a slightly adapted AIW was designed. In this AIW design, the coverslip is placed on a small ring that can be inserted as an inset on top of the window frame. This design allows the coverslip to be placed at the same height as in the original AIW. This prevents any limitations in movement of the objective over the coverslip. The main advantage of this design is that the inset can be replaced if excess exudate is limiting imaging depth. The exudate can easily be removed during replacement of the coverslip.

AIW surgery

A major issue during intravital imaging is organ movement, caused by respiration or animal movement, during and between imaging sessions. Several approaches are used to minimize organ movement. First, tissue movement can be reduced by using an inverted microscope, in

which gravity helps to hold the organs of interest in position. Second, a custom designed imaging box, which fits the stage of the multiphoton microscope, fixes the AIW above the objective. Thirdly we secure the organs of interest in the window by gluing them (n-butyl cyanoacrylate or ethyl-cyanoacrylate glue) to the ring of the AIW. The glue is applied only to the titanium of the inner rim of the AIW and not to the coverslip.
Due to the anatomical position of the liver partly underneath the rib cage and attached to the diaphragm, extra surgical steps are necessary for hepatic imaging through the AIW, as well as for reduction of respiratory movement. First, the xyphoid process of the sternum is resected, as it protrudes from the rib cage and hampers fixation of the AIW in the upper abdominal wall and skin. Before resection, the xyphoid process is clamped most proximal to the sternum for approximately 5 minutes with Hartman forceps to obtain hemostasis. Next, the falciform ligament is dissected, which allows manipulation of the liver to a caudo-ventral position to an extent that it can be fixed to the AIW. This procedure also reduces movements from respiration. Next, a sterile cotton gauze roll is placed in the space created between the diaphragm and the liver to further absorb respiratory movement and to keep the liver stabilized at its caudal position. No systemic inflammatory response was observed in response to the implantation of the cotton gauze[5]. After 2-3 weeks in situ the cotton gauze was completely encapsulated. Consequently, one cannot exclude local inflammation by the gauze at the site of insertion. Lastly, glue is applied to ensure firm positioning of the liver behind the window. These manipulations do not lead to alterations in tissue architecture, cell death, or influx of immune cells in the area located directly behind the window[5].

Imaging

Sequential imaging of the exact same location over multiple days is accomplished by a combination of methods. First, fiduciary landmarks like the vasculature are used to retrace area location[11]. Second, a numbered, gridded coverslip can be used for exactly retracing previously imaged areas[5]. Third, when using multiphoton excitation, a second harmonic generation signal of the type I collagen network can be generated to retrace area location with subcellular accuracy over time[5,11]. Fourth, single tumor cells can be traced by using expression of the photoconvertible fluorophore Dendra2 and switching single cells from the green to the red emission state[12,13].

Control experiments

When surgery is performed for the first time, it is recommended to test whether the surgical insertion of the AIW is successfully performed without the induction of local or systemic immune responses. For this, blood and tissue sections from animals carrying an AIW and controls animals that do not carry an AIW should be compared to one another. Additionally, the animals should be monitored to ensure that vital signs and body weight are returning to pre-surgery scores within 1 and 4 days respectively[5]. Furthermore, if an experiment with the AIW has a duration of multiple days, it is wise to include an animal treated similarly, with the exact same conditions, but without the AIW. End stage parameters should be comparable for both conditions.

MATERIALS

Reagents

Critical: All reagents and equipment can be substituted with appropriate alternatives from other manufacturers.

- Mice (strain and sex depending on experiment) preferably aged 10 weeks or older. We have used BALB/c mice, C57BL/6 mice, 129P2/OlaHsd;FVB/n mice, and mice from a mixed background. Preferably use mice between 10 and 15 weeks of age when implanting an AIW on the small intestine. In older mice it can be more difficult to visualize the cells of the crypt and villus compartment.
  Caution: All animal studies must be reviewed and approved by the institutional animal care and use committees to ensure that they conform to relevant ethics regulations.
- Buprenorphine hydrochloride (Temgesic®) (0.3mg/ml, BD pharmaceuticals limited, 0283732). Can be stored at room temperature (20-24°C) until date of expiration.
  Caution: Buprenorphine hydrochloride may cause prolonged respiratory depression. Wear protective clothing to avoid contact or inhalation. Buprenorphine is a controlled substance and should be handled according to relevant rules of the host institutions
- Opthalmic ointment (Duodrops veter kela 10ml, Kela Veterinaria, 1321355)
- Isoflurane (100% w/w solution for inhalation anesthetic, IsoFlo, Abbott, 05260-05)
- Cyanoacrylate glue (Super gel, Pattex)
  Caution: Avoid contact with skin, and wear gloves when handling.
- PBS (sterile)
- Ethanol (100% Ethyl alcohol 70%, Nedalco)
- Acetone (100%, JT Baker, 5002)
- 0.1 mg/ml PLL(20)-g[3.5]-PEG(2) (poly-L-lysine-graft-ply(ethyleneglycol), 20mg, SuSoS)
- MilliQ

Equipment

- Custom made titanium AIW (see Figure 1) (STMF136-02A that meets ISO5832 part 3 and EN10204-3.1.B (FMI instrumed: www.fmi.nl).
- 4-0 non-resorbable polypropylene sutures (sterile) (Ethicon, 8817H)
- Cotton swaps (sterile) (EMRO Medical, 123011700)
- Coverslip (Menzel Glazer 12 mm,Thermo Scientific, CB00120RA1)
- Gridded coverslip (Electron Microscopy Sciences, 72265-12)
- Sterile cotton gauze 8.5 x 5 cm (Klinion, 4111001)
- 1 ml syringe (BD plastipak, 300013)
- 25 gauge needle (BD microlance, 300600)
- HEPES (Sigma, H4034)
- Anesthetics machine (Anesthetics machine, Vet Tech solutions LTD)
- Ventilator (Active scavenger unit, Vet tech solutions LTD)
- Laminar flow
- Induction cage with autoclavable filter top (Techniplast, 1284L + 400SUC)
- Clipper (Wella, Contura)
- Microdissection scissors 3.5 inch (Roboz Surgical Instruments Co, RS-5880)
- Scissors (Aesculap, OC 492 R)
- Forceps no. 5 (Smooth tying platform, Neolab–DUMONT, 21033)
- Graefe forceps curved (serrated, Roboz Surgical Instruments Co, RS-5135)

- Hartman mosquito hemostatic forceps straight (3,5 inch, Roboz Surgical instruments Co, RS-7100)
- Heating pad (Inventum Holland BV, HNK513)
- Surgical drape (Medline Industries, GEM2140)
- Needle holder (Aesculap, BM01 3R)
- Surgical tray (Aesculap, BM 242)
- Sterile surgical gloves (SemperMed, SEM10255)
- Facemask (Vet tech solutions LTD)
- Custom made imaging box
- Medical oxygen (Linde, AIRAPY (O2 21,5% v/v, N2 78,5% v/v))
- Two-photon microscope surrounded by a heatable black box (Leica Microsystems, Leica TCS SP5 MP)
- 50 ml Greiner centrifuge tube (Sigma Aldrich, T2318)
- 0.22 µm Millex GS filter unit (Millipore, SLGS033SS)
- MouseOx® (Starr Life Sciences Corp.)
- Markers (Stabilo, 842)

Reagent Setup

Buprenorphine hydrochloride

- Dissolve 1 ml of the 0.3 mg ml^{-1} stock solution in 9 ml of PBS. Store dissolved solution at 4°C for up to 3 days.

PLL-g-PEG

- Make a 1 M HEPES stock by dissolving 23.83 gram HEPES in 100ml MilliQ and set the pH to 7.4. Prepare 10 mM HEPES pH 7.4 by diluting 500 µl 1M HEPES stock solution in 49.5 ml MilliQ. Filter sterilize 10 mM HEPES pH 7.4 using a 0.22 µm filter. Dissolve 20 mg PLL-g-PEG into 20ml 10 mM HEPES pH7.4 to make a 10 times stock with a final concentration of 1mg/ml and filter sterilize with a 0.22 µm filter. This stock solution can be stored at 4°C for at least 5 months. Shortly before use, dissolve 20 ul 10x PLL-g-PEG solution into 180 ul 10mM HEPES buffer.

Cotton Gauze

- Prepare a cotton gauze roll by cutting the sterile gauze into a 2.5 x 1 cm piece (Figure 2a). Grab the short edge of the gauze with an atraumatic forceps (forceps no. 5) and dip it into PBS. Use another pair of forceps to roll the piece around the forceps. Take it off and roll it between your gloved fingers. Cut the edges off using sterile scissors so a 1 cm long wet cotton gauze roll is left (Figure 2b).

Equipment Setup

Surgical station

- The surgery must be performed in an aseptic working environment, preferably involving a laminar flow HEPA-filtered hood, with an isoflurane anesthetics machine and ventilator. Position the electric heating pad and disinfect it using 70% ethanol. Ensure there is sufficient medical oxygen in the tank and isoflurane in the vaporizer to perform surgery.

Surgical kit preparation

- Before surgery the following items must be sterilized; scissors, microdissection scissors, forceps no. 5, graefe forceps curved, Hartman hemostatic forceps, needle holder, cotton swaps. Autoclave the kit together with some surgical drapes.

Surgical station preparation

- After shaving the mouse, place the sterile drape over the heating pad, and put the ethanol cleaned facemask on top. Place the surgical tray containing the tools open on the edge of the wrap, and carefully drop the sterile needle, sterile cotton gauze and window in it. Open a 50ml tube and add 40 ml sterile PBS. Make sure to wear sterile surgical gloves during surgery.

Animal housing

- Animals can be housed under standard conditions. They can be caged with other mice that had AIW surgery, but never with mice which did not undergo surgery. Make sure there is enough bedding to prevent the AIW from too much contact with the bottom of the cage.

PROCEDURE

Steps 1-9 Window preparation

1 Apply cyanoacrylate on the entire ring of the etched inset of the AIW using the back of a cotton swab.
2 Use forceps no. 5 to place the (gridded) coverslip in the inset of the window and gently apply pressure to the coverslip for one minute using a cotton swab.
3 Apply glue at the interface of the coverslip and window.
Critical: the glue should secure a watertight seal between the metal and the coverslip to prevent exogenous bacteria from entering the body as well as to prevent leakage of abdominal fluids.
4 Place the window on its side in a flow cabinet for at least 2 hours to allow the glue to dry completely.
Critical: Positioning the window side-ways during this desiccation process is favorable due to evaporation of the glue.
5 Remove excessive and condensed glue from the coverslip using a cotton swab soaked in 100% acetone.
6 Remove the acetone using a cotton swab soaked in 70% ethanol.
7 Examine if the window is watertight by filling it with water after placing it glass side down on a tissue. The tissue should still be dry after 5 minutes.
TROUBLESHOOTING
8 Disinfect the window. This can be done by placing the window in 70% ethanol for at least 30 minutes, in a flow cabinet underneath a UV lamp for 10 minutes on each side, by using steam sterilization for 1.5 hours at 121-134^{0}C, or by using ethylene oxide for 1-4 hours at 40-55^{0}C followed by a cooling period of 72 hours.
Caution: Do not autoclave the window with a glued coverslip on top, as heating will liquefy the cyanoacrylate. The window and coverslip can be autoclaved separately if desired.
9 Place the window into a sterile 50ml tube (**PAUSE POINT**, The window can be kept in the sterile 50ml tube for a maximum of 1 week).

Steps 10-16 Surgery preparation

10 In a sterile flow cabinet, apply a PEG-coating to the interior side of the coverslip by placing 200 ul PLL-g-PEG solution (1ng/ml) in the window and incubating it for 1 hour at RT. Next, wash the AIW using PBS and keep the window in PBS.
11 Anesthetize a mouse in an induction chamber using 2.5% (v/v) isoflurane.

12 Place the unconscious mouse with its nose in a facemask and lower the isoflurane to 1.5% isoflurane (v/v). Make sure the mouse is on a heat pad to maintain body temperature during surgery.
Critical: continuously monitor the mouse reflexes.
Caution: do not overheat the mouse because this enhances the depth of the anesthetics and might be lethal due to respiratory failure.
13 Position the mouse on its back and fix all four legs in an X shape with tape. After fixation shave the complete ventral side of the mouse from head to tail (Figure 2c).
Caution: make sure not to dislocate any joints when fixing
Critical: hair is strongly autofluorescent, therefore it is essential to remove as much hair as possible to prevent hampering imaging.
14 Use a 1ml syringe with a 25-gauge needle to inject 100µl of 0.03mg/ml buprenorphine intramuscularly in one of the hind legs.
15 Lubricate both eyes with eye ointment.
Caution: dehydration of the eyes can cause permanent damage.
16 Disinfect shaved area with 70% ethanol, which will also help to remove residual hairs.

Steps 17 AIW Surgery

17 Different protocols should be followed depending on which organs are to be placed behind the AIW. Option A is for the liver AIW, option B is for pancreas or spleen AIW and option C is for a small intestinal AIW.

TROUBLESHOOTING

A Liver AIW

i Hold the skin using the graefe forceps and make a 15 mm midline incision through the skin using microdissection scissors starting down from the xyphoid process (Figure 2d). Incise the linea alba to separate the mm-recti abdominis and open the abdomen (Figure 2e).
Caution: spare the large vessels by performing a midline incision in the abdominal wall.
Caution: make sure not to damage abdominal organs during the incision.
This can be prevented by lifting the abdominal wall with the forceps and bluntly opening the peritoneal cavity. Wait for air to flow into the abdomen and any organs adhering to the anterior abdominal wall to release, prior to enlarging the laparotomy incision.

ii Grab xyphoid process with the Hartman hemostatic forceps as cranially as possible and clamp it (Figure 2f and g).

iii Lift the Hartman hemostatic forceps in cranio-ventral direction, meanwhile visualize the falciform ligament by gently manipulating the liver caudally using a moist (PBS) cotton swab (Figure 2h). Dissect the falciform ligament onto the suprahepatic inferior vena cava (IVC) using micro dissection scissors.

Critical: it is important to completely dissect the falciform ligament to be able to manipulate the liver.

Caution: be careful not to damage the diaphragm (including diaphragmatic veins), abdominal aorta or inferior vena cava.

TROUBLESHOOTING

iv Dissect and remove the xyphoid process 5 minutes after clamping the xyphoid with the Hartman hemostatic forceps (Figure 2i).

v Use cotton swabs to manipulate the liver caudal and use graefe forceps to insert the cotton gauze roll transversely to the dissected falciform ligament in the space created between liver and diaphragm (Figure 2j).

vi Use the needle holder to apply a purse-string suture surrounding the midline incision through abdominal wall and skin. Start at the caudal end of the incision, approximately one mm from the edge, and pass the suture thread first through skin and then through opposing abdominal wall from outside to inside. Next, move 5mm up along the incision and pass the suture thread through the abdominal wall and skin again, from inside to outside (Figure 2k). Create a circular suture by repeating this along the entire wound edge. In order to be able to secure sutured skin/abdominal wall into the ring-groove, it is important not to make the incision too large. The last stitch should be located approximately 5 mm away from the first entrance. Make sure to leave loops on the outside, which will be used to tightly secure the suture in the window groove (Figure 2l).
Critical: it is important that the suture is not placed too close to the wound edge, risking tearing of tissue. If the suture is placed too far away from the incision, excess skin will be pulled into the groove, resulting in a skin flap which is more susceptible for infections and which makes it harder to place the AIW in the opening of the imaging box.

vii Apply glue on the interior ring surface of the AIW (Figure 2m) using the back of a cotton swab and glue the AIW to the liver (Figure 2n) by applying gentle pressure to the AIW. Wait 5 minutes for the glue to dry. Make sure the liver surface is not covered with any fluids directly prior to gluing.
TROUBLESHOOTING

viii Use the graefe forceps to carefully place abdominal wall and skin in the groove of the AIW (Figure 2o).
Caution: make sure not to detach the liver from the AIW.

ix Pull the loops of the purse-string suture one by one, tightening the suture in the groove of the AIW (Figure 2p).
Critical: to prevent animals from biting the suture, make sure the sutured knots are 'hidden' underneath the upper ring of the AIW.

TROUBLESHOOTING

B Pancreas/Spleen AIW

i Make a 15 mm lateral incision in the flank of the mouse above the organ of interest as described in step 17Ai.
Critical: it is important to make the incision in the flank of the mouse to reduce exudate accumulation between organ and the AIW.

ii Insert a purse-string suture through muscle layer and skin surrounding the incision as described in step 17Avi.

iii Extracorporate the organ of choice using cotton swabs.

iv Put glue on interior titanium facing of the AIW and place the AIW, glass down, adjacent to the organ.

v Fix the AIW to the organ by placing the organ in the AIW against the coverslip and glue. Wait 5 minutes for the glue to dry. Make sure the pancreas/spleen surface is not covered with any fluids directly prior to gluing.

vi Turn the window and gently position it in the mouse. Place the muscle and skin in the groove of the AIW as described in step 17Aviii and ix.

C Small intestine AIW

i Follow steps 17Bi to Biii

ii Place the small intestine in the window, leaving a small space between the small intestine and the titanium AIW.

iii Use the back of a cotton swab to apply small amounts of glue at two spots at the interface of the coverslip and small intestine. Make sure the surface of the small intestine is not covered with any fluids directly prior to gluing.

Critical: peristaltic movement will be reduced close to the glue which will improve imaging. However, excessive amounts of glue will lead to obstruction which may cause fatal ileus within a few days.

Steps 18-23 immediate imaging of the mouse (optional)

18 Either put the mice back into the home cage to recover and proceed from step 24 or, for immediate imaging, place the mouse with its head in the facemask of the custom designed imaging box. Position the mouse so the AIW is affixed in the hole of the metal frame of the imaging box (Figure 3a).

Critical: monitor the mouse vitals carefully during imaging by checking the breath rate at least every half hour or make use of a MouseOx for constant monitoring of vital signs.

19 When properly inserted in the imaging box, mark the window and metal frame of the box at two positions using differently colored markers. This will allow for similar positioning of the window and organ during sequential imaging sessions (Figure 3b).

Caution: the marked spots may disappear from the window after several days so make sure to repaint the marks every day.

20 Place the imaging box on top of the stage of the microscope (Figure 3b). To reduce aberrations during imaging make sure that the window is exactly perpendicular to the objective (prevent tilting of the window).

Critical: the temperature within the box surrounding the microscope is important because an anesthetized mouse is unable to regulate its body temperature.

21 Look through the objective of the microscope to determine whether the organ has a stable position and is not affected by respiratory movement. If affected, apply tape over the back of the mouse to stabilize the body against the imaging box. This will reduce tissue motion by respiration.

TROUBLESHOOTING

22 Record images in 12-bit mode to enhance the information on fluorescence intensity of proteins or cells if large differences in expression are found.

23 If you wish to image the same region over multiple days, use one or a combination of the following approaches (option A, motorized stage; option B, gridded coverslip; option C, vasculature road map; option D, collagen fibers; option E, large tile scans):

A Motorized stage

i) Search for a suitable region to image and store the coordinates of that region. This will help to retrace the same area over multiple days.

B Gridded coverslip

i) Mount a gridded coverslip on top of the AIW. Determine the grid number corresponding to the location of the area. The grid number can be visualized by reflectance imaging. The numbers in the grid are edged providing low efficiency of reflection, thereby offering contrast in the reflectance image. To obtain the reflectance image, the laser light has to be focused on the transition of the coverslip and the tissue and the reflected light should be

collected on the detector. In our Leica SP5 multiphoton-OPO system, we use visible laser light for this, for example 488 nm wavelength from an argon laser. Next, we detect the reflected photons within a 10 nm range surrounding the excitation wavelength. So, in case one uses 488 nm excitation, emitted photons between 483 and 493 nm should be collected. This results in a reflectance image of the coverslip, showing the number of the grid that is imaged (Figure 4a and b).

C Vasculature roadmap

i) Use a contrast agent of the vasculature or widefield microscopy. With a 450-490 nm excitation filter and a longpass 515 nm emission filter the vasculature is dark and an image can be obtained by placing a camera in the eyepiece of the multiphoton microscope (Figure 4c).

D Collagen fibers

i) Record the fluorophore of interest simultaneously with the second harmonic generation (SHG) signal of the type I collagen fibers using a multiphoton laser. For some organs, like the liver, the type I collagen fibers are very prominent, and can be used to retrace areas with subcellular accuracy (Figure 5)[5]. To collect the SHG signal, excite the tissue using a wavelength between 750 and 1040 nm, and collect the photons at half the excitation wavelength.

E Large tile scans.

i) If allowed by the time frame, make large tile scans to provide you with more spatial information and to facilitate retracing of multiple areas over multiple days.

Steps 24-25 Recovery after surgery

24 Put the mouse back in the cage and monitor it closely during recovery. Mice should be housed solitary under standard laboratory conditions, with water and food available at libitum. The first day after surgery a food pellet should be provided on the cage floor. Postoperatively, vital signs of the mouse should be monitored every day until parameters return to pre-surgery scores. These parameters include respiration, reactivity, excessive weight loss, abnormal behavior and posture. One day after surgery these parameters should return to pre-surgery scores. Once the scores are back to pre-surgery scores monitoring should be performed at least once a week. Also, monitor the skin surrounding the window for inflammation and necrosis.

25 Use a 1ml syringe with a 25-gauge needle to inject 100µl of 0.03mg/ml buprenorphine intramuscularly in one of the hind legs. This should be done between 8 and 12 hours after the first dose of buprenorphine was administered.

TROUBLESHOOTING

PAUSE POINT, when pre-surgery scores are met and no necrosis or inflammation is present, the mouse can be kept in its cage for a maximum period of 1 month.

Steps 26-28 Reimaging of the mouse (optional)

26 At the desired time point, anesthetize the mouse by placing it in the induction chamber with 2.5% (v/v) isoflurane.

27 When the mouse is completely unconscious, place the mouse with its head in the facemask of the imaging box. Position the mouse with its window down and affix the window in the hole of the metal frame of the imaging box, using the marks applied during the initial imaging session.

Critical: monitor the mouse vitals carefully during imaging by checking the breath rate at

least every half hour or make use of a MouseOx for constant monitoring of vital signs.

28 Repeat steps 18-24

Steps 29-30 Image analysis

29 After recording and saving, the images can be exported as TIF tiles and can be imported in ImageJ or ImageJ FIJI. Image corrections such as contrasting, changes in brightness, smoothing of the images or the application of certain filters like a median filter should always be done on the 12 bit images. After corrections, an RGB image can be created by merging the images.

30 If breathing movement created a shift in the x,y or z position of your area of interest, registration can be used to realign the images. This can be done manually in ImageJ or ImageJ FIJI. For a large number of images, software can be used in which this process is automated. For this, we use custom written software using algorithms based on the Pearson correlation coefficient as described by van Rheenen and colleagues18, or using ImageJ FIJI plugins.

Timing

Steps 1-9: Window preparation - Timing 3 hours

Steps 10-16: Preparing for surgery – Timing 15 minutes

Step 17: AIW Surgery – Timing between 15 and 45 minutes, depending on organ of interest and experience

Steps 18-23: Immediate imaging – Timing between 30 minutes and multiple hours, depending on the research question

Steps 24-25: Recovery – Timing 1 day or until recovered

Steps 26-28: Re-imaging – Timing between 40 minutes and multiple hours, depending on the research question

Steps 29-30: Image analysis – Timing between 10 minutes and one hour, depending on the amount of corrections

TROUBLESHOOTING

Step	Problem	Possible reason	Solution
7	The AIW is not watertight	Glue was not distributed evenly around the ring	Repeat steps 3-7
17	Mouse dies during surgery	Hyperthermic	Hyperthermia will amplify the effect of the anesthetics leading to depression of respiration. Reduce the power of the heating pad to recover from respiratory distress.
17 A-C	Heavy bleeding	Vascular damage	Try to control blood loss by gently pressing a cotton swab on top of the focus of bleeding for 1 minute
			Use a cautery and burn the leaky vessel to close it
			When performing a lateral incision in the muscular wall, try to spare large vessels that are visible by eye, or use trans-illumination to visualize the vessels
	The mouse has difficulty breathing	The mouse is hyperthermic	Hyperthermia will amplify the effect of the anesthetics leading to depression of respiration. Reduce the power of the heating pad to recover the mouse from respiratory distress.
17 Aiii	The mouse has difficulty breathing	The diaphragm was punctured	A punctured diaphragm will result in a pneumothorax. The mouse should be sacrificed to prevent suffocation. To avoid this, carefully manipulate the liver caudally with a cotton swab and dissect the falciform ligament during exhalation. Also, a blunt tipped scissors can be used
17 Avii	The liver is not located against the coverslip after placing the AIW	The AIW was not inserted correctly on top of the liver or too little glue was used to fix the liver to the AIW	Turn the mouse on its feet. Gravity will press all abdominal organs towards the coverslip.
17 Aix	Suture breaks	Sutures were pulled too tight	Replace purse string suture. The strength of the suture depends on the material being used. If breaking occurs often change to different non-resorbable suture material, or one size thicker suture
17 Aix	The incision does not completely close around the window	Initial incision is too long	Place a stitch at one of the ends to reduce the incision. This can be prevented by initially making a small incision and trying to fit the AIW. When too small, carefully enlarge the incision with a few millimeters until the AIW fits
21	The liver is still moving	The falciform ligament was not dissected far enough	If the movement is too severe, image distortions will occur. This can be circumvented by fast image acquisition. For example by reducing the averaging, by scanning in a bi-directional mode or by using a resonant scanner. Furthermore, image corrections after acquisition can be performed like registration in XY and/or Z
		The cotton gauze roll was not positioned correctly	
	The small intestine is still moving	Too little glue was used	

Step	Problem	Possible reason	Solution
	Poor visibility	Bleeding or accumulation of liquid	Try to remove liquid by inserting a 25-gauge needle underneath the window attached to a 1ml syringe. Make sure not to hit any organs. Once the needle is underneath the window, the liquid can be removed by slowly filling the syringe. If the bleeding is too heavy and does not stop or if the visibility does not improve, the animal should be sacrificed. Note that this cannot be done when imaging the liver, since the liver is completely glued to the window
24	Mouse is slow to recover from anesthesia	The mouse is hypothermic	Increase the temperature of the recovery cage by heating it with a heating pad or a lamp
		Excessive fluid loss	To rehydrate the mouse, inject 200 u l of PBS intraperitoneally
	Coverslip fracture	Mouse might have bumped into a hard material	The tissue will be dehydrated and seriously affected, imaging is not possible anymore. The mouse should be sacrificed
	Necrosis of the skin next to the AIW	The suture is pulled too tight into the AIW	The necrosis will cause pain to the animal and the AIW will eventually fall out. Therefore, the mouse should be sacrificed
	The AIW falls out	The suture is placed too close to the edge of the incision	Necrosis of the skin will occur due to insufficient blood supply. The mouse should be sacrificed
	The skin next to the AIW becomes red	The skin is inflamed	Work in a sterile environment and position the skin correctly and circularly in the window groove avoiding any openings of the abdominal cavity

ANTICIPATED RESULTS

Typical results that can be obtained with the liver AIW are shown in figure 5. For insertion of the AIW in the abdominal wall, a midline incision through skin and muscles was made. Colorectal tumor cells were injected into the splenic parenchyma as described[19,20]. The images show the progression of C26-GFP tumor cell outgrowth in the liver over multiple days and the second harmonic generation (SHG) signal that visualizes type I collagen fibers. The SHG signal can be used to retrace the same location over consecutive imaging sessions[5].

In figure 6, OT1 $CD8^+$ T cells from a GFP-transgenic mouse were adoptively transferred into a recipient mouse[5]. The spleen was then fixed to the AIW for imaging. T cells were imaged through the AIW over time after injecting OVA peptide into the tail base of the mouse, thus inducing an immune response. The OT1 $CD8^+$ T cells were found migrating along type I collagen fibers that were visualized using SHG imaging. T cells migrating along type I collagen fibers have previously been observed in the lymph node[21].

Fixation of the pancreas to the AIW allows imaging of, for instance, the pancreatic vasculature (Figure 7). Color contrast is achieved by intravenous injection of Texas-Red Dextran (70 kDa).

In stem cell biology it is of great importance to be able to follow the fate of individual stem cell lineages over time. In figure 8 we show that the AIW can be used to follow stem cell fate in the small intestine by using double heterozygous *Lgr5-EGFP-Ires-CreERT2/R26R-Confetti* mice (The Jackson Laboratory, 013731). In these mice, all Lgr5^{+}- intestinal stem cells express EGFP. Furthermore, the Lgr5 promotor also drives a tamoxifen inducible CreERT2, which will sporadically induces one of the confetti colors (nuclear green, membrane blue, yellow and red), which are inherited by all respective daughter cells[22]. By tracing these confetti-marked stem cells over multiple days through the AIW and by using the microvessels as fiduciary landmarks, it is possible to trace individual intestinal stem cell lineages, as each lineage is an accumulation of cells with the same confetti color.

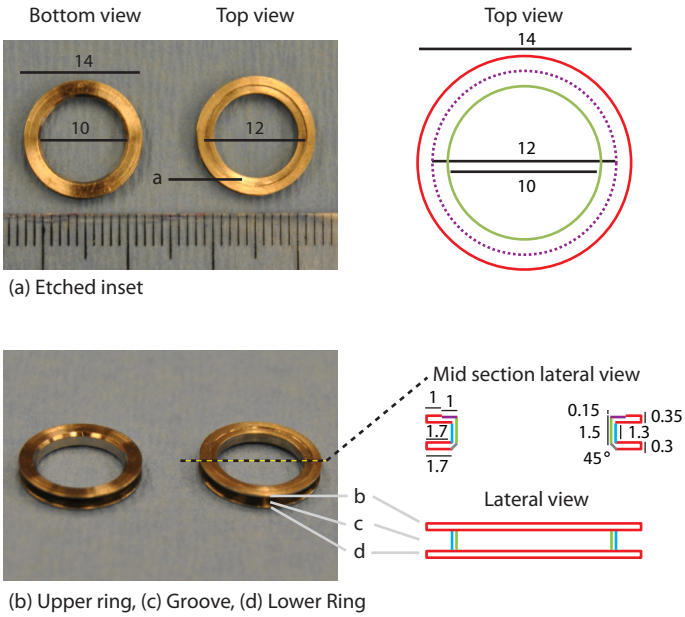

Figure 1. The specifics of the AIW. The AIW is shown from the top (upper left picture), bottom (upper left picture) and from the side (lower left picture). The etched inset (a), upper (b) and lower (d) ring and groove (c) are visible. The right cartoon shows the exact details of the dimensions of the ring.

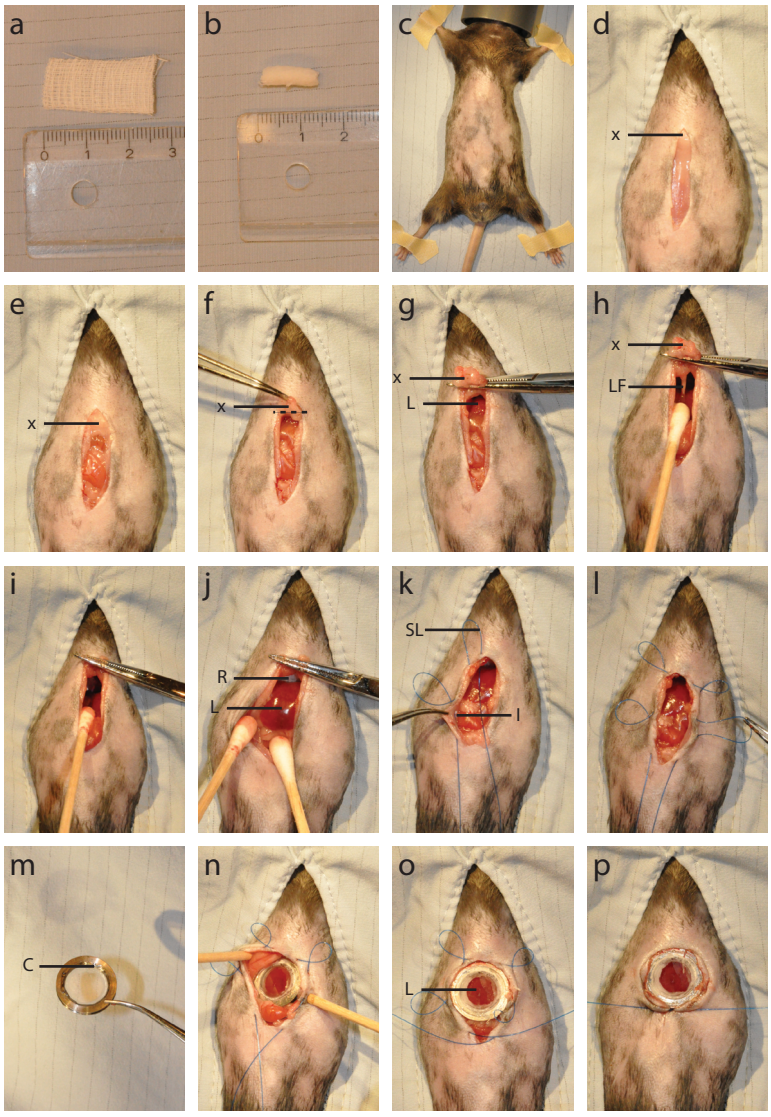

Figure 2. The AIW liver surgery. A. To prepare the cotton gauze roll, a sterile cotton gauze is cut to the appropriate size. **B.** The cotton gauze roll that will be inserted in between the liver and diaphragm. **C.** The shaved mouse is located with its face in a facemask and fixed in an X shape using tape. **D.** The skin incision starting just above the xyphoid process (x). **E.** An incision through the muscular layer is made exposing the abdominal organs and the xyphoid process (x). **F.** The xyphoid process (x) is lifted and the dashed line shows the position at which it should be clamped. **G.** The xyphoid process (x) is clamped and moved cranially, exposing the liver (L). **H.** The clamped xyphoid process (x) is moved cranio-ventrally, exposing the falciform ligament (LF). **I.** After hemostasis is obtained, the clamped xyphoid process is removed. The falciform ligament is dissected onto the suprahepatic IVC. **J.** The inserted cotton gauze roll (R) is inserted transversely in between the diaphragm and liver (L), moving the liver more caudally. **K.** A purse-string suture is placed. The first outer loop and second outer loop (SL) are visible, as well as the first inner loop (IL). **L.** The purse-string suture creates a continuous circular loop. **M.** Cyanoacrylate (C) is applied on the titanium edges of the inner ring of the AIW. **N.** The AIW is placed on top of the liver. **O.** The skin and muscular layer are placed in the AIW groove. The liver (L) remains attached to the AIW. **P.** Closure of the purse-string is performed by pulling the suture loops, and firmly tying the suture ends. This experiment was carried out in accordance with the guidelines of the Animal Welfare Committee of the Royal Netherlands Academy of Arts and Sciences, the Netherlands.

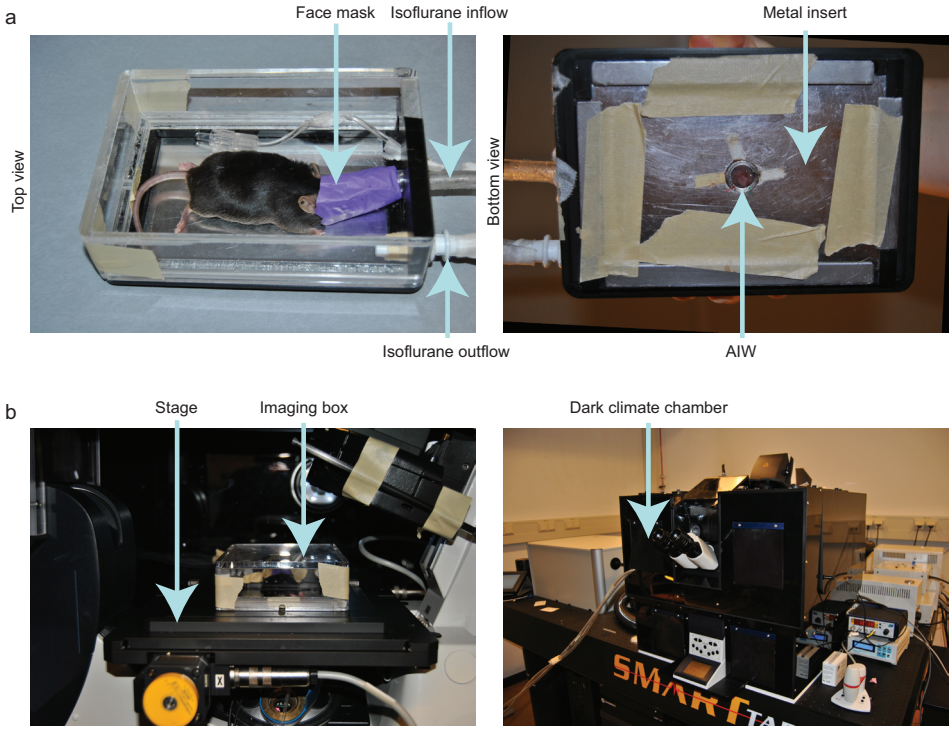

Figure 3. Fixation of the mouse in the imaging box. A. The custom made imaging box shown from different angles. **B.** The inverted Leica SP5 multiphoton microscope is shown. This experiment was carried out in accordance with the guidelines of the Animal Welfare Committee of the Royal Netherlands Academy of Arts and Sciences, the Netherlands.

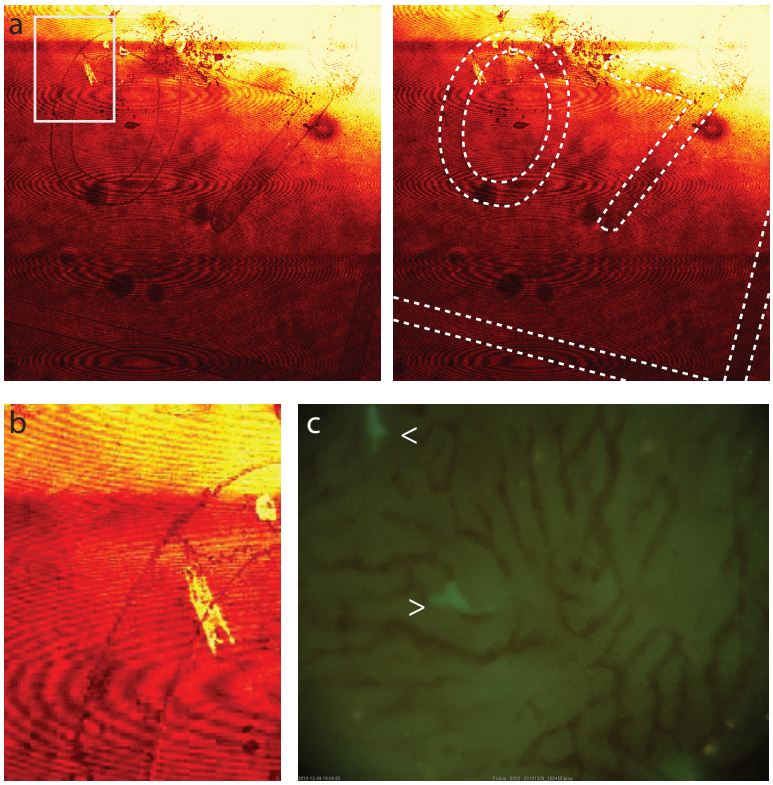

Figure 4. Tools to retrace areas of interest over multiple days. A. The grid and its corresponding number (07) visualized by reflectance imaging (left image, red hot lookup table). The grid is outlined in the right image (red hot lookup table). Scale bar represents 150 µm. **B.** A zoom in of the area highlighted by the square in (a). Scale bar represents 42 µm. **C.** An image taken through the eyepiece of a widefield microscope showing the vasculature in dark and fluorescent tumor cells in green (highlighted by the arrowhead). Scale bar represents 18 µm. This experiment was carried out in accordance with the guidelines of the Animal Welfare Committee of the Royal Netherlands Academy of Arts and Sciences, the Netherlands.

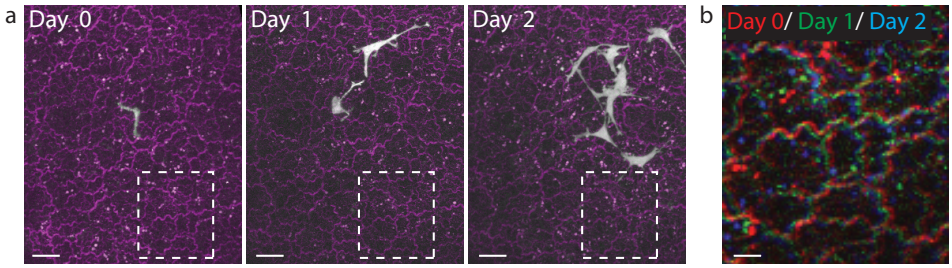

Figure 5. Imaging of the liver through the AIW. A. IVM images show multiple day tracing of a C26-Dendra2 tumor cell (white) that is surrounded by type I collagen (purple) fibers in the liver. To obtain the images, the region was imaged with a Leica TCS SP5 multiphoton (MP)-OPO microscope using an excitation wavelength of 960 nm. The SHG signal from the type I collagen fibers was detected between 455-490 nm, the Dendra2 signal was detected with two non-descanned detectors (NDDs) between 455-490 nm and 500-550 nm. A representative experiment from one out of ten mice is shown. Scale bar represents 20 µm. **B.** The squared area in the three pictures in (a) are merged and magnified. Position of the collagen fibres at different days were assigned a different color to show the subcellular retracing of the area. Scale bar represents 60 µm. This experiment was carried out in accordance with the guidelines of the Animal Welfare Committee of the Royal Netherlands Academy of Arts and Sciences, the Netherlands.

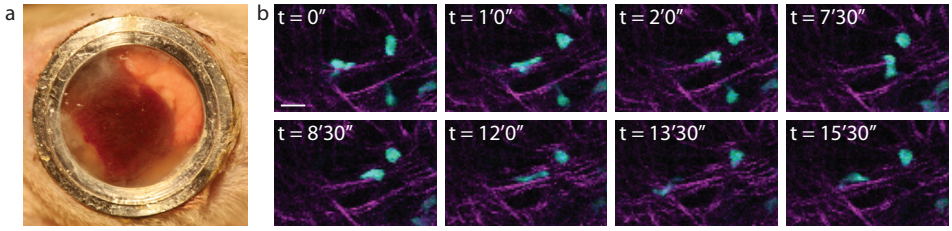

Figure 6. Imaging of the spleen through the AIW. A. The AIW is implanted on top of the spleen. **B.** OT1 CD8+ GFP T cells (blue) migrating along a type I collagen fiber (purple, SHG). To obtain the images, a Leica TCS SP5 MP-OPO microscope was used to excite the fluorophores with a wavelength of 900 nm. The SGH signal from the type I collagen fibers was detected <455 nm, the GFP signal was detected between 500-550 nm. A representative experiment from one out of four mice is shown. The scale bar represents 15 µm. This experiment was carried out in accordance with the guidelines of the Animal Welfare Committee of the Royal Netherlands Academy of Arts and Sciences, the Netherlands.

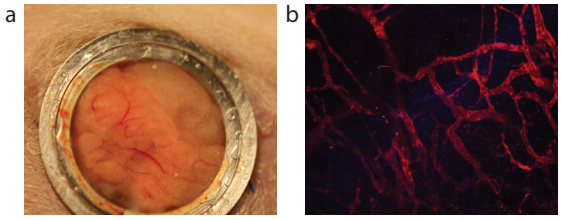

Figure 7. Imaging of the pancreas through the AIW. A. The AIW is implanted on top of the pancreas. **B.** The pancreatic vasculature is visualized by i.v. injection of 70kDa Texas-red labeled dextran (red). Texas-red was excited with a multiphoton laser tuned at 860 nm. Emitted photons were detected between 560-650 nm. A representative experiment from one out of three mice is shown. Scale bar represents 65 µm. This experiment was carried out in accordance with the guidelines of the Animal Welfare Committee of the Royal Netherlands Academy of Arts and Sciences, the Netherlands.

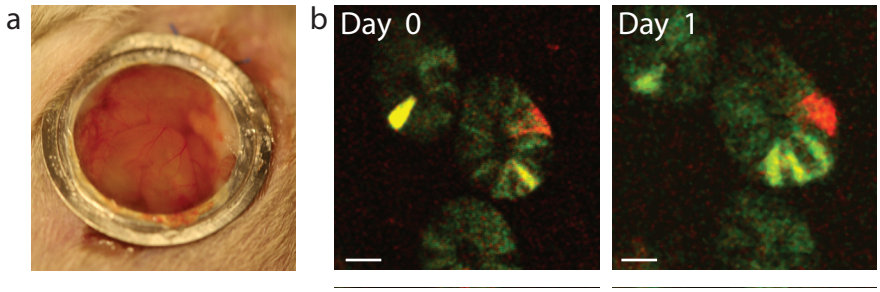

Figure 8. Imaging of the small intestinal through the AIW. A. The AIW is transplanted on top of the small intestine. **B.** Lgr5^{+} stem cell (green) tracing in the same intestinal crypt over multiple days. The confetti colors (red and yellow) were randomly activated in Lgr5^{+} cells and enabled tracing. The fluorophores were excited using a Leica TCS SP5 MP-OPO microscope. Excitation was performed at 960 nm and the emitted photons were collected using 3 NDDs that detect photons with a wavelength between 455-490 nm, 500-550 nm and 560-650 nm. A representative experiment from one out of ten mice is shown. Scale bar represents 8 µm. This experiment was carried out in accordance with the guidelines of the Animal Welfare Committee of the Royal Netherlands Academy of Arts and Sciences, the Netherlands.

REFERENCE LIST

1. Beerling, E et al. Intravital microscopy: new insights into metastasis of tumors. 124, 299-310. 2011.
2. Ritsma, L et al. Intravital imaging of cell signaling in mice. 1, 3-11. 2012.
3. Theer, P et al. Two-photon imaging to a depth of 1000 ?m in living brains by use of a Ti:Al2O3 regenerative amplifier. 28, 1022-1024. 2003.
4. Egeblad, M et al. Visualizing stromal cell dynamics in different tumor microenvironments by spinning disk confocal microscopy. 1, 155-167. 2008.
5. Ritsma, L et al. Intravital microscopy through an abdominal imaging window reveals a pre-micrometastasis stage during liver metastasis. Sci. Transl.Med. 4, 158ra145. 2012.
6. Kienast, Y et al. Real-time imaging reveals the single steps of brain metastasis formation. 16, 116-122. 2010.
7. Pan, F et al. Two-photon imaging of dendritic spine development in the mouse cortex. 68, 771-778. 2008.
8. Yuan, F et al. Vascular Permeability and Microcirculation of Gliomas and Mammary Carcinomas Transplanted in Rat and Mouse Cranial Windows. 54, 4564-4568. 1994.
9. Lehr, HA et al. Dorsal skinfold chamber technique for intravital microscopy in nude mice. 143, 1055-1062. 1993.
10. Palmer, GM et al. In vivo optical molecular imaging and analysis in mice using dorsal window chamber models applied to hypoxia, vasculature and fluorescent reporters. Nature protocols 2011/09/03, 1355-1366. 2011.
11. Perentes, JY et al. In vivo imaging of extracellular matrix remodeling by tumor-associated fibroblasts. 6, 143-145. 2009.
12. Gligorijevic, B et al. Dendra2 photoswitching through the Mammary Imaging Window. J.Vis.Exp. 2009.
13. Kedrin, D et al. Intravital imaging of metastatic behavior through a mammary imaging window. 5, 1019-1021. 2008.
14. Shan, S et al. A novel rodent mammary window of orthotopic breast cancer for intravital microscopy. 65, 109-117. 2003.
15. Farrar, MJ et al. Chronic in vivo imaging in the mouse spinal cord using an implanted chamber. 9, 297-302. 2012.
16. Holtmaat, A et al. Long-term, high-resolution imaging in the mouse neocortex through a chronic cranial window. 4, 1128-1144. 2009.
17. Niinomi, M. Recent research and development in titanium alloys for biomedical applications and healthcare goods. 4, 445-454. 2003.
18. van Rheenen, J et al. EGF-induced PIP2 hydrolysis releases and activates cofilin locally in carcinoma cells. J.Cell Biol. 179, 1247-1259. 2007.
19. Drixler, TA et al. Continuous Administration of Angiostatin Inhibits Accelerated Growth of Colorectal Liver Metastases after Partial Hepatectomy. 60, 1761-1765. 2000.
20. Stock, P et al. The generation of hepatocytes from mesenchymal stem cells and engraftment into murine liver[ast]. 5, 617-627. 2010.
21. BajÃ©noff, M et al. Stromal Cell Networks Regulate Lymphocyte Entry, Migration, and Territoriality in Lymph Nodes. 25, 989-1001. 2006.
22. Snippert, HJ et al. Intestinal Crypt Homeostasis Results from Neutral Competition between Symmetrically Dividing Lgr5 Stem Cells. 143, 134-144. 2010.

PART III | DISCUSSION AND SUMMARY

CHAPTER 8

8

DISCUSSION

The role of CD95 in intestinal homeostasis, colorectal tumor development and liver metastasis formation

The exact role of CD95 signaling in the homeostasis of the gastrointestinal tract remains obscure. Leithauser *et al* and Moller *et al* have studied the expression patterns of CD95 and its ligand (CD95L) in the intestinal tract[1,2]. CD95 is uniformly expressed at the basolateral surface of all epithelial cells along the crypt-villus axis[1,2]. CD95L is exclusively expressed in the Paneth cells of the intestinal epithelium and in scarce lymphohistocytic infiltrates in the lamina propria. These patterns were based on immunohistochemistry staining of intestinal tissue and as such completely rely on the specificity of the CD95 and CD95L antibodies[1,2]. Especially the specificity of the CD95L antibodies has been questioned[3]. However, in situ hybridization experiments on mRNA of CD95L showed a similar expression pattern[4]. Expression of the receptor and its ligand are thus confined to specific and distinct intestinal compartments. The homeostasis of the rapidly renewing epithelial layer of the intestinal tract and the typical CD95/CD95L expression pattern raises the question if CD95/CD95L signaling has a role in maintaining this equilibrium. A potential function of CD95/CD95L in intestinal homeostasis is to stimulate apoptosis of CD95-expressing epithelial cells of the rapidly renewing mucosa. This hypothesis is contradicted by studies reporting no morphologic intestinal abnormalities or differences in apoptotic cell count in mice lacking functional CD95 or CD95L[5,6]. Alternatively, CD95/CD95L signaling could influence migration of the epithelial cells along the crypt-villus axis as it has been shown to be a potent inducer of migration and invasion[7-9] (chapter 4). Furthermore, CD95/CD95L pathway stimulation has been implicated in neuronal stem cell maturation and differentiation[10,11]. Similarly, the differentiation of transit amplifying cells into enterocytes, goblet cells, enteroendocrine cells and paneth cells could be influenced by CD95/CD95L signaling.
Paneth cells are the only cells in the intestinal mucosa which express CD95L. Individual stem cells are surrounded by Paneth cells which produce niche signals essential for the phenotypic maintenance of stem cells[12]. CD95L signaling could be involved in this paneth cell-stem cell preservation even though the stem cell function and phenotype is retained by the expression of EGF, Wnt3 and Notch in paneth cells[12]. Possibly, the expression of CD95L on paneth cells could help protect the stem cell by inducing apoptosis of infiltrating CD95 expressing lymphocytes as such creating an immune privileged site, a theory similar to "the tumor counter attack" hypothesis[13-15].
In addition to the possible functions of CD95/CD95L signaling in the homeostasis of the gastrointestinal tract, it also remains unclear if faulty CD95/CD95L signaling is involved in tumorigenesis in the gut. Chapter 3 shows that CD95L does not only induce apoptosis but can also act as a chemotactic cytokine stimulating migration and invasion. Earlier work has shown that CD95 stimulates proliferation in primary tumors and promotes invasion and liver metastasis formation[7,16,17].
To further elucidate the role of CD95/CD95L signaling in the physiology of the intestine and in the initiation of tumor formation the following experimental models are proposed:

ALPS patients

Autoimmune lymphoproliferative syndrome (ALPS) is the clinical presentation of a non-functional mutation in the CD95 or CD95L gene[18]. Typical clinical observations in ALPS are lymphadenopathy, splenomegaly and autoimmune cytopenias[18]. ALPS is associated with lymphoma and carcinoma of breast, thyroid, liver, skin and tongue[18]. There is no description in the literature about ALPS and its effect on morphology, function or tumor development in the

gastrointestinal tract. Close observation of the morphology as well as the cytology of the gastrointestinal tract of ALPS patients over time could reveal alterations in the physiology of the intestine caused by non-functional CD95 signaling. This will help in understanding if CD95 signaling influences the homeostasis of the gut. Long term follow-up of ALPS patients will show any alterations in the incidence of colorectal tumorigenesis in comparison to the healthy population.

Mouse models

This ALPS phenotype was also observed in mice lacking expression of CD95 (*lpr*) and in mice with dysfunctional CD95L (*gld*). These mouse models allow for research on the function of CD95/CD95L in the gut. A disadvantage of these models is the important function of CD95 signaling in lymphocyte immunity causing lymphoproliferation. This makes it hard to differentiate if dysfunctional CD95/CD95L signaling directly affects intestinal epithelial cells or if changes in epithelial morphology and function result from the effect on infiltrating immune cells. Park *et al* developed a mouse model lacking CD95 expression selectively in the intestinal epithelial cells[19]. While chemically induced carcinogenesis in the intestinal tract of these mice compared to controls is not altered, it is not reported if the lack of CD95 signaling influences gastrointestinal homeostasis or physiology[19]. Close analysis of the morphology and function of the gut in these mice over time could hint to a possible function of CD95. A similar mouse model with a selective CD95L knockout in the gut should be developed to asses the role of CD95L in gut homeostasis.

Several groups have created a mouse model of spontaneous colorectal tumor development[20-22]. Genetic engineered mouse (GEM) with a germline loss-of-function APC and oncogenic Kras mutation spontaneously developed intestinal tumors[21-23]. However, these tumors were predominantly located in the small intestine and did not develop metastases[22]. Hung *et al* improved the APC/Kras GEM model by creation of a mouse with an adeno-cre inducible homozygous APC inactivating mutation as well as an inducible heterozygous activating Kras mutation[20]. When adenovirus was selectively injected in the distal colon colorectal tumors developed spontaneously and represented the entire adenoma-carcinoma-metastasis axis over time[20]. Despite the almost perfect representation of human colorectal cancer this model is limited by the inconsistency of metastasis development[20]. If a genetic mouse model can be created in which metastases occur reproducibly, it would be ideal for studying CD95/CD95L function in tumor and metastasis formation when crossed with intestine selective non-functional CD95/CD95L mice.

Human xenograft models

GEM cancer models are very practical in investigating the effect of signaling pathways on carcinogenesis. However, these models are based on mutations in the intestinal epithelial cells resulting in genetically homogeneous tumors. Furthermore, all mice harbor the same mutations and the same genetic background. Human colorectal cancer however is characterized by a large genetic heterogeneity[24].

A different approach to investigate the effect of CD95/CD95L signaling in CRC development is the use of xenograft models in which primary cancer cell lines are established from human CRC followed by implantation into immunodeficient mice. RNA interference targeting CD95 or CD95L in these cell lines prior to injection into the mouse creates the possibility to alter CD95 signaling selectively in tumor cells.

Injection of the primary human cell lines in an orthotopic or ectopic location results in consistent xenograft growth in immunodeficient mice. Metastasis formation of these tumors has been reported in studies using serial implantation of human tumor cells into mice[25,26]. Spontaneous metastasis only occurred after an average of 10-11 *in vivo* passages[26]. The question remains if the serial implantation does not select for a highly malignant population which is not consistent with the original heterogeneous tumor cell population. Another study reported spontaneous metastasis formation in a xenograft model after cecal wall injection of selected CD26 expressing human CRC cells in mice[27]. This study demonstrated for the first time that it is possible to obtain spontaneous metastasizing tumors from human resection specimens[27]. Therefore, it would be an interesting model to asses the function of CD95/CD95L in metastasis formation by blocking CD95/CD95L in the CD26 positive metastasizing cells. Alternatively CD95 or CD95L high versus low expressing cells could be selected and injected separately in the cecal wall wherafter metastasis formation could be assessed.
A drawback of the xenograft model is that the survival of human cells in rodents requires a defective or suppressed host immune system in order to avoid rejection of the cells. However, while a deficient immune system allows for human tumor development in mice it does not resemble human tumor development in which the immune system has anti- and pro-carcinogenic functions. Indeed, inflammatory reactions in CRC development play an important role in controlling malignant growth and metastasis formation[28].

Gene expression profiling

The development and progression of colorectal tumors is known to be caused by the accumulation of genetic alterations, resulting in altered function of oncogenes, tumor suppressor genes, and mismatch repair genes[29,30]. These alterations affect the expression of a variety of downstream genes, including those involved in regulating the cell cycle, apoptosis, adhesion, and angiogenesis[31]. Gene expression profiling of human CRC samples could aid in giving insights into the exact function of CD95/CD95L. It has been shown that CD95 expression is downregulated during colorectal tumor development by immunohistochemistry as well as by mRNA expression of CD95[1,2,32]. On the contrary, increased CD95L expression is an early event in colonic carcinogenesis and was associated with colorectal tumor development[33,34]. Large sampling of healthy, adenoma, primary tumor and metastatic colorectal tissue and subsequent mRNA expression profiling could reveal a distinct signature for CD95/CD95L low and high tumors. This signature could be related to disease progression, disease free survival, treatment and overall survival through correlation analysis of the resulting genes. In chapter 5 of this thesis such a method was applied to investigate PDGFR expression in CRC. In this approach bioinformatic software applications were used in the search for processes, pathways and single genes associated with PDGFR expression. Gene Ontology (GO) analyses of the resulting gene lists related PDGFR expression in CRC to extracellular matrix receptor signaling, platelet activation, TGFB signaling and EMT. Similar, this method could be applied to CD95/CD95L expression in CRC. Furthermore, GO analysis of the CD95/CD95L CRC signature could reveal an association with proliferation, survival, migration/invasion or metastasis formation pathways. These possible associated pathways should then be validated *in vitro* and *in vivo* in primary human colorectal cancer cell lines before conclusions can be drawn about the functions of CD95/CD95L signaling in colorectal cancer.

Colorectal liver metastasis formation and EMT

Metastasis formation is a multiphasic process in which a carcinoma cell has to become migratory, avoid or resist lethal attacks of immune cells and survive mechanical forces like shear stress[35]. In breast or lung cancer it is well accepted that the transition from an epithelial to a mesenchymal phenotype (EMT) results in a more migratory, invasive and apoptosis resistant tumor cell population which is more prone to metastasize[36,37].

For CRC it was observed that tumor cells in the invasive front dedifferentiate[19]. This is characterized by a loss of epithelial and gain of mesenchymal-like morphology[38,39]. This process of dedifferentiation, or budding, is very similar to EMT and correlates with liver metastasis formation and poor survival[40-43]. Because most liver metastases from CRC resemble the morphology of the primary tumor it is believed that the mesenchymal-like cells disseminating from the primary tumor and colonizing the liver undergo a mesenchymal-to-epithelial transition in the liver[38]. The above morphological changes are accompanied by the translocation of β-catenin from the cell membrane, where it interacts with e-cadherin and is involved in cell-cell adhesion, to the nucleus in the dedifferentiated cells at the invasive front. In the nucleus β-catenin is a transcriptional regulator and main effector of the Wnt signaling pathway which can induce EMT[44]. This indicates a functional connection between EMT in budding tumor cells and the nuclear localization of β-catenin.

Additionally, the presence of an EMT gene expression signature in CRC predicts tumor recurrence in stage II and stage III disease[42]. Pollution by tumor stroma in the sample could have contributed to the observed EMT-signature in this study as macrodissection from formaline fixed paraffin embedded tissue was used for RNA extraction. However, it was also shown by quantitative proteomic microarrays of microdissected tissue that the cell signaling pathway profile of stroma versus epithelium was closer related in tumors than in normal colon[45]. This supports the concept that EMT occurs in the tumor. Only recently a direct, functional role of EMT in CRC liver metastasis formation was demonstrated in a mouse model. Labelle *et al* showed that the well known EMT inducer TGFβ is released from platelets that interact with circulating tumor cells in the bloodstream[46]. Subsequently, the TGFβ/Smad and NF-κB pathways are activated resulting in EMT and enhanced metastasis formation *in vivo*[46]. In chapter 6 it is shown that the aggressive mesenchymal phenotype is also supported by PDGF signaling from platelets, resulting in an invasive phenotype and more efficient formation of liver metastases. Both *in vivo* models however are based on artificial metastasis formation in which colorectal tumor cells are injected in the tail vein or in the spleen. As explained above, mouse models resembling the adenoma-carcinoma sequence for CRC development were created but do not form metastases or do so very inconsistent and/or inefficient[20,21]. When consistent spontaneous mouse models are created EMT and CRC metastases formation could be studied by fluorescent labeling of epithelial and/or mesenchymal proteins. Subsequently, markers can be analyzed at the different phases of dissemination and liver colonization.

More evidence for EMT in cancer metastasis comes from mesenchymal circulating tumor cells (CTCs) in breast cancer which have far better metastatic potential and are associated with a poor survival compared to epithelial CTCs[47,48]. The detection of CTCs in CRC has been very difficult possibly due to the use of epithelial markers for the detection of disseminated mesenchymal-like tumor cells. However, these epithelial markers may be downregulated by the mesenchymal-like cells. Moreover, tumor cells get coated by platelets in the circulation which could camouflage cell markers. These difficulties can be overcome with spontaneously metastasizing mouse tumor models, in which tumor cells express epithelial and/or mesenchymal

fluorescent markers. Subsequently, simple portal vein blood analysis could not only detect CTCs but also reveal the phenotype of these cells. Using abdominal imaging windows as described in chapter 7 and 8 intravital imaging could be used to study whether mesenchymal-like CTCs are in deed more efficient in forming liver metastases when compared to epithelial-like CTCs.

EMT also poses a challenge for anti-cancer therapy. This is caused by the resistance to conventional systemic therapies associated with EMT. In colon and ovarian carcinoma cell lines it has been shown that an EMT phenotype was associated with resistance to oxaliplatin and paclitaxel[49]. In addition, Snail and Twist, two proteins linked to EMT, mediate resistance to radiotherapy and chemotherapy in several human tumor types[49]. When EMT is shown to play an important role in colorectal cancer progression future research should be directed towards specific targeting of the mesenchymal-like colorectal tumor cells with new chemotherapeutics.

Imaging of metastasis

The understanding of how tumors metastasize is expanding rapidly. However, most insights are derived from studies using static image analysis while most processes involved in carcinogenesis are dynamic[50]. How does the tumor cell behave when dormant and how does it react to the environment or other tumor cells? And importantly, what defines the highly dynamic process of metastasis formation and its response to therapeutic intervention? *In vivo* imaging of cancer is potentially able to provide insight into these questions.

Clinical imaging of cancer has been possible since the development of ultrasound (US) and positron emission tomography (PET) in the sixties of the previous century[51]. The development of computed tomography (CT) and magnetic resonance imaging (MRI) allowed for high contrast visualization of tumors[51]. Enhancement of the above mentioned techniques together with the development of specific probes made it possible to image tumor processes (i.e. angiogenesis or apoptosis) and the expression of molecular markers on tumors. These clinical imaging techniques greatly improved cancer diagnostics, treatment, relapse monitoring and therapy evaluation through visualization of physiology, tumor anatomy and molecular expression[51]. However, despite great advances to pre-clinical and clinical tumor imaging, all these techniques are limited to macroscopic assessment of tumor dynamics.

Intravital microscopy (IVM) in conjunction with the *in vivo* expression of fluorescent markers has created the possibility to image single cell dynamics in cancer biology. In chapter 7 and 8 we present the abdominal imaging window (AIW) through which primary tumor development, metastasis formation at a distant site and the effect of therapeutic intervention on tumor cells can be visualized by IVM over time. The development of this window next to already available window designs (i.e. cranial window model, dorsal skin fold chamber, mammary imaging window) allows for sequential imaging of the identical cell or region at subcellular resolution over time. With the help of genetic engineered mouse models in which different cell types (e.g. tumor cells, stromal cells or immune cells) are labeled with different fluorophores the interplay and dynamics of primary tumor development and metastasis formation in relation to its microenvironment can be studied in depth. We were able to identify a pre-micrometastatic phase of liver colonization in which migration/invasion of the disseminated tumor cells through the liver parenchyma is a limiting step in metastasis formation[52].

Moreover, it is even possible to visualize specific signaling pathways by labeling proteins with a fluorophore. For example, by labeling histone H2B with mCherry (red) and α-tubulin with

EGFP (green) in tumor cells it was shown that the initiation of mitosis *in vivo* was a far less frequent event than *in vitro*[53]. Currently IVM is applied for studies into cell division, cell death, cell migration, cell communication, cell fate and vascular networks, all important processes in carcinogenesis[50].

The advantages of IVM are mainly applicable to experimental tumor biology research in animals. Especially for imaging windows it is hard to imagine how they could be applied in a clinical human setting due to size, microscopy limitations and lack of fluorescence in human disease. Nevertheless IVM aids greatly in understanding and elucidating the cellular and molecular processes involved in cancer development. The great possibilities created by IVM in animal research resulted in efforts to develop clinical applications for tumor visualization. This led to studies in which IVM is already used in a clinical setting[54]. For example, laser endomicroscopy and surgical imaging potentially enable real-time microscopy imaging and *in vivo* diagnosis of gastro-intestinal tumors[54,55]. Other developments in IVM such as optical frequency domain imaging, which does not need contrast agents to visualize angiogenesis, lymphangiogenesis and tissue viability, could possibly help in monitoring treatment of human disease in situ[56].

Further innovations in IVM may give even better insights into the real-time formation of metastases. In conjunction with spontaneous mouse colorectal tumor models, in which molecular processes or cells are labeled, the small subpopulation of disseminated cells, which are able to form metastasis, could be potentially identified. Subsequently, directed treatment of these specific cells could be developed.

REFERENCE LIST

1. Leithauser, F *et al*. Constitutive and induced expression of APO-1, a new member of the nerve growth factor/tumor necrosis factor receptor superfamily, in normal and neoplastic cells. Lab Invest 69, 415-429. 1993.
2. Moller, P *et al*. Expression of APO-1 (CD95), a member of the NGF/TNF receptor superfamily, in normal and neoplastic colon epithelium. Int.J.Cancer 57, 371-377. 1994.
3. Strater, J *et al*. CD95 ligand (CD95L) immunohistochemistry: a critical study on 12 antibodies. Cell Death.Differ. 8, 273-278. 2001.
4. Moller, P *et al*. Paneth cells express high levels of CD95 ligand transcripts: a unique property among gastrointestinal epithelia. Am.J.Pathol. 149, 9-13. 1996.
5. Cohen, PL *et al*. Lpr and gld: single gene models of systemic autoimmunity and lymphoproliferative disease. Annu.Rev.Immunol. 9, 243-269. 1991.
6. Strater, J *et al*. CD95 (Fas/APO-1)/CD95L in the gastrointestinal tract: fictions and facts. Virchows Arch. 442, 218-225. 2003.
7. Hoogwater, FJ *et al*. Oncogenic K-Ras turns death receptors into metastasis-promoting receptors in human and mouse colorectal cancer cells. Gastroenterology 138, 2357-2367. 2010.
8. Kleber, S *et al*. Yes and PI3K bind CD95 to signal invasion of glioblastoma. Cancer Cell 13, 235-248. 2008.
9. Nijkamp, MW *et al*. CD95 is a key mediator of invasion and accelerated outgrowth of mouse colorectal liver metastases following radiofrequency ablation. J.Hepatol. 53, 1069-1077. 2010.
10. Corsini, NS *et al*. The death receptor CD95 activates adult neural stem cells for working memory formation and brain repair. Cell Stem Cell 5, 178-190. 2009.
11. Zuliani, C *et al*. Control of neuronal branching by the death receptor CD95 (Fas/Apo-1). Cell Death. Differ. 13, 31-40. 2006.
12. Sato, T *et al*. Paneth cells constitute the niche for Lgr5 stem cells in intestinal crypts. Nature 469, 415-418. 2011.
13. Bennett, MW *et al*. The Fas counterattack *in vivo*: apoptotic depletion of tumor-infiltrating lymphocytes associated with Fas ligand expression by human esophageal carcinoma. J.Immunol. 160, 5669-5675. 1998.
14. Houston, A *et al*. Fas ligand mediates immune privilege and not inflammation in human colon cancer, irrespective of TGF-beta expression. Br.J.Cancer 89, 1345-1351. 2003.
15. Munakata, S *et al*. Expressions of Fas ligand and other apoptosis-related genes and their prognostic significance in epithelial ovarian neoplasms. Br.J.Cancer 82, 1446-1452. 2000.
16. Chen, L *et al*. CD95 promotes tumour growth. Nature 465, 492-496. 2010.
17. Li, H *et al*. Human and mouse colon cancer utilizes CD95 signaling for local growth and metastatic spread to liver. Gastroenterology 137, 934-44, 944. 2009.
18. Bleesing, JJ *et al*. Immunophenotypic profiles in families with autoimmune lymphoproliferative syndrome. Blood 98, 2466-2473. 2001.
19. Park, SM *et al*. CD95 is cytoprotective for intestinal epithelial cells in colitis. Inflamm.Bowel.Dis. 16, 1063-1070. 2010.
20. Hung, KE *et al*. Development of a mouse model for sporadic and metastatic colon tumors and its use in assessing drug treatment. Proc.Natl.Acad. Sci.U.S.A 107, 1565-1570. 2010.
21. Janssen, KP *et al*. APC and oncogenic KRAS are synergistic in enhancing Wnt signaling in intestinal tumor formation and progression. Gastroenterology 131, 1096-1109. 2006.
22. Taketo, MM *et al*. Mouse models of colon cancer. Gastroenterology 136, 780-798. 2009.
23. Sansom, OJ *et al*. Loss of Apc allows phenotypic manifestation of the transforming properties of an endogenous K-ras oncogene *in vivo*. Proc.Natl. Acad.Sci.U.S.A 103, 14122-14127. 2006.
24. Hart, IR *et al*. The implications of tumor heterogeneity for studies on the biology of cancer metastasis. Biochim.Biophys.Acta 651, 37-50. 1981.
25. Hoffman, RM. Orthotopic metastatic mouse models for anticancer drug discovery and evaluation: a bridge to the clinic. Invest New Drugs 17, 343-359. 1999.
26. Sun, FX *et al*. An ultra-metastatic model of human colon cancer in nude mice. Clin.Exp.Metastasis 17, 41-48. 1999.
27. Pang, R *et al*. A subpopulation of CD26+ cancer stem cells with metastatic capacity in human colorectal cancer. Cell Stem Cell 6, 603-615. 2010.
28. Taketo, MM. Reflections on the spread of metastasis to cancer prevention. Cancer Prev.Res. (Phila) 4, 324-328. 2011.
29. Kountouras, J *et al*. New concepts of molecular biology for colon carcinogenesis. Hepatogastroenterology 47, 1291-1297. 2000.
30. Takahashi, M *et al*. Gene mutations and altered gene expression in azoxymethane-induced colon carcinogenesis in rodents. Cancer Sci. 95, 475-480. 2004.
31. Calvert, PM *et al*. The genetics of colorectal cancer. Ann.Intern.Med. 137, 603-612. 2002.
32. Butler, LM *et al*. Down-regulation of Fas gene expression in colon cancer is not a result of allelic loss or gene rearrangement. Br.J.Cancer 77, 1454-1459. 1998.
33. Bennett, MW *et al*. Fas ligand upregulation is an early event in colonic carcinogenesis. J.Clin.Pathol. 54, 598-604. 2001.
34. Mann, B *et al*. FasL is more frequently expressed in liver metastases of colorectal cancer than in matched primary carcinomas. Br.J.Cancer 79, 1262-1269. 1999.
35. Steeg, PS. Tumor metastasis: mechanistic insights and clinical challenges. Nat.Med. 12, 895-904. 2006.

36. Jechlinger, M *et al*. Autocrine PDGFR signaling promotes mammary cancer metastasis. J.Clin. Invest 116, 1561-1570. 2006.
37. Thomson, S *et al*. Kinase switching in mesenchymal-like non-small cell lung cancer lines contributes to EGFR inhibitor resistance through pathway redundancy. Clin.Exp.Metastasis 25, 843-854. 2008.
38. Kirchner, T *et al*. Patterning and nuclear beta-catenin expression in the colonic adenoma-carcinoma sequence. Analogies with embryonic gastrulation. Am.J.Pathol. 157, 1113-1121. 2000.
39. Thiery, JP *et al*. Epithelial-mesenchymal transitions in development and disease. Cell 139, 871-890. 2009.
40. Jass, JR *et al*. APC mutation and tumour budding in colorectal cancer. J.Clin.Pathol. 56, 69-73. 2003.
41. Kevans, D *et al*. Epithelial-mesenchymal transition (EMT) protein expression in a cohort of stage II colorectal cancer patients with characterized tumor budding and mismatch repair protein status. Int.J.Surg.Pathol. 19, 751-760. 2011.
42. Loboda, A *et al*. EMT is the dominant program in human colon cancer. BMC.Med.Genomics 4, 9. 2011.
43. Pino, MS *et al*. Epithelial to mesenchymal transition is impaired in colon cancer cells with microsatellite instability. Gastroenterology 138, 1406-1417. 2010.
44. Brabletz, T *et al*. Invasion and metastasis in colorectal cancer: epithelial-mesenchymal transition, mesenchymal-epithelial transition, stem cells and beta-catenin. Cells Tissues.Organs 179, 56-65. 2005.
45. Sheehan, KM *et al*. Signal pathway profiling of epithelial and stromal compartments of colonic carcinoma reveals epithelial-mesenchymal transition. Oncogene 27, 323-331. 2008.
46. Labelle, M *et al*. Direct signaling between platelets and cancer cells induces an epithelial-mesenchymal-like transition and promotes metastasis. Cancer Cell 20, 576-590. 2011.
47. Gradilone, A *et al*. Circulating tumour cells lacking cytokeratin in breast cancer: the importance of being mesenchymal. J.Cell Mol.Med. 15, 1066-1070. 2011.
48. Raimondi, C *et al*. Epithelial-mesenchymal transition and stemness features in circulating tumor cells from breast cancer patients. Breast Cancer Res.Treat. 130, 449-455. 2011.
49. Sun, YF *et al*. Circulating tumor cells: advances in detection methods, biological issues, and clinical relevance. J.Cancer Res.Clin.Oncol. 137, 1151-1173. 2011.
50. Pittet, MJ *et al*. Intravital imaging. Cell 147, 983-991. 2011.
51. Condeelis, J *et al*. *In vivo* imaging in cancer. Cold Spring Harb.Perspect.Biol. 2, a003848. 2010.
52. Ritsma, L *et al*. Intravital microscopy through an abdominal imaging window reveals a pre-micrometastasis stage during liver metastasis. Sci. Transl.Med. 4, 158ra145. 2012.
53. Orth, JD *et al*. Analysis of mitosis and antimitotic drug responses in tumors by *in vivo* microscopy and single-cell pharmacodynamics. Cancer Res. 71, 4608-4616. 2011.
54. Paramsothy, S *et al*. Endoscopy: Fluorescein contrast in confocal laser endomicroscopy. Nat. Rev.Gastroenterol.Hepatol. 7, 366-368. 2010.
55. Li, WB *et al*. Diagnostic value of confocal laser endomicroscopy for gastric superficial cancerous lesions. Gut 60, 299-306. 2011.
56. Vakoc, BJ *et al*. Three-dimensional microscopy of the tumor microenvironment *in vivo* using optical frequency domain imaging. Nat.Med. 15, 1219-1223. 2009.

PART III | DISCUSSION AND SUMMARY

CHAPTER 9

9

Summary in Dutch
Nederlandse samenvatting

Kanker komt steeds vaker voor en is momenteel zelfs de meest voorkomende doodsoorzaak in de westerse wereld. Dikke darm- en endeldarm (colorectale) kanker is in Nederland de op één na meest voorkomende vorm van kanker met elk jaar ongeveer 12000 nieuwe gevallen en bijna 5000 sterfgevallen. De mortaliteit ten gevolge van dikke darm kanker wordt bijna in zijn geheel veroorzaakt door het uitzaaien (metastaseren) van de tumor vanuit de darm naar de lever. Nog steeds is het niet geheel duidelijk hoe het kan dat een cel die de darmwand bekleedt, kan overleven en uitgroeien in de lever. Wel is bekend welke stappen een darmkankercel allemaal moet doorlopen om uit te kunnen zaaien.
De primaire epitheliale darmtumor is een solide massa van cellen waartussen sterke cel-cel interacties bestaan die essentieel zijn voor intercellulaire signalering. Om in het omliggende weefsel te kunnen invaderen moeten deze cel-cel interacties worden verbroken. Als de omliggende basaal membraan is afgebroken kunnen invaderende cellen vervolgens van de tumor losbreken, ook wel disseminatie genoemd. Wanneer de gedissemineerde en migrerende tumorcel een bloedvat tegenkomt kan deze door de endotheel laag van het vat in de bloedbaan terecht komen. De tumorcel komt in de circulatie terecht welke al bloed van de darm afvoert naar de lever. In de bloedbaan moet de tumorcel eliminatie door het immuunsysteem vermijden. Daarnaast moet de cel de mechanische krachten, gegenereerd door de stroming van bloed ('shear stress'), overleven in de microcirculatie (sinusoïden) van de lever. Wanneer de cel is vastgelopen in de sinusoïden van de lever moet deze door middel van het invaderen van de endotheellaag en degradatie van de basaal membraan uit de bloedbaan extravaseren. In de lever moet de cel tenslotte aanvallen van het lokale immuunsysteem zien te overleven. Wanneer er zich door proliferatie van de tumorcel een micrometastase heeft gevormd zal de structuur (morfologie) van deze metastase vaak overeenkomen met de morfolgie van de primaire darmtumor. Uit het hierboven beschreven proces van metastasering blijkt dat invasie een essentiele eigenschap is voor colorectale tumorcellen om uit te kunnen zaaien naar de lever. In dit proefschrift wordt in deel 1 ingegaan op hoe invasie wordt gesignaleerd in colorectale tumorcellen. In deel 2 wordt door middel van live beeldvorming aangetoond wat het belang van invasie is bij tumor kolonisatie van de lever.

Deel 1
Apoptose signalering stimuleert invasie van dikke darm kanker.

Veel cellen in het lichaam brengen op de buitenkant van de cel membraan receptoren tot expressie welke cel dood kunnen signaleren. Als omliggende cellen merken dat een cel niet meer goed functioneerd kunnen deze door middel van het activeren van deze 'death' receptoren de slecht functionerende cel gecontroleerde suïcide (apoptosis) laten plegen. CD95 is één van de meeste bekende 'death' receptoren. De mogelijkheid om via 'death' receptoren celdood in kankercellen te induceren wordt gezien als potentiële therapie. Echter in recente jaren blijkt uit steeds meer onderzoek dat CD95, en andere 'death' receptoren, ook mechanismen kunnen activeren die geen apoptose tot gevolg hebben. Zo blijkt CD95 ook proliferatie, differentiatie, migratie, invasie en overleving te kunnen signaleren.
CD95 en zijn activerende ligand (CD95L) worden ook in colorectale tumoren tot expressie gebracht. Maar het is nog onduidelijk wat precies de functie van CD95 is bij tumor formatie in de darm. Er kan onderdrukking van tumor groei zijn ten gevolge van apoptose activatie door CD95. Ook is het mogelijk dat CD95 signalering tumorgroei stimuleert door de activering van niet-apoptotische mechanismen zoals proliferatie, invasie en overleving. In **hoofdstuk 2** van

dit proefschrift wordt een overzicht gegeven van wat er in de literatuur bekend is over CD95 signalering in colorectale kanker. Aan de hand hiervan wordt een model gepresenteerd waarin de anti-tumorigene en de pro-tumorigene signalering van CD95 en CD95L samen bepalen hoe de colorectale tumor zich gedraagt. Verder wordt er besproken hoe de veranderende inzichten in CD95 signalering invloed hebben op de de potentiële therapeutische opties voor colorectale tumoren. Omdat nog niet duidelijk is in welke tumoren de activatie van CD95 een anti-tumorigene werking heeft en in welke tumoren een pro-tumorigene werking, is directe stimulatie van de 'death' receptor wellicht geen goede therapeutische optie. Dit is waarom in dit hoofdstuk het (medicamenteus) vastzetten van CD95 signalering in apoptose modus wordt bediscussieerd als een veel belovende therapeutische optie voor colorectale tumoren.

Een tumorcel moet in het omliggend weefsel invaderen om uit te kunnen zaaien. CD95 stimulatie kan invasie signaleren in colorectale tumorcellen maar de verantwoordelijke intracellulaire signaal mechanismen zijn onbekend. In **hoofdstuk 3** wordt aangetoond dat bij colorectale tumorcellen die ongevoelig zijn voor CD95-gestimuleerde apoptose CD95 activatie kan leiden tot invasie. Deze invasie wordt gesignaleerd door het activeren van cofiline, een eiwit wat belangrijk is bij afbreken en opbouwen van het starre geraamte van de cel.
De epitheliale tumorcel heeft een star cytoskelet (geraamte) wat de cel erg rigide maakt. Om te kunnen migreren of invaderen moet het cytoskelet dynamisch worden door afbraak en opbouw van dit geraamte. Zodoende kunnen zich uitstulpingen van de celmembraan vormen die de richting van beweging bepalen. De cel trekt zich als het ware voort aan deze cel protrusies. Het cytoskelet is opgebouwd uit actine filamenten. Deze filamenten bepalen de vorm en mobiliteit van de cel. CD95 stimulering kan voor een meer dynamisch cytoskelet zorgen door middel van activering van de tyrosine kinase receptor PDGF ('platelet derived growth factor'). Binding van CD95L aan de CD95 receptor leidt tot fosforylering van Tyrosine783 op fosfolipase C-γ1 (PLC-γ1) via de PDGF-receptor beta. Activatie door fosforylering van PLC-γ1 leidt op zijn beurt weer tot de hydrolyse van fosfatidylinositol (4,5)-bifosfaat (PIP_2). PIP_2 houdt cofiline gebonden aan de cel membraan waardoor het niet actief kan zijn. Wanneer PIP_2 wordt gehydrolyseerd, wordt de connectie met cofiline verbroken en kan cofiline binden aan actine filamenten. Door de binding van cofiline worden de actine filamenten gebroken en kunnen er nieuwe filamenten worden gecreëerd, vergelijkbaar met een gesnoeide boom die opnieuw ontspruit. Deze remodelering maakt het cytoskelet dynamisch en zo kunnen er protrusies worden gevormd die ervoor zorgen dat de cel gaat invaderen. Wanneer deze signaaltransductie wordt onderbroken door middel van de remming van de PDGF-receptor (PDGFR), overexpressie van niet-actief cofiline of suppressie van de aanmaak van PLC-γ1 eiwit wordt de cel ongevoelig voor CD95 gestimuleerde invasie. Dit bewijst dat CD95 gestimuleerde invasie van colorectale tumor cellen wordt gesignaleerd via cofiline gemedieerde reorganisatie van het cytoskelet.

Terwijl hoofdstuk 3 specifiek ingaat op het signaal transductie mechanisme verantwoordelijk voor CD95 gemedieerde invasie in colorectale tumoren kan CD95 ook invasie signaleren in andere apoptose resistente cellen. Zo is beschreven dat CD95 activatie een belangrijke rol speelt bij de invasie van cellen in inflammatoire processen en in neurobiologische processen. In **hoofdstuk 4** wordt een overzicht gegeven van alle beschreven signaleringsroutes via welke CD95 invasie stimuleert. Uit dit literatuur overzicht blijkt dat CD95 remodelatie van het cytoskelet niet alleen via de PDGF-receptor signaleert maar dat er ook verscheidene andere signalerings routes zijn. Zo wordt de uitgroei van dendrieten en neurieten tijdens de embryonale neurale ontwikkeling mede mogelijk gemaakt door een CD95 gemedieerd dynamisch cytoskelet. Dit

is afhankelijk van de georkestreerde activatie en deactivatie van Rac, een GTPase van de Rho familie. Bij dit strak georganiseerde evenwicht is CD95 signalering waarschijnlijk betrokken door de activatie van PI3K wat Rac activeert. Rac op zijn beurt reguleert actine polymerisatie via Arp 2/3. Naast de remodelatie van het cytoskelet moet ook de extracellulaire matrix worden afgebroken zodat de cel daadwerkelijk ruimte maakt om te migreren. Door middel van de expressie van proteasen kan een cel afbraak van de extracellulaire matrix bewerkstelligen. Deze eiwitten breken de filamenten van de matrix af waardoor een pad wordt gevormd waarover de cel kan migreren. CD95 stimulatie zorgt voor verhoogde transcriptie van de genen voor MMPs (matrix metalloproteinasen) en uPA (urokinase plasminogeen activator), beide zeer potente matrix proteasen, via een nog onbekend mechanisme. Waarschijnlijk wordt dit gereguleerd door de activatie van verschillende tyrosine kinases (bijvoorbeeld Src, EGFR of PDGFR). Daarnaast lijkt de complex vorming van PI3K met caspase 8 aan het 'death' domein van de CD95 receptor tot activatie van verscheidenen transcriptie factoren te leiden welke weer MMP en uPA expressie stimuleren. Kortom, CD95 gemedieerde invasie lijkt afhankelijk van de stimulatie van twee processen; de remodelatie van het cytoskelet en de stimulatie van expressie van extracellulaire matrix proteases.

In hoofdstuk 3 is de PDGFR geïndentificeerd als een belangrijke component van CD95-gestimuleerde invasie in colorectale cellen. **Hoofdstuk 5** gaat dieper in op de functie van de PDGFR bij het uitzaaien van colorectale tumoren. Colorectale carcinomen ontstaan uit epitheliale cellen. Epitheliale tumorcellen zijn afhankelijk van cel-cel verbindingen voor overleving, migreren niet veel en zijn gevoelig voor apoptose. Om uit te kunnen zaaien moeten cellen onafhankelijk van cel-cel interactie overleven, kunnen migreren, invasief zijn en apoptose inductie gedeeltelijk kunnen weerstaan. De hypothese is dan ook dat cellen die uitzaaien vanuit de primaire tumor een transitie hebben ondergaan naar een mesenchymale verschijningsvorm (fenotype), ook wel epitheliale naar mesenchymale transitie (EMT) genoemd. Deze mesenchymaal-achtige colorectale tumorcellen zijn niet afhankelijk van cel-cel interacties, migreren en invaderen gemakkelijk en zijn niet heel gevoelig voor apoptose. De huidige gedachte is dat de PDGFR in colorectale tumoren voornamelijk tot expressie wordt gebracht op stromale cellen, welke van mesenchymale origine zijn. Maar wanneer epitheliale colorectale tumorcellen EMT ondergaan, kunnen deze mesenchymaal-achtige cellen wellicht de PDGFR tot expressie gaan brengen. **Hoofdstuk 5** laat zien dat in een subgroep van humane colorectale tumoren de PDGFR tot expressie wordt gebracht op de tumorcellen. Verder laten gen expressie profielen van verschillende cohorten van humane colorectale tumoren zien dat PDGFR expressie gecorreleerd is met een kortere overleving en kortere ziekte vrije overleving. Ook is PDGFR expressie geassocieerd met de expressie van genen betrokken bij plaatjes activatie, TGFbeta signalering en EMT. Buiten het lichaam (*in vitro*) brengen mesenchymaal-achtige colorectale tumorcellen de PDGFR tot expressie, dit in tegenstelling tot epitheliale tumorcellen. De mesenchymaal-achtige cellen verliezen de PDGFR expressie wanneer zij, door middel van TGFbeta inhibitie, mesenchymale naar epitheliale transitie ondergaan. Activatie van de PDGFR op de mesenchymaal-achtige colorectale tumor cellen stimuleert *in vitro* invasie en *in vivo* (in het lichaam) de formatie van uitzaaiïngen in de lever. Stimulatie van de PDGFR vindt plaats door binding van PDGF. Een belangrijke bron van PDGF zijn bloedplaatjes. Tijdens het uitzaaiïngsproces gaat de tumorcel via de bloedbaan van de darm naar de lever. In de bloedbaan binden ongeactiveerde bloedplaatjes aan de tumorcellen. Als de tumorcellen vastlopen in de microcirculatie van de lever worden de gebonden bloedplaatjes geactiveerd en komt PDGF vrij. Dit vrijgekomen PDGF bindt aan de PDGFR op de uitzaaiende mesenchymaal-achtige

tumorcel en stimuleert daardoor invasie van de tumorcellen in het leverweefsel. Hieruit kan geconcludeerd worden dat in colorectale tumoren de PDGFR de vorming van uitzaaiïngen in de lever stimuleert. Dit nieuwe inzicht in de metastase formatie van colorectale tumoren kan in de toekomst eventueel leiden tot de ontwikkeling van nieuwe therapie gericht op het blokkeren van PDGFR signalering.

Deel 2
Invasie is een essentieel proces bij de kolonisatie van de lever door colorectale tumoren

Gezien de dodelijke consequenties van metastasering naar de lever wordt er veel onderzoek gedaan naar de cellulaire processen die uitzaaiïngen mogelijk maken en wat mogelijke aangrijpingspunten zijn voor therapie. Ondanks het vele onderzoek is er nog steeds niet bekend wat er precies gebeurt als de gedissemineerde cel vanuit de darmtumor aankomt in de lever. In **hoofdstuk 6** wordt een nieuw muismodel gepresenteerd waarmee de aankomst en uitgroei van een individuele uitzaaiende tumorcel kan worden gevisualiseerd gedurende langere tijd (weken). In dit nieuwe model wordt er een raampje, het 'abdominal imaging window' (AIW), geïmplanteerd in de buik van een muis. Door het raampje over de lever te plaatsen kan er met behulp van een geavanceerde 'multiphoton' lasermicroscoop tot 1 mm diep en met subcellulaire resolutie in het leverweefsel worden gekeken. Uitzaaiïngen naar de lever werden in dit model geïnduceerd door het injecteren van fluorescente cellen afkomstig van een colorectale muistumor in de milt. Via de milt wordt een groot deel van deze cellen meegenomen naar de lever door de portale circulatie. De subcellulaire resolutie van de lasermicroscoop maakt het mogelijk om individuele tumorcellen 'live' aan te zien komen in de sinusoïden van de lever. Deze cellen kunnen dagelijks, gedurende enkele uren, worden gevisualiseerd wat ervoor zorgt dat de initiële fasen van invadering in en migratie door het leverweefsel in beeld kunnen worden gebracht. Uit analyse van deze fasen blijkt dat uitzaaiïngen in de lever worden gevormd uit één individuele tumorcel en dat invasie een cruciaal proces is bij de vorming van wat hier pre-micrometastasen worden genoemd. De pre-micrometastatische fase wordt gekenmerkt door erg bewegelijke tumorcellen, weinig cel-cel interacties en zodoende een lage tumor densiteit. Proliferatie vindt plaats echter zeer traag. Na enkele dagen worden de cellen minder motiel en neemt proliferatie de overhand, er ontstaan meer dense micrometastasen. Behandeling met een PLC-γ1 inhibitor zorgt, door het verminderen van de dynamiek van het cytoskelet, voor zeer selectieve reductie van de motiliteit van de geïnjecteerde tumorcellen. Om te bepalen of de motiliteit van de cellen ook daadwerkelijk bijdraagt aan de efficientie van metastase formatie zijn muizen behandeld met deze inhibitor na injectie van tumorcellen in de milt. In vergelijking met onbehandelde muizen migreren en invaderen de uitzaaiende tumor cellen in de behandelde groep veel minder tijdens de pre-micrometastatische fase. Uiteindelijk leidt dit tot minder micro- en macrometastasen. Hieruit kan geconcludeerd worden dat invasie niet alleen een cruciaal proces lijkt bij het loslaten van een tumorcel van de tumor in de darm maar ook zeer belangrijk is bij het koloniseren van de lever.

Geavanceerde lasermicroscopen en de expressie van fluorescentie hebben het mogelijk gemaakt om cellen maar ook intracellulaire eiwitten in detail te observeren. De ontwikkeling van zogenoemde 'imaging windows' die in muizen worden geïmplanteerd heeft ervoor gezorgd dat deze cellen en eiwitten ook in de natuurlijke omgeving van het lichaam in beeld kunnen worden gebracht. Tot nu toe was het met de bestaande raampjes alleen mogelijk om voor

langere tijd naar processen in de hersenen, borstklier of onder de huid te kijken. Het ontwerp van deze bestaande raampjes belemmert echter de langdurige visualisitie van processen in buikorganen. Om de uitgroei van een individuele tumorcel tot een tumor in de lever te kunnen volgen is het AIW ontwikkeld. Naast de visualisatie van tumor formatie in de lever beschrijft **hoofdstuk 6** ook andere organen en processen die met behulp van de AIW tot in detail kunnen worden bestudeerd. Zo is het ook mogelijk om individuele cellen in de dunne of dikke darm in beeld te brengen. Als voorbeeld hiervan is de deling van een stamcel van de darm gefilmd. Ook het pancreas en de insuline producerence eilandjes van Langerhans kunnen worden gevisualiseerd. En als laatste wordt een voorbeeld gegeven van het visualiseren van de milt en de immuuncellen in dit orgaan. **Hoofdstuk 7** geeft een meer gedetaileerde omschrijving van de specificaties en van de chirurgische procedure voor implantatie van dit raampje. Met behulp van deze informatie moet het voor andere onderzoekers mogelijk zijn om dit model toe te passen en zodanig nieuwe inzichten te verkrijgen in fysiologische en ziekte processen in de buik.

PART IV | APPENDICES

CHAPTER 10

10

Appendices

Authors and Affiliations
Review Committee
Dankwoord
List of publications
Curriculum Vitae Auctoris

AUTHORS AND AFFILIATIONS

University Medical Center Utrecht, The Netherlands
Department of Surgery
IHM Borel Rinkes, MD PhD
BL Emmink, MD
KM Govaert, MD
FJH Hoogwater, MD PhD
O Kranenburg, PhD
J Laoukili, PhD
DAE Raats, Bsc
N Snoeren, PhD
BF Westendorp, Bsc

Department of Oncogenomics
FCP Holstege, PhD
SR van Hooff, Msc

Department of Haematology and Molecular Cancer Research
C Maas, PhD
B Rutten, Msc

Hubrecht Institute-Royal Netherlands Academy of Arts and Sceinces (KNAW) and University Medical Center Utrecht, The Netherlands
E Beerling, Msc
SIJ Ellenbroek, PhD
A de Graaff, Bsc
L van Gurp, Bsc
EJP de Koning, PhD
CJM Loomans, PhD
J van Rheenen, PhD
L Ritsma, Msc
R Schäfer, Msc
D Seinstra, Bsc
N Vrisekoop, PhD
A Zomer, Msc

The Netherlands Cancer Institute, Amsterdam, The Netherlands
Department of Immunology
C Gerlach, Msc
TN Schumacher, PhD

Academic Medical Center, Univeristy of Amsterdam, The Netherlands
Department of Oncogenomics
J Koster, PhD

REVIEW COMMITTEE

Prof. dr. G.J.P.L. Kops
Professor of Molecular and Tumorcel Biology, University Medical Center Utrecht

Prof. dr. E.E. Voest
Professor of Medical Oncology, University Medical Center Utrecht

Prof. dr. P.J. van Diest
Professor of Pathology, University Medical Center Utrecht

Prof. dr. P. ten Dijke
Professor of Molecular Cel Biology, Leids Universitair Medisch Centrum

Prof. dr. R. Fodde
Professor of Experimental Pathology, Erasmus Medical Center Rotterdam

Other members of the opposing committee

Prof. dr. R van Hillegersberg
Professor of Surgery, University Medical Center Utrecht

Dr. J. van Rheenen
Senior groupleader and head of the Hubrecht Imaging Center

DANKWOORD

Dit proefschrift is tot stand gekomen met de hulp en steun van velen, waarvoor heel veel dank! Toch wil ik nog een aantal personen in het bijzonder bedanken.

Prof. dr. I.H.M. Borel Rinkes, beste Inne
Lang geleden kwam ik als een wijsneuzerige student vragen of ik nog wat onderzoek voor je kon doen. Uiteindelijk heeft dat geresulteerd in dit proefschrift. Ik heb in de tussenliggende jaren groot respect voor je gekregen als wetenschappelijk georiënteerd chirurg. Dank voor de momenten waarin je me afremde, stimuleerde, ondersteunde maar vooral enthousiasmeerde. Ik heb veel van je geleerd en hoop nog veel meer te leren. Het was een voorrecht om deel uit te maken van jouw succesvolle chirurgisch oncologische onderzoeksgroep. Daarom is het ook dat ik met zeer veel eer als jouw promovendus dit proefschrift ten over staan van de promotiecommissie verdedig.

Tenslotte denk ik dat het tijd wordt dat wij ons sterk maken voor een wijziging van het al oude chirurgisch adagium: "When in doubt, cut it out" naar het adagium van Jack Reacher "When in doubt, drink coffee".

Dr. O. Kranenburg, beste Onno
De onderzoekgroep van de experimentele chirurgische oncologie heeft één sterkhouder en dat ben jij. In een café in Boston overtuigde jij mij om voor een promotietraject in de Borel Rinkes/ Kranenburg groep te kiezen. Op het uiteindelijke resultaat ben ik zeer trots en dat is mede aan jou te danken. Niet altijd zaten we op één lijn maar dat is de inhoud van dit proefschrift misschien wel ten goede gekomen. Vaak verbaas ik me over je ongelofelijke kennis van de huidige biomedische wetenschap, een karaktereigenschap die naar mijn mening het niveau van de groep van een constant stijgende lijn voorziet. Heel veel succes met het tot een verdere hoogte opstuwen van de groep. Mijn dank voor je hulp bij het tot stand komen van dit proefschift is groot.

Dr. J. van Rheenen, beste Jacco
De combinatie van biomedisch wetenschapper in hart en nieren en een arts lijkt in theorie niet garant te staan voor succes. Maar onze gezamelijke praktische aanpak van vraagstukken bleek zeer vruchtbaar te zijn. Je hebt de wonderen wereld van de microscopie voor mij toegankelijk gemaakt door me de basisprincipes uit te leggen en te laten begrijpen. Door dit te combineren met de basisprincipes van de chirurgie konden we de black box van de leveruitzaaiingen live in beeld brengen. Voor mij het ultieme translationele oncologisch onderzoek. Dank voor de inhoudelijke en niet-inhoudelijke discussie over alles wat ter tafel werd gebracht en de prettige samenwerking met jouw onderzoeksgroep.

De leden van de promotiecommissie, Prof. dr.Kops, Prof. dr. Voest, Prof. dr. van Diest, Prof. dr. Fodde, Prof. dr. Ten Dijke, Prof. dr. van Hillegersberg,
Dank voor de interesse in mijn onderzoek, de bereidheid tot samenwerken, het delen van kennis maar bovenal voor het zitting nemen in de oppositie.

Dr. M.R. Vriens, beste Menno,
Hartelijk dank voor het vertrouwen bij de sollicitaties voor de heelkunde, geweldig om nu chirurg in opleiding te zijn! Ik kijk er naar uit om van je te leren aan de operatie-tafel van het UMCU.

Wijnand M. Pon stichting, geachte heer en mevrouw Schipper,
Ik ben u zeer erkentelijk voor het mogelijk maken van het onderzoek beschreven in dit proefschrift. Met veel plezier denk ik terug aan onze ontmoeting, uw enthousiasme en in het bijzonder uw kennis van de wetenschap.

Marielle Hoefakker en Romy Liesdek,
Jullie zijn de kritieke schakel tussen onderzoekers en de wel hooggeleerde heren. Heel heel heel veel dank voor alle ondersteuning en vele hulp.

Medewerkers van de biobank; **Natalie, Jan en Jan-Willem** mijn verzoeken voor coupes of weefsel waren altijd CITO met hoofdletters en dan nog wisten jullie me te verbazen met hoe snel alles klaar lag. Jullie werk heeft me veel tijdswinst opgeleverd, waarvoor heel veel dank.

Stafleden en arts-assistenten afdeling Heelkunde van het UMC Utrecht, dank voor de interesse in mijn onderzoek, ondanks het fundamentele karakter. Met veel plezier kijk ik terug op de mooie momenten buiten het werk.

Stafleden en arts-assistenten chirurgie van het St. Antonius ziekenhuis, dank voor de interesse in mijn onderzoek en voor de hulp bij het heropstarten van de dokter in mij.

Collega's medische en urologische oncologie; **Laura Hussen-Daenen,** tijdens vier jaar onderzoek in principe uit prinicipe altijd kritisch. Mooi om dat in de kliniek van het St. Antonius weer tegen elkaar te kunnen zijn. Dank je wel daarvoor! **Jeanine Roodhart, Julia Houthuijzen, Martijn Lolkema, Marco Koudijs, Ilse van Oosterom, Stephanie Kroeze** en de collega's van de **Derksen**, **Lens**, **Medema** en **Kops groep** het was niet alleen zeer leerzaam maar ook erg gezellig om samen met jullie onderzoek te doen.

Van Rheenen groep,
Jacco's Angels; met open armen word ik altijd ontvangen bij jullie op het lab. Jullie enthousiasme is erg aanstekelijk en zorgt voor een geweldige sfeer. Het was een feest om met jullie samen te werken.
Laila Ritsma, bij alles stel jij de vraag 'waarom?', iets wat ervoor heeft gezorgd dat onze gezamelijke projecten een ontzettend sterk fundament kregen. Daarnaast was jouw microscopiekennis van essentieel belang bij het visualiseren van onze hypothesen. Als rasechte onderzoekster was het ontzettend plezierig om met je samen te werken.

Lidewij Hoorntje, Niels Smakman, Annique Duyverman, als begeleiders tijdens mijn verschillende wetenschappelijke stages hebben jullie mij niet alleen enthousiast gemaakt voor de chirurgie maar is de basis gelegd van het onderzoek beschreven in dit proefschrift. Heel veel dank hiervoor.

Voorgangers bij de experimentele chirurgische oncologie. **Frederik Hoogwater**, geweldig om in jouw onderzoekslift te mogen stappen en een paar verdiepingen samen omhoog te reizen. Nu doen we hetzelfde tijdens de opleiding in het Antonius maar nemen we de trap. **Maarten Nijkamp, Menno de Bruijn, Nikol Snoeren, Winan van Houdt** dank voor jullie wijze lessen, enthousiasme en reflecteermomenten: het gaf mijn promotie een vliegende start.

Studenten **Kari Trumpi** en **Jermaine Goveia**. Dank jullie wel voor alle hulp en het vele werk wat jullie voor me hebben gedaan. In mijn ogen voor allebei het begin van een mooie carriere in de wetenschap.

Isengard vrienden: **Charlotte van Kessel, Anne den Hartog, Emily Postma, Jakob Kist, Pieter van der Sluis, Stein van Esser, Eline van Hattum, Tjaakje Visser, Claire Pennekamp, Jasper van Keulen** altijd ontspannend om de lange reis naar Isengard te maken voor een gezellig moment.

Promovendi chirurgie: **Okan Bastian, Marjolein Heeres, Dave Koole, Martin ter Aa, Siegrid de Meer, Pieter Leliefeld, Herman Zandvoort, Peter Paul Wisman, Samira Fegrachi, Vincent Scholtes, Femke Maurits, Margriet Prins en Leonie Haverkamp** dank voor alle gezellige momenten.

Alpe d'HuZes team 2012 'Chirurgen tegen kanker': **Inne, Menno, Q, Menno, Jakob, Lutske, Klaas, Signe, Emily, Kari en Imke.** OPGEVEN IS GEEN OPTIE!

JC Staboul, dank voor de interesse in mijn onderzoek. Maar vooral voor de zeer welkome afleiding daarvan.

OHG Equites, een hechte groep met ontzettend veel ambitie. Het is een voorrecht hier onderdeel van uit te mogen maken. Dank voor de vriendschap.

Borel Rinkes-Kranenburg lab:
Klaas Govaert (alias Klees of Goevenator) jouw oneindige enthousiasme is geweldig vooral als het aankomt op opereren in het GDL. Parallel opereren was altijd uitermate gezellig en productief. Onze congres bezoeken met bijbehorende muzieklijsten en de 6de beklimming van de Alpe waren absolute hoogtepunten. Mooi om in de kliniek nog steeds directe collega's te zijn, het duurt niet lang en dan opereren we parallel op macro-niveau.

Kamergenoten **Lutske Lodewijk** en **Kari Trumpi**, dank jullie wel voor de thee/koffie momenten. De vele gesprekken over alles behalve de wetenschap waren erg gezellig ook al werd ik er soms gek van. Ik weet zeker dat jullie het onderzoek bij de chirurgische oncologie weer een stapje hoger gaan brengen.
Lab-genoten van de Kranenburg-Borel Rinkes groep: **Jamila Laoukili, Szabolcs Fatrai, Andre Verheem, Susanne van Schelven, Tijana Borovski, Thomas Vellinga**. My gratitude is endless for all the help and expertise you gave me. It was a pleasure to work with you.

Danielle Raats, mijn steun en toeverlaat in het lab. Dank je wel voor je loyaliteit, harde werken en bereidwilligheid om mij, de soms hardnodige, ondersteuning in het lab te geven. Ik noem je vaak de baas van het lab en dat meen ik ook, jij bent de constante factor, hebt de meeste expertise wat betreft het doen van experimenten en bent het fundament die het lab draaiende

houdt. Elke keer als er nieuwe arts-onderzoekers in de groep beginnen (zonder ooit een pipet te hebben vastgehouden) help je hen enthousiast. Mijn respect voor je is dan ook groot. Nogmaals heel veel dank.

Mijn paranimfen,
Roy Verhage de omschrijving van vriend en collega, exact in die volgorde, neem ik graag van je over. Geweldig om zo een goede vriend als vakgenoot te hebben. Samen opereren binnen de heelkunde is het mooiste wat er is, ik kan niet wachten op onze gezamelijke jaren in het UMCU. Thanks, dat je me als paranimf wilt ondersteunen.
Benjamin Emmink, samen hebben we de ontberingen van het promotieonderzoek gedurende drie en een half jaar doorstaan. Het was goed dat we de frustraties af en toe van ons af konden slaan op de tennisbaan. Na al het gedeelde bloed, zweet en tranen is het geweldig dat jij als vriend en paranimf naast me staat.

Beste schoonfamilie,
Jeanet, Ad, Roosmarijn en Fleur heel veel dank voor jullie bijzondere interesse in mijn onderzoek. De wôarme kersen in Limburg geven me eindeloos nieuwe energie. Venray voelt als tweede thuis.

Willemine, Jan Jasper (Saar), Tjeerd, Willemijn, Taco en Eerke,
Dank voor het informeren naar deadlines, acceptaties van artikelen en voor de algemene interesse in mijn onderzoek. Jullie steun heeft me zeer gemotiveerd. Maar vooral veel dank voor de niet medisch getinte gesprekken over management, bestuur en scheepsbouw, het verruimt mijn blik enorm.

Pap en Mam,
Jullie interesse in mijn onderzoek en de voortgang daarvan heeft mijn altijd erg gemotiveerd om hard door te werken, met dit proefschrift als resultaat. Door jullie opvoeding, zorg en onvoorwaardelijke steun heb ik mij in een veilige omgeving kunnen ontwikkelen tot wie ik ben. Ik ben jullie daar ontzettend dankbaar voor!

Lieve Isa,
Ik weet niet of ik je ooit uit dit boek zal voorlezen maar ik leg het je graag nog een keer uit.

Lieve Im,
Dank je wel voor alles wat je voor me bent en voor me doet, dit boekje is van ons samen. Je t'aimais, je t'aime et je t'aimerais.

LIST OF PUBLICATIONS

Ritsma L, **Steller EJ**, Ellenbroek SI, Kranenburg O, van Rheenen J, Borel Rinkes IH. Surgical implantation of an Abdominal Imaging Window for intravital microscopy.
Nature Protocols 2013 Feb 21;8(3):583-94.

Steller EJ, Raats DA, Govaert KM, Emmink BL, Rutten B, Borel Rinkes IH, Kranenburg O. PDGFRβ promotes liver metastasis formation of mesenchymal-like colorectal tumor cells.
Neoplasia 2013 Feb;15(2):204-17.

Ritsma L, **Steller EJ**, Beerling E, Loomans CJ, Zomer A, Gerlach C, Vrisekoop N, Seinstra D, van Gurp L, Schafer R, Raats DA, de Graaff A, Schumacher TN, de Koning EJ, Borel Rinkes IH, Kranenburg O, van Rheenen J. Intravital microscopy through an abdominal imaging window reveals a pre-micrometastasis stage during liver metastasis.
Science Translational Medicine 2012 Oct 31;4(158) p. 158ra145

Hoogwater FJ, **Steller EJ**, Westendorp BF, Borel Rinkes IH, Kranenburg O. CD95 signaling in colorectal cancer.
Biochimica et Biophysica Acta 2012 Mar 31;1826(1):189-198.

Duyverman AM, **Steller EJ**, Fukumura D, Jain RK, Duda DG. Studying primary tumor-associated fibroblast involvement in cancer metastasis in mice.
Nature Protocols 2012 Mar 22;7(4):756-62.

Steller EJ, van Leeuwen MS, van Hillegersberg R, Schipper ME, Rinkes IH, Molenaar IQ. Primary lymphoma of the liver - A complex diagnosis.
World Journal of Radiology 2012 Feb 28;4(2):53-7.

Govaert KM, Nijkamp MW, Emmink BL, **Steller EJ**, Minchinton AI, Kranenburg O, Borel Rinkes IH. Effects of tirapazamine on experimental colorectal liver metastases after radiofrequency ablation.
Britisch Journal of Surgery 2012 Apr;99(4):567-75.

Steller EJ, Borel Rinkes IH, Kranenburg O. How CD95 stimulates invasion.
Cell Cycle 2011 Nov 15;10(22):3857-62.

Steller EJ, Ritsma L, Raats DA, Hoogwater FJ, Emmink BL, Govaert KM, Laoukili J, Rinkes IH, van Rheenen J, Kranenburg O. The death receptor CD95 activates the cofilin pathway to stimulate tumour cell invasion.
EMBO Reports 2011 Sep 1;12(9):931-7.

Nijkamp MW, Hoogwater FJ, Govaert KM, **Steller EJ**, Verheem A, Kranenburg O, Borel Rinkes IH. A role for CD95 signaling in ischemia/reperfusion-induced invasion and outgrowth of colorectal micrometastases in mouse liver.
Journal of Surgical Oncology 2011 Aug 1;104(2):198-204.

Raats DA, de Bruijn MT, **Steller EJ**, Emmink BL, Borel-Rinkes IH, Kranenburg O. Synergistic killing of colorectal cancer cells by oxaliplatin and ABT-737.
Cellular Oncology 2011 Aug;34(4):307-13.

Emmink BL, Van Houdt WJ, Vries RG, Hoogwater FJ, Govaert KM, Verheem A, Nijkamp MW, **Steller EJ**, Jimenez CR, Clevers H, Borel Rinkes IH, Kranenburg O. Differentiated human colorectal cancer cells protect tumor-initiating cells from irinotecan.
Gastroenterology 2011 Jul;141(1):269-78.

Duda DG, Duyverman AM, Kohno M, Snuderl M, **Steller EJ**, Fukumura D, Jain RK. Malignant cells facilitate lung metastasis by bringing their own soil.
Proceedings of the National Academy of Sciences 2010 Dec 14;107(50):21677-82.

Nijkamp MW, Hoogwater FJ, **Steller EJ**, Westendorp BF, van der Meulen TA, Leenders MW, Borel Rinkes IH, Kranenburg O. CD95 is a key mediator of invasion and accelerated outgrowth of mouse colorectal liver metastases following radiofrequency ablation.
Journal of Hepatology 2010 Dec;53(6):1069-77.

Hoogwater FJ, Nijkamp MW, Smakman N, **Steller EJ**, Emmink BL, Westendorp BF, Raats DA, Sprick MR, Schaefer U, Van Houdt WJ, De Bruijn MT, Schackmann RC, Derksen PW, Medema JP, Walczak H, Borel Rinkes IH, Kranenburg. Oncogenic K-Ras turns death receptors into metastasis-promoting receptors in human and mouse colorectal cancer cells.
Gastroenterology 2010 Jun;138(7):2357-67

van Olden GDJ, Kaasschieter EG, **Steller EJ**, Verberne GH. Complicatieregistratiesysteem in de heelkunde
Nederlands Tijdschrift voor Heelkunde 17; 2; 2008; 33-35

CURRICULUM VITAE AUCTORIS

Ernst Johan Abraham Steller was born on August 7th, 1981 in Capelle aan den IJssel, The Netherlands. In 1999, he graduated from secondary school, the Gymnasium Felisenum in Velsen-Zuid. After high school he received a scholarship from the Fulbrigth Center to study a year at Knox College in Galesburg Illinois, USA. After returning to the Netherlands he studied Pre-Medicine at University College Utrecht graduating with honors as a Bachelor of Science in 2002. In 2001 he started medical school at Utrecht University. During his bachelors and medical studies he was an active member of several student bodies and societies. In 2005 he performed his obstetrics and gyneacology clinical rotation at the Queen Elisabeth Central Hospital in Blantyre, Malawi. As a medical student he was involved in several research projects at the department of Surgical Oncology of the University Medical Center Utrecht (UMCU), The Netherlands. In 2007 he went to the Edwin L. Steele Laboratory for Tumor Biology, Massachusetts General Hospital and Harvard Medical School, Boston MA, USA (prof. dr. R.K. Jain, dr. D. Duda) for his research elective. He obtained his medical degree in August 2008 whereafter he started working at the department of Surgery of the Diakonessenhuis, Utrecht (dr. G.J. Clevers). When awarded a research grant from the Dutch Cancer Society and the Wijnand M. Pon foundation he commenced a PhD program at the department of Surgical Oncology in April 2009 under the supervision of prof. dr. I.H.M. Borel Rinkes and dr. O. Kranenburg. In January 2013 he started the residency program in general surgery under the auspices of dr. P.M.N.Y.H. Go at the St. Antonius Hospital Nieuwegein. The fourth and fifth year of his surgical training are scheduled at the UMCU under the supervision of dr. M.R. Vriens. For the sixth and final year of the program he will return to the St. Antonius Hospital Nieuwegein.